MACROCYCLIC CHEMISTRY.
FROM ANION RECOGNITION TO THE REACTIVITY OF THEIR COOPER COMPLEXES

Arnau Arbusé Font

Per citar o enllaçar aquest document:
Para citar o enlazar este documento:
Use this url to cite or link to this publication:

http://hdl.handle.net/10803/673534

http://creativecommons.org/licenses/by/4.0/deed.ca

Aquesta obra està subjecta a una llicència Creative Commons Reconeixement

Esta obra está bajo una licencia Creative Commons Reconocimiento

This work is licensed under a Creative Commons Attribution licence

Universitat de Girona

DOCTORAL THESIS

Macrocyclic chemistry. From anion recognition to the reactivity of their copper complexes.

Arnau Arbusé Font

2020

DOCTORAL THESIS

Macrocyclic chemistry. From anion recognition to the reactivity of their copper complexes.

Arnau Arbusé Font

2020

DOCTORAL PROGRAMME IN CHEMISTRY

Supervised by:
Antoni Llobet Dalmases
Ma Ángeles Martínez Lorente

Tutor:
Ma Ángeles Martínez Lorente

Presented to obtain the degree of PhD at the University of Girona

Universitat
de Girona

El **Dr. Antoni Llobet Dalmases**, Professor Catedràtic del Departament de Quimica de la Universitat Autònoma de Barcelona i Group Leader a l’Institut Català d’Investigació Quimica, i la **Dra. M. Angeles Martinez Lorente**, professora Titular del Departament de Química de la Universitat de Girona

DECLAREM:

Que el treball titulat “Macrocyclic chemistry. From anion recognition to the reactivity of their copper complexes”, que presenta **Arnau Arbusé Font** per a l’obtenció del títol de doctor, ha estat realitzat sota la nostra direcció.

I, perquè així consti i tingui els efectes oportuns, signen aquest document.

Girona, 23 de març de 2020

Universitat
de Girona

Dr **Dr. Antoni Llobet Dalmases**, of Universitat Autònoma de Barcelona and Group Leader in Institut Català d'Investigació Quimica, and **Dr. M. Angeles Martinez Lorente**, of Universitat de Girona,

WE DECLARE:

That the thesis entitled "Macrocyclic chemistry. From anion recognition to the reactivity of their copper complexes", presented by **Arnau Arbusé Font** to obtain a doctoral degree, has been completed under our supervision.

For all intents and purposes, I hereby sign this document.

Girona, 23th March, 2020.

Publications related to the thesis content

The studies presented in this work have given rise to the three following publications:

Arbusé, A.˚ Anda, C.˚ Martínez, M.˚ Pérez-Miron, J.˚ Jaime, C.˚ Parella, T.˚ Llobet, A. *Inorg. Chem*. **2007**, *46*, 10632−10638. DOI: 10.1021/ic701288n

Arbusé, A.˚ Font, M.˚ Martínez, M.˚ Fontrodona, X.˚ Prieto, M.J.˚ Moreno, V.˚ Sala, X.˚ Llobet, A. *Inorg. Chem*. **2009**, *48*, 11098–11107. DOI: 10.1021/ic901488j

Arbusé, A.˚ Mandal, S.˚ Maji, S.˚ Martínez, M.˚ Fontrodona, X.˚ Utz, D.˚ Heinemann, F. W.˚ Kisslinger, S.˚ Schindler, S.˚ Sala, X.˚ Llobet, X. *Inorg. Chem*. **2011**, *50*, 6878–6889. DOI: 10.1021/ic0261833

List of abbreviations

AFM	Atomic Force Microscopy
BArF	tetrakis[3,5-bis(trifluoromethyl)phenyl]borate anion
CD	Circular Dichroism
CV	Cyclic Voltammetry
CIS	Complexation induced shifts
D	Self-diffusion coefficients
DNA	Deoxyribonucleic acid
DMSO	Dimethyl sulfoxide
EM	Electrophoretic Mobility
h	Hours
HRMS	High Resolution Mass Spectrometry
I	Ionic Force
IR	Infrared spectroscopy
min	Minutes
Me	Methyl group CH_3
MPA	3-Mercaptopropionic acid
MW	Molecular Weigh
NMR	Nuclear magnetic resonance spectroscopy
NOE	Nuclear Overhauser effects
MS	Mass spectrometry
m/z	Mass to charge ratio
OTf	Trifluoromethanesulfonate anion
SQWV	Squarewave voltammetry
TE	Tris-EDTA Buffer
TMAFM	Tapping Mode Atomic Force Microscopy
w/v	Weight / volume ratio
X-Ray	X-ray diffraction analysis
µL	Microliter
µM	Micromolar concentration
OC form	Plasmid Open Circular Form
CCC Form	Plasmid Covalently closed Circular Form
L	Ligand
S	Substrate

Substrates:

da: dicarboxylic acid

is: isophthalic acid.

ph: phthalic acid.

te: terephthalic acid.

Ligands and complexes nomenclatures:

Ligand	Ligand Abbreviation	Complex	Complex abbreviation
bsm2py$_{2+2}$	**L73**	[Cu$_2$(**L73**)]$^{2+}$	**1^{2+}**
bsm2phOH$_{2+2}$	**L74**	[Cu$_2$(**L74**)]$^{2+}$	**2^{2+}**
bsm2Et$_{2+2}$	**L75**	[Cu$_2$(**L75**)]$^{2+}$	**3^{2+}**
bsm2py$_{3+3}$	**L76**	[Cu$_2$(**L76**)]$^{3+}$	**4^{3+}**
bsm2phOH$_{3+3}$	**L77**	[Cu$_2$(**L77**)]$^{3+}$	**5^{3+}**
bsm2Et$_{3+3}$	**L78**	[Cu$_2$(**L78**)]$^{3+}$	**6^{3+}**
bsp3py	**L79**	[Cu$_2$(**L79**)]$^{2+}$	**7^{2+}**
bsm3py	**L80**	[Cu$_2$(**L80**)]$^{2+}$	**8^{2+}**
bsp2py	**L81**	[Cu$_2$(**L81**)]$^{2+}$	**9^{2+}**

TABLE OF CONTENTS:

List of Schemes

List of Tables

List of Figures

List of Figures in the Annex

Abstract

Resumen

Resum

1. INTRODUCTION 1

1.1. Bioinorganic chemistry 3

1.2. Macrocycle chemistry 4

1.3. Supramolecular Chemistry 9

1.3.1. Molecular receptors 9

1.3.2. Supramolecular chemistry of anions 10

1.3.3. Carboxilate anions Recognition 11

1.3.4. Inorganic phosphates and mononucleotides recognition 20

1.3.4.1. Phosphate, pyrophosphate and triphosphate anions recognition 21

1.3.4.2. Mononucleotide anions recognition 25

1.4 – Nucleic acids – metal complexes interactions 34

1.5 – Metal – DNA interaction modes 35

1.6 – Metal mediated DNA cleavage 37

1.6.1 – The Oxidative Pathway 39

1.6.2 – Factors influencing the oxidative pathway 40

1.6.3 – Artificial Copper nucleases 41

1.6.4 – Multinuclear nuclease systems 43

1.6.5 – Macrocyclic ligands in artificial dinuclear copper nucleases 44

2. OBJECTIVES 51

3. METHODOLOGY 55

3.1 – Materials 57

3.2 – Physical methods 57

3.2.1. Potentiometric titrations 58

3.2.2. NMR spectroscopy 59

3.2.3. Theoretical calculations 59

3.2.4. X-ray Diffraction Studies 60

3.2.5. Circular dichroism – CD Spectroscopy 61

3.2.6. EM in Agarose Gel 63

3.2.7. Atomic Force Microscopy, AFM 64

3.3 – Synthetic procedures 64

3.3.1. Ligand precursor Synthesis 64

3.3.2. Macrocyclic Ligand Synthesis 70

3.3.3. Synthesis of Cu(I) Complexes 72

3.3.4. Solubility and Stability of the copper complexes 77

4. RESULTS AND DISCUSSION 79

4.1. Fine-Tuning Ligand–Receptor Design for Selective Molecular Recognition of Dicarboxylic Acids 81

4.1.1. Abstract 81

4.1.2. Formation and selectivity of Ternary Species H:**L9**:S 82

4.1.3. Interaction Sites 88

4.1.4. Theoretical Calculations. 91

4.1.5. Final remarks. 93

4.2. Ligand Influence over the Formation of Dinuclear [2+2] versus Trinuclear [3+3] Cu(I) Schiff Base Macrocyclic Complexes 95

4.2.1. Abstract 95

4.2.2. Synthesis of the macrocyclic ligands 95

4.2.2.1. Synthesis of the triamine precursors 96

4.2.2.2. Synthesis of metal free [2+2] macrocyclic ligands 97

4.2.3. Synthesis of Cu(I) Complexes 98

4.2.4. Solid State Characterization 101

4.2.5. Stability of the complexes to oxidation 104

4.2.6. Mass Spectroscopy and the [2+2] vs. [3+3] Evolution Process 105

4.2.7. Final remarks 107

4.3. DNA-Cleavage Induced by New Macrocyclic Schiff base Dinuclear Cu(I)Complexes Containing Pyridyl Pendant Arms 109

4.3.1. Abstract 109

4.3.2. Synthesis, Structure, and Redox Properties of the complexes 109

4.3.3. DNA–Copper Complex Interaction Studies 115

4.3.3.1. CD Spectroscopy 115

4.3.3.2. EM in Agarose Gel 117

4.3.3.4. AFM. Atomic Force Microscopy 120

4.3.4. Final remarks 122

5. CONCLUSIONS 125

6. REFERENCES......129

ANNEX. Supporting Information......147

List of Schemes

Scheme 1.1. Synthetic pathways of [1+1] polymeric (a), cyclic [1+1] (b), [2+2] (c), [3+3] (d) or [4+4] (e) and macrobicyclic Schiff base derivatives (f) 5

Scheme 4.2.1. (A) General synthetic strategy for the preparation of substituted triamines: H_2NC_2PhOH, H_2NC_2py and H_2NC_2Et. (B) Alternative pathway for the synthesis of H_2NC_2Et 97

Scheme 4.2.2. Potential condensation products from reaction of isophthalaldehyde and the corresponding substituted triamine, including the 2+2 and 3+3 macrocyclic ligands and proton labeling used 98

Scheme 4.2.3. Summary of the reactions performed involving ligands or precursors and Cu(I) and the products obtained 99

Scheme 4.3.1. Synthetic Scheme for Ligands and Complexes discussed in Chapter 4.3 111

List of Tables

Table 3.1. Cristallographic data for the crystallized ligands and complexes..62

Table 4.1.1. Cumulative (β_{HiL}, β_{HiS}) and stepwise (K^{H}_{i}) logarithms of the protonation constants for Ligand **L9** and substrates (S = *ph*, *is* and *te*) at 25.0 ºC and I=0.10M (NMe_4Cl), as long as macrocyclic species **L8**, **L34**, **L12** and **L9** in KCl 0.1M from other works, comparison purposes. 83

Table 4.1.2. Logarithms of stepwise association constants (K_i^R) for the interaction of the ligand **L9** with substrates (S = *ph, is* and *te*) at 25ºC and I = 010 M (NMe_4Cl) 85

Table 4.1.3. NMR data of 1:1, 2 mM binary **L9**-*da* complexes..89

Table 4.1.4. Measured self-diffusion coefficients for **L9** and *is* in free and complex states......90

Table 4.1.5. Total energies and complexation energies for the Anionic complexes **L9**-*da*…..91

Table 4.2.1. Summary of synthesis of the described complexes. Experiments were done at room temperature.. 100

Table 4.2.2. Nomenclatures used for the ligands and complexes discussed in this chapter…100

Table 4.2.3. Selected bond distances and angles for the first coordination sphere of one of the Cu(I) metal centers of complexes **2**($(CF_3SO_3)_2$), **4**($(PF_6)_3$), **5**($(CF_3SO_3)_3$), and **6**((CF_3SO_3)) 103

Table 4.3.1. Selected Bond Lengths (Å) and Angles (deg) for **7**($(CF_3SO_3)_2$), **8**($(SbF_6)_2$), and **9**($(CF_3SO_3)_2$)..112

List of Figures

Figure 1.1. Ligand **L1** obtained through barium templation 7

Figure 1.2. Synthesis of ligand **L2** through terephthalate templation 7

Figure 1.3. Synthesis of ligand **L3** through sulphate templation 8

Figure 1.4. Macrocyclic polyammonium species studied as receptors for dicarboxilates by Kimura and Lehn 12

Figure 1.5. Ditopic macrocycle **L7** synthesized by Martell's group 13

Figure 1.6. Macrocyclic ligands with different aromatic geometry and aliphatic spacer length studied as oxalic acid receptors 14

Figure 1.7. Ligand **L12** selectively binds terephthalate anion over other aromatic diacids 14

Figure 1.8. Family of macrocyclic receptors used by Garcia-España and coworkers as glutamate receptors 15

Figure 1.9. Drawing of (a) macrocyclic ligands **L13** and **L14** and (b) pyridine dicarboxylic acids used as receptors and substrates 15

Figure 1.10. Chiral macrocyclic ligand **L15** 16

Figure 1.11. Kemp's triacids and the receptor **L16** 17

Figure 1.12. Tritopic receptors **L17**, **L18** and **L19**, and tricarbocylic acids 1,3,5-BTC, 1,2,4-BTC, 1,2,3-BTC and 1,3,5-BTAc 18

Figure 1.13. Cryptands bearing different aromatic spacers studied as receptors for dicarboxylates by Nelson and co-workers 18

Figure 1.14. L23 and **L24**. Cryptand ligands studied as receptors for dicarboxylates by Delgado and coworkers 19

Figure 1.15. L25. Cryptand with an amido binding site studied as a receptor for aliphatic dicarboxylates 20

Figure 1.16. Isomeric (*orto-, meta- and para*-substitued) macrotricyclic ligands used as receptors for inorganic phosphates 23

Figure 1.17. Bismacrocyclic ligands used as receptors for inorganic phosphates 23

Figure 1.18. Macrocyclic ligands **L33** and **L34**, used as receptors for monophosphate and pyrophosphate 24

Figure 1.19. Most biologically relevant triphosphate mononucleotides 25

Figure 1.20. Receptor **L35** and nucleotide TTP (top). Crystal structure of [(H_4**L35**)(HTTP)] (bottom) 27

Figure 1.21. Geometric isomeric macrocyclic and acyclic receptors studied as receptors for nucleotides 28

Figure 1.22. Macrobicyclic ligand **L40** 28

Figure 1.23. Open polyammonium ligands with an aromatic spacer (pyridyl spacer, X = N, **L41** and *meta* benzyl spacer, X = CH, **L42**) 30

Figure 1.24. Bismacrocyclic ligand with bis-cresol spacer **L43**, studied as a receptor for inorganic phosphates and ATP 30

Figure 1.25. Macocyclic receptor bearing anthracene (**L44**) or pyridyl (**L45**) pendant arms 32

Figure 1.26. Bismacrocyclic systems with a pyridine spacer (**L46**) and with a phenanthroline system (**L47**) 32

Figure 1.27. Macrocyclic ligands with tertiary amines **L34** and **L48** 33

Figure 1.28. XR structure of double stranded DNA containing adduct of Cisplatin 1,2d(GpG) intrastrand crosslink 36

Figure 1.29. Types of hydrophobic non-covalent binding: (A) Intercalation of proflavine between two pairs of adjacent bases of the double helix. (B) DNA minor-groove recognition of a tris-benzimidazole drug 37

Figure 1.30. Summary of hydrolytic cleavage pathway for nucleic acids, promoted by metal complexes 38

Figure 1.31. Generation of reactive oxygen species through molecular oxygen reduction 39

Figure 1.32. Summary of DNA Oxidative Cleavage pathway by hydroxyl radical through Hydrogen (H1′) abstraction of the desoxyribose backbone 39

Figure 1.33. Most relevant RMOS involved in DNA damage, in mono- and dicopper complexes 40

Figure 1.34. Phenanthroline derivative ligands used to study the effect of ligand substitution in copper nuclease models 42

Figure 1.35. Family of macrocyclic ligands, each bearing different heteroatoms 43

Figure 1.36. Mono-, tri- and isomeric dinuclear copper(II) complexes used to study the nucelarity effect by Guo and coworkers. Charges omitted for clarity 44

Figure 1.37. Ditopic macrocyclic ligands with different spacers. **L53** aliphatic spacer° **L54** xylene spacer° **L55** naphthalene spacer 45

Figure 1.38. General drawing of mono- and dinuclear copper(II) complexes of acyclic ligands with different spacers. Charges omitted for clarity 46

Figure 1.39. Polymacrocyclic ligands **L66**, **L67**, **L68**, **L69** 47

Figure 1.40. Dicopper complexes of macrocyclic ligands with different substituents on the aromatic spacer (R, R′ = –Br° –CH$_3$° –C(CH$_3$)$_3$). Charges omitted for clarity 48

Figure 1.41. Macrocyclic ligands with different number of nitro groups in the benzyl pendant arms 49

Figure 2.1. Macrocyclic ligand **L9** and the dicarboxylic substrates 53

Figure 2.2. General structure of the new family of macrocyclic ligands with pendant arms 53

Figure 2.3. General structure of the dicopper(I) complexes of the synthesized macrocyclic ligands with pyridyl pendant arms 54

Figure 4.1.1. Drawing, abbreviations and proton labeling for ligands and substrates discussed in the section 4.1 82

Figure 4.1.2. Species distribution diagram for the **L9** ligand as a function of pH 84

Figure 4.1.3. Species distribution diagram as a function of pH for the **L9**-*ph* (top), **L9**-*is* (middle) and **L9**-*te* (bottom) systems 86

Figure 4.1.4. Log K_i^R versus *n*H (the different ternary species with various degrees of protonation) for the three systems **L9**-*da* 87

Figure 4.1.5. Competitive calculated species distribution diagram and total species distribution diagrams for systems with equimolar amounts of L-S (**L9***, is, ph, te*) 88

Figure 4.1.6. Space fillig (left) and stick (right) views of average calculated structures studied by molecular dynamics for (A) **L9**-*is* (B) **L9**-*ph* and (c) **L9**-*te* systems 92

Figure 4.2.1. General structure for the macrocyclic ligand obtained as a 2+2 condensation between a triamine and isophthalaldehyde 96

Figure 4.2.1. Ball and stick diagrams for the X-ray crystal structure for Cu(I) complexes: (A) $\mathbf{2}^{2+\circ}$ (B) ligand $\mathbf{L74}^{\circ}$ (C) $\mathbf{5}^{3+\circ}$ (D) $\mathbf{4}^{3+\circ}$ (E) $\mathbf{6}^{\mathbf{3}}$ 102

Figure 4.2.3. View of the π−π and CH-π interactions leading to a dimer of trinuclear complexes in the packing structure of $\mathbf{4}(SbF_6)_3$ 104

Figure 4.2.4. ESI-MS spectra obtained for $\mathbf{2}(CF_3SO_3)_2$ (top) and $\mathbf{5}(CF_3SO_3)_3$ (bottom) in CH_3CN 106

Figure 4.3.1. Drawing of the macrocyclic ligands discussed in chapter 4.3 together with the abbreviations and proton labeling 110

Figure 4.3.2. Square Wave Voltammetrys of complexes $\mathbf{7}(CF_3SO_3)_2$, $\mathbf{8}(CF_3SO_3)_2$ and $\mathbf{9}(CF_3SO_3)_2$ 113

Figure 4.3.3. ORTEP plots (80% probability) for the cationic structures of the Cu(I) complexes: $\mathbf{7}^{2+}$ (top), $\mathbf{8}^{2+}$, (middle) and $\mathbf{9}^{2+}$ (bottom) 114

Figure 4.3.4. FT-IR spectroscopy of the CO adducts measured in a CH_2Cl_2 solution of each BARF-complex after bubbling with CO for a couple of minutes 115

Figure 4.3.5. CD Spectra of Calf Thymus DNA incubated with Cu(I) Complexes 116

Figure 4.3.6. Forms adopted by circular plasmid depending on the nicking degree 117

Figure 4.3.7. Summary of the Electrophoretic Mobility of each form of the circular plasmid 118

Figure 4.3.8. Agarose gel EM of pBR322 plasmid DNA treated with Cu(I) compounds 118

Figure 4.3.9. TMAFM images of pBR322 plasmid DNA treated with Cu(I) compounds 121

Figure 4.3.10. TMAFM images of pBR322 plasmid DNA treated with Cu(I) complex **9**................. 122

List of Figures in the Annex

Figure A1.1. ^{1}H-NMR (500 MHz) spectra in D_2O at pD = 5.84 and T = 298 K (A) free **L9** (2 mM)˚ (B) free *is* (2 mM) and (C) **L9**-*is* system (2 mM, 1:1) 149

Figure A1.2. 2D ^{1}H-^{1}H NOESY (500 MHz) spectra of **L9**-*is* system (2 mM, 1:1) in D_2O at pD = 5.84, T = 298 K 150

Figure A1.3. Expansions of the 2D ^{1}H-^{1}H NOESY (500 MHz) spectra of the **L9**-*is* system (2 mM, 1:1) in D_2O at pD = 5.84, T = 298 K 151

Figure A1.4. Diffusion experiments in D_2O at pD = 5.84 and T = 298 K (A) free **L9** (B) free *is* (C) ternary **L9**-*is* system (2 mM, 1:1). 152

Figure A1.5.Spectra of **L9**-*is* systems in D_2O, pD = 5.84, T = 298 K, [**L9**] = 2mM in different **L9**:*is* ratio 155

Figure A1.6. 2D ^{1}H-^{1}H NOESY (500 MHz) spectra of **L9**-*ph* system (2 mM, 1:1) in D_2O at pD = 5.84, T = 298 K 156

Figure A1.7. Expansions of the 2D ^{1}H-^{1}H NOESY (500 MHz) spectra of **L9**-*ph* system (2 mM, 1:1) in D_2O at pD = 5.84, T = 298 K 157

Figure A1.8. 2D ^{1}H-^{1}H NOESY (500 MHz) spectra of **L9**-*te* system (2 mM, 1:1) in D_2O at pD = 5.84, T = 298 K 159

Figure A1.9. Expansions of the 2D ^{1}H-^{1}H NOESY (500 MHz) spectra of **L9**-*te* system (2 mM, 1:1) in D_2O at pD = 5.84, T = 298 K 160

Figure A1.10. Two stick views of 25 overlayed lower energy structures (out of a total of 100) taken from 1 fs dynamic simulation. (A) **L9**-*is*, (B) **L9**-*ph*, and (C) **L9**-*te* systems 161

Figure A2.1. ^{1}H-NMR (400 MHz) spectra (A) and the ^{13}C-NMR (400 MHz) (B) of the compound ftNC$_2$PhOH in $CDCl_3$ 163

Figure A2.2. ^{1}H-NMR (400 MHz) spectra (A) and the ^{13}C-NMR (400 MHz) (B) of the compound H$_2$NC$_2$PhOH spectra in $CDCl_3$ 164

Figure A2.3. ^{1}H-NMR (400 MHz) spectra (A) and the ^{13}C-NMR (400 MHz) (B) of the compound $EtN(CH_2CN)_2$ in $CDCl_3$ 165

Figure A2.4. ^{1}H-NMR (400 MHz) spectra (A) and the ^{13}C-NMR (400 MHz) (B) of the compound ftNC$_2$Et in $CDCl_3$ 166

Figure A2.5. ^{1}H-NMR (400 MHz) spectra (A) and the ^{13}C-NMR (400 MHz) (B) of the compound H$_2$NC$_2$Et in $CDCl_3$ 167

Figure A2.6. ^{1}H-NMR (400 MHz) spectra (A) and the ^{13}C-NMR (400 MHz) (B) of the compound **bsm2py** (**L73**) in $CDCl_3$ 168

Figure A2.7. ^{1}H-NMR (400 MHz) spectra (A) and the ^{13}C-NMR (400 MHz) (B) of the compound **bsm2PhOH** (**L74**) in $CDCl_3$ 169

Figure A2.8. ^{1}H-NMR (400 MHz) spectra (A) and the ^{13}C-NMR (400 MHz) (B) of the compound **bsm2Et** (**L75**) in $CDCl_3$ 170

Figure A2.9. HRMS of the compound **bsm2py** (**L73**) 171

Figure A2.10. HRMS of the compound **bsm2PhOH** (**L74**). 171

Figure A2.11. HRMS of the compound **bsm2Et** (**L75**) 171

Figure A2.12. ^{1}H-NMR (400 MHz) spectra in CD_3COCD_3 of the complex $[Cu_2($**L73**$)](SbF_6)_2$, **1**$(SbF_6)_2$ and $[Cu_3($**L76**$)](SbF_6)_3$, **4**$(SbF6)_3$ 172

Figure A2.13. ^{1}H-NMR (400 MHz) spectra in CD_3COCD_3 of the complex $[Cu_2($**L74**$)](OTf)_2$, **2**$(OTf)_2$ and $[Cu_3($**L77**$)](OTf)_3$, **5**$(OTf)_3$ 172

Figure A2.14. ^{1}H-NMR (400 MHz) spectra in CD_3COCD_3 of the complex $[Cu_3($**L78**$)](OTf)_3$, **6**$(OTf)_3$ 173

Figure A3.1. ^{1}H-NMR (200 MHz) spectra in $CDCl_3$ (A) and FT-IR spectra (B) of the compound $ftNC_3H$ 174

Figure A3.2. ^{1}H-NMR (200 MHz) spectra in $CDCl_3$ (A) and FT-IR spectra (B) of the compound ftNC3py 175

Figure A3.3. ^{1}H-NMR (200 MHz) spectra in $CDCl_3$ (A) and FT-IR spectra (B) of the compound H_2NC_3py 176

Figure A3.4. ^{1}H-NMR (200 MHz) spectra in $CDCl_3$ (A) and FT-IR spectra (B) of the compound $ftNC_2H$ 177

Figure A3.5. ^{1}H-NMR (200 MHz) spectra in $CDCl_3$ (A) and FT-IR spectra (B) of the compound $ftNC_2py$ 178

Figure A3.6. ^{1}H-NMR (200 MHz) spectra in $CDCl_3$ (A) and FT-IR spectra (B) of the compound H_2NC_2py 179

Figure A3.7. ^{1}H-NMR (200 MHz) spectra in $CDCl_3$ FT-IR spectra (B) and ESI-MS spectra (C) of the compound **bsp3py** (**L79**) 180

Figure A3.8. ^{1}H-NMR (200 MHz) spectra in $CDCl_3$ FT-IR spectra (B) and ESI-MS spectra (C) of the compound **bsm3py** (**L80**) 182

Figure A3.9. ^{1}H-NMR (200 MHz) spectra in $CDCl_3$ (A), FT-IR spectra (B) and ESI-MS spectra (C) of the compound **bsp2py** (**L81**) 184

Figure A3.10. ^{1}H-NMR (400 MHz) spectra in D_2O:d_6-DMSO (4:1) (A), ^{13}C-NMR (100 MHz) spectra in d_6-DMSO (B) and ESI-MS spectra (C) of the compound **7**$(CF_3SO_3)_2$ 186

Figure A3.11. ^{1}H-NMR (400 MHz) spectra in d_6-DMSO (A), ^{1}H-NMR (400 MHz) spectra in D_2O:d_6-DMSO (4:1) (B), ^{13}C-NMR (100 MHz) spectra in d_6-DMSO (C) of the compound **8**(CF_3SO_3)$_2$........187

Figure A3.12. ^{1}H-NMR (400 MHz) spectra in D_2O:d_6-DMSO (4:1) (A), ^{13}C-NMR (100 MHz) spectra in d_6-DMSO (B) and ESI-MS spectra (C) of the compound **9**(CF_3SO_3)$_2$........189

Figure A3.13. ^{1}H-NMR (200 MHz) spectra in CD_3CN of the compound **7**(BArF)$_2$........ 190

Figure A3.14. ^{1}H-NMR (200 MHz) spectra in CD_2Cl_2 A) and ESI-MS spectra (B) of the compound **8**(BArF)$_2$........ 191

Figure A3.15. ^{1}H-NMR (200 MHz) spectra in CD_2Cl_2 (A), ^{1}H-NMR (200 MHz) spectra in CD_3CN (B) of the compound **9**(BArF)$_2$........ 192

Figure A3.16. Agarose Gel Electrophoretic Mobility of pBR322 plasmid DNA........ 193

Figure A3.17. Agarose Gel Electrophoretic Mobility of pBR322 plasmid DNA treated with Cu(I) Compounds under nitrogen atmosphere........193

Abstract

Macrocyclic ligands have been used in a wide variety of fields such as anion recognition or coordinated to metal ions as biomimetic systems. In this context, the behaviour of different polyazamacrocyclic compounds in different conditions is reported in this thesis, paying special attention on how small variations of the ligand lead to different behaviour of the compound.

On one hand, it is reported the host-guest interaction of the hexaazamacrocyclic ligand **L9** towards three different aromatic dicarboxylic acids, varying in the relative disposition of the acid groups: terephthalic acid (*te*), isophthalic acid (*is*) and phthalic acid (*ph*). The interaction between the receptor and the substrates has been studied by means of potentiometric titrations, HRMN studies and computational calculations. It has been observed that the strength of the L-S interaction increases with the order **L9**:*is* > **L9**:*ph* > **L9**:*te*. This is in contrast with the behaviour of the similar ligand **L12** with these substrates, as it is presented in the literature. Indeed, the methylation of the central amines of the ligand lead to a decrease and to a change of the order of the selectivity for the substrates, being the most stable the complex of the **L12** receptor, the complex with the terephthalic acid **L12**:*te*.

On the other hand, it has been synthesised a new family of imine macrocyclic ligands with pyridyl pendant arms, through a 2+2 condensation of an aromatic dialdehyde and a pendant arm triamine. The ligands of the family differ in the geometry of the aromatic spacer (*meta* or *para*) as well as in the length of the aliphatic spacers (two or three methylenes).

Within this family, the macrocyclic ligand with meta geometry and spacer of 2 methylenic units (**bsm2py**) undergoes a ring expansion when complexed with Cu(I) in acetonitrile solution, obtaining the trinuclear complex of the 3+3 ligand, in contrast with the other three pendant arm imine macrocyclic ligands of the family (**bsp3py**, **bsm3py** and **bsp2py**), which do not perform any ligand expansion in presence of Cu(I). In order to study this backbone rearrangement, two analogous ligands to **bsm2py** but with different pendant arms have been synthesised, one bearing a phenol group (**bsm2phOH**) and another bearing an ethyl group (**bsm2Et**), all of them undergo ring expansion when complexed with Cu(I) in acetonitrile, as shown by mass studies and X-ray structures of the obtained complexes. The ligand rearrangement of these ligands with pendant arms (**bsm2py**, **bsm2phOH** and **bsm2Et**) is in sharp contrast with the analogous imine macrocyclic ligand without pendant arms **bsM2** described in the literature, which does not undergo any ligand rearrangement when complexed with Cu(I).

The dinuclear Cu(I) complexes with the ligands **bsp3py, bsm3py** and **bsp2py** have been synthesized and fully characterized, and their nuclease activity has been studied by means of Electrophoresis Mobility in Agarose Gel, Circular Dichroism spectroscopy and Atomic Force Microscopy. All complexes interact with DNA and produce nicking in presence of H_2O_2, clearly being the complex with the ligand **bsp2py** the one with less activity. The interaction mode of the complexes with DNA is non intercalative in all three cases as evidenced by CD spectroscopy. In absence of H_2O_2 the order of the complexes interaction with DNA is [Cu$_2$(**bsp3py**)]$^{2+}$ > [Cu$_2$(**bsm3py**)]$^{2+}$ > [Cu$_2$(**bsp2py**)]$^{2+}$, while with H_2O_2, the nuclease activity of the complexes follows the order [Cu$_2$(**bsm3py**)]$^{2+}$ > [Cu$_2$(**bsp3py**)]$^{2+}$ > [Cu$_2$(**bsp2py**)]$^{2+}$. The difference in reactivity among the complexes can be associated with the properties of the products, both electronic and geometric.

Resumen

Ligandos de tipo macrociclo se han usado en una gran variedad de campos como reconocimiento de aniones o coordinados a metales como sistemas biomiméticos. En este contexto, en esta tesis se presenta el comportamiento de diferentes compuestos poliazamacrocíclicos en diferentes condiciones, poniendo especial atención a como pequeñas variaciones en el ligando llevan a diferentes comportamientos de los complejos.

Por una parte se reporta la interacción entre receptor y substrato cuando el receptor es el ligando hexaaza macrocíclico **L9** y los substratos tres ácidos dicarboxílicos diferentes: el ácido tereftálico (*te*), el ácido isoftálico (*is*) y el ácido ftálico (*ph*). La interacción entre el receptor y los substratos se ha estudiado a través de valoraciones potenciométricas, estudios de HRMN y cálculos computacionales. Se ha observado que la fuerza de la interacción L-S aumenta en el orden **L9**:*is* > **L9**:*ph* > **L9**:*te*. Estos datos contrastan con el comportamiento del ligando similar **L12** con estos substratos, tal y como se presenta en la bibliografía. Así, la metilación de las aminas centrales del ligando inducen una disminución de la selectividad, así como un cambio en el orden de la misma respeto los tres substratos, siendo en este caso el complejo más estable del ligando **L12** el que forma con el ácido tereftálico **L12**:*te*.

Por otro lado se ha sintetizado una nueva família de ligandos macrocíclicos con funciones tipo imina, con brazos laterales tipo piridilo. La síntesis se ha llevado a cabo a través de una reacción de condensación 2+2 entre un dialdehido aromático y una triamina que presenta un brazo lateral. Los cuatro ligandos difieren en la geometría del espaciador aromático (*meta* o *para*) y también en la longitud de los espaciadores alifáticos (dos o tres metilenos).

Dentro de esta família, el ligando con geometría *meta* y dos metilenos entre aminas (**bsm2py**) experimenta una expansión del anillo cuando se compleja con Cu(I) en solución de acetonitrilo, obteniendo el complejo trinuclear del ligando 3+3. Esto contrasta con los otros tres ligandos de la família (**bsp3py**, **bsm3py** y **bsp2py**), que no padecen ninguna expansión del anillo en presencia de Cu(I). Para estudiar esta reorganización se han sintetizado dos ligandos análogos al **bsm2py** pero con diferentes brazos laterales˚ uno con un grupo fenólico (**bsm2phOH**) y otro con un grupo etil (**bsm2Et**). Todos ellos experimentan una expansión del anillo cuando se complejan con Cu(I) en acetonitrilo, como se demuestra por las estructuras obtenidas por difracción de rayos X así como los estudios de espectrometría de masas. Esta reorganización de estos ligandos con brazos laterales (**bsm2py**, **bsm2phOH** y **bsm2Et**) contrasta con el ligando imínico análogo sin brazos laterales bsM2 descrito en la bibliografía, que no experimenta ninguna expansión cuando se compleja a Cu(I).

Se han sintetizado y caracterizado los complejos dinucleares de Cu(I) con los ligandos **bsp3py, bsm3py** y **bsp2py**, y se ha estudiado su actividad nucleasa a través de estudios de movilidad electroforética en gel de agarosa, dicroísmo circular, y microscopía de fuerza atómica. Todos los complejos interaccionan con el ADN y le producen escisiones en presencia de H_2O_2, siendo claramente el complejo **bsp2py** el que presenta una menor actividad. La interacción de estos complejos con el ADN es de tipo no intercalativo en los tres casos, como evidencian los resultados de la espectroscopia de dicroísmo circular. En ausencia de H_2O_2, el orden de la intensidad de interacción con el ADN sigue el orden $[\mathrm{Cu}_2(\mathbf{bsp3py})]^{2+}$ > $[\mathrm{Cu}_2(\mathbf{bsm3py})]^{2+}$ > $[\mathrm{Cu}_2(\mathbf{bsp2py})]^{2+}$, mientras que en presencia de H_2O_2 la actividad nucleasa sigue el orden $[\mathrm{Cu}_2(\mathbf{bsm3py})]^{2+}$ > $[\mathrm{Cu}_2(\mathbf{bsp3py})]^{2+}$ > $[\mathrm{Cu}_2(\mathbf{bsp2py})]^{2+}$. La diferencia en la reactividad de los complejos se puede asociar con las propiedades de los compuestos, tanto electrónicas como geométricas.

Resum

Lligands de tipus macrocíclic s'han usat en una àmplia varietat de camps, tals com reconeixement d'anions o, coordinats a metalls, com a sistemes biomimètics. En aquest context, en aquesta tesi es presenta el comportament de diferents compostos poliazamacrocíclics en diferents condicions, posant especial atenció en com les petites diferències entre lligands comporten diferents comportaments dels compostos.

Per una part, es presenta la interacció entre receptor i substrat quan el receptor és el lligand hexaazamacrocíclic **L9** i els substrats són tres àcids dicarboxílics diferents: l'àcid tereftàlic (*te*), l'àcid isoftàlic (*is*) i l'àcid ftàlic (*ph*). La interacció entre receptor i substrats s'ha estudiat a través de valoracions potenciomètriques, estudis de H-RMN i càlculs computacionals. S'ha observat que la intensitat de la interacció L-S augmenta amb l'ordre **L9**:*is* > **L9**:*ph* > **L9**:*te*. Aquestes dades contrasten amb el comportament del lligand similar **L12** amb aquests substrats, tal i com es presenta a la bibliografia. Així, la metilació de les amines centrals del lligand indueixen una disminució en la selectivitat del receptor respecte dels substrats, així com un canvi d'ordre en aquesta. En aquest cas, el complex més estable és el format pel lligand **L12** i l'àcid tereftàlic, **L12**:*te.*

Per altra banda s'ha sintetitzat una nova família de lligands macrocíclics amb funcions tipus imina amb braços laterals tipus piridil. La síntesi s'ha dut a terme a través d'una reacció de condensació 2+2 entre un dialdehid i una triamina funcionalitzada amb el braç lateral. Els quatre lligands (**bsp3py**, **bsm3py**, **bsp2py** i **bsm2py**) difereixen en la geometria de l'espaiador aromàtic (*meta* o *para*) i també en la longitud de l'espaiador alifàtic (dos o tres metilens).

Dins d'aquesta família, el lligand sintetitzat amb geometria *meta* i dos metilens entre les amines de l'espaiador alifàtic **bsm2py** presenta una expansió de l'anell macrocíclic quan es complexa al Cu(I) en solució d'acetonitril, obtenint el complex trinuclear 3+3. Aquest fet contrasta amb els altres tres lligands de la família, que no experimenten cap expansió del lligand en presència de Cu(I). Per tal d'estudiar aquest comportament s'han sintetitzat dos lligands macrocíclics anàlegs al bs**m2py** però amb diferents braços laterals: un amb un braç de tipus fenol (**bsm2phOH**) i un altre amb un etil (**bsm2Et**). Tots ells experimenten una expansió de l'anell macrocíclic quan són complexats a Cu(I) en solució d'acetonitril, tal i com demostres les estructures obtingudes per difracció de raigs X així com també els estudis d'espectrometria de masses. Aquesta reorganització d'aquests lligands amb braços laterals (**bsm2py**, **bsm2phOH** i **bsm2Et**) contrasta amb el lligand anàleg sense braç lateral **bsM2** descrit a la bibliografia, que no presenta cap expansió al ser complexat amb Cu(I).

S'han sintetitzat i caracteritzat els complexos dinuclears de Cu(I) amb els lligands **bsp3py**, **bsm3py** i **bsp2py**, i s'ha estudiat l'activitat nucleasa a través d'estudis de mobilitat electroforètica en gel d'agarosa, dicroisme circular i microscòpia de força atòmica. Tots els complexos interaccionen amb el ADN i produeixen escissions en presència de H_2O_2,essent el complex amb el lligand **bsp2py** clarament el que té menys activitat. La interacció d'aquests complexos amb l'ADN és de tipus no intercalatiu en els tres casos, com s'evidencia per espectroscòpia de dicroisme circular. En absència de H_2O_2, l'ordre de la intensitat de la interacció amb l'ADN segueix l'ordre [Cu_2(**bsp3py**)]$^{2+}$ > [Cu_2(**bsm3py**)]$^{2+}$ > [Cu_2(**bsp2py**)]$^{2+}$,. Mentre que en presència de H_2O_2, l'activitat nucleasa segueix l'ordre [Cu_2(**bsm3py**)]$^{2+}$ > [Cu_2(**bsp3py**)]$^{2+}$ > [Cu_2(**bsp2py**)]$^{2+}$. La diferència en la reactivitat d'aquests complexos es pot relacionar amb les seves propietats, tant electròniques com geomètriques.

1. Introduction

1.1. Bioinorganic chemistry.

Bioinorganic chemistry is the discipline present at the interphase between biochemistry and inorganic chemistry. It deals with the role of metal ions or inorganic compounds in biological systems. These inorganic compounds can be metal ions (such as K^+, Ca^{2+} or Fe), coordination compounds (like cisplatin) or other inorganic molecules (such as PO_4^{3-}, CO, O_2).[1–4]

The major components of bioinorganic chemistry are (i) the study of the metallic active sites in metalloenzymes, and (ii) the study of the interactions between metal ions or inorganic compounds and biomolecules.

Metalloenzymes are enzymes which require a metallic atom in order to carry out their catalytic roles. One of the goals of bioinorganic chemistry is the synthesis and characterization of robust low molecular weight chemical models capable of reproducing and mimicking the reactive and spectroscopic properties of these biological centres.

The study of the interactions between metal ions or inorganic compounds and biomolecules, is the other main objective of the bioinorganic chemistry, either to study their toxicity mechanisms, or to develop new inorganic drugs. These subject of study include a wide range of interactions, such as the coordination of the metallic center of a metalloprotein to their substrate° the selective recognition phenomena of ions through ion channels or in phosphate binding proteins° or the binding of inorganic compounds to biological systems.

One of the most successful inorganic drugs is cisplatin, a coordination compound used in the treatment of several type of cancers. It is a platinum complex capable of binding DNA and interfering with its replication. The hindrance of DNA replication induces programmed cell death. This process affects the most to the fastest proliferating cells, which in theory are carcinogenic, thus killing them.[5]

Furthermore, new inorganic chemistry can be learned and developed through the study of biological systems.[6,7]

1.2. Macrocycle chemistry.

The chemistry of macrocyclic ligands and their complexes have attracted the interest of both inorganic and bioinorganic chemists in recent years due their unique structural and functional properties and biological activities. Indeed, the versatility of macrocyclic ligands and their complexes has been proven in many fields, such as molecular and ion recognition, catalysis, and bioinorganic chemistry to mimic the structure and function of metalloproteins, as well as biology and medicine, and in processes which require extreme kinetic and thermodynamic stability toward metal release.[8–20]

In this context, there is a particular interest in the preparation and characterization of coordination compounds with aza-macrocyclic ligands with pendant substituents. The complexation properties of polyaza-macrocycles are governed mainly by the macrocyclic ring size, but *N*-Functionalization of these macrocycles may enhance their metal-ion selectivity and the stability of metal complexes depending on the coordination properties of the pendant arms.[21]

Macrocyclic ligands have been especially used in the field of supramolecular chemistry.
The discovery of synthetic macrocyclic molecules which form stable metal complexes was a fundamental stage in the start of modern supramolecular chemistry, since the pioneering work of Pedersen and Lehn in the late 1960s. They observed a great increase in the stability of the complexes with macrocyclic ligands when compared to the complexes with analogue but acyclic ligands. They called this phenomenon the “macrocyclic effect”.[22–25]

Indeed, nature chooses macrocyclic derivatives which give enhanced kinetic and thermodynamic stabilities, such that the metal ion is very firmly held in the central cavity of the ligand, so the biological function is not impaired by competing demetallation processes. For example, the porphyrin ring of the iron-containing haem proteins, the related (partially reduced) chlorin complex of magnesium in chlorophyll, or the corrin ring of vitamin B 12. Also, naturally occurring cyclic peptides like Valinomicyn are capable of binding and transporting metal atoms across membranes.[26]

On the other hand, the effectiveness of ions in promoting cyclization reactions via the ‘‘template reaction’’ procedure contributed to keep up the interest towards metals in supramolecular chemistry while supramolecular chemistry was facing its spectacular spreading.[19,27]
Schiff base (imine) macrocycles are a family of ligands which have been extensively used in many fields. [10–12,20,28–34]

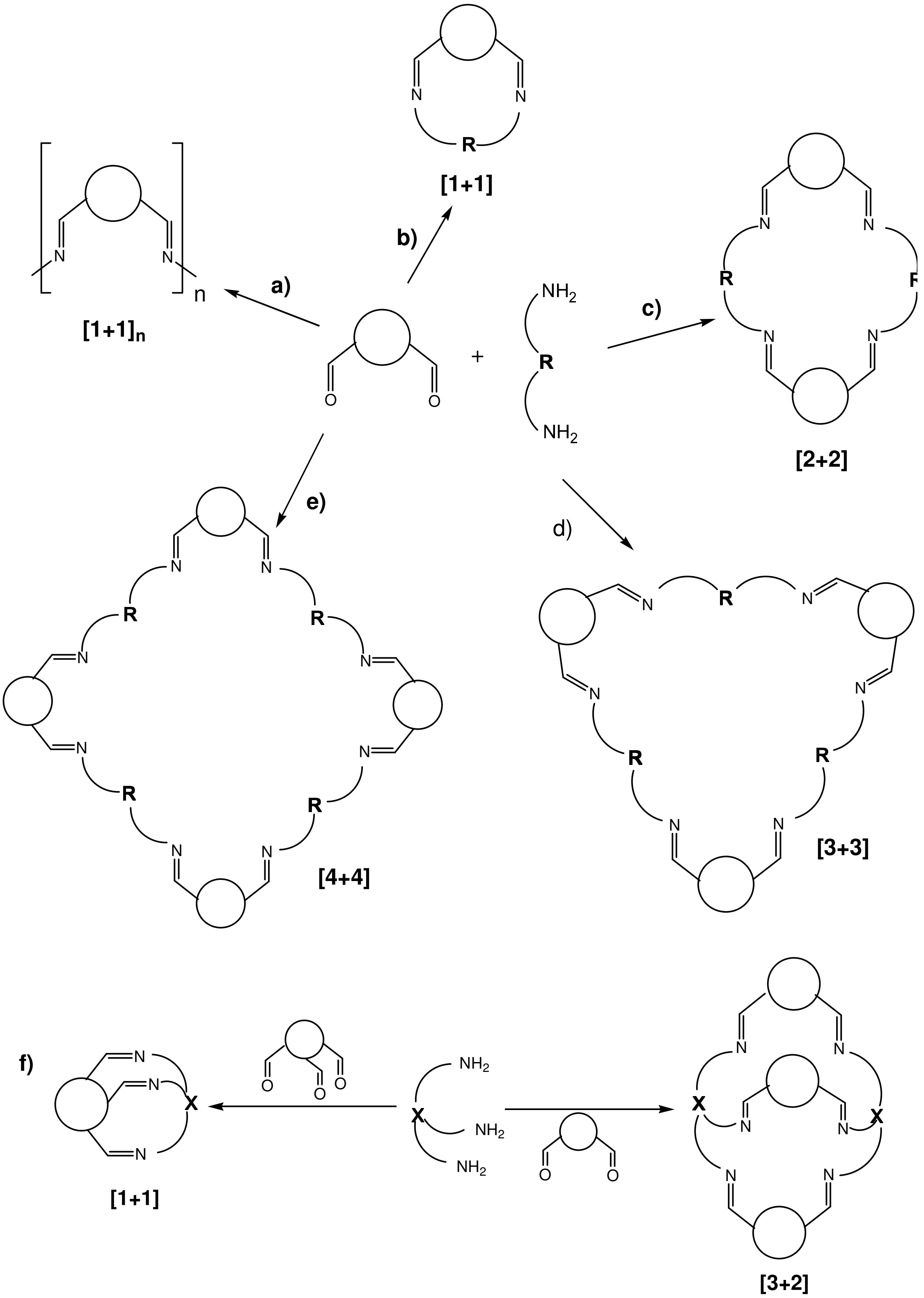

Scheme 1.1. Synthetic pathways of [1+1] polymeric (a), cyclic [1+1] (b), [2+2] (c), [3+3] (d) or [4+4] (e) and macrobicyclic Schiff base derivatives (f).

One of the most extended synthetic pathways to obtain symmetric imine macrocycles is a simple one-pot self-condensation of formyl- or keto- and primary amine precursors. Multiple self-condensations processes lead to planar or tridimensionals compounds in one step. So, the size and shape of the cavity, as well as other properties of the ligand can be tuned by choosing different formyl- and amine precursors.

Depending on the shape and properties of the formyl- and amine precursors (*linkers*), and/or the metal ion used as templating agent, different ring sizes can be formed during the cyclization reaction (*Scheme 1.1*).

If one dicarbonyl moiety reacts with one diamine moiety a [1+1] macrocycle results˚ when two dicarbonyl precursors react with two diamines then a [2+2] macrocycle results, and so on. This synthetic procedure may form [3+3] or [4+4] superior macrocyclic homologues, or can lead to [1+1] polymeric species.

Similarly one tricarbonyl precursor reacts with a tripodal triamine to form a [1+1] macrobicyclic compound while three dicarbonyl precursors react with two tripodal amines to form [3+2] macrobicyclic compounds.

These imine macrocycles can be further modified by different methods, for example by inserting appropriate groups in the aliphatic or aromatic chains, or also by reducing the imine groups to the related amines. In turn, these NH groups can also be functionalized, giving rise to a wide variety of macrocycles.

In general, amine ligands are more robust than their imine analogs, in reproducibility and stability. Amines do not suffer hydrolytic processes encountered with the Schiff base analogues˚ they show also a higher flexibility while maintaining the capacity to form complexes with transition metal ions. Nonetheless, the secondary amines can also undergo some reactions with metal ions, such as oxidative dehydrogenation of the NH-CH bound to give back the imine.[35]

This cyclation reaction can also be carried out through template procedures, with the aid of a metal, obtaining directly the metal complex. Sometimes this template synthesis is the easiest, or even the only way to obtain a certain macrocyclic ligand. In many occasions, the direct reaction between the carbonyl and amine precursors lead to oligomeric, non-macrocyclic species, but adding a specific metal allows the isolation of the macrocyclic complex.[11,28,36,37]

For example, the macrocyclic ligand **L1** (*Figure 1.1)* can only be obtained through template synthesis with Ba^{2+}. Direct, not template synthesis, or template procedure with Pb cations does not lead to any clean reaction product.[38]

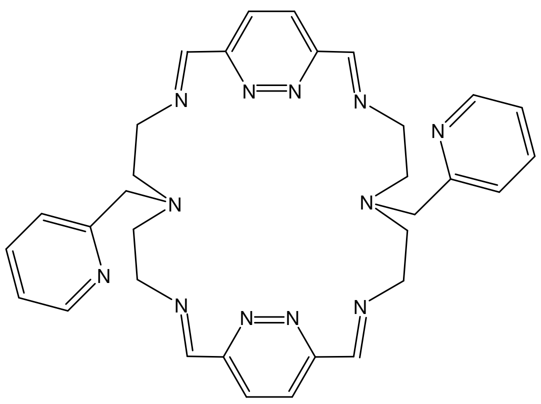

Figure 1.1. Ligand **L1** obtained through barium templation.[38]

Actually, the presence of a metal can also determine the formation of one or another macrocycle, or even reorganize an already obtained macrocyclic complex.[39–55] So, the Schiff base condensation to form the corresponding macrocycle can, in some occasions, be controlled to yield one or another macrocyclic ligand. For example, the formation of a [2+2] or [4+4] macrocycle, or a acyclic part can depend on the solvent, temperature, anion or stochiometry of the template agent.[11,56–60]

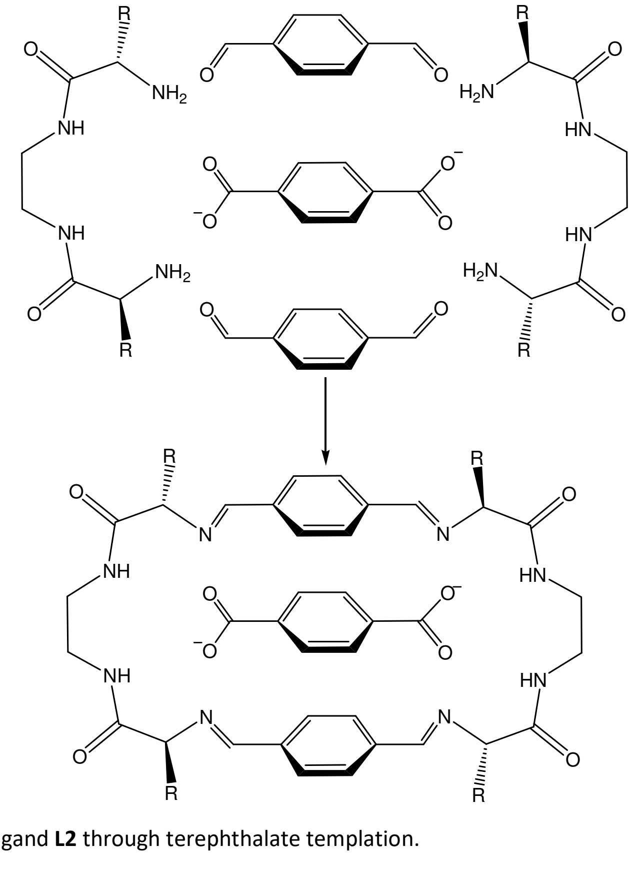

Figure 1.2. Synthesis of ligand **L2** through terephthalate templation.

On the other hand, the template synthesis can also be carried out with anionic substances as templating agents.[61–63] As an example, the reaction between the diamine and the dialdehyde without template affords only oligomeric species. But when an aromatic dicarboxylate was added, the [2+2] macrocycle L2 was obtained (*Figure 1.2*).

Another example comes from the cyclation reaction between the diamine **R1.1** and the diformylbipyrrole **R1.2.** [64] It is an acid catalysed cyclization, but the obtained product depends on the anion of the acid, which acts as a template agent. When HBr, HCl or HNO_3 were used, only oligomers of high molecular weight are obtained. When acetic, trifluoroacetic, and phosphoric acids led to the formation of the [2+2] macrocycle **L3** but contaminated with high quantities of oligomers. Finally, the use of sulfuric acid produced the [2+2] macrocycle **L3**, nearly free of other side products.

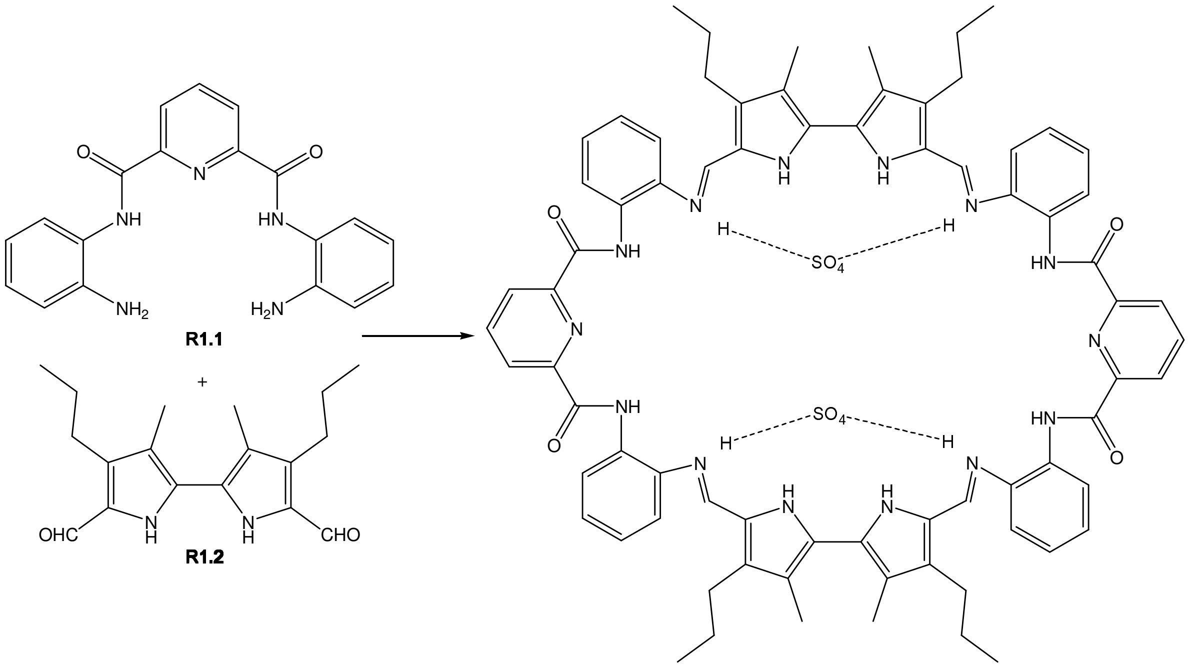

Figure 1.3. Synthesis of ligand **L3** through sulphate templation.

This behavior is related to the supramolecular interactions between the macrocyclic product and the templating agent, in this case, the sulphate recognition by the protonated macrocyclic complex, as a recognition and interaction between reacting groups and template agent must exist so that the cyclisation reaction is carried out. Indeed, in this case, interaction studies have shown sulphate anion to be the best guest for the ligand, with the highest complexation constant. On the other hand, the anions whose acids did not perform this cyclation reaction, were found to not to effectively interact with the macrocyclic product.[64,65]

1.3. Supramolecular Chemistry.

Supramolecular chemistry can be defined as “chemistry beyond the molecule”. In contrast to molecular chemistry, which focuses on covalent bonding, supramolecular chemistry focuses on the study of structures and functions of the supermolecules resulting from the union of a substrate with its molecular receptor. [66–68]

The term supermolecule is related to highly complex entities resulting from the association of two or more chemical species through intermolecular forces.[68] The interval of this forces ranges from weak bonds such as hydrogen bonding to strong bonds such as metal ions coordination.

Intermolecular interactions are the basis of highly specific processes of recognition, transport, regulation etc. that take place at biological level, such as the union of a substrate to a proteic receptor, enzymatic reactions, or transcription and replication of the genetic code. [67]

The specific union of a substrate and a receptor with the corresponding formation of a supermolecule implies a molecular recognition process. If the receptor is also able of performing a chemical reaction, it can carry out a chemical transformation on the substrate, as a catalyst.

For a receptor to recognize and associate to a substrate, it is necessary a complementarity in terms of size and geometry of the binding sites, and also in terms of chemical functions.

The supramolecular species are characterised by the spatial arrangement of their components, their architecture and the nature of their intermolecular bonds. They have well defined structural, thermodynamic, kinetic and dynamic characteristics. Given that the intermolecular forces are in general weaker than covalent bonds, the supramolecular species are thermodynamically less stable, kinetically more labile and dynamically more flexible than the molecules. [66–68]

1.3.1. Molecular receptors.

A molecular receptor can be defined as an organic structure, formed by covalent bonds, which is capable of selectively binding molecular or ionic substrates through intermolecular interactions, forming a supermolecule.[18]

For an effective molecular recognition the receptor must be able to interact with the substrate through non-covalent bonds, and to wrap it with a match of size and shape. Thus, artificial receptors must have a cavity big enough for the substrate to fit in, and also they must have a balance between rigidity and flexibility in order to interact better.

The phenomena determining the affinities are: i) size and shape of substrate and receptor. ii) Chemical complementarity between substrate and receptor, and iii) many different interacting sites.[25]

Monotopic receptor is the term used to refer to the receptors which have a single receptor unity, so, which is capable of binding a single substrate. Those receptors capable of binding more than one receptor unit are called politopic receptors.

The aim of the molecular recognition studies is to prepare molecules that are able to selectively bind complementary species through intermolecular forces, forming a supermolecule.

It is at a biological level where molecular recognition is more complex, with reaction, transport, regulation and union processes with a high level of selectivity. These natural processes, of which we attempt to understand the basic principles, will be the inspiration of the receptor model systems.

1.3.2. Supramolecular chemistry of anions.

Anions have a great relevance from a biological point of view since over 70% of all cofactors and substrates involved in biologic processes are of anionic nature.[69]

From the biological point of view, these studies and applications require aqueous conditions. Still, most of the examples of synthetic selective anion receptors work on organic media, or in an organic-aqueous mixture. Indeed, water itself is a highly competitive polar solvent, able to hydrate the host and the guest through hydrogen bond donation and acceptance. This solvatation hinders even more the interaction host-guest.[62]

Anions present characteristic properties that have to be taken into account in order to prepare adequate receptors. First, anions are large when compared with metal ions. This leads to weaker electrostatic interactions with a positively charged host. The second aspect concerns the variety of shapes that anions have covering spherical, triangular, tetrahedral, square planar, octahedral or even more complex shapes that biologically relevant species adopt, like polycarboxylates, nucleotides and dinucleotides, and they also display a much greater range of

hydrophilicity/hydrophobicity.[70] Another obvious characteristic is that often the existence of an anion lies within a limited pH range, when they are conjugated bases of protic acids, being able in many occasions of exhibiting multiple protonation equilibria. Finally, anions are coordinatively saturated species, so electrostatic interactions, or more or less weak intermolecular forces like hydrogen-bonding, π-π -stacking or hydrophobic effects can be used for their recognition.
Although electrostatic attraction is the main driving force for adduct formation, sometimes other of the above mentioned forces can be the driving force for the formation of the adduct.[71]

In this context, one of the most used families of compounds used in anion recognition in aqueous media have been polyammonium species.
From the work of Kimura and Lehn in the early 80s[68,72] about the interactions between nucleotides and macrocyclic polyamines, these macrocyclic systems has been extensively studied as receptors for anionic molecules, as they bind to a great variety of anionic species through electrostatic forces and hydrogen bonding between the positively charged ammonium groups and the corresponding anionic substrate.
In these charged polyaza receptors the recognition commonly takes place through a combination of coulombic and hydrogen bond interactions. Nevertheless, an important drawback of these systems is the pH- sensitivity. Indeed, this type of receptors in aqueous solution evolves into species with different protonation degrees, which can interact with anionic species. The stability of the corresponding complexes will be defined by electrostatic and hydrogen bonding interactions. In consequence, the formation of these species will depend on the pH of the aqueous solution.
Within this family of polyammonium systems, polyazamacrocycles have been extensively studied in the literature as anion receptors.[12,25]

1.3.3. Carboxilate anions Recognition.

Dicarboxylic species such as malonate, succinate, fumarate, malate, glutamate, etc, are of special relevance as they are widely spread in living systems, taking part in several metabolic processes, and also being related to some diseases.[73–76] Moreover, some polycarboxylates are used in different industries, such as food additives, in cosmetics or pharmaceutical industries, or in the production of plastics.[76,77]

All these examples exemplify the relevance of dicarboxylic species as analytical targets to be detected. In this context, the design of synthetic receptors for the selective targeting of dicarboxylate and polycarboxylate anions has constituted a preferential goal in host–guest chemistry and even nowadays still persists.[25,78–80]

Two common approaches have been used in the design of synthetic receptors for carboxylate binding in aqueous solution: the incorporation of polyammonium groups and of metal cations acting as Lewis acid centres. Thus polyamine groups have been included in macrocyclic and macrobicyclic architectures to be used in the protonated form for the direct interaction with anions, or in the neutral form for the coordination to metal ions.[17,71,81–85]

The polytopic nature of the dicarboxylic species requires special attention in the design of receptors – they should include several interacting sites, which should be able to be adequately oriented and to operate in a cooperative way in order to selectively bind one substrate, and distinguishing it from other structurally and chemically similar species.

The use of ammonium salts to create carboxylate receptors began with studies on polyammonium salts derived form polyaminic macrocycles, as exemplified by the work of Kimura and Lehn.[72,83,86,87] They synthesized a series of macrocyclic species (*Figure 1.4*), with different number of amino groups and different spacers and sizes, and studied the interaction of these species and their protonated derivatives towards different anions, including mono- and polycarboxylates. They observed that the main driving forces for the host-guest binding were electrostatic interactions, but there was also a selectivity of the receptors for the substrates whose chain length complemented the size of the cavity: the smallest macrocycles (**L4** and **L5**) had preference for the smallest dicarboxylates such as oxalate, but when moving to bigger, ditopic receptors (**L6)**, the receptors were able to bind longer chain dicarboxylates such as glutarate or pimelate, depending on the size of the macrocycle.

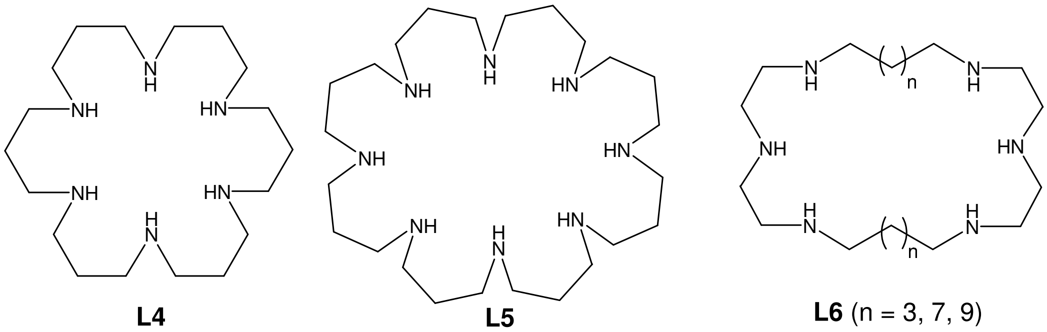

L4 **L5** **L6** (n = 3, 7, 9)

Figure 1.4. Macrocyclic polyaminic species studied as receptors for dicarboxilates by Kimura and Lehn.

Martell and coworkers synthesized later a macrocycle with furan aromatic spacers, **L7**.[60] It was found to bind oxalate, malonate and pyrophosphate in water, but oxalate displayed a better interaction than other anions due to a good structural match with the cavity of the macrocyclic receptor.

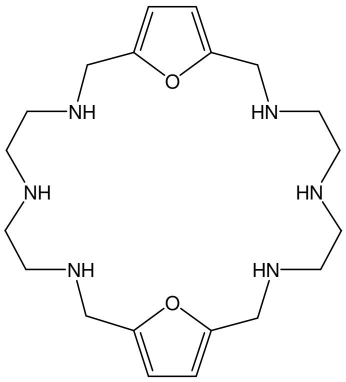

Figure 1.5. Ditopic macrocycle **L7** synthesized by Martell's group.

Analogous ditopic macrocycles with benzene units as spacers have also been synthesized and their protonated ammonium salts evaluated as receptors for diacids. [88] Four different macrocycles have been described, differing in the aromating substitution (*meta* or *para*) and also in the number of methylenic units linking the secondary amines (2 or 3) (see *Figure 1.6*). These differences induce electronic differences in each macrocycle as well as in the size and shape of the cavity. All of them have been evaluated as receptors towards oxalic acid (small and rigid diacid) and oxydiacetic acid (larger and more flexible diacid).

It has been observed that the receptors with two methylenic units between amines (**L8** and **L10**, the two ligands with smallest cavities) have a similar affinity for oxalate, meaning that the shape of the cavity does not affect the strength of the binding, only the size.

On the other hand, the bigger cavity of the other receptors produces a much poorer fit with the substrate and in consequence a decrease in recognition.

A variation of these macrocyclic receptors, with the central amine methylated (**L12**, *Figure 1.7*), was evaluated as receptor for aliphatic and aromatic dicarboxylates of different sizes and geometries.[89] The experiments and simulations showed that this receptor had a clear preference for terephthalate over isophthalate and phthalate aromatic dicarboxylates, as the therephthalate can be included inside the cavity of the receptor and stabilized through electrostatic interactions, hydrogen bonding and π-π stacking forces.

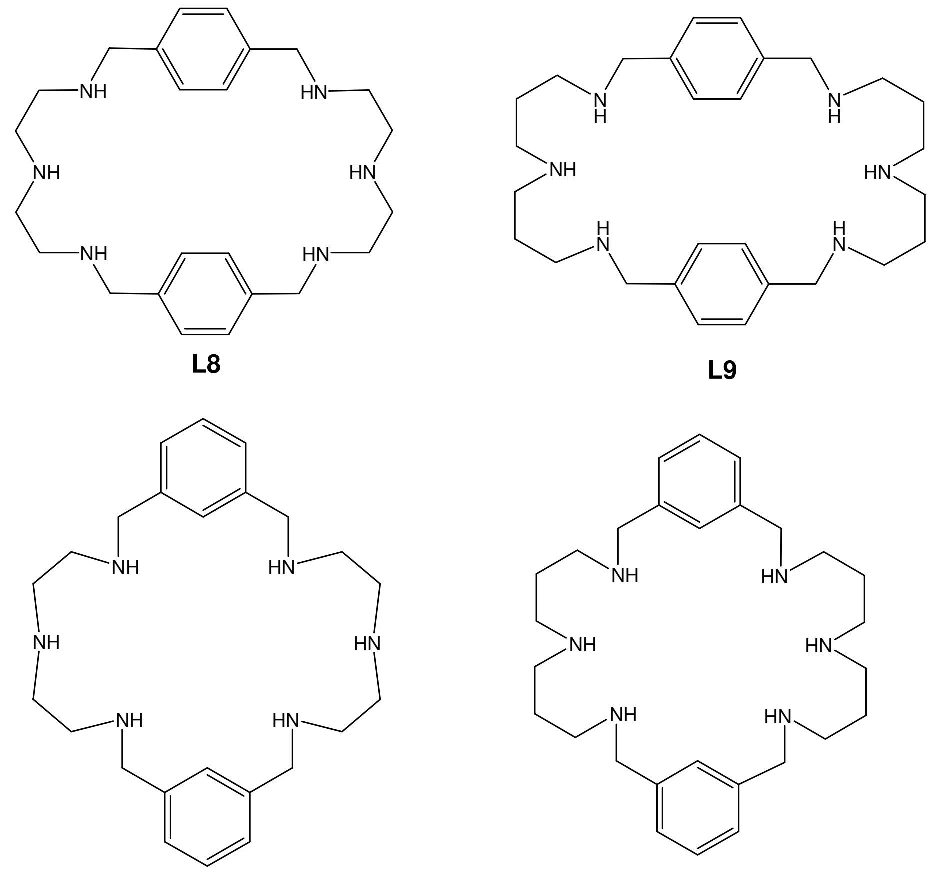

L8 **L9**

L10 **L11**

Figure 1.6. Macrocyclic ligands with different aromatic geometry and aliphatic spacer length studied as oxalic acid receptors. [88]

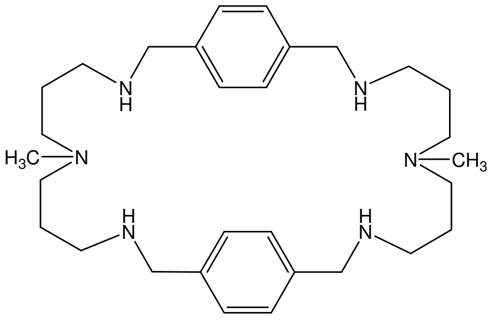

L12

Figure 1.7. Ligand **L12** selectively binds terephthalate anion over other aromatic diacids. [89]

Another variation of these macrocyclic receptors was developed by García-España and coworkers, synthesizing a family of macrocycles with pyrazole as aromatic spacer. These receptors have the central amino nitrogen and the pyrazolic nitrogen functionalized with aromatic or aliphatic radicals. [90]

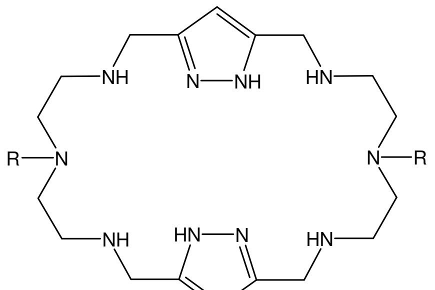

Figure 1.8. Family of macrocyclic receptors used by García-España and coworkers as glutamate receptors. [90]

These macrocyclic ligands have been studied as receptors for glutamate. A strong bond between the receptor and substrate has been found for the receptor with the central amine bearing a benzyl (R = bz). Others substitutions led to a sharp decrease in stability. This behavior is due to a combination of hydrogen bonding, electrostatic and π–cation interactions between the ammonium glutamate group and one of the benzene rings. All these factors lead to a high stability of the benzyl receptor – glutamate complex.

A different type of aromatic dicarboxylates, isomeric pyridinedicarboxylic acids, were studied as substrates for two different macrocyclic ligands (*Figure 1.9*).[91]

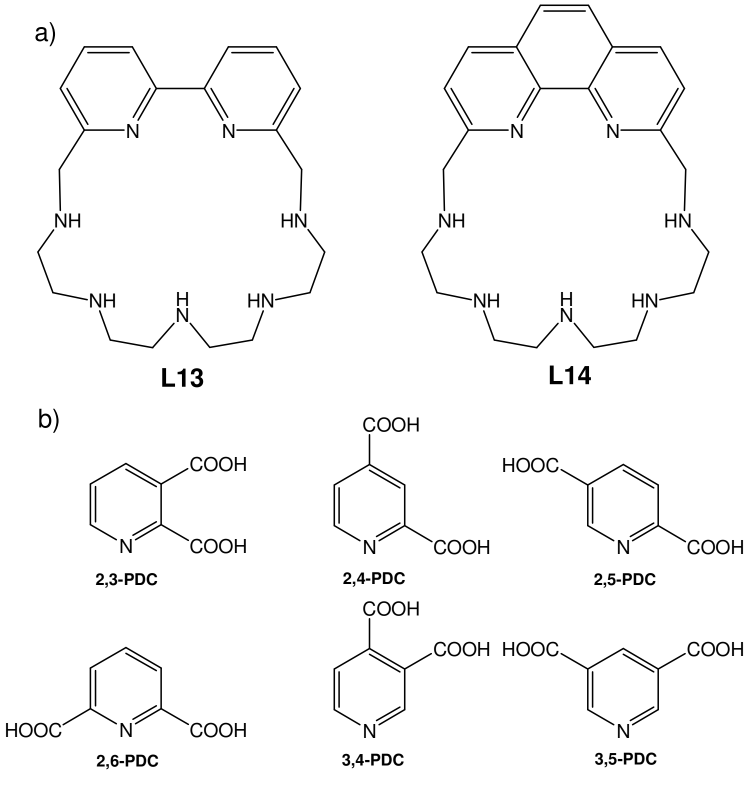

Figure 1.9. Drawing of (a) macrocyclic ligands **L13** and **L14** and (b) pyridine dicarboxylic acids used as receptors and substrates.

The receptor **L13** and **L14** showed a selective binding for 2,6-PDC, due to the position of the two carboxylate groups and the nitrogen atom of the pyridyl group, that provide a synergetic binding of the substrate. On the other hand, it has been found that the receptor **L13** is able to bind this substrate stronger than **L14** though electrostatic interaction, hydrogen bonding and π-π stacking as a result of a better match between receptor and substrate, favoured by the more flexible bipyridine spacer compared to phenantroline.

The work with biological targets often deals with the chirality of the molecules of interest.[78,92,93] A large portion of biological substrates are chiral being only one of the enantiomers biologically active. In this context, enantioselectivity has been the goal of many studies. As an example, the macrocyclic ligand **L15** has been synthesized as an enantiomerically pure macrocycle and evaluated for enantioselective recognition of chiral dicarboxylates.[94,95]

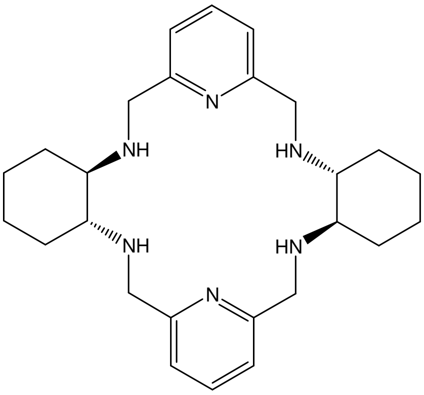

Figure 1.10. Chiral macrocyclic ligand **L15**.

For the majority of the chiral diacids studied, the ligand is capable of binding more strongly an enantiomer over the other, displaying also a better enantioselectivity at physiological conditions, where the uncharged complex predominates. These results reinforce the idea that hydrogen bonding, rather than coulombic interactions, are the driving force for the formation of the complex.

Another type of substrates of special interest are the carboxylates derived from benzenetricarboxylic acids, as they can be considered as ideal model for rigid anionic substrates with well defined shapes. On the other hand, Kemp's triacids, are also interesting species, as they have relatively rigid structures and the carboxylate can be either in axial or equatorial positions, leading to the isomers *cis,cis*-1,3,5-trimethyl-1,3,5-cyclohexanetricarbonylic acid (*c,c*-TMCT) and *cis,trans*-1,3,5-trimethyl-1,3,5-cyclohexanetricarbonylic acid (*c,t*-TMCT).

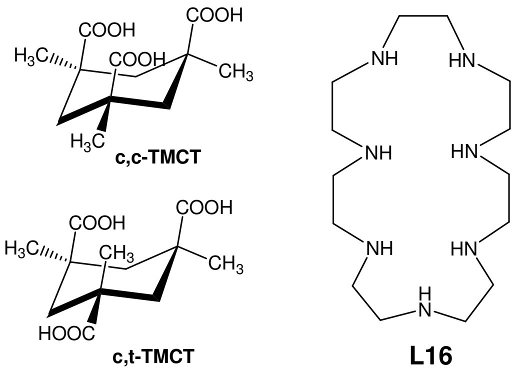

Figure 1.11. Kemp's triacids and the receptor **L16**.

When studying the interaction of the protonated macrocycle **L16** as receptor [96,97] with both isomers it is found a selectivity for the *c,c*-TMCT isomer over the *c,t*-TMCT isomer. The polyammonium host behaves as a flat charge surface, that interacts better with all three carboxylates in *c,c*-TMCT which are on the same side, than with the *c,t*-isomer, which has only two carboxylate groups in the same side.

Furthermore, when comparing the interaction of the same guest with these species and the dicarboxylate 1,2-benzenedicarboxylic acid (1,2-DBC), it is found that, despite a lower charge, there is a stronger interaction of the ligand with 1,2-DBC than with c,t-TMCT, which can be explained with the same reasoning.

On the other hand, an interesting example of the importance of the shape-complementarity in the selective recognition of carboxylic acids has been carried out when studying the interaction of these three carboxylate isomers with the macrocycle based ligands **L17**, **L18** and **L19** (*Figure 1.12*).[98]

In all the cases, recognition for 1,3,5-benzenetricarboxylic acid (1,3,5-BTC) over 1,2,4-BTC and 1,2,3-BTC is achieved, due to the ternary symmetry of hosts and 1,3,5-BTC. The acid fits in the cavity and it is encapsuled by the hosts.

Furthermore, it has been studied the interaction between the ligand **L19** and the larger triacid 1,3,5-benzenetriacetic acid (1,3,5-BTAc), observing in this case a mismatch of size between host and guest.

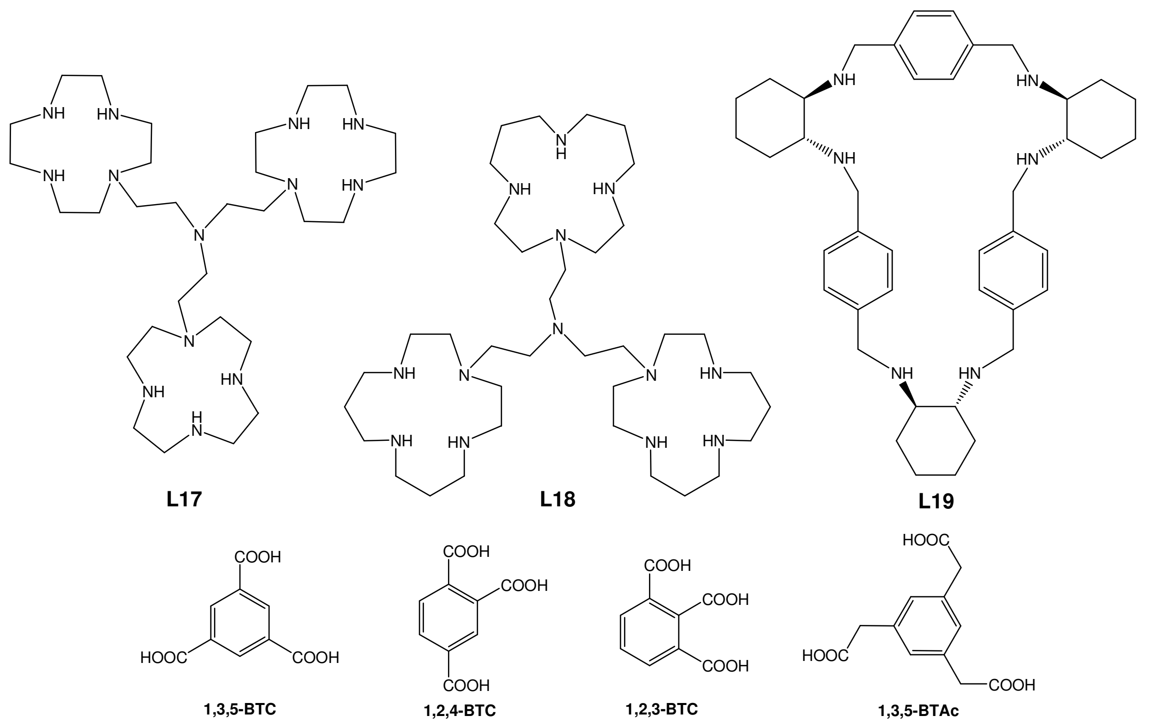

L17 **L18** **L19**

1,3,5-BTC 1,2,4-BTC 1,2,3-BTC 1,3,5-BTAc

Figure 1.12. Tritopic receptors **L17**, **L18** and **L19**, and tricarbocylic acids 1,3,5-BTC, 1,2,4-BTC, 1,2,3-BTC and 1,3,5-BTAc.

In these cases the receptors behave no longer as a charged surface, but they have been prepared to adapt specifically to the shape of 1,3,5-BTC over the other species.

Bicyclic cryptands can be considered as an evolution of macrocyclic receptors. Polyammonium salts of this type of receptors have also been studied in dicarboxylate recognition.

Nelson and coworkers have studied the interaction of three cryptand receptors bearing different aromatic spacers (m- xylyl, furane and pyridine, *Figure 1.13*) with different dicarboxylates in water.[99,100]

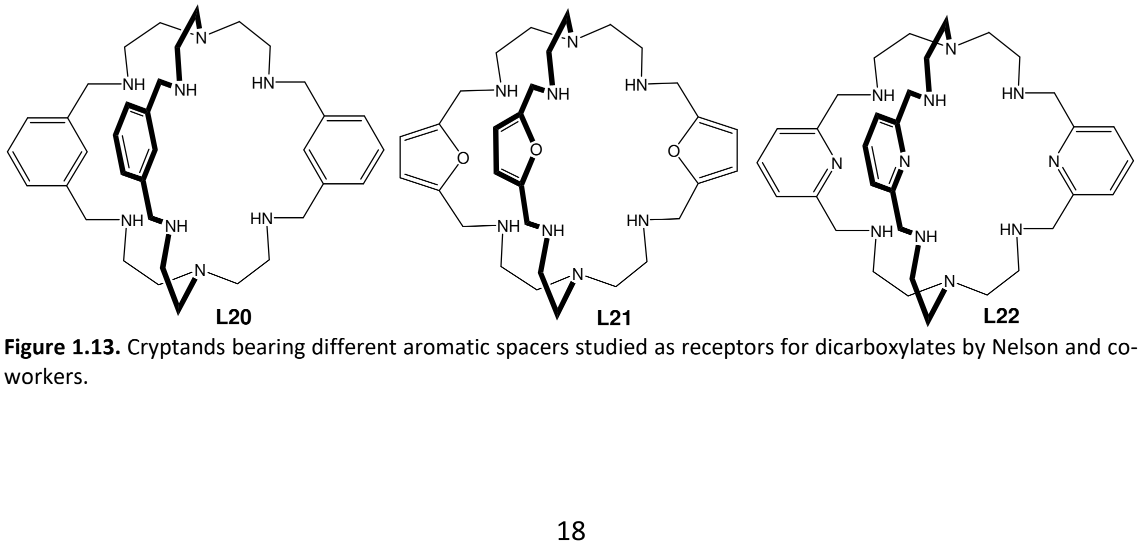

L20 **L21** **L22**

Figure 1.13. Cryptands bearing different aromatic spacers studied as receptors for dicarboxylates by Nelson and co-workers.

In all cases, especially strong interactions have been found with oxalate, and low selectivity towards diacids bearing longer aliphatic chain.

Delgado and co-workers studied the interaction of two other ditopic criptand receptors (one bearing a flexible amine spacer **L24** and the other bearing a rigid aromatic spacer **L23**, *Figure 1.14*) towards some dicarboxylates of varying chain length, in aqueous solution.[101]

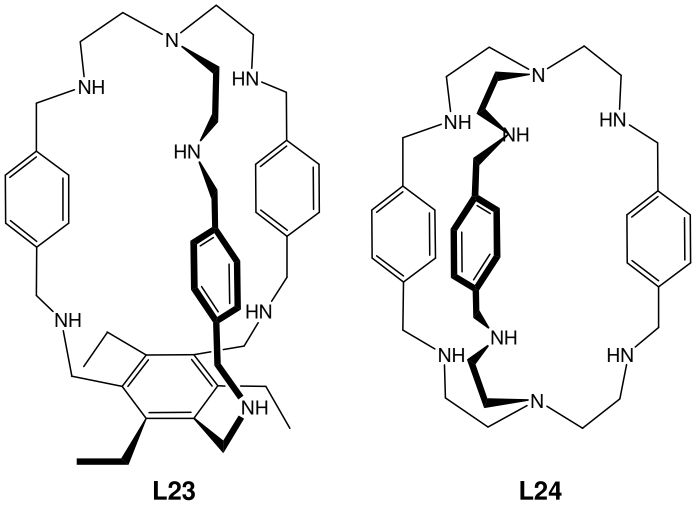

Figure 1.14. Cryptand ligands **L23** and **L24** studied as receptors for dicarboxylates by Delgado and coworkers.[101]

The results showed no differences between the selectivity pattern of the dicarboxylates since it was the same for both criptands (preferentially binding oxalate and fumarate) although not the strengths of the complexes. This is because, despite the structural differences between the two receptors, the binding subunits remain very similar, and so is the size and shape of the cavity where the substrates are accommodated. On the other hand, the differences in binding strength between the two receptors are explained by the difference in flexibility. When no preorganization exists, the more rigid the ligand, the more cost has its conformational rearrangement and thus the more difficult it is to accommodate a substrate, leading to a less stable complexes with the more rigid but not preorganised criptand **L23**.

Another criptand, with an amido binding site (**L25**, *Figure 1.15*), has been used as a receptor for aliphatic dicarboxylates.[79]

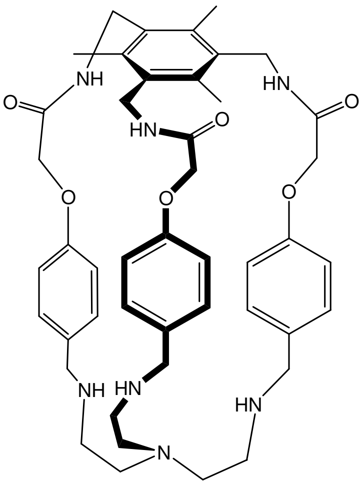

L25

Figure 1.15. Cryptand **L25** with an amido binding site studied as a receptor for aliphatic dicarboxylates.

This criptand interacts with all studied diacids, but it has a strong selectivity with succinate diacid, and clearly shows a correlation between the strength of the interaction and the length of the dicarboxylate chain. It is interesting to note that the driving forces for the complexes formation are electrostatic, as evidenced by the higher binding constant of the most charged species. Nevertheless, hydrogen bonding interaction with the amido moieties are also of special relevance, which are not protoned and still strongly interacts with one end of the dicarboxylates accommodated within the criptand cavity.

1.3.4. Inorganic phosphates and mononucleotides recognition.

Inorganic phosphates and nucleotides are ubiquitously present in biological systems and play crucial roles in many cellular functions, such as transport across membranes, DNA synthesis, cell signalling and energy or electron-transfer processes.[69,102,103] It was estimated that ATP, ADP and inorganic phosphate, from which they are formed, take part in more chemical reactions than any other compound except water.[104] In most cases, these functions are regulated by recognition processes involving proteins able to selectively bind the appropriate phosphate or nucleotide anion by using essentially highly specific non covalent interactions, both polar and apolar, such as charge–charge and charge–dipole interactions, hydrogen bonding and hydrophobic effects.

To study these complex events, one of the approaches has been the design and study of synthetic (abiotic) receptors that are able to bind phosphate derivatives anions in aqueous solution. This has become a common strategy to mimic biological recognition of nucleotides by proteins since the earliest works of Kimura and Lehn in the early 1980s, where they studied the interaction between polyazamacrocyclic structures and inorganic phosphates and nucleotides such as AMP, ADP and ATP. Since then many examples of host molecules specifically designed for nucleotide binding, mostly of the polyammonium type, have been used to study these phenomena, showing a diversity of binding contributions between receptor and substrate to study and enhance the selectivity.

1.3.4.1. Phosphate, pyrophosphate and triphosphate anions recognition.

From the earliest works from Kimura and Lehn about anion recognition many studies have been performed dealing with the studies of interaction between inorganic phosphates (*monophosphate, pyrophosphate and triphosphate*) and macrocyclic polyammonium receptors. In these initial cases, the electrostatic interaction, along with the substrate-receptor fit, is the main driving force for complex formation and stability: the higher the charge of the receptor and substrate, the more the stability of the resulting complex.

In these cases, when comparing the stability of a receptor with the different phosphates, the most stable complexes are formed with the more charged anion triphosphate $P_3O_{10}^{5-}$, followed by the complexes with pyrophosphate anion $P_2O_7^{4-}$, and the less stable complexes being formed with the less charged monophosphate PO_4^{3-} anion.

As mentioned above, all these species are specially pH-sensitive, as the degree of protonation, and therefore the charge of the substrates and receptors, depend on the H^+ concentration. Thus, when the driving forces are the electrostatic attractions, at very basic or very acidic pH, stable complexes are not formed: indeed, at highly acidic pH the substrates are fully protoned and therefore they have not got any charge to interact with the receptor. On the other hand, at basic pH it is the ligand which is not protoned, and thus this neutral receptor has not any positive charge which would allow an interaction with the anionic substrate.

Within this trend, several studies have been done dealing with the conformation, geometry and cavity size of the receptor in relation to the stability of its complexes with a phosphate derivative substrate, given a certain protonation degree. Most of the receptors are azamacrocycles constituted by two or more polyamines groups separated by different spacers, such as aliphatic chains or aromatic units. These spacers modulate the distance between the ammonium chains, which act as binding sites, as well as sometimes the geometry and flexibility of the receptors, the distance between binding moieties and the cavity size and conformation.

When Anda et al.[105] compared the interaction of the macrocyclic receptor **L9** (*Figure 1.6*) towards monophosphate (PO_4^{3-}) and pyrophosphate ($P_2O_7^{4-}$), stronger interaction of the ligand with pyrophosphate was found, due to the higher negative charge of the latter, which leads to stronger coulombic interaction between substrate and receptor and thus to a more stable complex.

On the other hand, in the same work a comparison of the interaction between pyrophosphate and two macrocyclic receptors **L9** and **L11** (*Figure 1.6*) has been carried out. These two receptors are isomeric species, with the same aliphatic spacer but where the aromatic spacers are linked in the *meta* position or *para* position, which leads to different cavity shapes and sizes (*Figure 1.6*).

A stronger interaction between pyrophosphate substrate and **L11** receptor over **L9** was found. Given the similarity in the chemical nature of **L11** and **L9**, this selectivity arises only because of the different shape and/or size of the cavity of those two ligands, being the **L11** more fitting for this substrate and thus forming more stable species.
Furthermore, monophosphate substrate binds these two ligands in a similar manner, since the small size of the substrate prevent from discrimination by any of the two receptors.[105]

Another example of the effect of the substitution comes from the work by Handel and coworkers.[106] A series of macrotricyclic ligands, having different substitution of the aromatic spacer, have been tested towards inorganic substrates and the stability of the complexes evaluated (*Figure 1.16*).

For the receptors with *meta* (**L24**) and *para* (**L25**) substitution, the strength of the complexes increases in the order monophosphate < pyrophosphate < triphosphate. This can be ascribed to electrostatic interaction. Nontheless, the *ortho*- substituted receptor **L23** shows high complex stability with monophosphate and pyrophosphate in comparison with the other *para*- and *meta*-receptors. This is due to the distance between binding ammonium moieties, which in the *ortho*-isomer, which has the smallest, is the best tuned to fit monophosphate and pyrophosphate.
So, even if the complexes are strongly stabilized by charge-charge interaction, a good fitting of the receptor in the substrate is also essential.

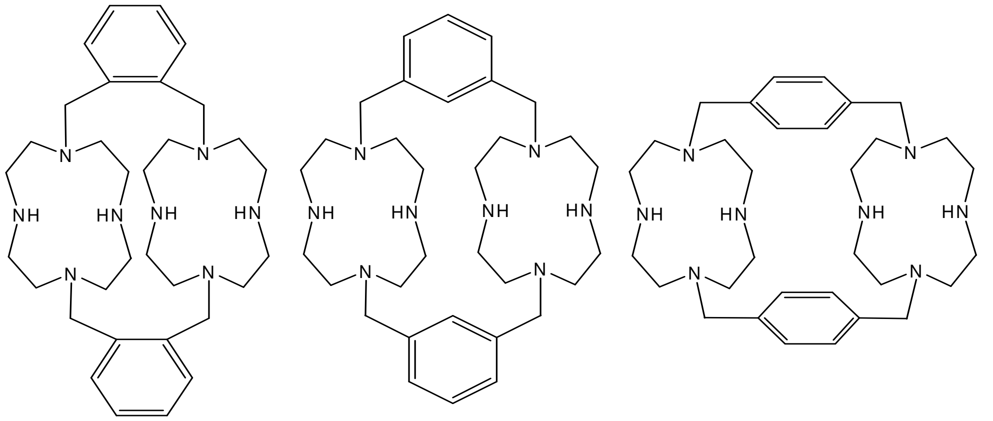

L26 **L27** **L28**

Figure 1.16. Isomeric (*orto-, meta- and para*-substitued) macrotricyclic ligands used as receptors for inorganic phosphates.

The analog compounds podand open chain of these macrocyclic complexes have also been studied in their complexation towards inorganic phosphates, to test the differences between macrocycles and open ligands.[107]

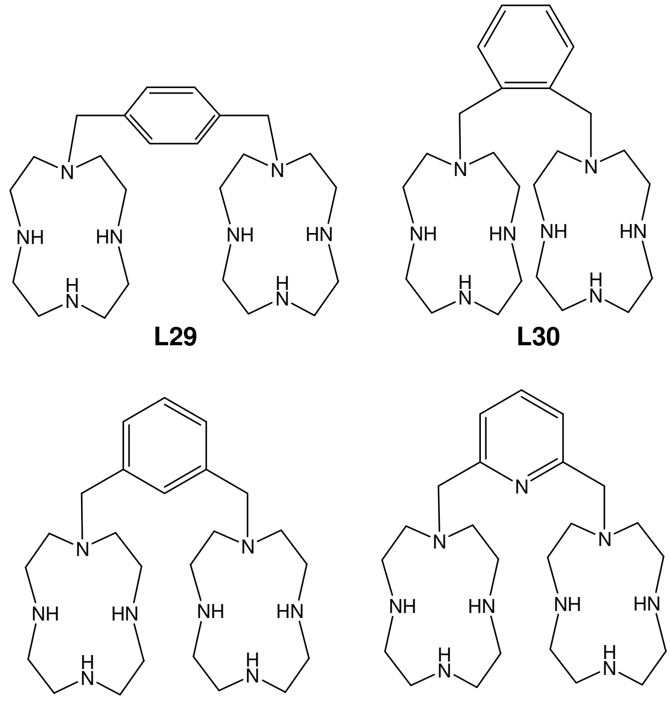

L29 **L30** **L31** **L32**

Figure 1.17. Bismacrocyclic ligands used as receptors for inorganic phosphates.

The stability constants for the phosphate – receptor ternary systems with the bismacrocycles (podands) are largely lower than with its macrotricycle analogs. Another feature of the macrotricycles over bismacrocycles is a higher selectivity of the host-guest recognition, which arises from a higher rigidity of the macrotricyclic receptors.

Although normally these electrostatic forces are the driving force for formation of complexes with anions, in the case of complexes phosphate – polyammonium receptors, other forces like hydrogen bonding may be the ones that define the final stability of the complex, in contrast with the general trend of increasing stability with increasing charge of receptors and anions

In this context, not always strict trends are found in the stability of the complexes between phosphate and polyammonium receptors in relation to their coulombic charges: given a degree of protonation, the less charged anion can form more stable complexes. Actually, even the reverse relation can be found.

A good example is given when the interaction between two macrocyclic ligands and monophosphate and pyrophosphate is studied.[108]

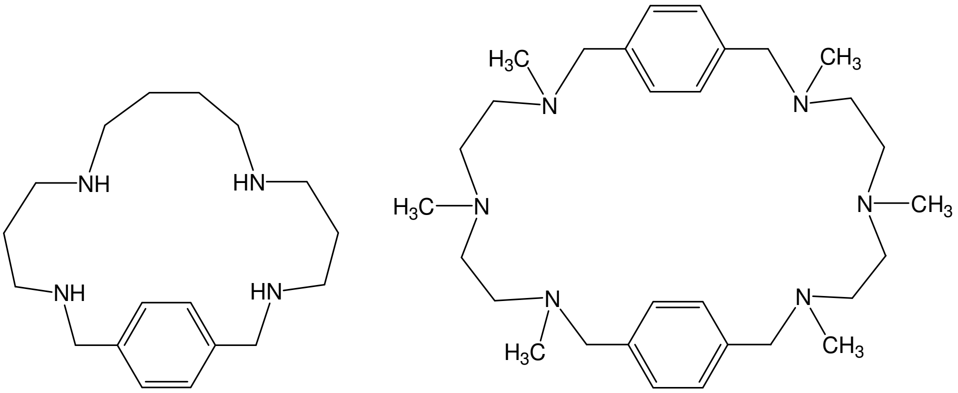

L33 **L34**

Figure 1.18. Macrocyclic ligands **L33** and **L34**, used as receptors for monophosphate and pyrophosphate.

The stability of the complex of HPO_4^{2-} with the mono-, di- and triprotonated forms of **L33** decreases when increasing the charge on the ligand. On the other hand, the stability of the complexes formed by the tetraprotonated form H_4**L34**$^{4+}$ with $HP_2O_7^{3-}$, $H_2P_2O_7^{2-}$ and $H_3P_2O_7^{-}$, increases with the decreasing charge of the anion.

This behaviour is attributed to the particular ability of the phosphate species in behaving as acceptors and donors of hydrogen bonds. Phosphate and pyrophosphate anions can interact with polyammonium receptors through many hydrogen bonds, in which both anions and receptors can act as acceptors or donors.

So, although the electrostatic attraction brings the substrate and the receptor in contact with each other, then several types of hydrogen bonds can be established, depending on the complex structure and the protonation degree of both species. This contribution of different hydrogen bonds are decisive in the stability of the complex.

Another possible driving force for the formation and stability of the phosphate complexes with polyammonium receptors is the dessolvation process occurring upon complexation. In some cases, the cavity of the polyammonium receptor is folded forming a pocket where many water molecules can be hosted. The process of inclusion of the anion to form the host-guest complex causes the exclusion of these water molecules from the cavity, which is accompanied by a favorable entropic effect.[109]

1.3.4.2. Mononucleotide anions recognition.

Nucleotides are the building blocks of nucleic acids. They are composed of three subunit molecules: a nitrogenous base, a five-carbon sugar (ribose or deoxyribose), and at least one phosphate group. They can have one phosphate group (monophosphate), two phosphate groups (diphosphate) or three (triphosphate). Nitrogenous bases typically can be derivatives of two possible compounds: pyrimidine or purine.

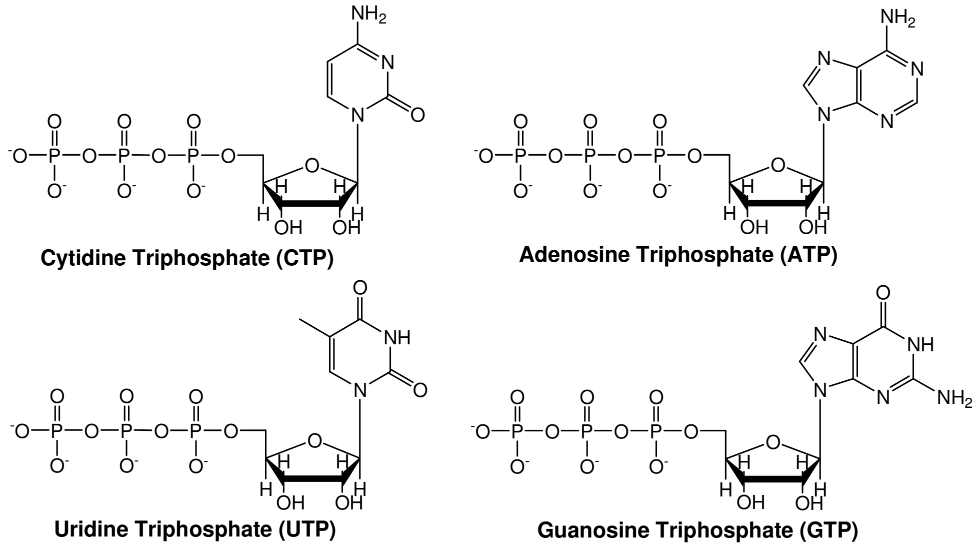

Cytidine Triphosphate (CTP)

Adenosine Triphosphate (ATP)

Uridine Triphosphate (UTP)

Guanosine Triphosphate (GTP)

Figure 1.19. Most biologically relevant triphosphate mononucleotides.

The addition of a nitrogenous base, which is an aromatic moiety, in respect of the inorganic phosphates, adds the possibility of a π -interaction between the receptor and the substrate.

π -π stacking is one of the forces that can be used to complement coulombic interactions and hydrogen bonding forces in nucleotide recognition. While the phosphate chain of the nucleotide represents a good electrostatic binding point, the aromatic moieties may operate as an adequate site for π -π stacking interactions with the appropriate functionalities of the ligand.

Several studies have been carried out dealing with the interaction of phosphate and nucleotide substrates with polyammonium receptors. Some of them show that the main driving force for the complex formation is electrostatic attraction, despite the possible π -π interaction.

For example Anda et al studied the interaction of both inorganic phosphates PO_4^{3-}, $P_2O_7^{4-}$ and $P_3O_{10}^{5-}$ and nucleotides AMP, ADP and ATP with two macrocyclic receptors **L10** and **L11** (*Figure 1.6*, page 14).[110]

It was found that the strength of the ternary complexes is only proportional to the charge of receptor and substrate, following the order of strength $P_3O_{10}^{5-} > P_2O_7^{4-} > PO_4^{3-}$ for these inorganic phosphates, and ATP > ADP > AMP for nucleotides. In addition, comparing inorganic phosphates and nucleotides, the stability of the complexes bearing a substrate of the same charge (diphosphate and ATP, which are both tetranegative) are more similar than when comparing the stability of the complexes with a substrate with the same number phosphorous atoms (triphosphate and ATP, which have both 3 phosphorous atoms), supporting that the main driving force for complex formation is electrostatic attraction.

In many other studies, on the other hand, the π -π interaction between aromatic moieties of substrate and receptor play a major role in recognition and stability of the complex. Nontheless, other factors such as the receptor flexibility, basicity or rigidity can also be relevant in the substrate selectivity and in the stability of a complex.[111,112]

Bianchi and coworkers reported the first crystal structure of a nucleotide bound to a synthetic receptor.[113] It was shown that the receptor **L35** interact with the nucleotide Thymidine triphosphate (TTP) (*Figure 1.20*) through different binding interactions, mainly hydrogen bonds and salt bridges involving the ammonium groups of the ligand and the substrate phosphate oxygen atoms, and also π–stacking between the nucleobase and ligand heteroaromatic groups.. These interactions were revealed to also be active in solution.

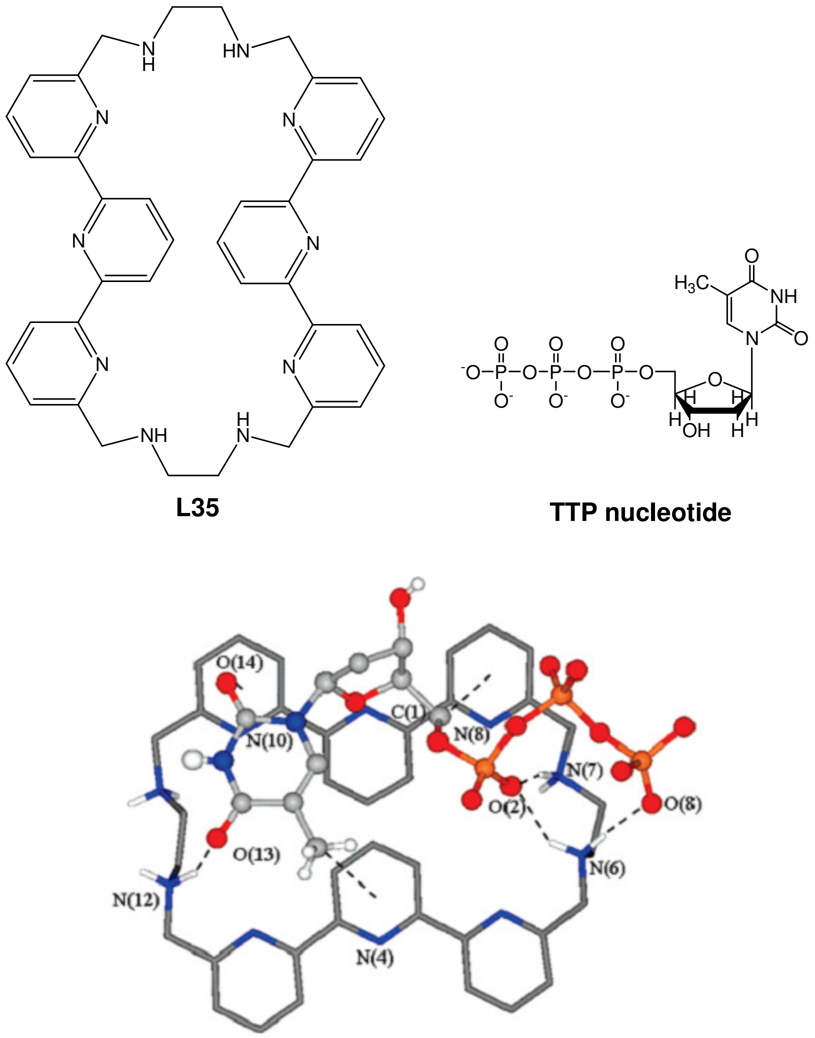

Figure 1.20. top: Receptor **L35** and nucleotide TTP. Bottom: Crystal structure of [(H_4**L35**)(HTTP)]. [113]

In order to study the influence of the substitution of the aromatic spacer, a series of receptors formed by a polyamine chain attached to a *ortho-, meta-* or *para-* xylyl spacer have been developed and its interaction towards nucleotides studied, focusing on the influence of the aromatic substitution of the macrocyclic receptor in its selectivity towards nucleotides.[114–116]

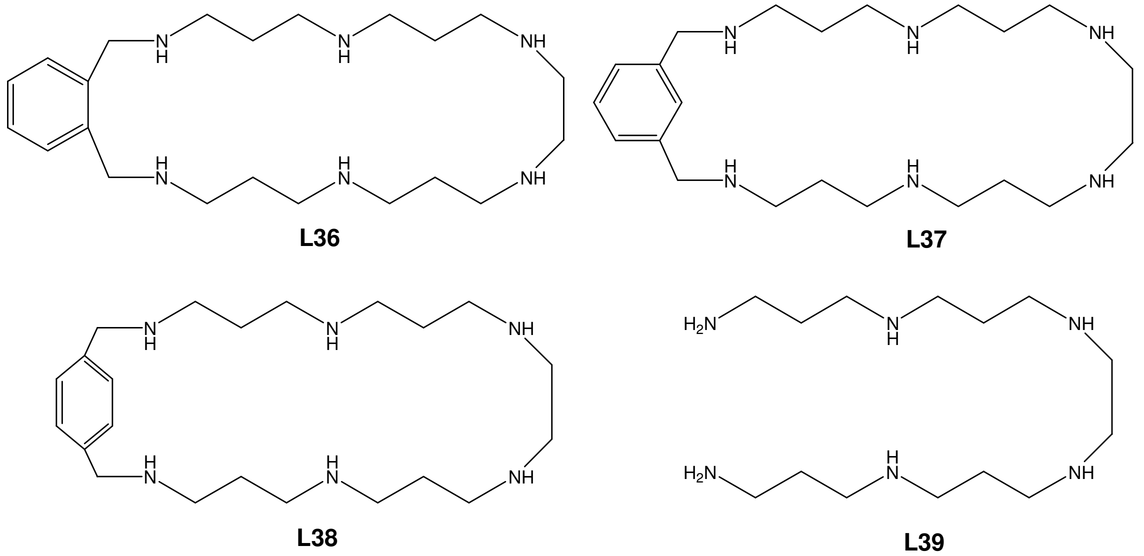

L36 **L37** **L38** **L39**

Figure 1.21. Geometric isomeric macrocyclic and acyclic receptors studied as receptors for nucleotides.

It has been found that all the receptors strongly interact with ATP, and that its interaction strength deeply depends on the aromatic substitution. Within macrocyclic receptors, the stability order found for the complex L-ATP followed the sequence *ortho* > *meta* > *para*-substitution (**L36** > **L37** > **L38**). All macrocyclic receptors form more stable complexes than its open-chain counterpart **L39**. The π – π interactions between the aromatic part of the receptor and the one from the nucleobase play an important role in the stability of the complexes.

Other receptors, macrocyclics and acyclics, containing other aromatic parts have been used to evidence the importance of pi stacking in the stability of the complexes with nucleotides. Nonetheless, these kinds of interactions not always provide enough stabilization to the complex. Llobet and coworkers studied the interaction of the nucleotides ATP and ADP and their corresponding inorganic phosphates with the macrobicyclic ligand **L40** (*Figure 1.22*).[109]

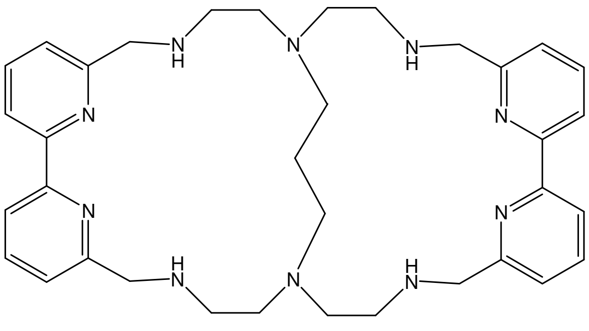

L40

Figure 1.22. Macrobicyclic ligand **L40**.

It was found that complexes with inorganic phosphates were more stable than complexes with the corresponding nucleotide, which is rather surprising since the stability of the adducts of inorganic phosphates with polyammonium macrocycles is generally lower than that of the nucleotides complexes. In this case, π-stacking interaction between adenosine from the nucleotide and bipyridine moiety from the receptor is formed, as seen from ^{1}H-RMN and molecular mechanics calculation. The higher affinity for inorganic phosphates is due to the fact that they are small enough to perfectly fit in the pocket created by the folded conformation of the macrocycle. On the other hand, the phosphate chains of the bulky ATP or ADP cannot be completely encapsulated and the adenine moiety remains outside the ligand cleft, resulting in fewer or weaker salt bridges between the receptor ammonium functions and the phosphate chains of nucleotides, destabilizing these complexes.

An interesting synergy between π interactions and coulombic forces is exhibited in the complex between the ligands **L31** and **L32** (see *Figure 1.17* on page 23), and nucleotides ATP, ADP and AMP.[117] The two receptors are a family of bismacrocyclic ligands, consisting of two macrocyclic moieties linked by a meta-benzyl (**L31**) or a pyridine (**L32**).

This two receptors at neutral and basic pH are able to bind the nucleotides through electrostatic forces, in a similar manner than to inorganic phosphates, through H bonds, as and also by supplementary π stacking interactions between the aromatic linker and the nitrogenous base. At acidic pH the pyridine moiety of the **L32** ligand is protonated, what allows it to interact with the phosphate group through H bonding. This allows this ligand to form stable complexes with nucleotides over all the pH range, even at acidic pH, where complexes with **L31** receptors are not so stable.

Another set of receptors similar to these, an aromatic spacer (pyridyl **L41** or xylyl **L42**) but with linear amines have been studied with ATP and triphosphate.[118] There is a strong electrostatic component in the formation of both complexes, although in some cases the formation of especially strong H bonding overtakes the electrostatic effect.

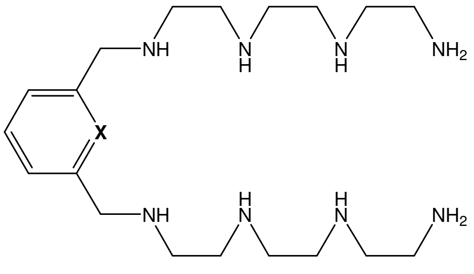

L41: X = N
L42: X = CH

Figure 1.23. Open polyammonium ligands with an aromatic spacer (pyridyl spacer, X = N, **L41** and *meta* benzyl spacer, X = CH, **L42**).

It has been observed also an involvement of π–stacking forces between the aromatic linker and the adenine moiety in the stabilization of the ternary complexes with ATP, although they are not the driving forces for the complex formation.

Taking all this into account, the ATP complex structure is as follows: the polyammonium moieties interact strongly with the more charged terminal phosphates, as can be deduced from a downfield shift of the Pγ and Pβ, in ^{31}P-RMN studies, and almost none for Pα. This have been observed also in other similar systems.[117,119] The complex is further stabilized through π-staking interactions between the aromatic moieties of substrate and receptor.

Another bismacrocyclic ligand, where the linker is a bis-cresol moiety as a spacer, forms stable complexes with pyrophosphate, triphosphate and ATP but not with monophosphate.[120]

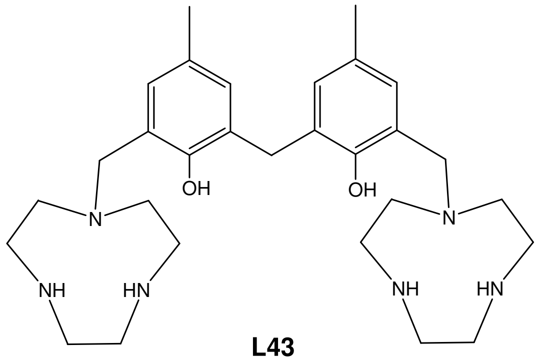

L43

Figure 1.24. Bismacrocyclic ligand with bis-cresol spacer **L43**, studied as a receptor for inorganic phosphates and ATP.

The anionic substrates interact with the ligand through a cooperativity effect of the two macrocyclic ammonium moieties. Monophosphate anion is too small and with too low charge to interact with this receptor. The other substrates interact with the protonated form of the receptor with the increasing order diphosphate < triphosphate < ATP. This trend can be explained taking into account the number of possible charge-charge interactions, and the π–stacking interactions between the nitrogenous base of ATP and the aromatic moiety of the bis cresol, which gives to the complex with ATP the higher stability.

In another work, macrocyclic receptors bearing anthracene (**L44**) or pyridine (**L45**) pendant arms (*Figure 1.*25) were used as receptors for different nucleotides.[121]

When studying the interaction of ATP with these two receptors, different behaviour was noticed between the receptor with anthracene arm **L44** and the receptor with pyridyl arm **L45** in acidic pH.

Indeed, at neutral and basic pH values, the substrate is not protonated and the interaction strength is based on electrostatic attraction between the ATP anion and the different pH-dependent polyammonium receptors, being stronger the interaction as pH decreases. Nevertheless in acidic pH, below pH = 6, an interesting behaviour difference is found between pyridyl and anthracene pendant arm receptors. The interaction of ATP and pyridyl derivative receptor **L45** does not increase, or even decreases, as pH decreases. This behaviour is ascribed to less coulombic interaction as the anionic ATP protonates. On the other hand, the anthracene moiety of the **L44** receptor can interact in a more favourable way through π-π stacking with the more electron deficient aromatic part of the protonated adenine, leading to a π–π interaction based, more stable complex.

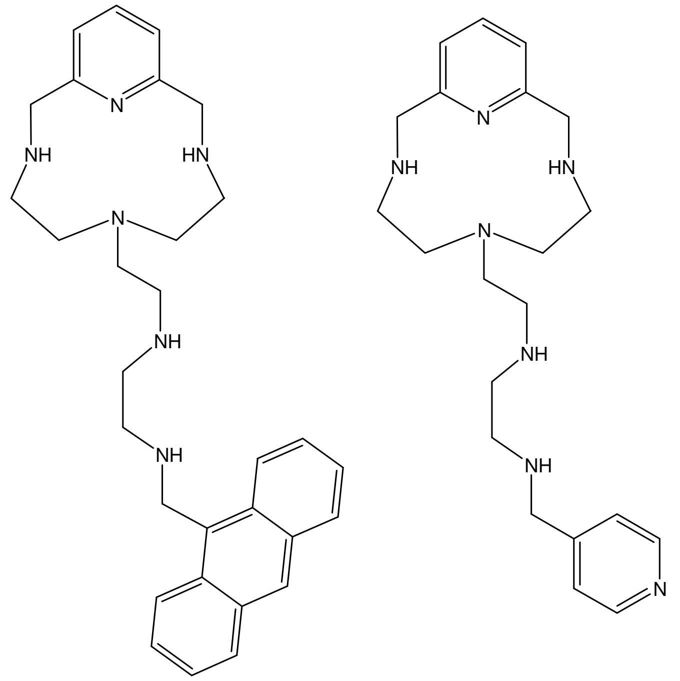

L44 **L45**

Figure 1.25. Macocyclic receptor bearing anthracene (**L44**) or pyridyl (**L45**) pendant arms.

Very similar results were obtained when studying the interaction between monophosphate nucleotides and two receptors consisting in two macrocyclic moieties linked by an aromatic spacer – a pyridine and a phenantroline.[122,123]

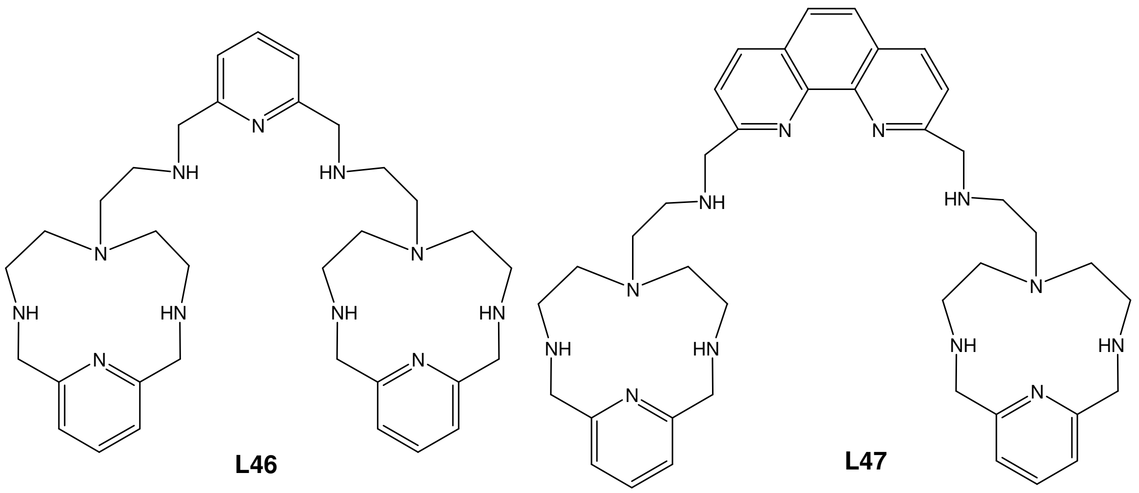

L46 **L47**

Figure 1.26. Bismacrocyclic systems with a pyridine spacer (**L46**) and with a phenanthroline system (**L47**).

At basic pH values the driving force for complex formation is electrostatic force, but in acidic range when nucleotides protonate and electrostatic force is lower, the π-π interactions between the aromatic moieties of the ligand and of the nucleotides lead to an increasing stability of the complex between the substrate and the receptor with the larger π system phenanthroline in **L47**, and a decrease of stability of the complex with the smaller π system pyridine **L46** receptor.

A similar synergistic effect of electrostatic and aromatic stacking interactions is even able to reverse the almost immutable trend selectivity towards the nucleotide ATP/ADP/AMP series.[124]

Many studies have also focused on the relationship between selectivity and receptor structure. For example, Bianchi and coworkers studied the binding patterns towards ADP and ATP of the two macrocyclic ligands **L34** and **L48**, which are composed of two polyamine subunits linked by aromatic spacers, leading to rigid macrocyclic frameworks.[125]

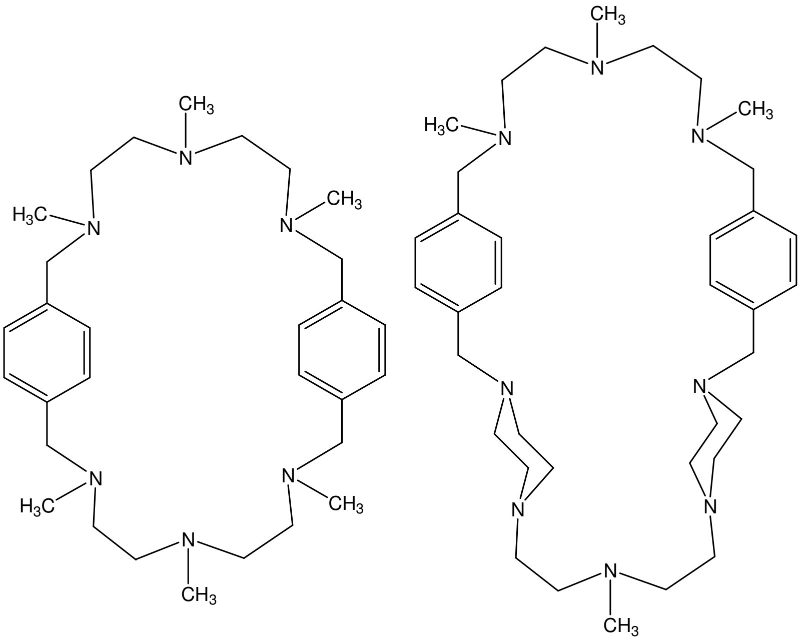

L34 **L48**

Figure 1.27. Macrocyclic ligands with tertiary amines **L34** and **L48**.

The partially protonated form of both macrocyles has a very similar structure and charge distribution. Nontheless, **L34** forms stable complexes with ATP and ADP, but no interaction between ATP, ADP and the **L48** receptor is observed. This difference in behavior is due to different conformation of the N-H$^+$ groups, which in the case of **L34** receptor are convergent, allowing the receptor to form stable complexes with the substrate, but in the case of the **L48** are divergent, preventing the two polyamine subunits from forming simultaneously contacts with the phosphate groups of nucleotides. So, despite having both receptors a similar charge distribution, their respective conformation allows one of them to form stable complexes with nucleotides and prevents the other receptor from forming them.

In other words, charge-charge attraction, although it is the driving force for most ion pairing processes, it is not always able enough to stabilize anion complexes with polyammonium receptors, but has to be further reinforced through other forces such as hydrogen bonding and/or π–π stacking.

Beyond recognition processes, when two molecules interact, if one of them has a reactive site, it may carry out a chemical change on the other molecule, like a catalyst, or an enzyme.

1.4 – Nucleic acids – metal complexes interactions.

Nucleic acids are highly stable polymers resulting from the condensation of phosphoric acid with alcohol groups of ribose (RNA) or desoxyribose (DNA) moieties, which possess heterocyclic purine or pyrimidine bases derivatives as side chains. Each phosphate group contributes with one negative charge to the overall charge of the polymer that is electrostatically balanced by a layer of alkali metal and Mg(II) ions.[126,127] Their anionic nature facilitates the interaction with cationic species, such as metal complexes.

Because binding and cleavage of DNA is at the heart of cellular transcription and translation, it is an obvious target for therapeutic intervention and the development of diagnostic structural probes. Indeed, the interactions between metal complexes and DNA can be exploited for medicinal purposes, as they can cause damage to DNA in cancer cells by means of binding or cleavage and so rendering DNA replication impossible, which would lead to cell death. [128–132]

Among natural species, there are several metalloenzymes capable of selectively bind and perform DNA cleavage. These nucleases are used within the cell as a strategy of defense against exogenous nucleic acids, but also for DNA repair or as a strategy to clean dead or aged cells.[133,134] They can often recognize and bind very selectively a specific nucleotide sequence, and perform a hydrolytic single or double strand scission in the DNA double chain. This ability of these metalloenzymes has found applications in fields like genetic engineering or medicine. [34,135–137]

Nonetheless, the use of natural enzymes has some disadvantages, such as poor stability, difficulty in separation and purification, and high cost. Thus, it is necessary to mimic the structure of natural nucleases, through metal complexes which can act as chemical nucleases possessing high catalytic activity as long as specific recognition, like natural systems. Chemical nucleases are small molecules with an active site with the same reactivity of cleaving enzymes and a simpler structure, which should be able to perform the catalytic reaction with high efficiency and specificity, mimicking the function of the enzyme, but with other advantages, such as simple preparation, cheap cost, and without the limitations of the natural nucleases. Compared to natural nucleases, mimetic systems are a kind of new non-enzymatic breakage tool, which can mimic the function of an enzyme and can catalyse the cleavage of DNA or RNA highly efficiently and selectively.[129,134,138–141]

In this context, medicinal inorganic chemistry is a field of increasing prominence as metal-based compounds offer possibilities for the design of therapeutic agents not readily available to organic compounds. Numerous metal ions play a vital role in biological systems and currently many metal-based drugs are routinely administered to patients for therapeutic and diagnostic benefit.[127,128,131,142–144] Among these, anti-cancer drug screening is becoming the most attractive field due to the increasing threats of cancer to our health, and thus complexes able to bind and/or cleave DNA play a crucial role within this field.

1.5 – Metal – DNA interaction modes.

Metal complexes which interact with DNA can bind it through either covalent or non covalent mechanisms. [126,130,145,146]

Strong covalent interactions between DNA and a soft metal are generally established between the metal and a nitrogen atom of the nitrogenous base. When the metal is a hard Lewis acid, it can sometimes establish coordination bonds with the oxygen atoms of the phosphate groups. Finally, although less frequent, sometimes there are covalent interaction of the metal center and oxygen atoms of the sugar moiety.[126,147,148]

Among the complexes which covalently bind to DNA, of special interest is the cisplatin. This complex, cis-diamminedichloroplatinum(II), was serendipitously found to inhibit cell division by Rosenberg and coworkers in 1965,[149,150] and later it was shown to possess antitumor activity. Since then it has become an immense success, although its use has shown some drawbacks such as severe side effects and development of drug resistance.[151] Nonetheless, its discovery renewed the research interest in rationally designed metallodrugs with improved biological activities.

The activity of this complex comes from the coordination of the platinum center to the soft nitrogen atoms in the nitrogenated bases, mainly the N7 of the guanine base, yielding to a conformational change to DNA which irreversibly interferes with cell division and ultimately leads the cell to activate apoptosis.[145,152]

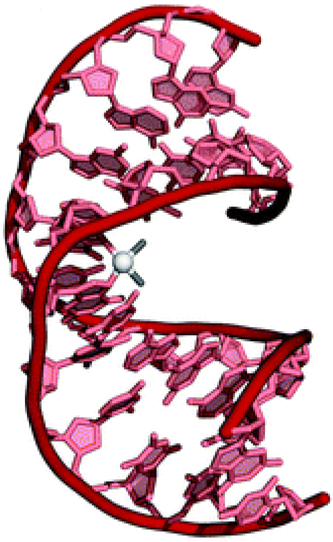

Figure 1.28. X-Ray structure of double stranded DNA containing adduct of Cisplatin 1,2d(GpG) intrastrand crosslink.[153]

On the other hand, a coordinatively saturated metal complex can establish weaker noncovalent interactions with the DNA, through either the metal center, or the ligand of the complex. Noncovalent interactions, which can be highly selective, include intercalation, groove binding, hydrogen bond and electrostatic interactions. Intercalative binding can be established when planar aromatic heterocyclic ligands stack between DNA base pairs, stabilized through dipole-dipole interactions. Also, nonintercalative hydrophobic interactions of the ligand in the DNA grooves can occur as well. On the other hand, hydrogen bonds between the coordinated ligand and the polynucleotide are quite common, especially with the oxygen atoms of the phosphate backbone.[126,130,148,152,154–157]

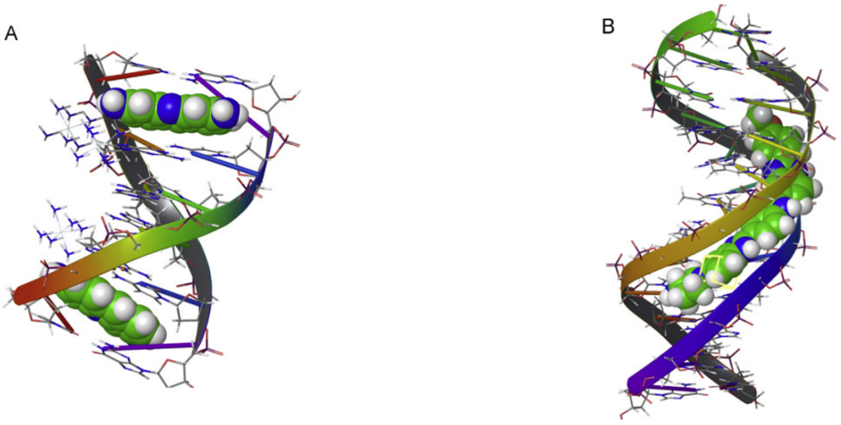

Figure 1.29. Types of hydrophobic non-covalent binding: (A) Intercalation of proflavine between two pairs of adjacent bases of the double helix. (B) DNA minor groove recognition of a tris-benzimidazole drug.[158]

Understanding of how small molecules bind DNA could potentially be useful in the design of new compounds, in order to induce selective recognition, and in possible applications in medical therapy.[159]

1.6 – Metal mediated DNA cleavage

Metal complexes are not only able to bind to DNA but they may also be able to induce scissions in the polynucleotide chain.

Cleavage of DNA or RNA can occur through three major pathways: (i) oxidative, generating reactive oxygen-containing species or other radicals for DNA oxidation˚ (ii) nucleophilic, hydrolytically cleaving the phosphodiester linkages˚ and (iii) photolytic, performing direct redox reactions with DNA.[126,129,137,139,145,155,160–165] The cleavage pathway of a complex will largely depend on the metal center.

Transition redox-active metals such as Cr, Mn, Co, Fe, or Cu are often involved in metallonucleases showing oxidative cleavage, through the breakdown of the sugar and base moieties.[138,139,163,166]

Complexes with redox-inert, hard Lewis acids are expected to operate through hydrolytic cleavage. Zinc is the paradigm of this pathway, but other metals like Cu or Mn, even if they can be redox-active centers, can also perform hydrolytic DNA cleavage.[167,168]

The mechanism of DNA hydrolysis by metallonucleases involves the formation of a metal-phosphate intermediate, which facilitates the nucleophilic attack of an oxygen atom from a water molecule, or from a metal-bound hydroxide nucleophile, and so leading to strand scission.[134,162,167–170]

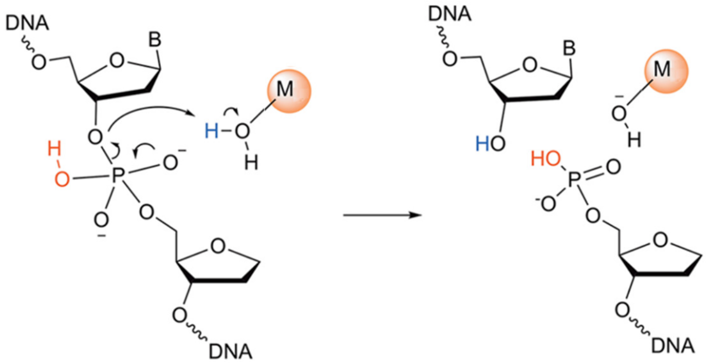

Figure 1.30. Summary of hydrolytic cleavage pathway for nucleic acids, promoted by metal complexes.

The Lewis acidity of the metal is what promotes the activation of the phosphate group towards the attack of the nucleophile, increasing the leaving group ability of the departing alcohol and also activating a coordinated water molecule as a nucleophile.

Finally, many metals can be involved in DNA photo-cleavage. In these cases, DNA cleavage is performed by reactive species (either an excited form of the complex or other reactive species), which are produced after light exposure.[171–173] Copper metallonucleases have also shown in some occasions to perform this cleaving pathway.[174–179]

Among all the investigated metals, copper is an interesting candidate because of its bioavailability. In artificial metallonucleases, the amino acids of the natural enzymes are replaced by simple organic ligands. Depending on the ligand moiety, hydrolytic, oxidative (or both) or photoinduced reaction pathways can be followed.[129,139,148,157,180–182]

1.6.1 – The Oxidative Pathway.

Many transition metal complexes bearing different metal centers have been reported to mediate DNA oxidation in the presence of oxidants or reductants or without any assistant agents. The oxidative pathway involves the attack of the sugar or base moieties of DNA by highly reactive species and can be highly efficient in inducing strand scission of DNA.[138,139,163]

The mechanism of the oxidative DNA cleavage involves reactive oxygen species (ROS), or reactive metal-oxo species (RMOS), which are the ones responsible for the cleavage. Indeed, the DNA-cleavage ability of different metallonucleases is largely determined by the reactivity of the reactive species formed.[129,163,183]

A redox active metal, with an appropriate reduction potential is needed to produce these reactive species.

Most reactive intermediates are indeed produced through a redox cycle of the metal center in aerobic environment or in the presence of co-oxidants. Indeed, the sequential reduction of molecular oxygen can generate a group of reactive oxygen species: the molecular oxygen can be excited to singlet oxygen ($^1O_2$), or reduced to superoxide (O_2^-), peroxide (O_2^{2-}), or hydroxyl radical.[163,170,184–187]

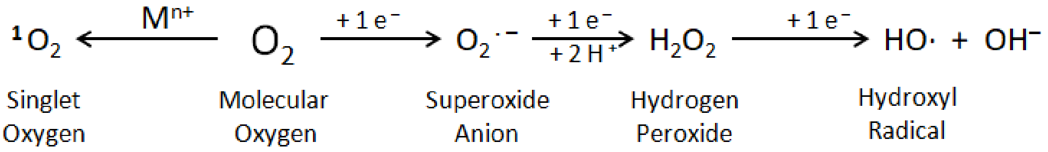

Figure 1.31. Generation of reactive oxygen species through molecular oxygen reduction.

These ROS are diffusible molecules capable of damaging DNA, either by hydrogen atom abstraction from the sugar moiety, or by damaging the DNA bases. .[163,183,188]

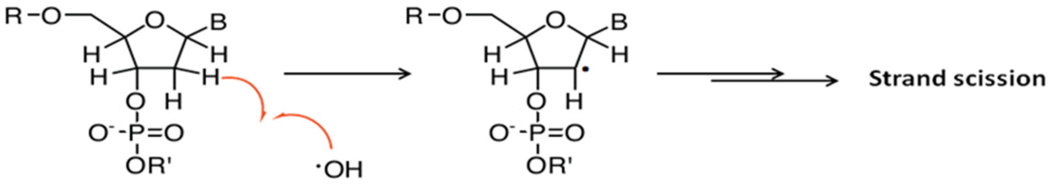

Figure 1.32. Summary of DNA Oxidative Cleavage pathway by hydroxyl radical through Hydrogen (H1’) abstraction of the desoxyribose backbone.

On the other hand, the produced reactive oxo species can be also bound to the metal center, obtaining Reactive Metal-Oxo species (RMOS). RMOS are non diffusible species, more diversified than ROS and also able to induce DNA damage leading to strand scission by the same pathways.[28,163,170,189]

RMOS include end-on and side-on peroxo and superoxo metal species, from mono and dimetallic centers, and even high valent metal oxo species (M=O). [163,186,189,190]

One metal center	**Two metal centers**
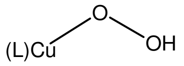 *Hidroperoxo*	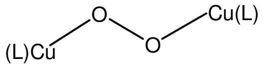 *End on*-η-1,2-peroxo
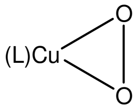 *Side-on* η^2 peroxo	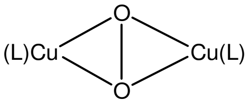 *Side-on* μ- η^2: η^2-peroxo
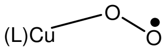 *End-on* η^1 superoxo	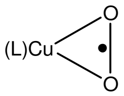 *Side-on* η^2 superoxo

Figure 1.33. Most relevant RMOS involved in DNA damage, in mono- and dicopper complexes.

1.6.2 – Factors influencing the oxidative pathway.

Apart from the nature of the metal center, other factors affect the cleavage ability of the nuclease. Metal centers control mainly the redox potential, the formation of reactive species and DNA binding ability. Ligands act as the unit of functional regulation. In some cases, the ligands alone are responsible to a large degree for the overall cleavage ability of specific metallonucleases.[34,159,163,184,191–196]

Therefore, in copper based artificial nucleases, the redox potential is a useful index for the evaluation of the oxidative cleavage ability. Normally, the DNA-cleavage ability of Cu-based nucleases is highly dependent on the Cu(II)/Cu(I) redox potentials.[129,159,163,197,198]

Another of the factors to take into account is the charge of the complex. Since DNA is negatively charged, the higher positive charges of metallonucleases could enhance their affinity to DNA through electrostatic forces and thus increase their DNA-cleavage ability.[199,200]

Ligand planarity is another favorable factor for improving DNA-cleavage ability of metallonucleases. Planar heteroaromatic structures such as phenanthroline (phen) can strengthen the DNA binding potential of metallonuclease by intercalation and π-π interactions between the aromatic parts of the nucleobases and of the ligand. Larger planar structures can enhance the DNA-cleavage efficiency. On the other hand, steric factors can also influence the metallonucleases DNA binding abilities and as a consequence their efficiency and selectivity.[129,152,163,201–205]

Another factor influencing metallonucleases with oxidative cleavage is the concentration of co-factors. Indeed, in order to perform the oxidative DNA cleavage in copper nucleases, oxidizing cofactors such as $KHSO_5$ or H_2O_2, or reductants like ascorbic acid or 3-mercaptopropionic acid (MPA), are often necessary to produce the reactive species which will cleave the DNA, either ROS or MROS.[126,127,129,145,163]

1.6.3 – Artificial Copper nucleases.

In this context, copper complexes have been widely studied as artificial nucleases, mainly because of its versatility, bioavailability, low toxicity and high activity, its biologically relevant redox properties and its high affinity for nucleobases.[139,148,160]

The first copper complex to be recognised as an artificial nuclease was described by Sigman et al in 1979. It was a bis(1,10-phenanthroline)copper(I), which when activated either with hydrogen peroxide or with molecular oxygen and a reducing agent, showed DNA cleavage activity after binding to the minor groove of the DNA.[206,207] Since then the nuclease activity of this type of complexes, and the relationship between the structures of the complexes and their activity has been a recurring issue of study.[148,208–211]

From the beginning it became clear that the ligand was an essential issue to take into account in the design of metallonucleases. When Sigman and co-workers compared the activity of the bis(1,10-phenanthroline)copper(I) complex with the nuclease activity of its analogous with methyl substituted phenanthroline ligands, it was seen that if the methyl groups were in positions 2 and 9 the steric hindrance prevented a strong interaction between the complex and the DNA.[212]

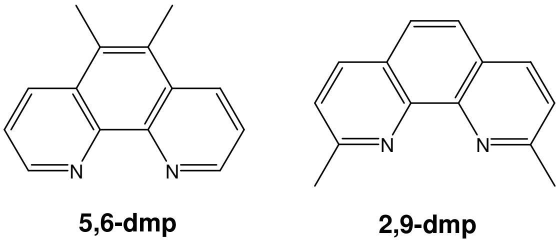

Figure 1.34. Phenanthroline derivative ligands used to study the effect of ligand substitution in copper nuclease models.

Furthermore, these steric effects between the two ligands bound to the same copper atom destabilized and prevented the formation of the reactive intermediate, a planar Cu(II) species, and thus this complex lacks of nuclease activity. On the other hand, when the methyl substituents were at positions 5 and/or 6, they didn't interfere with the bonding to the DNA or with the redox cycle, and the nuclease activity was not affected.

Other studies focused on the effect of the copper atom coordination. In order to highlight the environment of the metal ion in artificial copper nucleases, copper(II) complexes of cyclen and analogous cyclen derivatives, where the nitrogen coordinating atoms of the original cyclen macrocycle have been substituted by other heteroatoms, have been studied as oxidative DNA cleavers in presence of a reductive agent.[192,213] The results show a relevant dependence between the complex performance and the number and type of heteroatoms. Indeed, in these cases, substitution of one nitrogen atom of the cyclen for an oxygen atom notably increases the complex activity. Furthermore, not only did the number of different heteroatoms modify the complex activity, but also the position of these heteroatoms in the macrocyclic backbone. These studies emphasise again the high effect that the ligand plays on the complex activity.

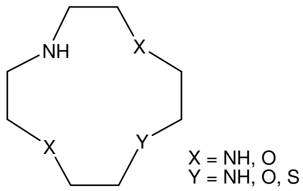

Figure 1.35. Family of macrocyclic ligands, each bearing different heteroatoms.

1.6.4 – Multinuclear nuclease systems.

Since many cleaving enzymes contain two or three metal centres at their active site that operate in a synergistic and cooperative fashion to cleave their substrates, it is not surprising that the last decades have seen intense interest in the development of bi- and trinuclear metal complexes as a route to generating more active synthetic cleavage agents.[11,12,28,33,34,129,163,167,187,214–217] Indeed, multinuclearity is one of the successful strategies to increase the efficiency and selectivity of the metallonucleases. This cooperative effect between metal centers can facilitate the formation of the active intermediate involving multinuclear species, and also plays an important role in DNA recognition. Many studies have focused in the cooperative effect of multinuclear complexes.[10–12,32,34,129,163,217,218]

As an example, Guo and coworkers synthesized two dinuclear copper complexes and they were tested as oxidative nuclease models in presence of mercaptopropionic acid (MPA), and compared with their mononuclear and trinuclear analogs. The ligands consisted in one, two or three BPA motifs (BPA = bis(2-pyridylmethyl)amine) linked by an aromatic spacer (see *Figure 1.36*).[219] In order to elucidate the structural dependence of synergy between metal centers in DNA cleavage, the two dinuclear complexes bear aromatic linkers with different geometry, either *meta*- or *para*- xylylene spacers.

Results clearly show that the two dinuclear complexes have a higher DNA cleaving capacity than the mononuclear complex, suggesting a synergy between the two copper centers concerning the cleavage activity.

On the other side, the trinuclear complex [Cu_3(**L50**)Cl_6], despite the fact that it showed the highest DNA binding affinity, showed a lower efficiency than the dinuclear models, being comparable to the mononuclear complex [Cu(**L49**)Cl_2]. This result suggests a quenching effect of the third copper center, possibly due to an alteration of the active motive which leads to an inhibition access of the MROS to the cleaving target.

The difference in the activity between the two dinuclear complexes [Cu_2(**L51**)Cl_4] and [Cu_2(**L52**)Cl_4] is explained through a geometrical dependence of the complexes in the DNA cleavage – the *meta* motif is necessary for both a better DNA binding and also a more efficient O_2 activation, leading to complex **C3** to be more active and thus showing a higher cleaving performance, when compared to the *para* analog (complex **C4**).

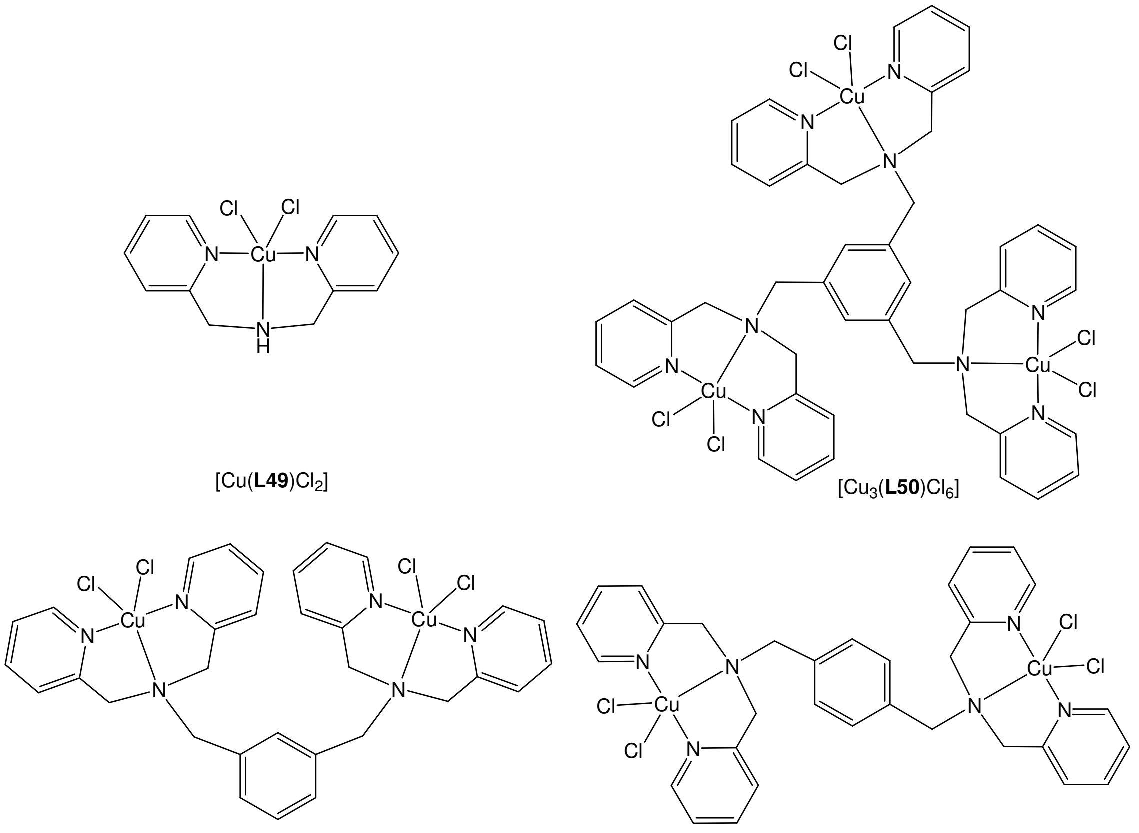

[Cu(**L49**)Cl_2]

[Cu_3(**L50**)Cl_6]

[Cu_2(**L51**)Cl_4]

[Cu_2(**L52**)Cl_4]

Figure 1.36. Mono-, tri- and isomeric dinuclear copper(II) complexes used to study the nuclearity effect by Guo and coworkers. [219] Charges omitted for clarity.

1.6.5 – Macrocyclic ligands in artificial dinuclear Cu nucleases

A widely used strategy in the design of multinuclear complexes is the use of ditopic macrocyclic moieties, either via the use of ligands capable of simultaneously complexing two or more metal centers within a single macrocyclic framework (the macrocyclic strategy) or by linking two or more discrete metal-binding motifs together by spacer units (the spacer strategy). Ditopic macrocyclic ligands are rigid systems which allow a tuning of the intermetallic distances and the disposition of the metallic centers through the control of the macrocycle ring size and the spacer type and geometry.[11,12,34,148,220] Indeed, many studies have focused on establishing a relationship between the structure of the complex and its reactivity as oxidative nuclease mimics.

In a work done by Kandaswamy and coworkers, it has been studied the performance of three dinuclear copper macrocyclic complexes as oxidative nuclease mimics. The three complexes bear different spacers – one of them is aliphatic, and two are aromatics (xylene and naphthalene derivatives).[221]

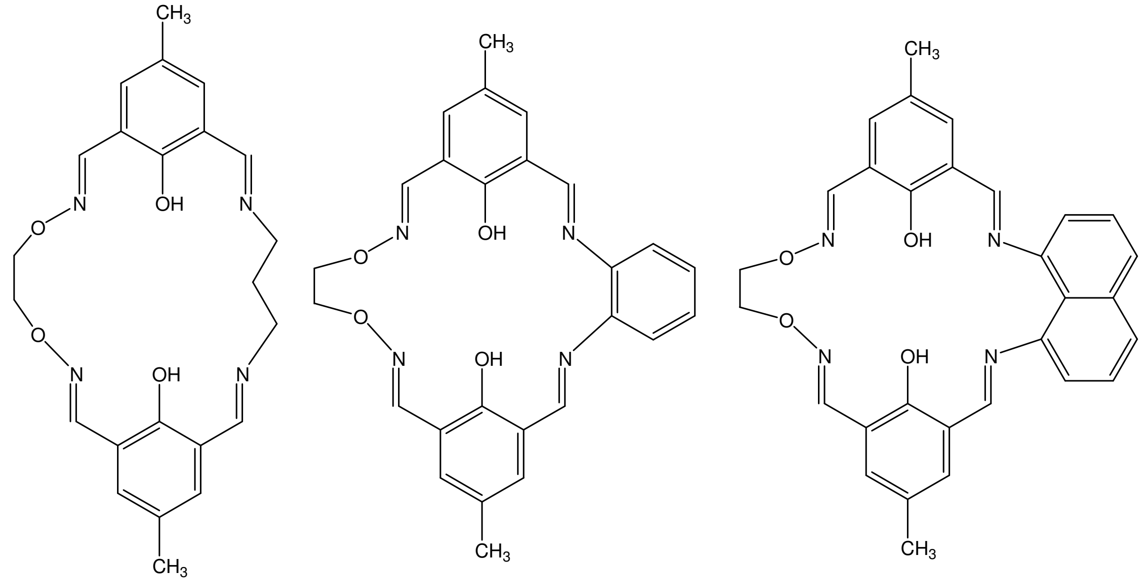

L53 **L54** **L55**

Figure 1.37. Ditopic macrocyclic ligands with different spacers. **L53** aliphatic spacer° **L54** xylene spacer° **L55** naphthalene spacer.

The results of this study show that all three complexes strongly bind DNA through an intercalative mode, and all three complexes show nuclease activity in presence of mercaptoethanol and oxygen. Nonetheless, there is a clear relationship between the nature of the linker and the nuclease activity – the complexes bearing ligands with aromatic spacers **L54** and **L55** are clearly more active than the complex bearing aliphatic spacer **L53**. This difference can be explained through the strength of the binding between the complex and the DNA: complexes with aromatic spacers bind nucleobases through π-π interactions between the aromatic parts of the nucleobases and the ones of the ligand, and thus more strongly than the complex with the aliphatic spacer. This difference in the strength of binding involves a difference in the nuclease performance of the complexes.

Very similar results were obtained by the same group when studying the oxidative nuclease activity of mono and dinuclear copper complexes of similar but acyclic ligands.[193,214]

Analogously to the macrocyclic systems, all complexes bind DNA through intercalation mode. In addition, mono and dinuclear copper complexes of the ligands **L60** and **L65** bearing naphthalene moiety interact with DNA more strongly than the other complexes, and also show a higher nuclease performance. On the other hand, it is interesting to note that, when comparing the nuclease activity of the mononuclear complex bearing a naphthalene moiety and its dinuclear analogous, it is more active the latter, indicating a possible cooperativity between the two metal centers.

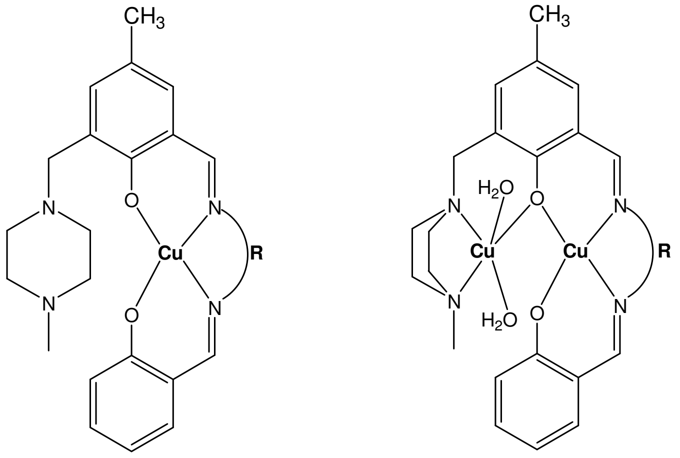

Mononuclear		**Dinuclear**
[Cu(**L56**)]	- $(CH_2)_2$ -	$[Cu_2($**L61**$)(H_2O)_2]^{2+}$
[Cu(**L57**)]	- $(CH_2)_3$ -	$[Cu_2($**L62**$)(H_2O)_2]^{2+}$
[Cu(**L58**)]	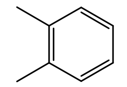	$[Cu_2($**L63**$)(H_2O)_2]^{2+}$
[Cu(**L59**)]	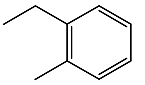	$[Cu_2($**L64**$)(H_2O)_2]^{2+}$
[Cu(**L60**)]	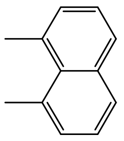	$[Cu_2($**L65**$)(H_2O)_2]^{2+}$

Figure 1.38. General drawing of mono and dinuclear copper(II) complexes of acyclic ligands with different spacers. Charges omitted for clarity.

Hosseini-Yadzi and coworkers sinthesised a series of polymacrocyclic ligands and the corresponding Cu(II) complexes, and studied their nuclease activity using 3-mercaptopropionic acid (MPA) as reducting agent under aerobic conditions.[222,223]

Ligands **L66**, **L67** and **L68** form mononuclear complexes, and ligand **L69** forms a dinuclear copper complex. It was found that the dinuclear complex (with tris-macrocyclic ligand **L69**) was the most active among them, suggesting a synergetic effect between the two copper centers.

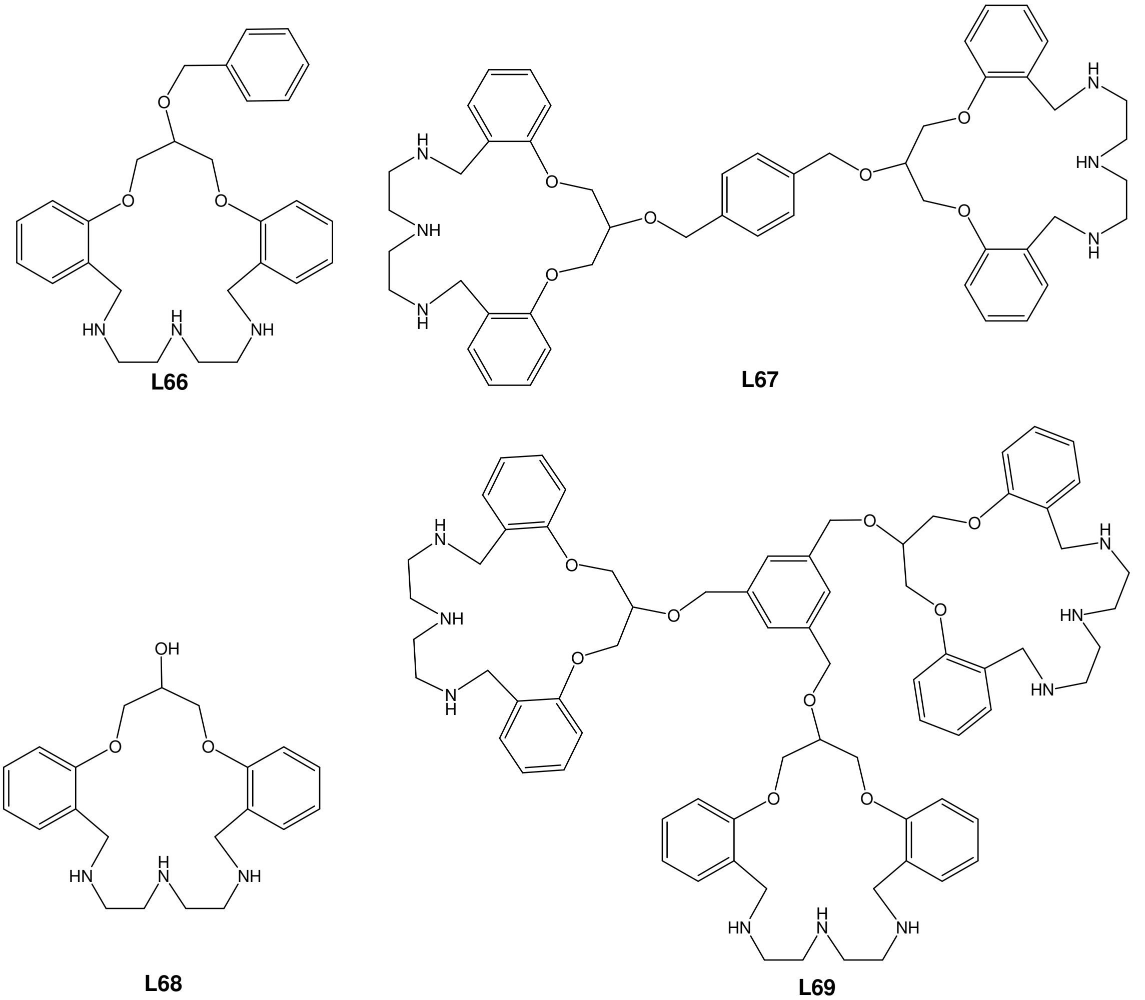

Figure 1.39. Macrocyclic ligands **L66**, **L67**, **L68**, **L69**.

Interestingly enough the complex with the bis-macrocyclic ligand **L67**, though mononuclear, was found to show a higher activity than mononuclear complexes with the monomacrocyclic ligands **L66** and **L68**.

In a recent example, several ditopic macrocyclic ligands differing only on the substituents of the aromatic linker and their corresponding dinuclear copper(II) complexes have been synthesised and their interaction with DNA as well as their nuclease activity, have been tested.[224]

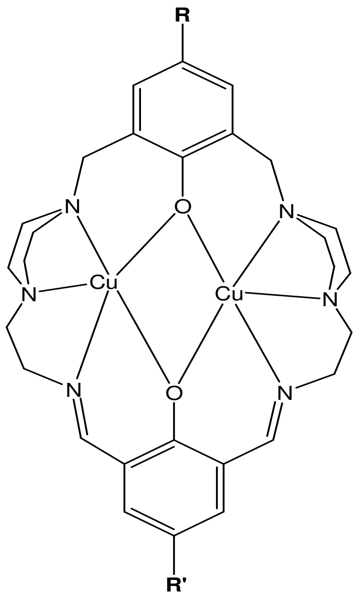

Figure 1.40. Dicopper complexes of macrocyclic ligands with different substituents on the aromatic spacer (R, R' = –Br˚ –CH_3˚ –$C(CH_3)_3$).[224] Charges omitted for clarity.

The complexes interact with DNA through different modes and present nuclease activity through oxidating pathway in presence of H_2O_2. Depending on de substituent in the aromatic linker, the different complexes have different binding modes with DNA. Indeed, the complexes bearing a tert-butyl group bind stronger to DNA, as the binding is enhanced by Van der Waals hydrophobic forces between the ligand and the DNA. On the other hand, the complex with two bromine substituents has the weakest interaction. Not only do the substituents affect the binding mode, but also do the active species in the nuclease oxidative mechanism. It has been proven that three of the complexes cleaved DNA through a peroxo intermediate, and another complex performed the oxidative cleaving through hydroxyl radical species.

Another series of iminic hexaaza macrocyclic ligands and their dicopper(II) complexes have been assayed as nuclease mimics (*Figure 1.41*).[225] In this study, the ligands differed in the number of nitro groups in the benzene pendant arms of the macrocyclic ligand.

The dicopper complexes bind DNA through an intercalative mode. The complex with the ligand **L65** with two nitro groups in the benzyl moiety has the strongest binding. In presence of H_2O_2, all complexes perform DNA cleavage through generation of hydroxyl radicals.

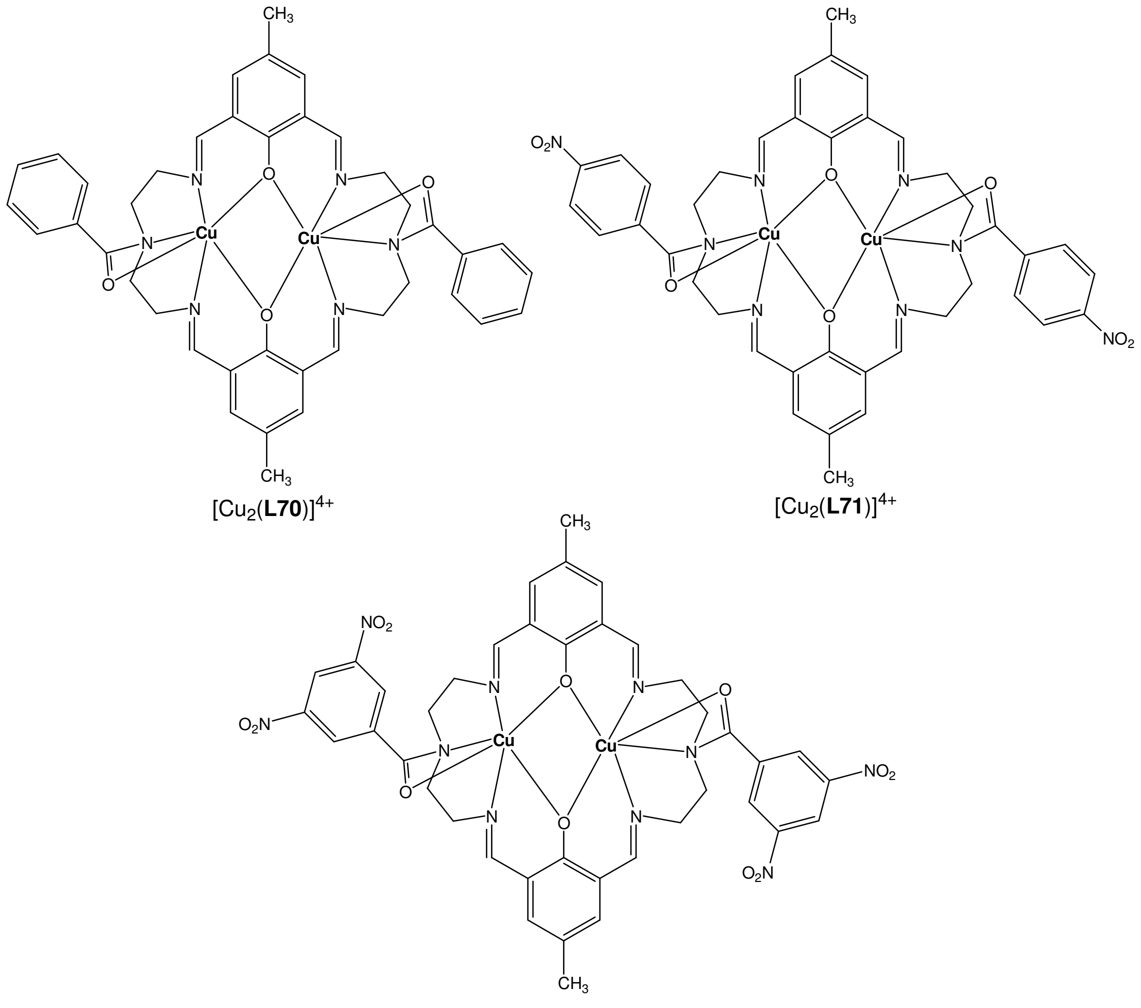

$[Cu_2(\mathbf{L70})]^{4+}$

$[Cu_2(\mathbf{L71})]^{4+}$

$[Cu_2(\mathbf{L72})]^{4+}$

Figure 1.41. Macrocyclic ligands with different number of nitro groups in the benzyl pendant arms.

Many other mono- and polycopper complexes of macrocycilic ligands have been shown to perform nuclease activity towards DNA in presence of an external oxidant,[148,180,181,198,226–231] exposing macrocyclic ligands and their complexes as good mimetic systems, where it is possible to tune many specifications of the ligands, the metallic centers and their environment. All these combined variables will define in turn the complex recognition of the DNA target, their interaction and selectivity, and in the end, the performance of the nuclease.

In view of all that has been mentioned above, and considering the large possibilities within the chemistry of macrocyclic compounds, our research has focused on developing the synthesis and characterization of macrocyclic compounds and the study of the interaction of these compounds towards substrates with biologic relevance.

These studies have led to this work, in which are presented both new recognition studies of macrocyclic derivatives already described in the literature with anionic species, as long as the development of new macrocyclic ligands and complexes and their recognition, binding and nuclease activity towards DNA.

We have focused especially on how subtle differences between different macrocyclic species lead to significant changes in their chemistry.

2. Objectives

The main objective of this work is to study the interactions of macrocyclic entities/species towards different molecules, and how differences in the backbone of the ligand affect the process.

More specifically:

- To study the recognition process of the macrocyclic ligand **L9** towards the following isomeric aromatic diacids: terephthalic acid, isophthalic acid and phthalic acid, and compare the results with other analogous macrocyclic receptors.

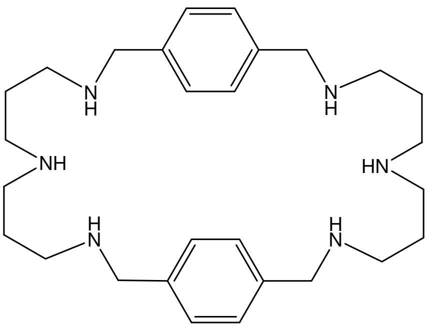

L9

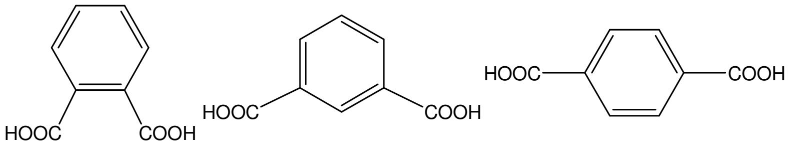

Phthalic acid Isophthalic acid Terephthalic acid

Figure 2.1. Macrocyclic ligand **L9** and the dicarboxylic substrates.

- To synthesise and characterise a new family of macrocyclic ditopic iminic ligands with a central pendant arm. These ligands will differ, in one hand, on the geometry and the length of the aromatic and aliphatic spacer, and on the other hand, on the nature of the central pendant arm.

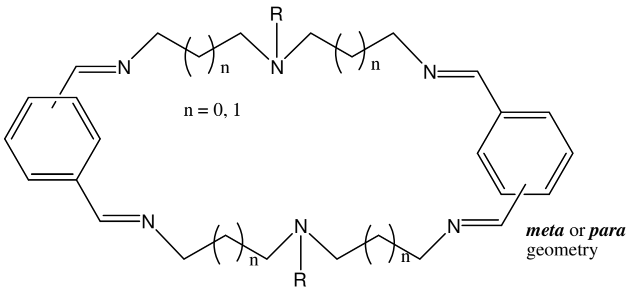

Figure 2.2. General structure of the new family of macrocyclic ligands with pendant arms.

- To synthesise and characterise the corresponding dicopper(I) complexes of these new family of macrocyclic ligands.

- To study the nuclease activity towards DNA of the pyridyl pendant family of dicopper complexes, paying special attention to the relationship between the geometry of the ligand and the performance of the complexes.

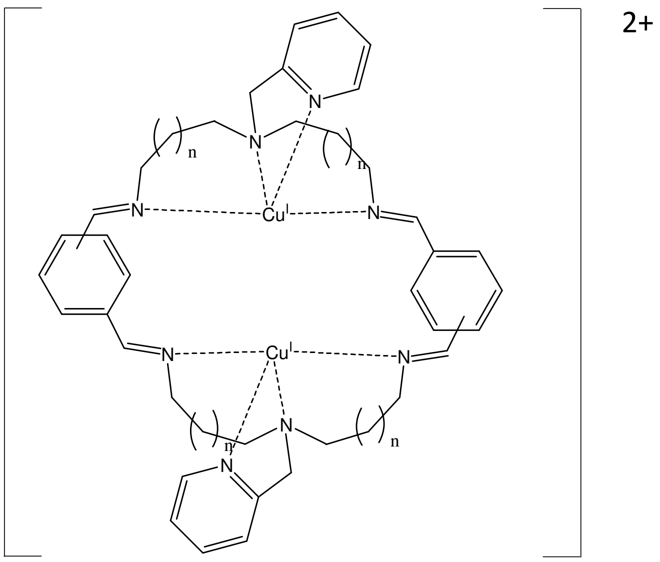

Figure 2.3. General structure of the dicopper(I) complexes of the synthesized macrocyclic ligands with pyridyl pendant arms.

3. Methodology

3.1 – Materials.

For the potentiometric studies, NMe_4Cl (purum > 98%), phthalic acid (ACS reagent > 99.5%), isophthalic acid (purum, 99%), and terephthalic acid disodium salt (purum 96%) were commercial products obtained from Aldrich and were used without further purification. Hydrochloric acid solution 0.1 mol/L and tetramethylammonium hydroxide solution 10% were purchased from Merck. The degasified solution of tetramethylammonium hydroxide was standardized with potassium hydrogen phthalate. Ligand **L9** was prepared as a colourless hexabromide salt (**L9**·6HBr) according to previously published procedures.[105]

For the synthesis of ligands and complexes, all reagents used were obtained from Aldrich Chemical Co. and were used without further purification unless otherwise stated. Solvents were purchased from SDS, and they were purified and dried either by passing them through an activated alumina purification system (MBraun SPS-800) or by conventional distillation techniques. Preparation and manipulation of Cu(I) complexes were carried out in a drybox (MBraun, N_2, or Ar) with O_2 and H_2O concentrations <1.0 ppm.

For the interaction studies of the dicopper(I) complexes with DNA, Calf thymus DNA (CT DNA), EDTA (ethylenediaminotetraacetic acid), and Tris-HCl (tris-(hydroxymethyl)aminomethane-hydrochloride) used in the CD study were obtained from Sigma (Madrid, Spain). pBR322 plasmid DNA used in the EM and AFM studies was obtained from Boehringer Mannheim (Germany). Ultrapure agarose was obtained from ECOGEN (Barcelona, Spain). HEPES (N–2–hydroxyethyl piperazine–N'–2–ethanesulfonic acid) was obtained from ICN (Madrid).

3.2 – Physical methods.

HRMS analyses were recorded on a Waters LCT Premier liquid chromatograph coupled time-of-flight mass spectrometer (HPLC/MS-TOF) with electrospray ionization (ESI). MS analyses were recorded on an esquire 6000 ESI ion trap LC/MS (Bruker Daltonics) equipped with an electrospray ion source.

The ESI-MS experiments were performed on a Navigator LC/MS chromatograph from Thermo Quest Finigan, using acetonitrile as a mobile phase.

Elemental analyses were performed using a CHNS-O EA-1108 elemental analyzer from Fisons.

Square wave voltammetry experiments were performed in an IJ-CambriaHI-660 potentiostat using a three electrode cell. Glassy carbon disk electrodes (3 mm diameter) from BAS were used as working electrode, platinum wire was used as auxiliary, and SSCE was used as the reference electrode.

IR spectra of solid samples were taken in a Mattson-Galaxy Satellite FT-IR spectrophotometer using a MKII Golden Gate single reflection ATR system. IR solution experiments were performed on a FTIR spectrometer Thermo Nicolet 5700, with DLaTGS and MCT detectors with KBr windows Omnicell from Specac.

3.2.1. Potentiometric titrations.

Potentiometric titrations were used to obtain the protonation constants of ligand ans substrates as long as the complexation constants of the supramolecular complex **L9**:diacid.

Potentiometric measurements were conducted in a jacketed cell thermostated at 25.0°C and were kept under an inert atmosphere of purified and humidified argon. For the potentiometric measurements, a Crison pHmeter (Model 2002) was used, equipped with a glass electrode and a Ag/AgCl reference electrode with saturated KCl as internal solution. The volume of titrating agent to be added to the reaction mixture was controlled by means of an electronic Crison burette with a nominal volume of 1 mL. The support electrolyte used to keep ionic strength constant at 0.10 M was NMe_4Cl. The combined glass electrode (Metrohm 6.0255.100) was calibrated as a hydrogen concentration probe by titrating known amounts of HCl with CO_2-free NMe_4OH solutions and by determining the equivalent point by Gran's method[232,233] that allows to calculate the standard potential (E_0) and the ionic product of water (pKw). Log Kw for the system, defined in terms of $\log([H^+][OH^-])$, was found to be -13.83 at 298.1 K in 0.1 mol/L NMe_4Cl and was kept fixed during refinements.

Acid dissociation constants for the phthalic and isophthalic acids were determined under exact conditions employed in this work and were found to agree well with data from the literature.[234] Because of its insolubility on the medium used, acid dissociation constants for the terephthalic acid were obtained from the literature.[235]

Potentiometric measurements of solutions either containing the ligand or the ligand plus equimolecular amounts of phthalic acid, isophthalic acid, or terephthalic acid were run at concentrations of 2.0×10^{-3} M and ionic strengths of $\mu = 0.10$ M (NMe_4Cl). At least 10 points per neutralization of every hydrogen ion equivalent were acquired, repeating titrations until satisfactory agreement was obtained. A minimum of three consistent sets of data was used in each case to calculate the overall stability constants and their standard deviations. The range of accurate pH measurements was considered to be 2-12. Equilibrium constants and species distribution diagrams were calculated using the program HYPERQUAD.[236]

3.2.2. NMR spectroscopy

NMR spectra of the different compounds were measured using a Bruker DPX 200 MHz, a Bruker DXP 300 MHz, or a Bruker DRX 400 MHz instrument.

For the interaction studies between the **L9** ligand and the diacid species ^1H NMR spectra in D_2O solution at different pH values were recorded at 298 K in a Bruker 500 MHz spectrometer. The peak positions are reported relative to the residual HOD at 4.79 ppm. Small amounts of 0.01 mol·dm^{-3} NaOD or DCl solutions were added to a solution of the ligand to adjust the pD. The pH was calculated from the measured pD values using the following relationship: pH=pD-0.40. (13) Self-diffusion experiments were performed using the BPLED pulse sequence using a diffusion time of 150 ms and an LED delay of 5 ms. For each experiment, sine-shaped pulsed-field gradients with a duration of 1.5 ms followed by a recovery delay of 100 µs were incremented from 2% to 95% of the maximum strength in 16 equally spaced steps. Diffusion coefficients were obtained by measuring the slope in the following linear relationship: $\ln(A_g/A_o) = -\gamma^2 g^2 \delta^2 (4\Delta - \delta)D$ where A_g and A_o are the signal intensities in the presence and absence of PFG, respectively, is γ the gyromagnetic ratio (rad s g^{-1}), g is the strength of the diffusion gradients (gauss cm^{-1}), δ is the length of the diffusion gradient (s), and Δ is the time separation between the leading edges of the two diffusion pulsed gradients (s).

3.2.3. Theoretical calculations.

The molecules studied theoretically were manually built using the program MacroModel[237] and were fully minimized with the AMBER* force field.[238,239] A conformational analysis was done for each of the molecules to obtain the most representative conformation. A Metropolis MonteCarlo method was used, and the most stable conformation was considered. The geometry of each molecule computed was fully optimized using Gaussian-98 program.[240] The theoretical calculation was carried out at MP2 level, and the electrostatic potential was computed using the 6-31G* basis set with the Merz-Singh-Kollman population analysis (pop = mk). The module RESP implemented in the AMBER 7 package was used to compute a final set of atomic charges for each molecule. The atomic charges were needed for the building of the molecules in AMBER.[241] In this study, the AMBER force field was used with a set of parameters gaff[242] implemented in the AMBER 7.0 package. Each molecule was first minimized in vacuum, and then the system was gradually heated from 1 to 298 K during 30 ps and was equilibrated for 70 ps at 298 K. This procedure was followed by another equilibration for 100 ps. The productive run was then performed in gas phase at 298 K using a time step of 1 fs and a length of 1 ns.

3.2.4. X-ray Diffraction Studies.

Crystals of **L74, 2$(CF_3SO_3)_2$, 4$(SbF_6)_3$, 4$(PF_6)_3$, 5$(CF_3SO_3)_3$, 6$(CF_3SO_3)_3$**, **7$(CF_3SO_3)_2$, 8$(SbF_6)_3$** and **9$(CF_3SO_3)_2$** were obtained as described in the synthetic procedure.

Crystals of **L74, 2$(CF_3SO_3)_2$, 4$(SbF_6)_3$, 5$(CF_3SO_3)_3$, and 6$(CF_3SO_3)_3$ 7$(CF_3SO_3)_2$, 8$(SbF_6)_3$** and **9$(CF_3SO_3)_2$** were mounted on a nylon loop and used for X-ray structure determination. The measurements were carried out on a Bruker Smart Apex CCD diffractometer. Single crystals of **4$(PF_6)_3$** were coated with polyfluorether oil and mounted on a glass fiber. The data were collected on a Nonius Kappa diffractometer with a CCD array detector at 173(2) K. Mo Kα radiation was used for all measurements (λ= 0.71073 Å).

The measurements were made in the range 2.29 to 28.34º for θ for the complexes **6$(CF_3SO_3)_3$**, **7$(CF_3SO_3)_2$, 8$(SbF_6)_3$** and **9$(CF_3SO_3)_2$**, from 1.88º to 28.37º for the ligand **L74**, from 2.14º to 29.35º for **4$(SbF_6)_3$** and from 1.94º to 28.23º for complexes **2$(CF_3SO_3)_2$** and **5$(CF_3SO_3)_3$.** Full-sphere data collection was carried out with ω and ϕ scans.

For **6$(CF_3SO_3)_3$** a total of 51292 reflections were collected of which 16109 [R(int) = 0.3133]were unique. For **L74** a total of 85514 reflections were collected of which 16923 [R(int) = 0.0706] were unique. For **4$(SbF_6)_3$** a total of 42888 reflections were collected of which 17338 [R(int) = 0.1404] were unique. For **2$(CF_3SO_3)_2$** a total of 79370 reflections were collected of which 12917 [R(int) = 0. 0461] were unique. For **5$(CF_3SO_3)_3$** a total of 85514 reflections were collected of which 16923 [R(int) = 0.0706] were unique. For **7$(CF_3SO_3)_2$**, a total of 77760 reflections were collected of which 12442 [R(int)=0.0443] were unique. For **8$(SbF_6)_2$** a total of 75425 reflections were collected of which 12135 [R(int) = 0.0379] were unique. For **9$(CF_3SO_3\ )_2$** a total of 35011 reflections were collected of which 10 688 [R(int) = 0.0958] were unique.

In all the cases, the data collection was executed using the SMART program version 5.631 (Bruker AXS 1997-02). The data reduction was made by the SAINT program + version 6.36A (Bruker AXS 2001). Structure solution and refinement were done using SHELXTL program version 6.14 (Bruker AXS 2000-2003).The structures were solved by direct methods and refined on F^2 using full-matrix least-squares techniques.21 The non-hydrogen atoms were refined anisotropically. The H-atoms were placed in a geometrically optimized arrangement and treated with a riding model, except the OH hydrogen atoms for the **2(CF_3SO_3)$_3$**, which are refined without constraints.

For the structure **5(CF_3SO_3)$_3$** and **8(SbF_6)$_2$** a considerable amount of electron density that is attributable to partially disordered solvent water molecules was removed with the SQUEEZE option of PLATON.[243] Structures **2(CF_3SO_3)$_3$**, **5(CF_3SO_3)$_3$**, and **6(CF_3SO_3)$_3$** present disorder on one of the CF_3SO_3 counterions. For the structure **4(PF_6)$_3$,** SAME-restraints were used to refine solvate molecules (THF and CH_3OH).

Further crystallographic experimental details are given in *Table 3.1*.

3.2.5. Circular dichroism – CD Spectroscopy.

All compounds were dissolved in an aqueous solution with 20% DMSO prepared with milli-Q water (4×10^{-4} M). The use of DMSO is to facilitate the dissolution of compounds to be evaluated. The stock solutions of complexes were freshly prepared before use. A stock solution (20 µg/mL) of CT DNA in TE buffer solution (50 mM NaCl, 10 mM tris-(hydroxymethyl)aminomethane hydrochloride (Tris-HCl), and 0.1 mM H_4edta, pH 7.4) was prepared and kept at 4 ºC before use. The final concentration of DNA was determined by measuring the absorbance at 260 nm in a UV-vis spectrophotometer. The samples were

Table 3.1. Cristallographic data for the crystallized ligands and complexes.

	L74	**$4(SbF_6)_3$**	**$4(PF_6)_3 \cdot 2.5\ THF \cdot 0.5\ H_2O \cdot 0.75\ CH_3OH$**	**$2(CF_3SO_3)_2 \cdot CH_3CN$**	**$5(CF_3SO_3)_3 \cdot 2H_2O$**	**$6(CF_3SO_3)_3 \cdot 1Et_2O$**	**$7(CF_3SO_3)_2$**	**$8(SbF_6)_2$**	**$9(CF_3SO_3)_2$**
empirical formula	$C_{38}H_{42}N_6O_2$	$C_{54}H_{59}Cu_3F_{18}N_{12}Sb_3$	$C_{64.75}H_{84}Cu_3F_{18}N_{12}O_{3.75}P_3$	$C_{48}H_{51}Cu_2N_9O_8F_6S_2$	$C_{66}H_{76}Cu_3F_9N_{12}O_{14}S_3$	$C_{55}H_{76}Cu_3N_{12}F_9O_{10}S_3$	$C_{46}H_{58}Cu_2F_6N_8O_7S_2$	$C_{42}H_{51}Cu_2F_{12}N_9Sb_2$	$C_{40}H_{43}Cu_2F_6N_9O_6$
formula weight	614.52	1774.00	1715.97	1163.16	1719.19	1523.08	1140.20	1280.50	1061.03
temperature, K	300(2)	100(2)	100(2)	100(2)	300(2)	373(2)	100(2)	100(2)	100(2)
wavelength, Å	0.71073	0.71073	0.71073	0.71073	0.71073	0.71073	0.71073	0.71073	0.71073
Crystal system	monoclinic	Triclinic	Triclinic	Monoclinic	Triclinic	Triclinic	Monoclinic	Monoclinic	Triclinic
Space group	P2(1)	$P\bar{1}$	$P\bar{1}$	P21/n	$P\bar{1}$	$P\bar{1}$	P21/n	P21/c	$P\bar{1}$
a, Å	13.357(5)	12.008(18)	11.4563(3)	15.203(3)	15.72(2)	11.383(6)	19.833(6)	11.9994(9)	10.7658(11)
α, deg	90	109.82(3)	80.620(2)	90	104.45(3)	84.485(10)	90	90	110.323(2)
b, Å	35.402(13)	15.72(2)	17.6766(6)	18.211(3)	16.73(2)	14.732(8)	12.470(4)	24.7847(18)	13.4453(14)
β, deg	101.776(7)	104.97(3)	81.518(2)	99.371(3)	111.79(3)	80.547(9)	111.172(5)	90	94.852(2)
c, Å	14.629(6)	20.01(3)	36.255(1)	19.084(3)	18.04(3)	20.652(11)	21.921(6)	16.6745(12)	16.5660(17)
γ, deg	90	97.76(3)	82.902(2)	90	106.39(3)	86.199(10)	90	90	98.578(2)
Volume, Å^3	6772(4)	3328(9)	7127.1(4)	5213.3(16)	3878(10)	3396(3)	5055(3)	4931.7(6)	2199.3(4)
Z	8	2	4	4	1	2	4	4	2
ρ (g/cm3)	1.205	1.770	1.599	1.482	1.462	1.489	1.498	1.725	1.587
R ^{a} [$I > 2\sigma(I)$]	0.0563	0.1057	0.0869	0.0399	0.0818	0.0898	0.0797	0.0473	0.0568
wR ^{b}	0.1371	0.2698	0.1976	0.0617	0.2416	0.2699	0.2612	0.1230	0.1155

${}^aR = \sum(F_0 - F_c) / \sum F_0$; ${}^bwR = [\sum(w(F_0^2 - F_c^2)^2) / \sum(w\,F_0^4)]^{1/2}$

prepared by addition of aliquot parts of the Cu-complex solutions to stock solutions of CT DNA in TE (5mL). The amount of complex added to the DNA solution was designated as r_i (the input molar ratio of Cu to nucleotide).[244] This parameter reflects the proportion between the dicopper complex and the base pair of DNA (mol of compound/mol of nucleotide). The CD spectra of DNA in the presence or absence of Cu(I) complexes (DNA concentration 20 µg/mL, molar ratios r_i = 0.10, 0.30, 0.50) were recorded at room temperature, after 24h incubation at 37 ºC, on a JASCO J-720 spectropolarimeter with a 450 W xenon lamp using a computer for spectral subtraction and noise reduction. As a blank, a solution in TE of free native DNA was used. Each sample was scanned twice in a range of wavelengths between 220 and 330 nm. The CD spectra drawn are the average of three independent scans. The data are expressed as average residue molecular ellipticity (θ) in deg·cm^2·dmol $^{-1}$.

3.2.6. EM in Agarose Gel.

pBR322 plasmid DNA of 0.25 µg/µL (8.84 x 10^{-8} M) concentration was used for the experiments. Stock solutions of the Cu complexes (4 x 10 $^{-4}$ M) in milli-Q water with 20% DMSO were freshly prepared before use. Aliquot parts of 21 µL of Cu complex solutions were added to aliquot parts of 3µLof the pBR322DNA in 20 µL of a TE (Tris-H_4edta, Tris-(hydroximethyl)aminomethaneethylendiaminetetracetic acid) buffer solution (50 mM NaCl, 10 mM Tris-HCl, 0.1 mM H_4edta, pH 7.4). The samples were prepared with an input molar ratio of the complex to nucleotide r_i = 6.9. The reaction mixture was incubated at 37ºC for 2 h, and then 4 µL of charge marker were added to aliquots parts of 20 µL of the adduct complex/DNA. The mixtures were electrophoretized in agarose gel (1% in TBE buffer, Tris-borate-EDTA) for 5 h at 1.5 V/cm. Afterward, the DNA was dyed with ethydium bromide solution (0.5µg/µL in TBE) for 20 min. A sample of free DNA was used as a control. The experiment was carried out in an ECOGEN horizontal tank connected to PHARMACIA GPS 200/400 variable potential power supply.

H_2O_2 (1 µL, 33% w/v) was always added after incubation to the reaction samples prepared as described above. Samples with H_2O_2 were run at room temperature for different times (t_1 = 3 min$^{\circ}$ t_2 = 30 min) and then quenched and analyzed according to the procedures described above. A control experiment with H_2O_2 in the absence of Cu complexes was included (see **Figure A3.16**, Supporting Information).

Experiments under inert atmosphere were carried out using Schlenk techniques. Solvents for the preparation of complex solutions were degassed prior to the dissolution of the complex under nitrogen. Eppendorfs containing the DNA and buffer solutions were submitted to vacuum and left under N_2 atmosphere before the addition of the complex solution. Eppendorfs were tightly sealed with parafilm in the nitrogen atmosphere and incubated at 37ºC for 2 h.

3.2.7. Atomic Force Microscopy, AFM.

pBR322 plasmid DNA of 0.25 µg/µL (8.84×10^{-8} M) of concentration was used for the experiments. Stock Cu complex solutions (4×10^{-4} M) in milli-Q water with 20% DMSO were freshly prepared before use. Aliquot parts of 7 µL of these solutions were added to aliquots parts of 1 µL of the pBR322 DNA in 50 µL of a 40 mM HEPES buffer solution (HEPES (N-2-hydroxyethyl piperazine-*N′*-2-ethanesulfonic acid), 10 mM $MgCl_2$, pH = 7.4). The samples were prepared with an input molar ratio of the complex to nucleotide r_i = 6.9. The different solutions as well as Milli-Q water were passed through 0.2 nm FP030/3 filters (Scheicher & Schueell GmbH, Germany) to provide a clear background when they were imaged by AFM. The resulting solutions were incubated for 2 h at 37 ºC. The samples were imaged in a Nanoscope III multimode atomic force microscope (Digital Instrumentals Inc., Santa Barbara) operating in tapping mode.

Samples were treated after incubation with 1 µL of H_2O_2 (33% w/v) for different times and then imaged according to the procedures described above.

3.3 – Synthetic procedures.

3.3.1. Ligand precursor Synthesis.

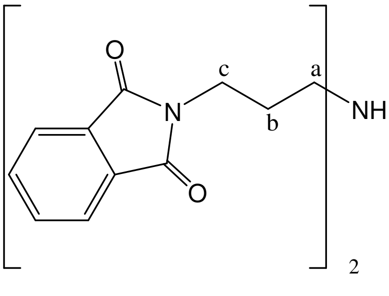

1,7-Diphthalimido-4-azaheptane. (ftNC$_3$H).This compound was synthesized by a procedure similar to that described for **ftNC$_2$H** (see below), but using *N*-(3-aminopropyl)-1,3-propanediamine (14.3 mL, 0.1 mol) and phthalic anhydride (33.2 g, 0.2 mol) in 160 mL of glacial acetic acid. Yield: 35.54 g (91%). ^{1}HNMR (200MHz,$CDCl_3$)δ(ppm): 1.92 (quint, J = 6 Hz,4H,Hb), 2.73 (t, J = 6 Hz, 4H, Ha), 3.75 (t, J = 6Hz, 4H, Hc), 7.64-7.82 (m, 8H, arom). FT-IR ν(cm^{-1}): 1701 (C=O), 1395 (CO–N), 718 (C–H ft), 531 (C–H ft).

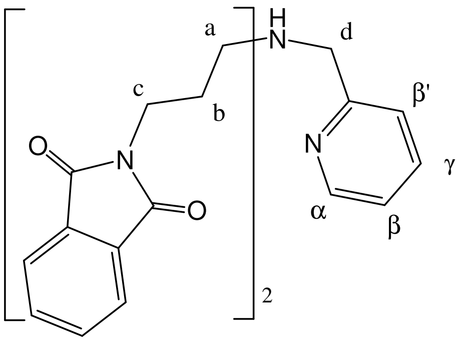

4-(2-Pyridylmethyl)-1,7-diphthalimido-4-azaheptane (ftNC$_3$py).A mixture of **ftNC$_3$H** (9.85g, 0.025 mol), 2-(chloromethyl)pyridine hydrochloride (5.01 g, 0.030mol), Na_2CO_3 (6.58g, 0.062 mol), and 150 mg of tetrabutylammonium bromide in 450 mL of acetonitrile was refluxed for 48 h. The solvent was then evaporated, and the dry residue was treated with H_2O and extracted with dichloromethane (3 x 100 mL). This extract was dried with anhydrous $MgSO_4$ and evaporated to give a solid, which was recrystallized in methanol. Yield: 7.59 g (62%). ^{1}H NMR (200MHz,$CDCl_3$) δ (ppm): 1.83 (quint, J= 7Hz, 4H, Hb), 2.56 (t, J=7Hz, 4H, Ha), 3.70 (s, 2H, Hd), 3.70 (t, J=7Hz, 4H,Hc), 7.0-7.1 (m, 1H,Hβ), 7.4-7.8 (m, 10H, arom + Hβ' + Hγ), 8.35-8.45 (m, 1H,Hα). FT-IR *ν* (cm^{-1}): 1702 (C=O), 1590 (C=C py), 1467 (C=C), 1396 (CO–N), 753 (C–H py), 716 (def C–H ft), 614 (C–H py), 530 (def C–H ft). MS (m/z): 483.3 (MH$^+$). Anal. Calcd (%) for $C_{28}H_{26}N_4O_{43}$ 0.5H_2O (MW = 491.54 g·mol^{-1}): C, 68.42˚ N, 11.40˚ H, 5.54. Found: C, 68.50˚ N, 11.42˚ H, 5.76.

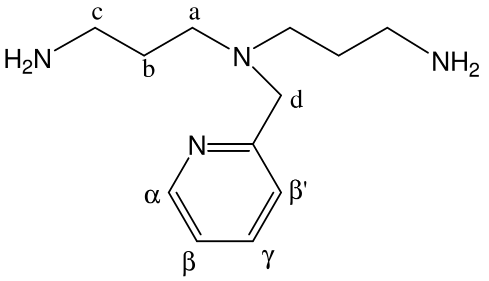

5-(2-Pyridylmethyl)-1,5,9-triazanonane (H$_2$NC$_3$py). A mixture of **ftNC$_3$py** (3,67 g, 7.57mmol) and hydrazine monohydrate (5.0 mL, 100 mmol) in 170 mL of ethanol and 35 mL of chloroform was allowed to react at room temperature for 24 h. The white solid was then filtered off, and the filtrate was evaporated under reduced pressure. A total of 150 mL of chloroform was added, and the solution was stirred for 24 h more, then filtered again, and evaporated to dryness to obtain a product as a yellow oil. Yield: 0.85 g (50%). ^{1}H NMR (200 MHz, $CDCl_3$) δ(ppm): 1.2-1.5 (4H, NH_2), 1.59 (quint, J = 7Hz, 4H, Hb), 2.50 (t, J= 7Hz, 4H, Ha), 2.68 (t, J = 7Hz, 4H,Hc), 3.68 (s, 2H,Hd), 7.00-7.15 (m, 1H,Hβ), 7.35-7.45 (m, 1H,Hβ'), 7.50-7.70 (m, 1H,Hγ), 8.0-8.5 (m, 1H,Hα). FT-IR *ν* (cm^{-1}): 3362, 3285 (NH_2), 2930, 2855, 2812 (C–H), 1589 (C=C py), 1568 (–NH_2), 1471, 1432 (– CH_2 –), 755 (def C–H py), 615 (C–H py).

1,5-Diphthalimido-3-azapentane (ftNC$_2$H). This compound was obtained as described in the literature[245] using diethylenetriamine (11.20 mL, 0.1 mol), phthalic anhydride (30.54 g, 0.2 mol), and 160 mL of acetic acid. Yield: 31.25 g (86%). ^{1}H NMR (200 MHz, CDCl$_3$) δ(ppm): 1.50 (s, 1H, N-H), 3.00 (t, J = 6 Hz, 4H, Ha), 3.81 (t, J = 6 Hz, 4H, Hc), 7.6-7.8 (m, 8H, arom). FT-IR ν(cm^{-1}): 3328 (N-H), 2943, 2868 (C–H), 1702 (C=O), 1393 (CO–N), 716 (C–H ft), 531 (C–H ft).

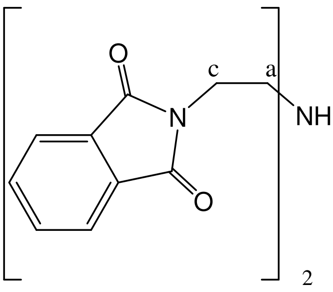

3-(2-pyridylmethyl)-1,5-diphthalimido-3-azapentane (ftNC$_2$py). A mixture of **ftNC$_2$H** (10.00 g, 0.0275 mol), 2-pyridinecarboxaldehyde (2.65 mL, 0.0275 mol), and sodium triacetoxyborohydride (8.52 g, 0.040 mol) in 100 mL of 1,2-dichloroethane was stirred under nitrogen atmosphere for 12 h. Then 100 mL of 2 M NaOH solution was added. The organic layer was extracted, and the aqueous phase was washed with 100 mL of dichloromethane twice. The extract was dried over sodium sulfate and evaporated to dryness. The product was purified through recrystallization with methanol. Yield: 8.21 g (66%). ^{1}H NMR (200 MHz,CDCl$_3$) δ(ppm): 2.83 (t, J = 6Hz, 4H,Ha), 3.75 (t, J = 6Hz, 4H,Hc), 3.83 (s, 2H, Hd), 6.8-7.0 (M, 1H, Hβ), 7.0-7.2 (m, 2H, Hβ' + Hγ), 7.6-7.8 (m, 8H, arom), 8.3-8.4 (m, 1H, Hα). FT-IR ν (cm^{-1}): 1699 (C=O), 1592 (C=C py), 1466 (C=C), 1433 (–CH$_2$–), 1394 (CO–N), 756 (C–H py), 714 (C–H ft), 616(C–H py), 529 (C–H ft). Anal. Calcd (%) for $C_{26}H_{22}N_4O_4 \cdot 0.6\ H_2O$ (MW = 465.29 g·mol^{-1}): C, 67.12˚ N, 12.04˚ H, 5.03. Found: C, 67.30˚ N, 12.09˚ H, 5.42.

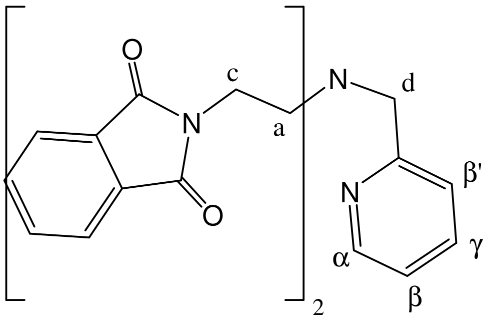

4-(2-pyridylmethyl)-1,4,7-triazaheptane(H$_2$NC$_2$py).The procedure was analogous to that used for the deprotection of **ftNC$_3$py**, using **ftNC$_2$py** (10.00 g, 0.022 mol) and hydrazine hydrate (14.0 mL, 0.283 mol) in 500 mL of ethanol and 100 mL of chloroform. Yield: 1.96 g (46%). ^{1}H NMR (200 MHz, CDCl$_3$) δ(ppm): 2.63 (t, J = 6 Hz, 4H, Ha), 2.82 (t, J = 6 Hz, 4H, Hc), 3.79 (s, 2H, Hd), 7.1-7.2 (m, 1H, Hβ), 7.4-7.5 (m, 1H,Hβ'), 7.6-7.7 (m, 1H,Hγ), 8.55-8.65 (m, 1H,Hα). FT-IR ν (cm^{-1}): 3353, 3279 (NH$_2$), 2936, 2861 (C–H), 1591 (C=C py), 1474, 1433 (–CH$_2$–), 758 (C–H py), 614 (def C–H py).

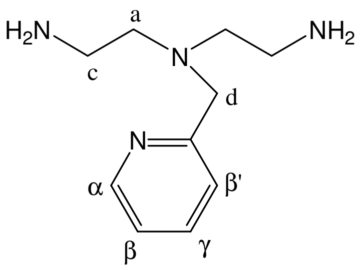

ftNC$_2$PhOH. Salicylaldehyde (3.0 mL, 28 mmol) was added to a mixture of ftNC$_2$H (10.00 g, 28 mmol) in 1,2-dichloroethane (150mL). The crude product was stirred for several minutes. Afterward, NaBH(OAc)$_3$ (8.60 g, 0.039 mol) was slowly added, and the mixture was stirred at room temperature for 24 h. The organic layer was extracted after adding 100 mL of water. The aqueous phase was washed with dichloromethane (2 x 100 mL). The organic fractions were dried over MgSO$_4$ and concentrated up to ~10 mL. Methanol (150 mL) was then added with stirring, producing the white solid precipitated product, which was filtered and dried under vacuum. Yield: 11.21 g (87%). Anal. Calcd (%) for $C_{27}H_{23}N_3O_5 \cdot 0.25\ H_2O$ (MW = 473.99 g·mol^{-1}): C, 68.42˚ H, 5.00˚ N, 8.87. Found: C, 68.33˚ H, 5.02˚ N, 9.01. ^{1}H NMR(400 MHz, CDCl$_3$) δ (ppm): 2.95 (t, J = 6 Hz, 4H, Ha), 3.89 (m, 6H, Hc + Hd), 6.24–6.29 (m, 1H, Hα), 6.71–6.78 (m, 1H, Hβ), 6.92–6.98 (m, 1H, Hβ'), 7.01–7.08 (m, 1H, Hγ), 7.70–7.84 (m, 8H, H$_{arom}$), 9.07 (s, br, PhO***H***). ^{13}C NMR (100 MHz, CDCl$_3$) δ (ppm): 34.8 (Cc), 51.5 (Ca), 58.1 (Cd), 116.0 (Cα$_{PhOH}$), 119.5 (Cγ$_{PhOH}$), 121.4 (Cqα$_{PhOH}$), 123.2 (C$_{arom}$) 129.0, 129.1 (Cβ$_{PhOH}$, Cβ'$_{PhOH}$), 132.2 (Cq$_{arom}$), 133.8 (C$_{arom}$), 156.8 (***C***–OH), 168.2 (C=O). FT-IR *ν* (cm^{-1}): 1700 (C=O), 1398 (CO–N), 754 (C–H PhOH), 708 (C–H ar), 532 (C–H ft). HRMS (*m/z*): [M + Na]$^+$, 492.1526 (100%)˚ calcd. Mass., 492.1535.

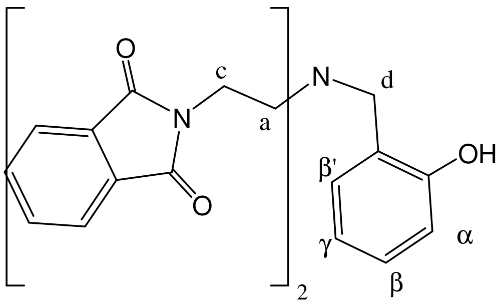

H$_2$NC$_2$PhOH. Hydrazine monohydrate (9.7 mL, 0.2 mol) was added to a solution of **ftC$_2$PhOH** (8.65 g, 18.42 mmol) in chloroform/ethanol (60:320 mL). The mixture was stirred at room temperature for 24 h, and the obtained white precipitate was filtered off and discarded. The resulting transparent solution was evaporated under reduced pressure. Chloroform (150 mL) was then added to the residue, and the mixture was stirred for another 24 h and filtered again. Evaporation of the chloroform fraction afforded the desired product as oil. Yield: 2.62 g (85%). Anal. Calcd (%) for $C_{11}H_{19}N_3O_3 \cdot 0.14\ CHCl_3$ (MW = 226.00 g·mol^{-1}): C, 59.20˚ H, 8.54˚ N, 18.59. Found: C, 59.39˚ H,8.81˚ N, 18.21. ^{1}H NMR (400MHz, CDCl$_3$) *δ* (ppm): 2.59 (t, J = 6Hz, 4H, Ha), 2.86 (t, J = 6 Hz, 4H, Hc), 3.36 (s, br, –N***H$_2$***), 3.73 (s, 2H, Hd), 6.69–7.22 (m, 4H, H$_{PhOH}$). ^{13}C NMR (100 MHz, CDCl$_3$) *δ* (ppm): 39.3 (Cc), 55.7 (Ca), 57.9 (Cd), 116.4 (Cα), 119.1 (Cγ), 122.7 (Cqα), 128.8 (Cβ), 129.3 (Cβ'), 157.5 (***C***–OH). FT-IR *ν* (cm^{-1}): 1587 (C=C),

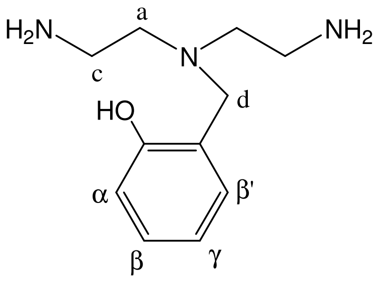

1472, 1446 (–CH_2–), 1269, 1256 (ArC–OH), 753 (C–H $_{arom}$), 708 (C–H PhOH), 532 (C–H arom). ESI-MS (*m/z*): $[M + H]^+$, 210.1 (100%).

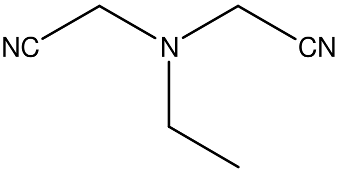

EtN(CH_2CN)$_2$. In a round-bottom flask containing 70% ethylamine (2 mL, 25 mmol), water (15 mL), and 37% HCl (6 mL), a 4.2 mL sample of 37% formaldehyde (55 mmol) was added, and the mixture was stirred for 30 min. The solution was then cooled to 0ºC, and NaCN (2.94 g, 55 mmol) was added. The mixture was allowed to react at room temperature for 24 h. Then, NaOH (1 g) and dichloromethane (15 mL) were added, the organic phase was extracted, and the aqueous phase was washed with dichloromethane (2 x 15 mL). The combined organic fractions were dried over $MgSO_4$, and the solvent was removed in the rotary evaporator. The oil obtained was then purified via flash chromatography in silica gel, using a hexane/ethyl acetate mixture (2:1) as eluent. Yield: 1.274 g (42%). Anal. Calcd (%) for $C_6H_9N_3 \cdot 0.25\ H_2O$ (MW = 127.66 g · mol $^{-1}$): C, 56.45° H, 7.50° N, 32.92. Found: C, 56.37°H,7.42° N, 32.71. ^1H NMR (400 MHz, $CDCl_3$) δ (ppm): 1.17 (t, J = 7 Hz, 3H, N–CH_2–C$\boldsymbol{H_3}$), 2.72 (q, J = 7 Hz, 2H, N–C$\boldsymbol{H_2}$–CH_3), 3.62 (s, 4H, N–C$\boldsymbol{H_2}$–CN). ^{13}C NMR (100 MHz, $CDCl_3$) δ (ppm): 12.4 ($\underline{\boldsymbol{C}}H_3$), 41.7 (–$\underline{\boldsymbol{C}}H_2$–$CH_3$), 48.01 (–$\underline{\boldsymbol{C}}H_2$–CN), 114.35 (–$\underline{\boldsymbol{C}}$N). FT-IR *v* ($cm^{-1}$): 2978, 2944, 2834 (C–H), 1428 (–CH_2–), 1106, 868.

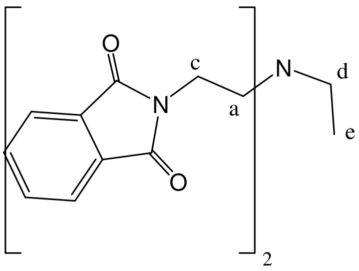

ftNC_2Et. A mixture of **ftNC_2H** (5.00 g, 13.76 mmol), K_2CO_3 (2.85 g, 20.64 mmol), and iodoethane (2.2 mL, 27.52 mmol) in 150mL of acetonitrile was refluxed for 18 h. After the reaction mixture was cooled to room temperature, it was filtered, and the solvent was evaporated to dryness. The residue was redissolved in 100 mL of $CHCl_3$ and was washed with 3 N aqueous NaCl solution. The aqueous phase was extracted three times with 3 x 20 mL $CHCl_3$. The combined organic phases were dried over Na_2SO_4. Evaporation of the solvent gave a yellow oil, which turned solid under high vacuum. Yield: 5.10 g (95%). Anal. Calcd (%) for $C_{22}H_{21}N_3O_4$ (MW = 391.42 g·mol^{-1}): C, 67.51° H, 5.41° N, 10.74. Found: C, 67.20° H, 5.42° N, 1085. ^1H NMR (400MHz, $CDCl_3$) δ (ppm): 0.95 (t, J = 6Hz, 3H, He), 2.65 (q, J = 6 Hz, 2H, Hd), 2.80 (t, J = 6 Hz, 4H, Ha), 3.75 (t, J= 6 Hz, 4H, Hc), 7.67–7.78 (m, 8H, H_{arom}). ^{13}C NMR (400 MHz, $CDCl_3$) δ (ppm): 11.91 (Ce), 35.92 (Cc), 47.24 (Cd), 51.21 (Ca), 123.05 (C_{arom}), 132.22 (Cq_{arom}), 133.68 (C_{arom}), 168.26 ($\underline{\boldsymbol{C}}$=O). HRMS (*m/z*): $[M + Na]^+$, 414.1436 (100%)° calcd mass, 414.1430.

H_2NC_2Et. The compound H_2NC_2Et was synthesized by the following two procedures: Method A and Method B.

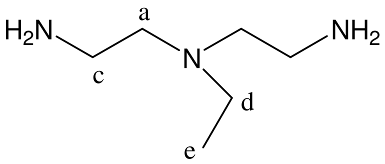

Method A. A round-bottom flask, kept under nitrogen, containing $LiAlH_4$ (3.737 g, 95 mmol) and dry THF (110 mL), was cooled to –10ºC. Concentrated H_2SO_4 (5 mL) was carefully added, the mixture was stirred for 30 min at –10ºC, and then, it was allowed to warm to room temperature. $EtN(CH_2CN)_2$ (1.274 g, 10.4 mmol) was dissolved in dry THF (10 mL), added carefully to the hydride mixture, and allowed to react overnight. Then, water (7 mL) was added slowly, the mixture was stirred for 24 h, and the solvent was evaporated through a N_2 stream. Afterward, dichloromethane (50 mL) and methanol (50 mL) were added, and the mixture was stirred again for 24 h. The solid obtained was then filtered off and discarded, and the filtrate was evaporated. The product was finally obtained through distillation under reduced pressure. Yield: 0.291 g (21%).

Method B. Hydrazine monohydrate (6.98 mL, 0.14 mol) was added to a solution of $ftNC_2Et$ (5.00 g, 12.77 mmol) in chloroform/ ethanol (50:280 mL). The mixture was stirred at room temperature for 24 h, and then, the obtained white precipitate was filtered off and discarded. The resulting transparent solution was evaporated under reduced pressure. Chloroform (150 mL) was then added to the residue, and the mixture was stirred for another 24 h and filtered again. Evaporation of the chloroform fraction afforded an oil which was purified by distillation at 150 ºC in vacuo. Yield: 0.920 g (55%). Anal. Calcd (%) for $C_6H_{17}N_3{\cdot}0.15\ H_2O$ (MW = 133.92 g·mol^{-1}): C, 53.81˚ H, 13.02˚ N, 31.38. Found: C, 53.64˚ H, 13.53˚ N, 31.59. ^1H NMR (400 MHz, $CDCl_3$) δ (ppm): 1.01 (t, J = 7 Hz, 3H, He), 1.31 (s, br, 4H,–N***H_2***), 2.40–2.60 (m, 6H, Hd + Ha), 2.75 (t, J = 7 Hz, 4H, Hc). ^{13}C NMR (400 MHz, $CDCl_3$) δ (ppm): 11.77 (Ce), 39.86 (Ca), 47.74 (Cd), 56.75 (Ca). FT-IR ν (cm^{-1}): 3354, 3289 (NH_2), 2962, 2934, 2870, 2804 (C–H), 1460 (–CH_2–, –CH_3), 918, 864 (NH_2).

3.3.2. Macrocyclic Ligand Synthesis.

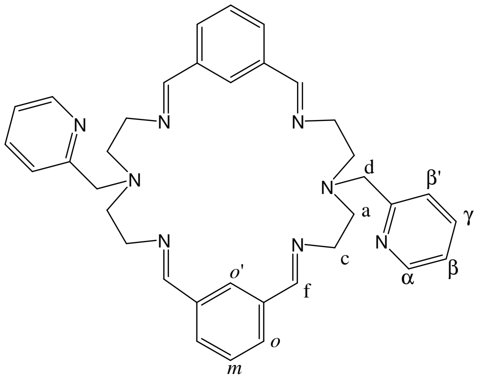

bsm2py (**L73**). A solution of isophthalaldehyde (0.228 g, 1.70mmol) in acetonitrile (40 mL) was slowly added (6.0 mL/h via syringe pump) to a solution of H_2NC_2py (0.330 g, 1.70 mmol) in acetonitrile (40 mL) at 0 ºC and allowed to react overnight at room temperature. It was then filtered to remove some solid particles, and the filtrate was then concentrated in the rotary evaporator, leading to the separation of an oil. The solvent was decanted, and the oil was dried under a vacuum. Yield: 0.380 g (76%). Anal. Calcd (%) for $C_{36}H_{40}N_8 \cdot 0.6\ H_2O \cdot 0.4\ CH_3CN$ (MW = 611.99 g·mol^{-1}): C, 72.22˚ H, 6.98˚ N, 19.23. Found: C, 72.24˚ H, 6.45˚ N, 19.21. ^{1}H NMR (400MHz, $CDCl_3$) δ(ppm): 2.98 (t, J = 4 Hz, 8H, Ha), 3.72 (t, J = 4 Hz, 8H, Hc), 3.87 (s, 4H, Hd), 7.04-7.07 (m, 2H, Hβ), 7.16 (s, 2H, $H_{ortho'}$), 7.29-7.33 (m, 2H, H_{meta}), 7.38-7.42 (m, 4H, Hβ' +Hγ), 7.84-7.87 (m, 4H, H_{ortho}), 8.08 (s, 4H, Hf), 8.49 (d, J = 3.82 Hz, 2H, Hα). ^{13}C NMR ($CDCl_3$, 400 MHz) δ (ppm): 55.22 (Ca), 59.72 (Cc), 61.38 (Cd), 121.78 (Cβ), 123.11 (Cβ'), 128.70 (C_{ortho}), 128.90 (Cγ), 129.75 ($C_{ortho'}$), 136.12 (C_{meta}), 136.67 (Cq_{arom}), 148.80 (Cα), 160.15 (Cqα), 161.09 (Cf). FT-IR *v*(cm^{-1}): 2838 (C–H), 1644 (C=N), 1588, 1568 (C–C py), 1473, 1433 (C–H), 797 (C–H ar), 756 (C–H py), 692 (C–H ar), 614 (C–H py). HRMS (*m/z*): [M + Na]$^+$, 607.3279 (100%)˚ calcd mass, 607.3274.

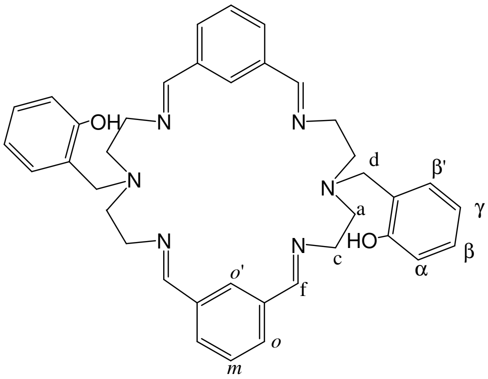

bsm2PhOH (**L74**). A solution of isophthalaldehyde (0.655 g, 4.88 mmol) in CH_3CN (50 mL) was slowly added (9 mL/h via syringe pump) to a solution of **H_2NC_2PhOH** (1.021 g, 4.88 mmol) in CH_3CN (50 mL) with stirring. After the mixture was stirred for 24 h, a white solid was obtained, filtered, and then dried under a vacuum. Yield: 0.797 g (53%). Crystals for X-ray diffraction were obtained by dissolving 0.015 g of **L74** in 1 mL of chloroform and then diluting the solution with MeOH. Slow evaporation of the solvents afforded white crystals suitable for X-ray diffraction. Anal. Calcd (%) for $C_{38}H_{42}N_6O_2$ (MW = 614.78 g·mol^{-1}): C, 74.24˚ H, 6.89˚ N, 13.67. Found: C, 73.88˚ H, 6.84˚ N, 13.67. ^{1}H NMR (400 MHz, $CDCl_3$) *δ* (ppm): 2.98 (t, J = 6Hz, 8H, Ha), 3.72 (t, J = 6Hz, 8H, Hc), 3.90 (s, 4H, Hd), 6.75–6.85 (m, 2H, $H\gamma_{PhOH}$), 6.85–6.90 (m, 2H, $H\alpha_{PhOH}$), 7.0–7.1 (m, 2H, $H\beta'_{PhOH}$), 7.06 (s, 2H, $H_{ortho',arom}$), 7.15–

7.25 (m, 2H, $H\beta_{PhOH}$), 7.35–7.45 (m, 2H, $H_{meta,arom}$), 7.8–7.9 (m, 4H, $H_{ortho,arom}$), 8.04 (s, 4H, Hf), 10.22 (s, br, PhO***H***). ^{13}C NMR (100 MHz, $CDCl_3$) *δ* (ppm): 55.6 (Ca), 58.9 (Cd), 59.6 (Cc), 116.6 ($C\alpha_{PhOH}$), 119.1 ($C\gamma_{PhOH}$), 123.0 ($Cq\alpha_{PhOH}$), 128.6, 128.7, 128.9, 129.0 (C_{ortho},C_{meta}, $C\beta_{PhOH}$, $C\beta'_{PhOH}$), 130.5 ($C_{ortho'}$), 136.2 (Cq_{arom}), 157.8 (**C**–OH), 161.7 (Cf). FT-IR *ν* (cm^{-1}): 3185 (OH), 2837, 2805 (C–H), 1642 (C=N), 799 (C–H_{arom}), 746 (C–H_{PhOH}), 691 (C–H_{arom}). HRMS (*m/z*): [M + H]$^+$, 615.3451 (100%)˚ calcd mass, 615.3448.

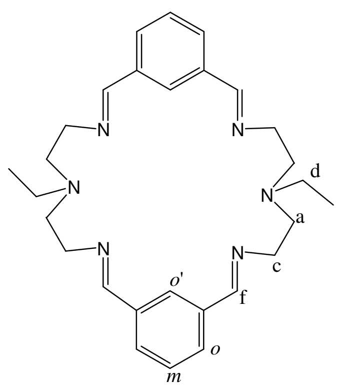

bsm2Et (**L75**)**.**The procedure is the same as that for **bsm2py** (**L73**), starting with H_2NC_2Et (0.300 g, 2.29 mmol) in CH_3CN (40 mL) and isophthalaldehyde (0.308 g, 2.29 mmol) in CH_3CN (40 mL). The product is obtained as a solid. Yield: 0.250 g (48%). Anal. Calcd (%) for $C_{28}H_{38}N_6$ (MW = 458.64 g·mol1): C, 73.33˚ H, 8.35˚ N, 18.32. Found: C, 73.29˚ H, 8.34˚ N, 18.24. ^{1}H NMR (400 MHz, $CDCl_3$) *δ* (ppm): 0.96 (t, J = 7 Hz, 6H, He), 2.55 (q, J = 7 Hz, 4H, Hd), 2.85 (t, J = 6 Hz, 8H, Ha), 3.66 (t, J= 6 Hz, 8H, Hc), 7.07 (s, 2H, $H_{ortho',arom}$), 7.43 (t, J = 7 Hz, 2H, $H_{ortho,arom}$), 7.91-7.96 (m, 4H, $H_{meta,arom}$), 8.04 (s, 4H, Hf). ^{13}C NMR (400 MHz, $CDCl_3$) *δ* (ppm): 12.37 (Ce), 48.57 (Cd), 54.35 (Cc), 60.00 (Ca), 128.32, 128.88, 129.72 ($C_{ortho'}$, C_{meta}, C_{ortho}), 136.72 (Cq_{arom}), 161.10 (Cf). HRMS (*m/z*): [M + Na]$^+$, 481.3051 (100%)˚ calcd mass, 481.3056.

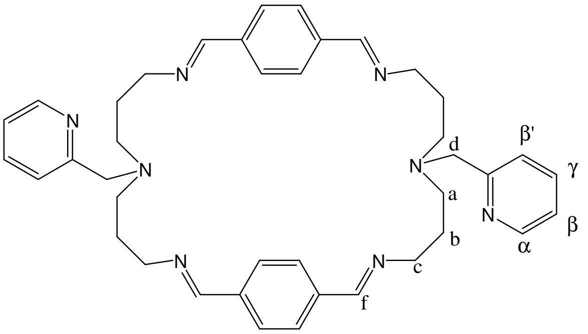

bsp3py (**L79**).To a solution of $\mathbf{H_2NC_3py}$ (0.30 g, 1.3 mmol) in 18 mL of acetonitrile was added, slowly and under an ice bath, a solution of terephthalaldehyde (0.18 g, 1.3 mmol) in 18 mL of acetonitrile. The mixture was stirred over 12 h at room temperature, precipitating a colourless oil. The solution was decanted, and the oil dried to vacuum, turning into a white solid. Yield 0.26 g (60%). ^{1}H NMR (200 MHz, $CDCl_3$) δ(ppm): 1.88 (quint, J = 7 Hz, 8H, Hb), 2.61 (t, J = 7 Hz, 8H, Ha), 3.64 (t, J = 7 Hz, 8H, Hc), 3.77 (s, 4H, Hd), 7.1-7.3 (m, 2H, Hβ), 7.4-7.8 (m, 12H, arom + Hβ + Hγ), 8.22 (s, 4H, He), 8.5-8.6 (m, 2H, Hα). FT-IR *ν* (cm^{-1}): 2970, 2927, 2871, 2839, 2796 (C–H), 1640 (C=N), 1590, 1568 (C=C py), 1476, 1431 (–CH_2–), 826 (C–H ar), 750 (def C–H py), 618 (C–H py). MS (m/z): 641.2(MH$^+$).

bsm3py (**L80**). The procedure was analogous to that used for the synthesis of **L79**, using **H$_2$NC$_3$py** (1.88 g, 8.5mmol) in 85 mL of acetonitrile and isophthalaldehyde (1.17 g, 8.5 mmol) in 85mL of acetonitrile. Yield: 2.22 g (82%). ^{1}H NMR (200 MHz, CDCl$_3$) δ(ppm): 1.88 (quint, J = 7Hz, 8H, Hb), 2.6 (t, J = 7Hz, 8H,Ha), 3.65 (t, J = 7Hz, 8H,Hc), 3.76 (s, 4H,Hd), 7.00-7.9 (m, 14H, 8H arom + 2Hβ' + 2Hγ + 2Hβ), 8.24 (s, 4H, HF), 8.4-8.6(m, 2H, Hα). FT-IR *ν* (cm^{-1}): 2927, 2835 (C–H), 1644 (C=N), 1590 (C=C py), 1434 (–CH$_2$–), 798 (C–H ar), 757 (C–H py), 691 (C–H ar), 616 (CcH py). MS(m/z): 641.2 (MH$^+$).

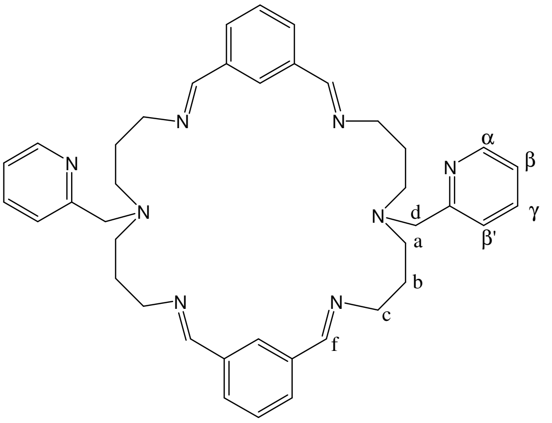

bsp2py (**L81**). The synthesis of **L81 (bsp2py)** was analogous to the synthesis of **L79,** using H$_2$NC$_2$py (1.03 g, 5.32 mmol) in 53 mL of acetonitrile and terephthalaldehyde (0.71 g, 5.32 mmol) in 53 mL of acetonitrile. Yield: 0.65 g (42%). ^{1}H NMR (200 MHz, CDCl$_3$) δ(ppm): 2.97 (t, J = 7 Hz, 8H, Ha), 3.77 (t, J = 7 Hz, 8H, Hc), 3.85 s, 4H, Hd), 7.1-7.3 (m, 2H, Hβ), 7.4-7.8 (m, 12H, 8 Harom + 2Hγ + 2Hβ'), 8.22 (s, 4H, Hf), 8.5-8.6 (m, 2H, HR). FT-IR *ν* (cm^{-1}): 2924, 2838 (C–H), 1642 (C=N), 1589, 1568 (C=C py), 1432 (–CH$_2$–), 828 (C–H ar), 756 (C–H py). MS (m/z): 585.3 (MH$^+$).

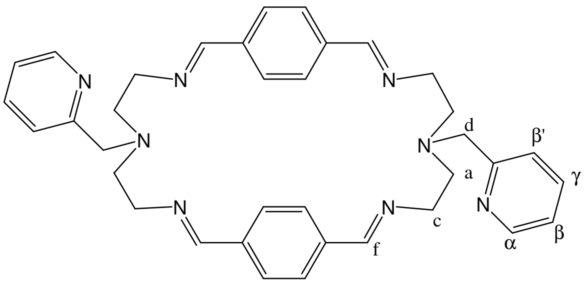

3.3.3. Synthesis of Cu(I) Complexes.

[Cu$_2$(L73)](PF$_6$)$_2$, 1(PF$_6$)$_2$. [Cu(CH$_3$CN)$_4$]PF$_6$ (0.373 g, 1 mmol) was added to a solution of **bsm2py** (0.292 g, 0.5 mmol) in CH$_3$OH (20 mL), and the mixture was stirred for 1 h at room temperature. The resulting yellow-orange precipitate was filtered and washed with Et$_2$O. The solid was then redissolved inCH$_2$Cl$_2$ and filtered. The obtained solid was discarded, and the solvent was removed under vacuum to obtain the product. Yield: 0.400 g (0.40 mmol˚ 80%). The diffusion of a mixture of THF/Et$_2$O (1:1) into the mother solution yielded a dark yellow powder. Anal. Calcd (%) for C$_{36}$H$_{40}$Cu$_2$F$_{12}$N$_8$P$_2$ · 0.5 CH$_2$Cl$_2$ (MW = 1044.24 g·mol1): C, 41.98˚ H, 3.96˚ N, 10.73. Found:

C, 41.87° H, 3.95° N, 10.77. FD-MS (70 eV,CH_3CN)(*m/z*): 857 (71%) $[Cu_2L1(PF_6)]^+$, 791 (20%) $[CuL1(PF_6)]^+$, 647 (100%) $[CuL1]^+$, 356 (17%) $[Cu_2L1]^{2+}$. IR (KBr) *ν* (cm^{-1}): 2914, 2857 (C-H), 1637 (C=N), 1440 (C-H), 842 (P-F), 764,689 (C-H).

$[Cu_3(L76)](PF_6)_3$, $4(PF_6)_3$. $[Cu(CH_3CN)_4]PF_6$ (0.373 g, 1 mmol) was added to a solution of H_2NC_2py (0.194 g, 1 mmol) and isophthalaldehyde (0.134 g, 1.00 mmol) in MeOH (20 mL), and the mixture was stirred for 2 h at room temperature. The resulting orange precipitate was filtered off, washed with a small amount of MeOH and Et_2O, and dried under vacuum. Yield: 0.342 g (0.288 mmol° 68%). Recrystallization of the crude product from CH_3CN and diffusion of a mixture of THF/ Et_2O (1:1) into the mother solution for about 2 weeks yielded red crystals suitable for X-ray diffraction analysis. Anal. Calcd (%) for $C_{54}H_{60}Cu_3N_{12}F_{18}P_3$ (MW = 1502.67 g·mol^{-1}): C, 43.16° H, 4.02° N, 11.19. Found: C, 43.34° H, 4.30° N, 11.06.IR (KBr) *ν* (cm^{-1}): 2916, 2854 (C-H), 1633 (C=N), 1439 (C-H), 842 (P-F), 763,766 (C-H). FD-MS (70 eV, CH_3CN) (*m/z*): 939 (95%) $[CuL4]^+$, 876 (100%) $[L4+H]^+$.

$[Cu_3(L76)](SbF_6)_3$, $4(SbF_6)_3$. A solution of $[Cu(CH_3CN)_4]SbF_6$ (0.048 g, 0.10 mmol) in CH_3CN (0.5mL) was added dropwise to a suspension of **L73** (0.029 g, 0.05 mmol) in CH_3CN (0.5 mL), and the solution was stirred for 1 h. Slow diethyl ether diffusion into the solution for about 2 weeks afforded orange crystals, which have been characterized by X-ray diffraction analysis. Yield: 0.042 g (69%). Anal. Calcd (%) for $C_{54}H_{60}Cu_3N_{12}F_{18}Sb_3$ (MW = 1775.02 g·mol^{-1}): C, 36.54° N, 9.47° H, 3.41. Found: C, 36.86° N, 9.70° H, 3.72.^1H NMR (400 MHz, CD_3COCD_3) *δ* (ppm): 2.8-3.3 (m, 8H, Ha), 3.4-4.0 (m, 8H, Hc), 4.19 (s, 4H, Hd), 7,2-8.8 (m, 20H, H_{arom}+ H_{py} + Hf). FT-IR *ν* (cm^{-1}): 2916, 2853 (C–H), 1633 (C=N), 1603 (SbF_6), 1440 (CH_2), 764 (C_{arom}-H), 653(SbF_6).

$[Cu_2(L74)(CH_3CN)_2](CF_3SO_3)_2$, $2(CF_3SO_3)_2$. A solution of $[Cu(CH_3CN)_4][CF_3SO_3]$ (0.050 g, 0.128 mmol) in CH_3CN (2mL) was added to a suspension of **L74** (0.040 g, 0.065mmol) in CH_3CN (1 mL). The yellow solution was stirred for 1 h, and then it was filtered. Addition of diethyl ether (50 mL) into the yellow solution generated a yellow powder. Yield: 0.060 g (80%). ESI-MS (*m/z*): 615.3 $[$**L74**$+H]^+$, 637.2 $[$**L74**$+ Na]^+$, 677.2. [**L74**+ Cu]+. ^1H NMR (200 MHz,CD_3COCD_3)δ(ppm): 2.9-3.3 (m, 4H, Ha), 3.9-4.4 (m, 6H, Hc + Hd), 6.8-7.4 (mm, 5H, PhOH), 7.8-9.2 (mm, 6H, H_{ar}+ Hf). FT-IR *ν* (cm^{-1}): 3320 (O–H), 2916, 2855 (C–H), 1628 (C=N), 1275, 1221, 1025 (CF_3SO_3), 758 (C–H, $_{PhOH}$), 634

(CF_3SO_3). Anal. Calcd (%) for $C_{60}H_{63}Cu_3N_9F_9O_{12}S_3 \cdot 2\ CH_3CN \cdot H_2O$ (MW = 1660.1 g·mol^{-1}): C, 46.31˚ N, 9.28˚ H, 4.31˚ S, 5.79. Found: C, 46.12˚ N, 9.31˚ H, 4.29˚ S, 5.77.

Slow diethyl ether diffusion into the acetonitrile solution of the compound **$2(CF_3SO_3)_2$** afforded a mixture of yellow and orange crystals after 12–15 days, which were both characterized by X-ray diffraction analysis and show the formation of **$[Cu_2(L74)(CH_3CN)_2](CF_3SO_3)_2$**, **$2(CF_3SO_3)_2$** and **$[Cu_3(L77)(CH_3CN)_3](CF_3SO_3)_3$**, **$5(CF_3SO_3)_3$**. MS(*m/z*): 615 [**L74**+H]+, 922 [**L77**+H]$^+$.

$[Cu_3(L78)(CH_3CN)_3](CF_3SO_3)_3$, $6(CF_3SO_3)_3$. A solution of $[Cu(CH_3CN)_4](CF_3SO_3)$ (0.025 g, 0.064 mmol) in CH_3CN (2 mL) was added to a suspension of **L75** (0.015 g, 0.032mmol) in CH_3CN (0.5mL), and the mixture was stirred for 1 h. Slow diethyl ether diffusion into the solution for about 2 weeks afforded yellow crystals, which have been characterized by X-ray diffraction analysis. Yield: 0.020 g (71%). Anal. Calcd (%) for $C_{45}H_{57}Cu_3N_9F_9O_{12}S_3 \cdot 2.25\ CH_3CN \cdot 0.75\ C_4H_{10}O$ (MW = 1473.66 g·mol^{-1}): C, 42.79˚ N, 10.69˚ H, 4.87˚ S, 6.53. Found: C,42.86˚ N, 10.58˚ H, 4.73˚ S, 6.38. ^{1}H NMR (400MHz, CD_3COCD_3) δ (ppm): 1.1-1.3 (m, 3H, He), 2.63.1 (m, 6H, Ha + Hd), 3.6-4.0 (m, 4H, Hc), 7.7-8.8 (mm, 6H, H_{arom} + Hf). FT-IR ν (cm^{-1}): 1631 (C=N), 1253, 1223 (CF_3SO_3), 1149 (–CH_2–), 1027 (CF_3SO_3), 634 (CF_3SO_3).

$[Cu_2^I(L)](CF_3SO_3)_2$ (L = **L79, L80, L81**) were prepared by the same general method in an anaerobic box, adding a solution of $Cu^I(CH_3CN)_4(CF_3SO_3)$ (0.040 g, 0.106 mmol) in CH_3CN (1 mL) to a suspension of particular ligand (0.034 g for **L79** and **L80**, 0.029 g for **L81**, 0.053 mmol) in CH_3CN (1 mL). The corresponding reaction mixture was stirred for 1-2 h. Addition of diethyl ether causes the precipitation of the resulting complex, which was isolated by decantation and dried under vacuum.

$[Cu_2^I(L)](BArF)_2$ (L = **L79, L80, L81**) were prepared, with the purpose of improving the solubility of the complexes in CH_2Cl_2, as follows: in an anaerobic box, to a suspension of 0.040 mmol of the corresponding triflate complex (0.043 g for **$7(CF_3SO_3)_2$** and **$8(CF_3SO_3)_2$** and 0.040 g for **$9(CF_3SO_3)_2$** in dichloromethane, 0.072 g of NaBArF (0.080 mmol) is added. The suspension is stirred for 3-4 h and then filtered so that the $NaCF_3SO_3$ is filtered off. Then 5 mL of pentane are added carefully so that it does not mix with the dichloromethane. Twenty-four hours later, decantation of the liquid and drying of the obtained solid lead to the pure BArF complexes.

$[Cu_2^{I}(L79)](CF_3SO_3)_2$ $(7(CF_3SO_3)_2)$. The product resulted in 0.052 g (92% yield) of a red solid. Single crystals of **$7(CF_3SO_3)_2$** suitable for X-ray diffraction analysis were obtained by slow diethyl ether diffusion into acetonitrile solution of the complex. Anal. Calcd (%) for $C_{42}H_{48}Cu_2F_6N_8O_6S_2$ · 1.5 H_2O (MW = 1093.11 g·mol^{-1}): C, 46.15° N, 10.25° H, 4.70, S, 5.87. Found: C, 46.02° N, 10.02° H, 4.60, S, 5.71. ^1H NMR (400 MHz, DMSO-d_6)δ(ppm): the corresponding spectre is identical to that obtained in a DMSO-d_6-D_2O (1:4) mixture. ^1HNMR (400MHz, DMSO-d_6-D_2O(1:4)) δ(ppm): 1.7-1.9 (m, 4H, Hb(1)), 2.0-2.1 (m, 4H, Hb(2)), 2.5-2.7 (m, 4H, Ha(1)), 2.9-3.1 (m, 4H, Ha(2)), 3.4-3.6 (m, 4H, Hc(1)), 3.78 (s, 4H, Hd), 3.9-4.0 (m, 4H, Hc(2), 7.53 (s, 8H, Har), 7.6-7.7 (m, 4H,Hβ), 7.9-8.0 (m, 2H,Hγ), 8.37 (s, 4H,N=CH), 8.6-8.7 (m, 2H Hα). ^{13}C NMR (100 MHz, DMSO-d_6) δ(ppm): 27.7 (Cb), 58.1 (Ca), 60.0 (Cd), 64.1 (Cc), 125.1 (Cβ), 127.9 (C-Har), 137.2 (Cq, ar), 138.5 (Cγ), 149.0 (Cα), 157.7 (Cα), 164.0 (C=NH). ESI-MS in aqueous DMSO (m/z): 917.2 [Cu_2 **L79**](OTf)$^+$. $E_{1/2}$(CH_3CN) = 0. 82 V vs SSCE.

$[Cu_2^{I}(L79)](BArF)_2$ $(7(BArF)_2)$. The product resulted in 0.078 g (78% Yield) of an orange solid. Anal. Calcd (%) for $C_{104}H_{72}B_2Cu_2F_{48}N_8$ · 2 H_2O (MW = 2530.41 g·mol^{-1}): C, 49.37° N, 4.43° H, 3.03. Found: C, 49.40° N, 4.64° H, 3.04. ^1H NMR (200 MHz, CH_3CN) δ(ppm): 1.8-2.0 (m, 4H, Hb(1)), 2.0-2.2 (m, 4H, Hb(2)), 2.6-2.8 (m, 4H, Ha(1)), 3.0-3.2 (m, 4H, Ha(2)), 3.5-3.7 (m, 4H, Hc(1)), 3.81 (s, 4H, py–CH_2–N), 3.9-4.1 (m, 4H, Hc(2)), 7.4-7.8 (m, 36H, 24HBArF + 8Harom + 4Hβ), 7.9-8.0 (m, 2Hγ), 8.27 (s, 4H,N=CH°), 8.6-8.8 (m, 2Hα).

$[Cu_2^{I}(L80)](CF_3SO_3)_2$ $(8(CF_3SO_3)_2)$. The product resulted in 0.043 g (76% yield) of a dark red solid. Anal. Calcd(%) for $C_{42}H_{48}Cu_2F_6N_8O_6S_2$ (MW = 1066.09 g·mol^{-1}): C,47.32° N, 10.51° H, 4.54, S, 6.02. Found: C, 47.59° N, 10.74° H, 4.70, S, 5.29. ^1H NMR (400 MHz, DMSO-d_6) δ(ppm): 1.7-2.0 (m, 8H, Hb), 2.5-2.7 (m, 8H, Ha), 3.2-4.0 (m, 12H, 8Hc + 4H py–C*H*$_2$–N), 7.4-8.1 (m, 12H, 6H_{arom} + 6H_{py}), 8.6-9.0 (m, 6H, $Hα_{py}$ + 4 N=C*H*–), 9.40 (s, 2H_{arom}). ^1H NMR (400 MHz, DMSO-d_6-D_2O) δ(ppm): 1.7-2.0 (m, 8H,Hb), 2.4-2.8 (m, 8H,Ha), 3.1-3.5 (m, 8H,Hc), 3.8-4.2 (m, 4H, py–C*H*$_2$–N), 7.3-8.0 (m, 12 H, 6 H_{arom} + 6 H_{py}), 8.5-8.9 (m, 6H, 2$Hα_{py}$ + 4H, N=C*H*-), 9.40 (s, 2H_{arom}). ^{13}C NMR (100 MHz, DMSO-d_6) δ(ppm): 28.9 (Cb), 59.4 (Ca), 63.8 (Cc + py–CH_2–N), 119.0 ($C_{arom,quat}$), 123.1 ($Cβ_{py}$), 123.3 ($Cβ_{py}$), 138.7 ($Cγ_{py}$), 149.3 ($Cα_{py}$), 158.2 N=CH–). $E_{1/2}$(CH_3CN) = 0.89 V vs SSCE.

$[Cu_2^I(L80)](SbF_6)_2$ $(8(SbF_6)_2)$. Compound **$8(SbF_6)_2$** was obtained by reacting **L80** with $Cu^I(CH_3CN)_4(SbF_6)$ in CH_3CN using the same general method for **$8(CF_3SO_3)_2$**. Slow diethyl ether diffusion in an acetonitrile solution of **$8(SbF_6)_2$** complexes afforded brownish crystals suitable forX-ray diffraction.

$[Cu_2^I(L80)](BArF)_2$ $(8(BArF)_2)$. The product resulted in 0.065 g (64% yield) of an orange solid. Anal. Calcd (%) for $C_{104}H_{72}B_2Cu_2F_{48}N_8$ (MW = 2494.38 g·mol^{-1}): C, 50.09° N, 4.49° H, 2.91. Found: C, 49.76° N, 4.68° H, 3.05. ^{1}H NMR (200 MHz, CD_2Cl_2) δ (ppm): 1.8-2.2 (m, 8H, Hb), 2.5-3.0 (m, 8H, Ha), 3.4-4.0 (m, 12H, 8Hc + 4H pyCH_2–N), 7.2-8.6 (m, 44 H, 24 H_{BArF} + 8H_{arom} + 8H_{py} + 4 N=C*H*–). ESI-MS (*m/z*): 1631.3 [Cu_2**L80**](BArF)$^+$.

$[Cu_2^I(L81)](CF_3SO_3)_2$ $(9(CF_3SO_3)_2)$. The product resulted in 0.053 g (94% yield) of a reddish orange solid. Slow diethyl ether diffusion in an acetonitrile solution of complex led to the formation of single crystals of **$(9(CF_3SO_3)_2)$** suitable for X-ray analysis. Anal. Calcd (%) for $C_{38}H_{40}Cu_2F_6N_8O_6S_2\cdot$ 2.5 H_2O (MW = 1055.03 g·mol^{-1}): C, 43.26° N, 10.62° H, 4.30° S, 6.08. Found: C,43.20° N, 10.50° H, 4.05° S, 6.02. ^{1}H NMR (400 MHz, DMSO-d_6) δ (ppm): the corresponding spectre is identical to that obtained in a DMSO-d_6-D_2O (1:4) mixture. ^{1}H NMR (400MHz,DMSO-d_6-D_2O(1:4)) δ (ppm): 2.9-3.0 (m, 4H, Ha(1)), 3.3-3.4 (m, 4H, Ha(2)), 3.75-3.85 (m, 4H, Hc(1)), 3.95-4.1 (m, 4H, Hc(2)), 4.40 (s, 4H, Hd), 7.4-7.5 (m, 2H, Hβ), 7.55-7.65 (m, 2H, Hβ), 7.9-8.0 (m, 2H, Hγ), 8.56 (s, 8H, H_{arom}), 8.67 (s, 4H, N=C*H*), 8.8-8.9 (m, 2H, Hα). ^{13}C NMR (100 MHz, DMSO-d_6) δ (ppm): 52.4 (Cc), 57.2 (Cd), 59.9 (Ca), 124.2, 124.3 (Cβ), 128.5 (CH_{arom}), 136.5 (Cq_{arom}), 138.0 (Cγ), 149.3 (CHα), 158.8 (CHα), 161.8 (N=CH). ESI-MS in aqueous DMSO: (*m/z*): 861.1 [Cu_2**L81**](OTf)$^+$. $E_{1/2}$ (CH_3CN) = 0.71 V vs SSCE.

$[Cu_2^I(L81)](BArF)_2$ $(9(BArF)_2$. The product resulted in 0.069 g (71% yield) of an orange solid. Anal. Calcd (%) for $C_{100}H_{64}B_2Cu_2F_{48}N_8\cdot$3 H_2O (MW = 2492.31 g·mol^{-1}): C, 45.30° N, 4.36° H, 2.52. Found: C, 45.54° N, 4.21° H, 2.65. ^{1}H NMR (200 MHz, CH_2Cl_2) δ (ppm): 3.0-3.2 m, 4H, Ha(1)), 3.3-3.5 (m, 4H,Ha(2)), 3.7-3.9 (m, 4H,Hc(1)), 3.9-4.2 (m, 4H, Hc(2)), 5.30 (s, 4H, py–CH_2–N), 7.0-8.5 (m, 34H, 24H_{BArF} + 8H_{arom} + 8*H*$_{py}$ + 4N=C*H*–). ^{1}HNMR (200 MHz, CH_3CN) δ (ppm): 2.9-3.3 (m, 8H, Ha), 3.8-4.1 (m, 8H, Hc), 4.3-4.5 (m, 4H, Hd), 7.0-8.5 (m, 44 H, 24H_{BArF} + 8H_{arom} + 8H_{py} + 4N=C*H*–).

3.3.4. Solubility and Stability of the copper complexes.

The copper complexes of **L79**, **L80** and **L81** were soluble in DMSO and aqueous DMSO. These binuclear complexes were found to be stable in the solution phases used, as evidenced by the NMR.

4. Results and discussion

4.1. Fine-Tuning Ligand−Receptor Design for Selective Molecular Recognition of Dicarboxylic Acids

4.1.1. Abstract.

The design of host molecules as receptors for the recognition of substrate anion guest molecules in aqueous solution is an important target from many points of view with multiple potential applications. In particular, polyaza macrocyclic species have been widely studied as receptor models for anionic substrates, having been observed many factors such as dimensionality, hydrogen bonding, topology, and charge complementarities, which influence the anion binding and selectivity. Moreover, dicarboxylate anion recognition is of special relevance from the biotechnological point of view.

Some previous studies have been carried out with a family of ditopic hexaazamacrocyclic ligands containing meta- and para-xylylic spacers and different content of methylenic units within amine groups. It has been shown how the appropriate hexaazamacrocyclic ligand, under the right conditions, can strongly and selectively bind a specific dicarboxylate species over other guests.

In this section it will be discussed the host−guest interaction between the hexaaza macrocyclic ligand **L9** and three rigid dicarboxylic acids (isophthalic acid, $H_2\textit{is}^{\circ}$ phthtalic acid, $H_2\textit{ph}^{\circ}$ and terephthalic acid, $H_2\textit{te}$). These interactions have been investigated using potentiometric equilibrium methods and NMR spectroscopy including the measurement of intermolecular nuclear Overhauser effects (NOEs) and self-diffusion coefficients (*D*).

Results show that ternary complexes (H_nLS) are formed in aqueous solution as a result of hydrogen bond formation and Coulombic interactions between the host and the guest. The maximum interaction is reached in the system $[(H_6\mathbf{L9})(\textit{is})]^{4+}$ complex. Competitive distribution diagrams and total species distribution diagrams are used to illustrate the main features of these systems. A high selectivity of the **L9** macrocycle for the formation of the *is* complexes over the *te* complexes is observed. Moreover, the recognition capacity of **L9** over dicarboxylic acids (*da*) is compared to the related hexaaza macrocycle **L12**. The latter binds *da* with a lesser strength and it is not selective. Finally, theoretical calculations performed at molecular dynamics level have also been carried out and point out that the origin of selectivity is mainly due to the

capacity of the **L9** ligand receptor to adapt to the geometry of the dicarboxylic acid to form relatively strong hydrogen bonds.

4.1.2. Formation and selectivity of Ternary Species H:**L9**:S.

In this work it has been obtained the protonation constants for the macrocyclic receptor **L9**, as long as for the diacid substrates *is*, *ph* and *te*. Moreover, the association constants for the receptor-substrate complexes have also been obtained. In this section it will be discussed the selectivity of the ligand **L9** towards each of the three diacids, and the obtained data will be compared with the analogous ligands previously described in the literature **L8***,* **L34** and **L12**.

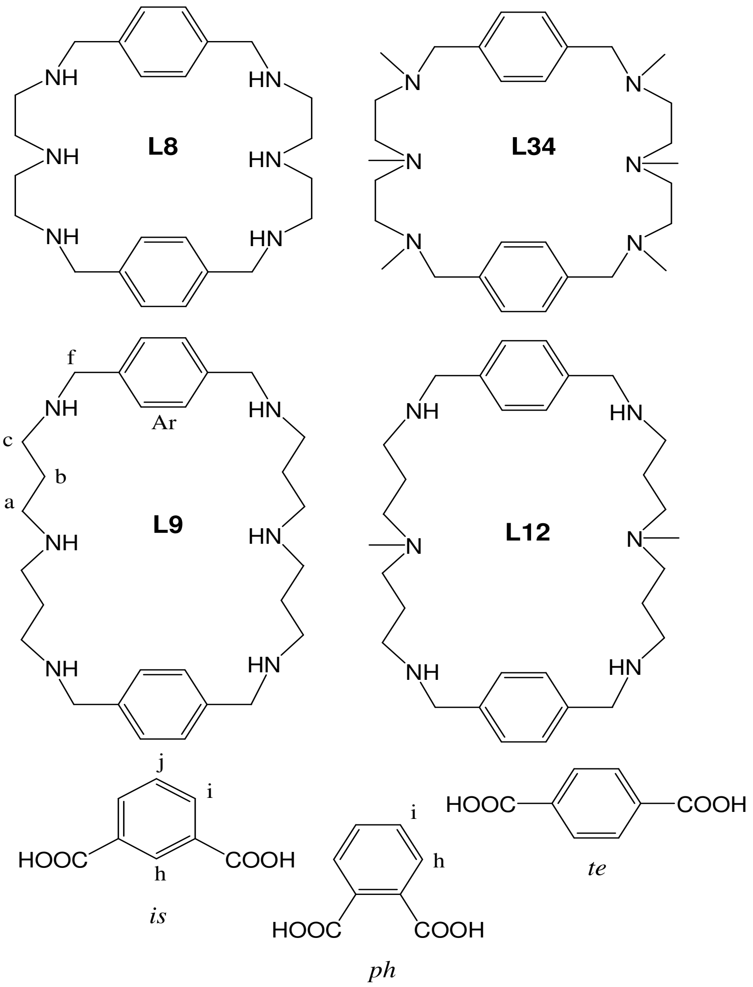

Figure 4.1.1. Drawing, abbreviations and proton labeling for the ligands and substrates discussed in the section 4.1.

The drawing and abbreviations for the ligands and substrates discussed in this section are shown in *Figure 4.1.1.* The receptors are hexaazamacrocyclic cyclophanes, with secondary or tertiary amines. The substrates are rigid, aromatic diacids with different geometries.

First, protonation constants of the fully protoned ligand and diacids have been obtained through potentiometric titrations with Me_4NOH, using a solution 0.1 M Me_4NCl, to keep the ionic strength constant. The protonation constants of the **L9** ligand in 0.1M Me_4NCl, obtained in this work, and also of the related **L8**, **L34**, and **L12** and **L9** in 0.1 M KCl from previous works are shown in *Table 4.1.1*. for comparison purposes.

Table 4.1.1. Cumulative (β_{HiL}, β_{HiS}) and stepwise (K^H_i) logarithms of the protonation constants for Ligand **L9** and substrates (S = *ph*, *is* and *te*) at 25.0 ºC and I=0.10M (NMe_4Cl), as long as macrocyclic species **L8**, **L34**, **L12** and **L9** in KCl 0.1M from other works, comparison purposes. Charges have been omitted for clarity. Values in parentheses are the standard deviations in the last significant figure.

Equilibrum quotient (L)	**L8** (KCl) [88]	**L34** (NaCl) [125]	**L9** (Me_4NCl)	**L9** (KCl)[105]	**L12** (KCl)[89]	Equilibrium quocient (S)	*ph*	*is*	*te*
β_{H1L} L + H = LH	9.54	8.93	10.20(2)	10.55	10.41	β_{H1S} S+H = LH	5.011(2)	4.42(2)	4.50
β_{Hi2L} L + 2 H = LH_2	18.44	17.15	20.27(1)	20.61	20.23	β_{H1S} S+H = LH_2	7.749(5)	7.90(2)	8.11
β_{H3L} L + 3 H = LH_3	26.7	24.5	28.79(1)	29.17	29.05				
β_{H4L} L + 4 H = LH_4	34.2	30.94	36.42(2)	36.84	36.92				
β_{H5L} L + 5 H = LH_5	37.38	32.44	43.44(2)	43.96	43.71				
β_{H6L} L + 6 H = LH_6	40.42	--	50.09(2)	50.66	49.98				
K^H_1 [HL]/[L][H]	9.54	8.93	10.20(2)	10.55	10.41	K^H_1 [HS]/[S][H]	5.011(2)	4.42(2)	4.50
K^H_2 $[H_2L]/[HL][H]$	8.90	8.22	10.07(2)	10.06	9.82	K^H_2 $[H_2S]/[HS][H]$	2.738(2)	3.48(3)	3.61
K^H_3 $[H_3L]/[H_2L][H]$	8.26	7.35	8.52(2)	8.56	8.82				
K^H_4 $[H_4L]/[H_3L][H]$	7.50	6.44	7.62(2)	7.67	7.87				
K^H_5 $[H_5L]/[H_4L][H]$	3.18	1.50	7.03(2)	7.12	6.79				
K^H_6 $[H_6L]/[H_5L][H]$	3.05	--	6.65(2)	6.70	6.27				
Σ log K^H_i	40.42	32.44	50.09(2)	50.66	49.98				

The logarithms of the stepwise protonation constants of the *n* degree of protonation are calculated by subtraction, from the log of cumulative protonation constant of the *n* degree of protonation, the log of the cumulative protonation constant of the previous degree of protonation (*n* – 1). As an example, Log K^H_3 is calculated subtracting β_{H2} from β_{H3}:

$$\text{Log } K^H_3 = \text{Log } \beta_{H3} - \text{Log } \beta_{H2}$$

From the obtained protonation constants the distribution diagram of the present species as a function of pH can be obtained. The distribution diagram of the **L9** ligand show that the hexaprotonated ligand H_6**L9** is the only existing species below pH = 5 (*Figure 4.1.2*). Above this pH until pH = 12, other species with all protonation degrees appear to exist throughout the pH range.

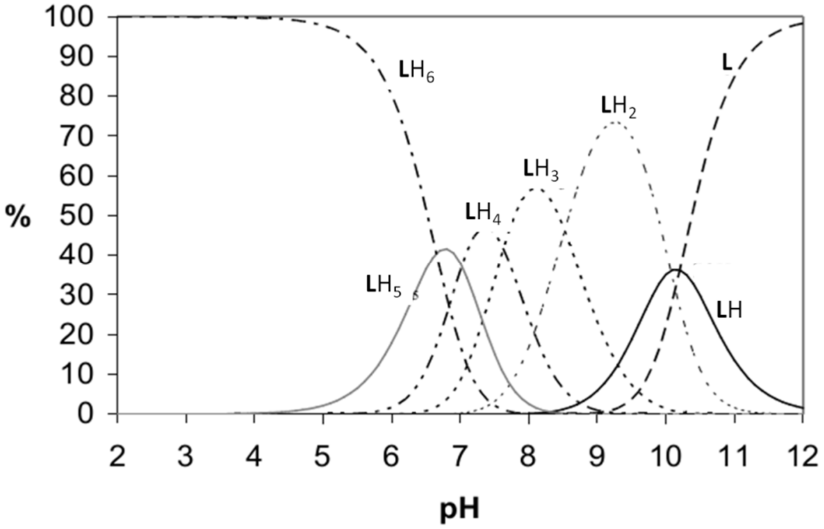

Figure 4.1.2. Species distribution diagram for the **L9** ligand as a function of pH.

When comparing **L8** and **L34** it can be seen that secondary amines (**L8**) are much more basic than the tertiary ones (**L34**), because the values of the protonation constants for **L8** are higher than those for **L34** *(Table 4.1.1)*.[88,125] Nevertheless, for the particular case of **L12** (two tertiary amines and four secondary amines) [89] and **L9** (six secondary amines),[105] they possess relatively similar overall basicity with values of 49.98 and 50.64, respectively.

Moreover, potentiometric titrations were used to obtain information about the strength of the ligand–substrate interaction. Once the individual protonation constants for the **L9** ligand and substrates are precisely known, the potentiometric data of a solution containing an equimolecular amount of ligand and substrate can be resolved to obtain the value of the interaction constants between the different species involved. This gives the log K^R values of the species generated from **L9** and the three dicarboxylic acids studied (*Table 4.1.2.*)° furthermore *Table 4.1.2*. also contains the log K^R values of related systems for purposes of comparison.

For the **L9**-*is* system, the presence of six equilibrium species is detected and can be expressed as shown in *Table 4.1.2*, where K_i^R is the recognition constant of protonation degree *i* for the ligand, and is listed in order of appearance from high to low pH.

From the obtained association constants of the **L9***:da* complexes, species distribution diagrams of the expositing species, both complexed and uncomplexed, can be obtained. These diagrams show the percentage of each species as a function of pH. *Figure 4.1.3.* displays the species distribution diagrams as a function of pH obtained for the three systems **L9**-*is*, **L9**-*ph*, and **L9**-*te*.

Table 4.1.2. Logarithms of stepwise association constants (K_i^R)[a] for the interaction of the ligand **L9** with substrates (S = *ph, is* and *te*) at 25ºC and I = 010 M (NMe_4Cl)[b]. Charges have been omitted for clarity. Values in parentheses are the standard deviations in the last significant figure.

Stoichometry L S H	Equilibrium (L = **L9**)	Logarithms of Association Constants Values[b]					
		L9-*is*	**L9**-*ph*	**L9**-*te*	**L12**-*is* [89]	**L12**-*ph* [89]	**L12**-*te* [89]
1 1 1	L + S + H = LSH	--	--	--			
1 1 2	L + S + 2H = LSH_2	--	23.02(6)	--			
1 1 3	L + S + 3H = LSH_3	31.87(9)	31.58(6)	31.4(1)			
1 1 4	L + S + 4H = LSH_4	40.38(5)	39.26(6)	39.3(1)			
1 1 5	L + S + 5H = LSH_5	47.2(1)	46.91(4)	46.3(2)			
1 1 6	L + S + 6H = LSH_6	54.83(5)	53.79(2)	53.5(1)			
1 1 7	L + S + 7H = LSH_7	58.80(7)	57.24(7)	--			
1 1 8	L + S + 8H = LSH_8	62.10(7)					
1 1 1	[HLS]/[HL][S]	--	--	--	--	--	
1 1 2	[H_2LS]/[H_2L][S]	--	2.75	--	--	1.79	
1 1 3	[H_3LS]/[H_3L][S]	3.07	5.79	2.58	--	2.42	
1 1 4	[H_4LS]/[H_4L][S]	3.96	2.85	2.80	2.41	2.67	
1 1 5	[H_5LS]/[H_5L][S]	3.73	3.47	2.83	2.68	3.05	
1 1 6	[H_6LS]/[H_6L][S]	4.74	3.70	3.45	3.02	3.38	
1 1 7	[H_6LS]/[H_6L][HS]	4.29	2.14	--	2.72	2.69	
1 1 8	[H_6LS]/[H_6L][H_2S]	4.11	--	--	--	--	
1 1 6 [a]	[H_6LS]/[H_6L][S]				3,2 [a]	3,3[a]	4,3 [a]

[a]Value calculated through H-NMR titrations. [b] Logarithm of stepwise association constants Log K_i^R are calculated by subtraction of the logs of the cumulative protonation constants of the individual ligands and substrates (Table 4.1.1, β_{HiL}, β_{HiS}) from the logs of the cumulative formation constants (Table 4.1.2, β_{HiLS}). As an example, LogK_8^R is calculated using the following equation:

$$\text{Log } K_8^R = \text{Log } \beta_{H8LS} - \text{Log}\beta_{H6L} - \text{Log } \beta_{H2S}$$

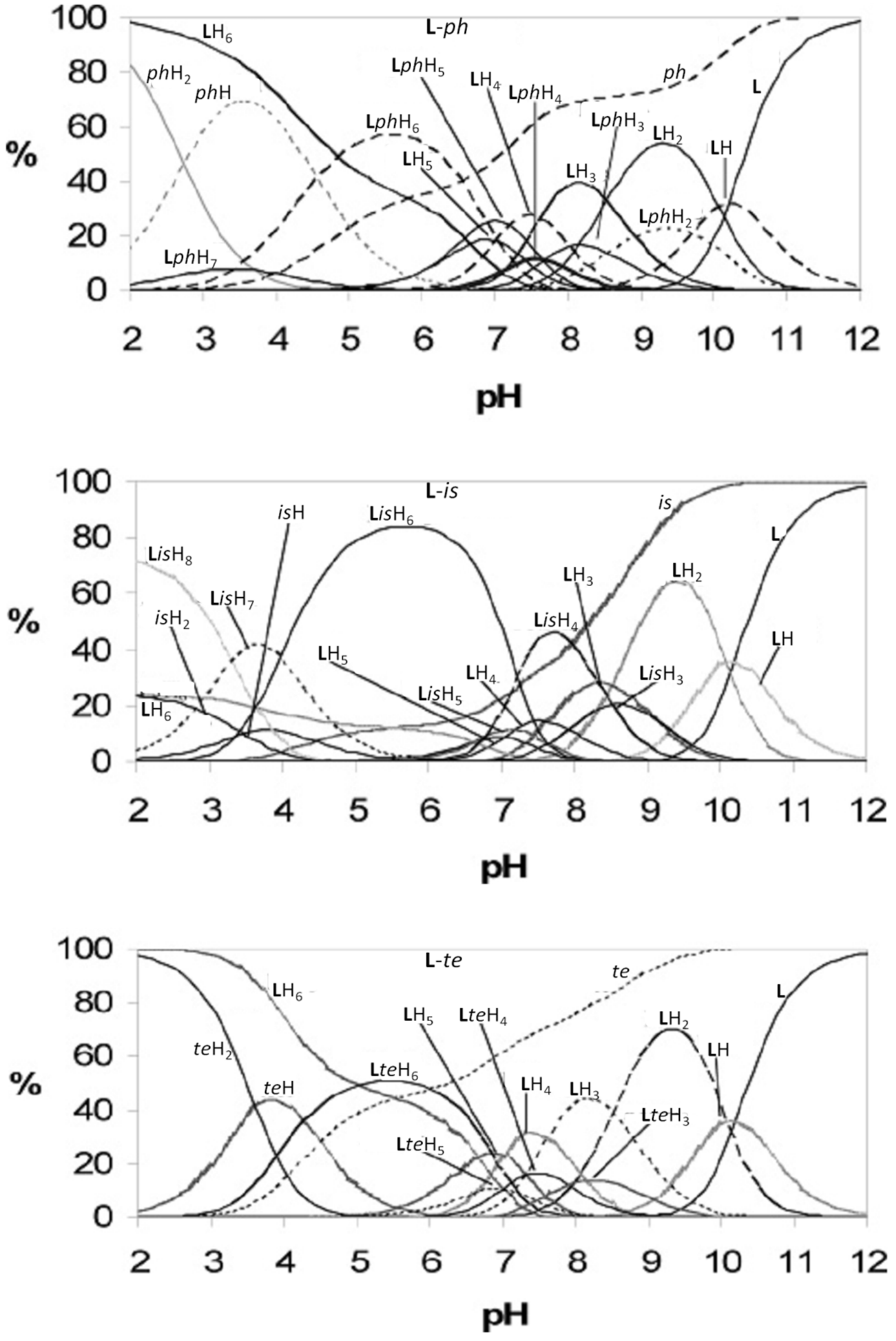

Figure 4.1.3. Species distribution diagram as a function of pH for the **L9**-*ph* (top), **L9**-*is* (middle) and **L9**-*te* (bottom) systems.

For the **L9**-*is* system, it is interesting to note that over the pH range 2-8 the predominant species is H_i:**L9**:*is* rather than the individual species derived from protonation of the ligand and substrates (this range is reduced to 5-6.8 and 5-6.2 for the **L9**-*ph* and **L9**-*te* systems, respectively). The highest equilibrium constant corresponds to the formation of the species H_6**L9***is*$^{4+}$, log K_6^R

=4.74, where Coulombic interaction and potential hydrogen bonding reach a maximum. This species is largely predominant over the pH range 4-7 as can be observed in *Figure 4.1.3*.

The recognition constants for the other carboxylic acids studied (*ph* and *te*) are displayed in *Table 4.1.2*. These association constants are lower than for the case of **L9**-*is* system.-Furthermore, for purposes of comparison, *Table 4.1.2* also shows the recognition constants of the same substrates but using the **L12** ligand. It must be noted that those recognition constants are in general lower than the ones for the corresponding **L9**.

A graphical representation of the values of the Log K_i^R (stepwise association constant) as a function of the degree of protonation of the ternary species (nH, the proton content obtained for the **L9** systems formed with three diacidic substrates) is shown in *Figure 4.1.4*.

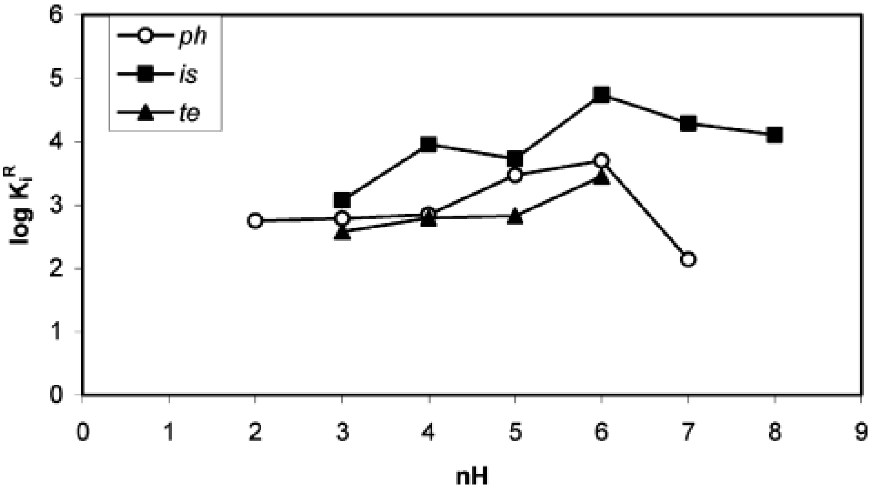

Figure 4.1.4. Log K_i^R versus *n*H (the different ternary species with various degrees of protonation) for the three systems **L9**-*da*.

From the graph, it is clear that the log K_i^R and thus the bonding strength follow the sequence **L9**-*is* > **L9**-*ph* > **L9**-*te* clearly manifesting the importance of the geometrical fit between substrate and receptor. This is further illustrated in *Figure 4.1.5*. where for the **L9**-*is*-*te* competitive system, the **L9**:*is*:H_i species always predominates over the **L9**:*te*:H_i species.

At pH 5.0 for instance, the selectivity of *is* containing species over *te* is 89%˚ the selectivity for *is* containing species over *te* at a particular pH is defined according to the following equation:

$$\sum_i (\%L:is:H_i)/[\sum_i (\%L:is:H_i) + \sum_i (\%L:te:H_i)]$$

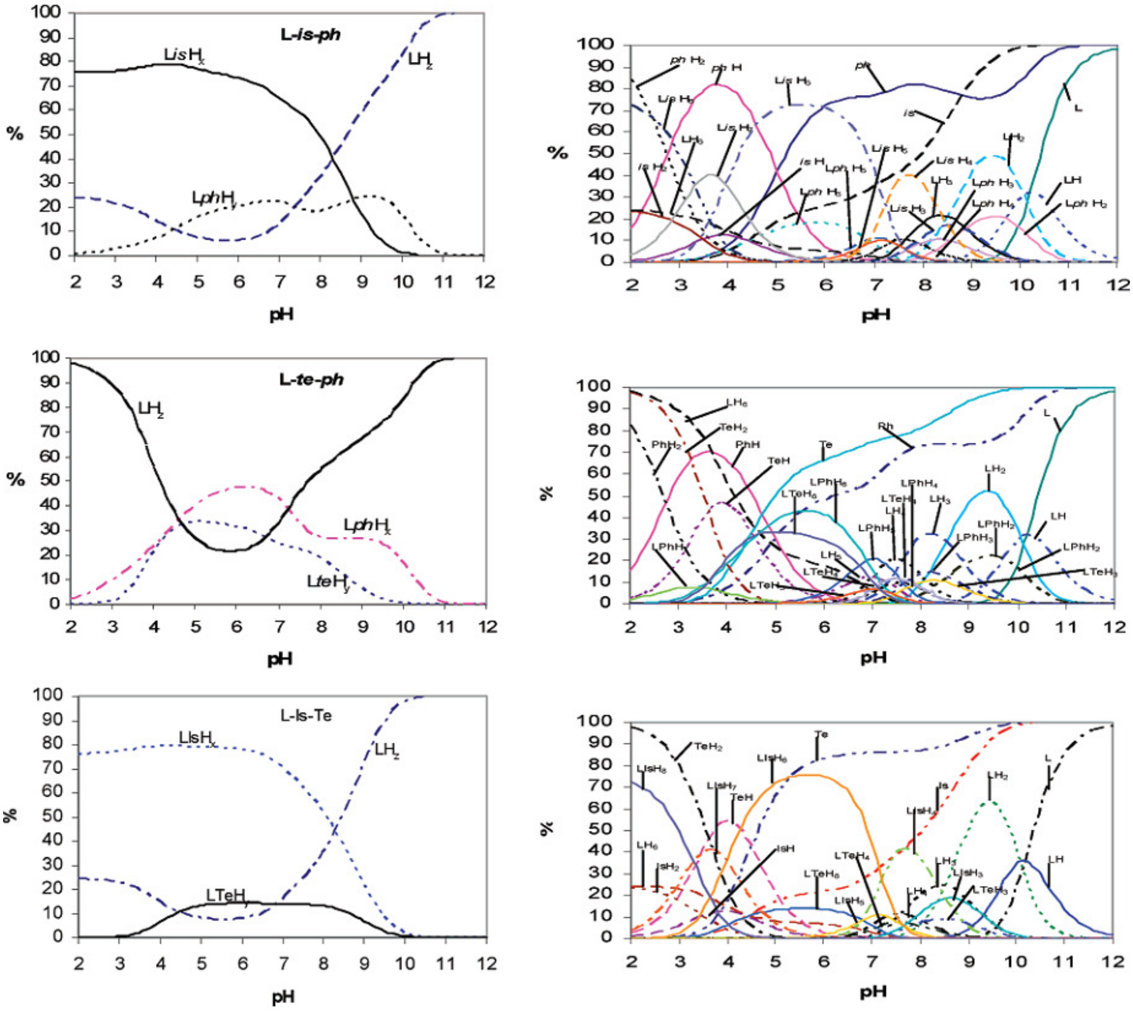

Figure 4.1.5. Competitive calculated species distribution diagram and total species distribution diagrams for systems with equimolar amounts of L-S (**L9**, *is, ph, te*).

4.1.3. Interaction Sites

^{1}H NMR spectroscopy was also used to characterize the complexation process and to identify the site of interaction between the **L9** macrocycle and three aromatic dicarboxylic derivatives.

NMR spectra were recorded at pH = 5.5 because of the large abundance of the H_6**L9**:*is* species. *Table 4.1.3* summarizes the most important NMR related features including CISs (complexation induced shifts), intermolecular nuclear Overhauser effects (NOEs), and self-diffusion coefficients (*D*) of the studied complex, whereas a full set of key NMR spectra is included in the Annex.

Table 4.1.3. NMR data of 1:1, 2 mM binary **L9**-*da* complexes.

	CIS[a]	NOEs[b]	D(**L9**)x10^{-10} cm^2/s [c]	D(*da*) x10^{-10} cm^2/s [d]
L9-*is*	H_h: 8.28 – 8.06 H_i: 7.98 – 7.91 H_j: 7.52 – 7.47 Ar: 7.56 – 7.45 $(CH_2)_b$: 2.05 – 2.00 $(CH_2)_c$: 3.06 – 3.00 $(CH_2)_a$: 3.06 – 3.00 $(CH_2)_f$: 4.31 – 4.19	$(CH_2)_{a,c}$ – Ar(*is*) (*s*) $(CH_2)_{b,f}$ – Ar(*is*) (*m*) Ar(***L9***)–Ar(*is*) (*w*)	3.0 ± 0.2	4.3 ± 0.2
L9-*ph*	H_h: 7.47 – 7.32 H_i: 7.41 – 7.23 Ar: 7.56 – 7.44 $(CH_2)_b$: 2.05 – 1.92 $(CH_2)_c$: 3.06 – 2.88 $(CH_2)_a$: 4.31 – 4.17 $(CH_2)_f$: 4.31 – 4.17	$(CH_2)_{a,c}$ – Ar(*ph*) (*s*) $(CH_2)_{b,f}$ – Ar(*ph*) (*m*) Ar(***L9***)–Ar(*ph*) (*w*)	3.0 ± 0.2	3.8 ± 0.2
L9-*te*	H_i: 7.88 – 7.63 Ar: 7.56 – 7.51 $(CH_2)_b$: 2.05 – 1.97 $(CH_2)_c$: 3.06 – 3.01 $(CH_2)_a$: 3.06 – 2.91 $(CH_2)_f$: 4.31 – 4.23	$(CH_2)_{a,c}$ – Ar(*te*) (*s*) $(CH_2)_{b,f}$ – Ar(*te*) (*m*) Ar(***L9***)–Ar(*te*) (*w*)	3.0 ± 0.2	3.9 ± 0.2

[a] Experimental chemical shift changes in ppm upon complexation in a ratio 1:1. [b] s: strong, m: medium, w: weak. [c] The D value of the free **L9** ligand is 3.1 ± 0.2 x 10^{-10} cm^2/s. [d] The D values of the free substrates are 5.2 x 0.2x 10^{-10} cm^2/s for *is*, 5.2x 10^{-10} cm^2/s for *ph*, and 5.1x 10^{-10} cm^2/s for *te*.

Both CIS and self-diffusion coefficients (D) values support the existence of host-guest complexation, whereas the intermolecular host-guest NOEs allow us to get more insight about the geometry and the main contact points between the different diacid compounds and the macrocycle.

It can be shown that an equimolecular mixture of **L9** and *da* produces a general CIS effect that mostly affects the aromatic protons of both diacid and cyclophane (*Table 4.1.3*). Furthermore, the aliphatic chain of **L9** is also slightly affected by the complexation process specially the CH_2 benzylic protons labeled as $(CH_2)_f$ in *Figure 4.1.1* (see page 82).

In the case of the **L9**-*is* system, the major CIS effect is observed for the H_h proton, and strong intermolecular NOEs are observed between $(\text{-N-CH}_2)_c$ and $(\text{-N-CH}_2)_a$ of **L9** and all the aromatic protons of *is*, putting forward the most important contact points in the receptor-substrate complex. Very importantly, only weak NOEs can be detected between the aromatic *is* protons and the $(CH_2)_b$ and $(CH_2)_f$ menthylenic protons and between the aromatic protons of **L9** and *is*, indicating that π-stacking interactions are not predominant in this system. Relatively similar behaviors are also observed for the other two diacid systems.

The formation of the complex is evident from the large variation of the experimental diffusion coefficient obtained for the small dicarboxylic acid molecule, *D*(*da*), as a function of its concentration whereas *D* of the macrocycle, *D* (**L9**), remains practically unaltered (*Table 4.1.3*).[246] Both the large chemical shift deviations and also the similar *D* values observed for both **L9** and *is* resonances in high [**L9**]:[*is*] ratio confirm that the acid is strongly attached into the cationic ligand receptor. When [*is*] increases, dynamic processes combining several possible free and complexed geometries are active where the guest is in fast equilibrium between the outside and the inside of the macrocyclic cavity (see *Table 4.1.4*).

Table 4.1.4. Measured self-diffusion coefficients for ***L9*** and *is* in free and complex states.

[**L9**]:[*is*]	*D*(**L9**) x 10^{-10} cm^2/s	*D*(*is*) x 10^{-10} cm^2/s
1:0	3.1 ± 0.2	
0:1		5.2 ± 0.2
1:0.1	3.1 ± 0.2	3.2 ± 0.2
1:0.5	3.0 ± 0.2	4.0 ± 0.2
1:1	3.0 ± 0.2	4.3 ± 0.2
1:1.5	3.2 ± 0.2	4.6 ± 0.2
1:2	3.1 ± 0.2	4.8 ± 0.2

4.1.4. Theoretical Calculations.

Theoretical calculations were performed at MP2 level using the 6-31G* set of basis to get further insight into the site of interaction between receptor and substrate. Those calculations also allow visualizing the complexed structures and a quantitative evaluation of their bonding strength. *Figure 4.1.6* displays two views (left, compact° right, stick) of the average calculated structure for the three systems studied.

An overlaying of the 25 most significant structures is presented as Supporting Information. *Table 4.1.5* displays the energies obtained for the free ligand and substrates and also of the complexed species. From *Figure 4.1.6*, it can be observed that the **L9** ligand interacts with substrate *is* through four strong H-bonds whereas substrate *ph* interacts through three and *te* only through two. This number of strong H-bonds for each complex species correlates with the obtained complexation energies displayed in *Table 4.1.5* where the energy released upon complexation follows the order meta (**L9**-*is*) > orto (**L9**-*ph*) > para (**L9**-*te*). The zone of interaction between the **L9** receptor and the ligand substrates is in agreement with the structural description acquired by the NMR experiments described in the previous section.

Table 4.1.5. Total energies and complexation energies for the Anionic complexes **L9**-*da*.

	E_{tot} (kcal/mol)	Standard deviation	E_c (kcal/mol)
is^{2-}	– 194.2528	0.2348	
ph^{2-}	– 193.1369	0.2880	
te^{2-}	– 177.7070	0.1807	
$H_6\mathbf{L9}^{6+}$	– 671.0568	16.6535	
$is^{2-} + H_6\mathbf{L9}^{6+}$	– 939.4684	25.9589	– 74.1588
$ph^{2-} + H_6\mathbf{L9}^{6+}$	– 923.3875	24.9323	– 59.1938
$te^{2-} + H_6\mathbf{L9}^{6+}$	– 894.6212	38.3180	– 45.8574

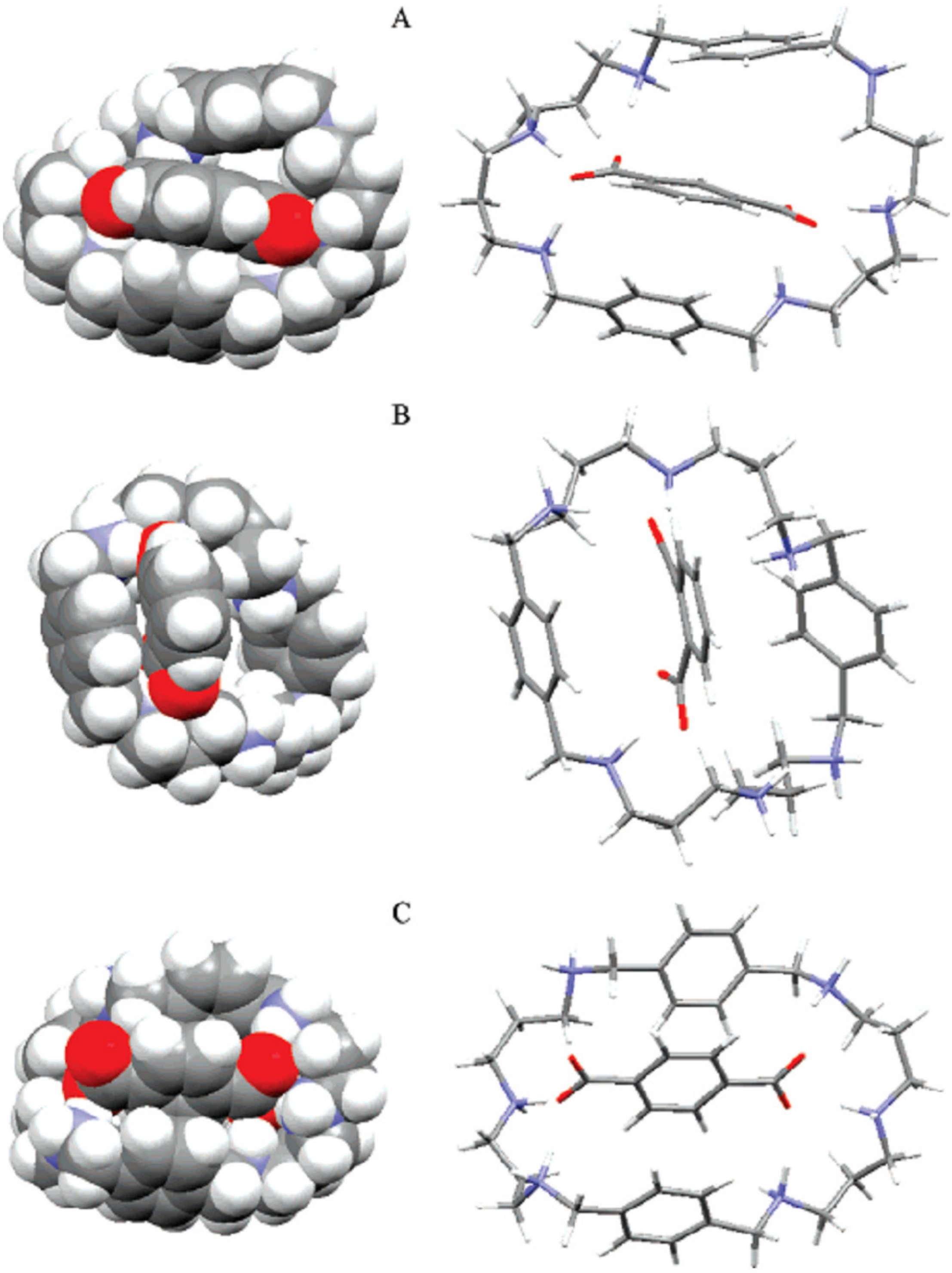

Figure 4.1.6. Space fillig (left) and stick (right) views of average calculated structures studied by molecular dynamics for (A) **L9**-*is* (B) **L9**-*ph* and (c) **L9**-*te* systems.

4.1.5. Final remarks

Bringing all the results together, additional remarks can be highlighted.

The basicity of a given ligand receptor usually plays a key role [88,98,105,247] with regard to its anionic bonding capacities together with its size, shape, and flexibility. The ligands **L9** (six secondary amines) and **L12** (two tertiary amines + four secondary amines) have very similar overall protonation constants. The fact that the first four protonation constants differ in only 0.14 – 0.26 log units indicates that the main protonation sites in both cases are the secondary amines. For the fifth and sixth protonation constants, the differences now increase only up to 0.33-0.43 log units. These small differences clearly manifest that in this particular case charge separation becomes a dominant factor over the secondary versus tertiary amine effects.

Potentiometric titrations and NMR spectroscopy unambiguously reveal the formation of cationic complexes between dicarboxylic acids (*da*) and the **L9** ligand receptor (*Tables 4.1.2* and *4.1.3*) as had also been previously shown for the **L12** case[89] (see *Table 4.1.2*). In sharp contrast, however, for the latter the ligand interacts with *is* and *ph* substrates with comparable strength between them, and interacts stronger with *te.* On the other hand, for the former there is a large difference between the recognition capacities for the three different *da* substrates. As an example, the recognition capacity of the **L9** ligand receptor over the *da* substrate is exemplified by a selectivity of over 89% at pH = 5.0 in favor of the *is* substrate versus the *te*. Furthermore, whereas the largest recognition constant log K_6^R is 3.02 for **L12** and *is*, for **L9** it increases by more than 1.7 orders of magnitude to a value of 4.74. Given the close similarities in the basicity and size of the two ligands, the discriminatory effect can only be attributed to the more restricted rotation of tertiary versus secondary central amines with the conformational consequences that this implies. In addition, the relative capacity of these central amines to form H-bonds with the substrates will also be responsible for the discriminating phenomenon. In this sense and as shown in *Figure 4.1.6*, the **L9** central amines are involved in the formation of H-bondings with all three substrates. While for the *te* substrate these are the only formed H-bondings, for the *ph* and *is* substrates, the H-bonding is further extended to the benzylic amines thus providing multiple H-bonding sites whose strength depends on the geometry of the substrate and the capacity of the **L9** ligand to adapt to the substrate geometry. These results in four strong H-bonds with *is*, three with *ph*, and two with *te* which also correlates with the calculated complexation energies (see *Table 4.1.4*) as mentioned above.

It has been then shown that the replacement of tertiary central amines in **L12** by secondary amines in **L9** produces a new conformational scenario that together with their stronger capacity to form H-bonds with the dicarboxylic acid substrates is responsible for the spectacular change in selectivity of the mentioned ligand receptors versus the substrates.

This chapter must be seen as an example of how subtle ligand variations cause dramatic recognition capacities and thus is useful for the design of future ligand receptors.

4.2. Ligand Influence over the Formation of Dinuclear [2+2] versus Trinuclear [3+3] Cu(I) Schiff Base Macrocyclic Complexes

4.2.1. Abstract.

A macrocyclic ligand obtained from the condensation of isophthalaldehyde and a diethylenetriamine (**bsM2**), as well as its dinuclear Cu(I) complexes have been described previously.

In this chapter it is discussed the synthesis of new analogs of **bsM2** ligand, bearing a substituent R in the central amine. It is also discussed the effect that these substituents have on the coordination behavior of the corresponding Cu(I) complexes. The corresponding macrocycles with R = ethyl, 2-methylpyridyl, and 2-methylphenol groups have been used to this aim.

More specifically, here it is described the synthesis of the [2+2] imine macrocyclic ligands bearing pendant arms, through the condensation of the isophthaldehyde and the corresponding substituted triamine. It has been found that when these [2+2] ligands react with Cu(I), a mixture of dinuclear $[(\boldsymbol{L_{2+2}})Cu_2]^{2+}$ and trinuclear $[(\boldsymbol{L_{3+3}})Cu_3]^{3+}$ complexes is found in solution, being the trinuclear complex the result of a rearrangement of the ditopic ligand ($\boldsymbol{L_{2+2}}$) due to the breaking of the imine bonds and formation of new ones, affording an expanded macrocyclic tritopic ligand ($\boldsymbol{L_{3+3}}$).

Finally, all the Cu(I) complexes described here, with the only exception of the phenol substituted ligand, react only very slowly with molecular oxygen at room temperature and thus manifest the capacity of the Schiff base ligand to stabilize the Cu(I) oxidation state in a CH_3CN solution.

4.2.2. Synthesis of the macrocyclic ligands.

Macrocyclic organic ligands, with a general structure represented in *Figure 4.2.1.*, are prepared through a 2+2 condensation of isophthalaldehyde and the corresponding triamine, which has to be previously obtained with the corresponding pendant arm in the central nitrogen atom.

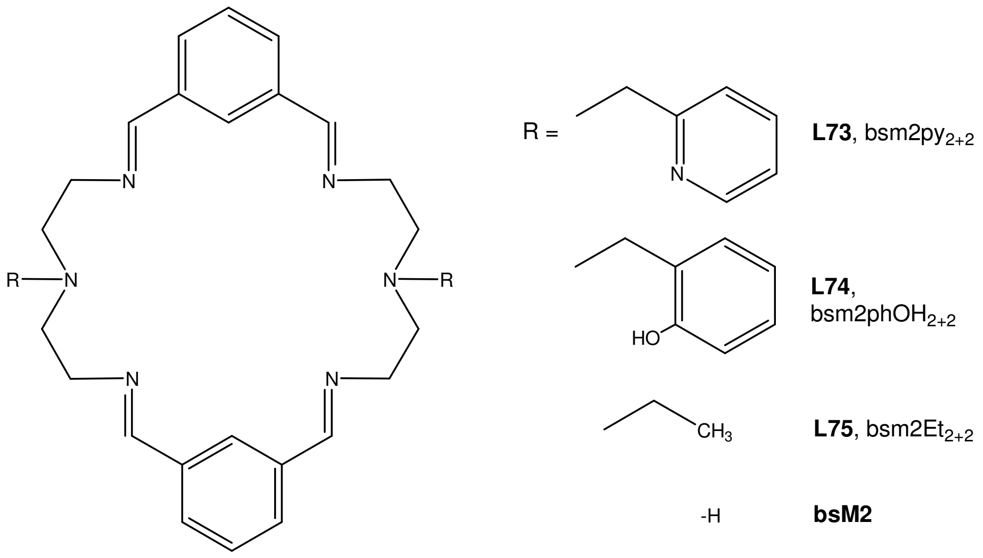

Figure 4.2.1. General structure for the macrocyclic ligand obtained as a 2+2 condensation between a triamine and isophthalaldehyde.

4.2.2.1. Synthesis of the triamine precursors .

For the preparation of the amine precursors, or substituted triamines, a multistep process was followed. For the synthesis of the triamines with a pyridyl- and phenol- arms, this process included: (a) the protection of the primary amines with phthalic anhydride to form the corresponding phthalimides (ftNC$_2$NH)$^{\circ}$ (b) a reductive amination substitution, including the addition of the pyridyl or phenol aldehyde to the central amine in presence of NaBH(OAc)$_3$, yielding the substituted, protected amines ftNC$_2$Npy and ftNC$_2$NphOH (c) deprotection of the phthalamides with hydrazine to yield the corresponding primary amines H$_2$NC$_2$py and H$_2$NC$_2$phOH.

For the triamine with an ethyl pendant arm, two methods were assayed. The first method was very similar to the method for the synthesis of pyridyl and phenol substituents, but with a variation in the substitution method, and included a) protection of the primary amines of diethylenetriamine with phthalic anhydride to form the phtalimide ftNC$_2$NH b) substitution of the secondary amine through a substitution reaction with ethyl iodide to yield the ethyl substituted, protected triamine ftNC$_2$Et, and c) deprotection with hydrazine to obtain the substituted primary amine precursor H$_2$NC$_2$Et.

The second pathway to obtain the ethyl substituted precursor is depicted in *Scheme 4.2.1-B*. Ethylamine is substituted with two methylcyano groups, which are later reduced to primary amines by LiAlH$_4$.

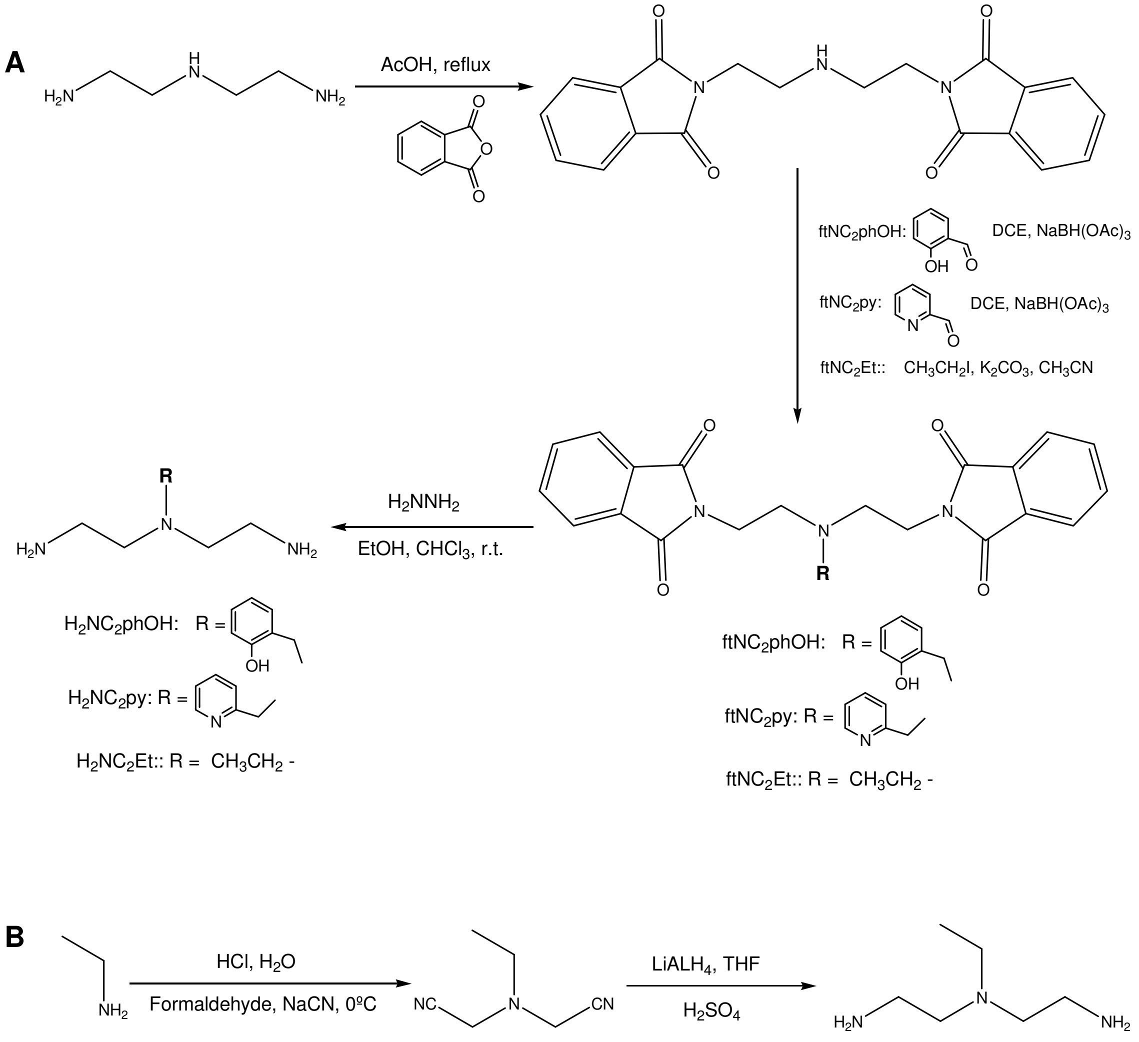
A
AcOH, reflux
ftNC2phOH:
DCE, NaBH(OAc)3
ftNC2py:
DCE, NaBH(OAc)3
ftNC2Et:: CH3CH2I, K2CO3, CH3CN
H2NNH2
EtOH, CHCl3, r.t.
H2NC2phOH: R =
H2NC2py: R =
H2NC2Et:: R = CH3CH2 -
ftNC2phOH: R =
ftNC2py: R =
ftNC2Et:: R = CH3CH2 -
B
HCl, H2O
Formaldehyde, NaCN, 0ºC
LiALH4, THF
H2SO4

Scheme 4.2.1. (A) General synthetic strategy for the preparation of substituted triamines: H_2NC_2PhOH, H_2NC_2py and H_2NC_2Et. (B) Alternative pathway for the synthesis of H_2NC_2Et.

4.2.2.2. Synthesis of metal free [2+2] macrocyclic ligands.

The direct, metal-free, reaction of a dialdehyde and a substituted triamine can yield a large range of condensation products both macrocyclic and acyclic, that can be in equilibrium. The relative amount of each product depends basically on entropic and geometric factors (*Scheme 4.2.2*). From an enthalpic viewpoint, it involves the formation and breaking of the same type of bond, and highly strained systems will be enthalpically disfavored. The relative formation of these products is also influenced by the solvent, the reaction temperature, the reaction time, and, very importantly, their solubility. This wide range of condensation compounds has been previously described in the literature for related systems (e. g. for the pyridyldialdehyde system).[10,27,249]

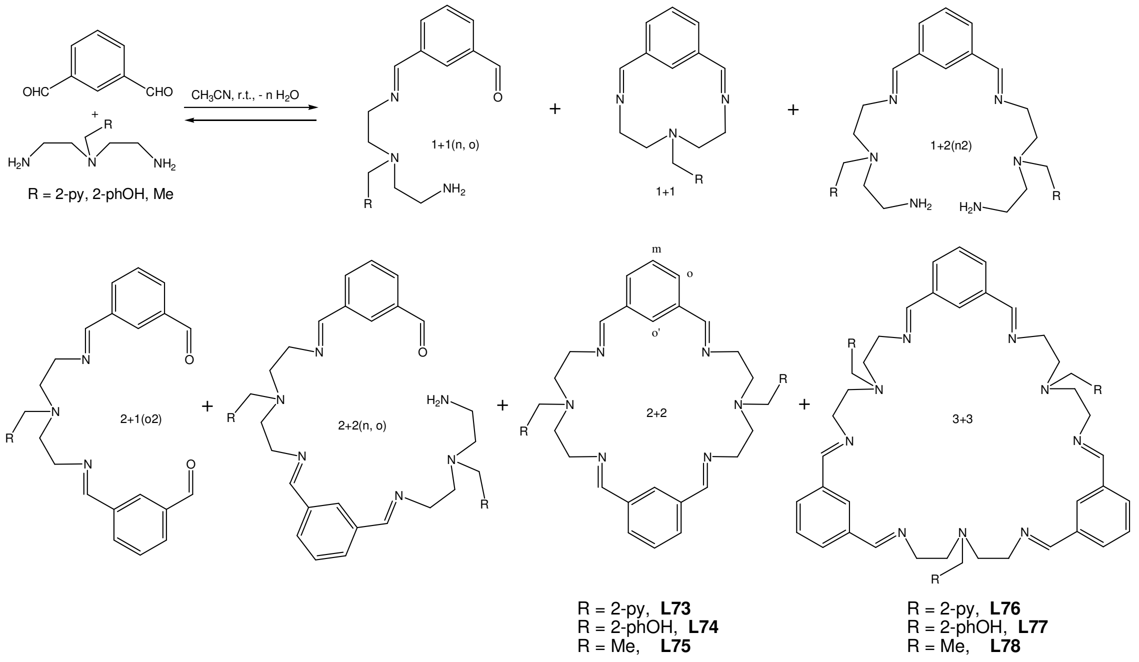

Scheme 4.2.2. Potential condensation products from reaction of isophthalaldehyde and the corresponding substituted triamine, including the 2+2 and 3+3 macrocyclic ligands and proton labeling used.
Nomenclature note: the numerical values indicate the number of reacted units and, in parentheses, the unreacted groups. For instance [1+1](n,o) means a condensation of one molecule of isophthalaldehyde and one of triamine. In parentheses the (n) indicates an unreacted amine and (o) indicates anunreacted aldehyde.

In our case, the [2+2] macrocyclic ligands **L73**, **L74** and **L75** (see *Scheme 4.2.2*) were prepared by a condensation of a 1:1 molar ratio of the corresponding substituted triamine and isophthalaldehyde. The latter was very slowly added to the triamine solution to favor both lower oligomeric compounds as well as macrocyclic type products. The relatively low yields obtained indicate the formation of other products and potentially unreacted starting materials. In all the cases, once the [2+2] condensation product was formed, it was redisolved in either CH_3OH or CH_3CN and was stirred at room temperature for 24 h. MS analysis of the resulting solution indicated the presence of the [2+2] condensation product only. Thus, this result indicated that once the macrocycle is formed, and in the absence of a catalyst, it is stable enough and there is no equilibration process that could generate a mixture of other species or oligomers, at least on the time scale of days.

4.2.3. Synthesis of Cu(I) Complexes.

An important factor that can strongly influence reactivity in the cycle formation in these ligands is the presence of a metal cation that can act as a templating agent and thus stabilize the formation of a condensation product that possesses a cavity size and shape that is complementary to those of the templating cation. Therefore, the synthesis of the Cu(I) complexes of the macrocyclic ligands **L73**, **L74** and **L75** was assayed either by mixing 2 equivalents of the $[\mathrm{Cu^I(CH_3CN)_4}]^+$ salt and one of the [2+2] free ligand. Additionally, a template procedure was also performed. The following equations 1-5 schematize these reactions.

Equation 1 $$2\,[\mathrm{Cu^I(MeCN)_4}]^+ + \mathbf{L73} \xrightarrow{\text{MeOH, r.t.}} \underset{\mathbf{1}^{2+}}{[\mathrm{Cu^I_2}(\mathbf{L73})]^{2+}} + 8\,\mathrm{MeCN}$$

Equation 2 $$3\,[\mathrm{Cu^I(MeCN)_4}]^+ + \mathbf{L73} \xrightarrow{\text{MeCN, r.t.}} \underset{\mathbf{4}^{3+}}{[\mathrm{Cu^I_3}(\mathbf{L76})]^{3+}} + 12\,\mathrm{MeCN}$$

Equation 3 $$3\,[\mathrm{Cu^I(MeCN)_4}]^+ + 3\,[1{,}3\text{-}\mathrm{ph(CHO)_2} + 3\,\mathrm{H_2NC_2py} \xrightarrow{\text{MeOH, r.t.}} \underset{\mathbf{4}^{3+}}{[\mathrm{Cu^I_3}(\mathbf{L76})]^{3+}} + 12\,\mathrm{MeCN}$$

Equation 4 $$[\mathrm{Cu^I(MeCN)_4}]^+ + \mathbf{L74} \xrightarrow{\text{MeCN, r.t.}} \underset{\mathbf{2}^{2+}}{[\mathrm{Cu^I_2}(\mathbf{L74})(\mathrm{MeCN})_2]^{2+}} + \underset{\mathbf{5}^{3+}}{[\mathrm{Cu^I_3}(\mathbf{L71})(\mathrm{MeCN})_3]^{3+}}$$

Equation 5 $$6\,[\mathrm{Cu^I(MeCN)_4}]^+ + 3\,\mathbf{L75} \xrightarrow{\text{MeCN, r.t.}} 2\,\underset{\mathbf{6}^{3+}}{[\mathrm{Cu^I_3}(\mathbf{L78})(\mathrm{MeCN})_3]^{3+}}$$

Scheme 4.2.3. Summary of the reactions performed involving ligands or precursors and Cu(I) and the products obtained.

Different conditions were assayed for the complexation of the ligands and the template synthesis. In the case of the complexation of **L73** ligand, the solvent and crystallization time have a strong influence over the complexes obtained. In CH_3OH, the main product obtained was the dinuclear complex $\mathbf{1}^{2+}$ (80% yield), as indicated in equation 1. On the other hand, and in sharp contrast, when using CH_3CN as the solvent it is generated the analogous trinuclear complex $\mathbf{4}^{3+}$ in 70% yield (Equation 2).

As discussed above in the ligand synthesis section, the **L73** ligand does not isomerizes in solution. Therefore, this suggests that the presence of a metal assisted in the transformation that generates **L76** out of **L73**, which will be discussed later. Further, a one pot synthesis using the triamine and dialdehyde and Cu(I) as a template metal generates the $\mathbf{4}^{3+}$ complex in 68% yield, as shown in equation 3.

In the case of the **L74** ligand, only the dinuclear complex, $\mathbf{2}^{2+}$, is obtained in either CH_3OH or CH_3CN in good yields (approximately 80%) after 1 h of mixing the reagents at room temperature. However, if the solution is allowed to stand for 12-15 days, a mixture of dinuclear, $\mathbf{2}^{2+}$, and trinuclear, $\mathbf{5}^{3+}$, complexes is obtained (equation 4).

Finally, for the case of the **L75** ligand, when mixed with Cu(I) only the trinuclear complex $\mathbf{6}^{3+}$ was obtained in 71% yield, indicating the formation of the **L78** ligand, as shown in equation 5.

A summary of the conditions for the synthesis of the different obtained complexes, either undergoing ligand rearrangement or not, as long as the experimental conditions used, is shown in *Table 4.2.1*.

Table 4.2.1. Summary of the synthesis of the described complexes. Experiments were done at room temperature.

	Reaction for Synthesis	Solvent	Isolation	Ring size	Yield	Colour
1$(PF_6)_2$	**L73** + 2 $Cu(MeCN)_4(PF_6)$	i) MeOH ii) CH_2Cl_2	i) Precipitation ii) Evaporation	2+2	80%	Dark yellow
4$(PF_6)_3$	$Cu(MeCN)_4(PF_6)$ + dialdehyde + diamine	MeOH	Precipitation	3+3	68%	Orange
4$(SbF_6)_3$	**L73** + 2 $Cu(MeCN)_4(PF_6)$	MeCN	Slow Et_2O diffusion (about 2 weeks)	3+3	69%	Orange
2$(CF_3SO_3)_2$ **and** **5**$(CF_3SO_3)_3$	**L74** + 2 $Cu(MeCN)_4(OTf)$	MeCN	Slow Et_2O diffusion (about 2 weeks)	2+2 and 3+3	81%	Yellow and Orange
6$(CF_3SO_3)_3$	**L75** + 2 $Cu(MeCN)_4(OTf)$	MeCN	Slow Et_2O diffusion (about 2 weeks)	3+3	71%	Yellow

The nomenclatures used for the ligands and for the corresponding complexes discussed in this chapter are summarized in *Table 4.2.1*.

Table 4.2.2. Nomenclatures used for the ligands and complexes discussed in this chapter.

Ligands		Complexes	
bsm2py$_{2+2}$	**L73**	$[Cu^{I}_2(\mathbf{L73})]^{2+}$	$\mathbf{1}^{2+}$
bsm2phOH$_{2+2}$	**L74**	$[Cu^{I}_2(\mathbf{L74})(MeCN)_2]^{2+}$	$\mathbf{2}^{2+}$
bsm2Et$_{2+2}$	**L75**	Complex Not Isolated	
bsm2py$_{3+3}$	**L76**	$[Cu^{I}_3(\mathbf{L76})]^{3+}$	$\mathbf{4}^{3+}$
bsm2pOH$_{3+3}$	**L77**	$[Cu^{I}_3(\mathbf{L77})(MeCN)_3]^{3+}$	$\mathbf{5}^{3+}$
bsm2Et$_{3+3}$	**L78**	$[Cu^{I}_3(\mathbf{L78})(MeCN)_3]^{3+}$	$\mathbf{6}^{3+}$

4.2.4. Solid State Characterization.

Crystals suitable for X-ray diffraction studies were obtained from these reactions, and the solid state structures for the dinuclear complex **2**$^{2+}$, the trinuclear complexes, **4**$^{3+}$, **5**$^{3+}$, and **6**$^{3+}$ as well as for the ligand **L74** were obtained. The ball and stick representation of these structures are depicted in *Figure 4.2.1*.

The crystal structure of the ligand **L74** consists of eight discrete **L74** molecules. The X-ray analysis shows four crystallographically independent but chemically identical **L74** units, which present very slight variations in bond distances and angles. It is interesting to note that, for each molecular structure, the two benzene rings are nearly parallel to one another and that the phenol groups are placed in mutually *trans* position in an inversion center arrangement around the tertiary amine, permitting the establishment of H-bonding with the nearby units.

For the dinuclear complex, **2**$^{2+}$, the *meta* substitution of the aromatic ring places the two copper centers at a distance of 7.97 Å˚ whereas the two benzene rings are nearly parallel to one another with an angle of 29.1º. Each copper center has a distorted tetrahedral arrangement as a result of the constraints imposed by the triaza moiety of the macrocyclic ligand. This generates a long Cu–N (2.208 Å) distance with the central amine group, two medium Cu–N (2.022 Å and 2.061 Å) distances with the imines, and a short distance with the CH_3CN monodentate ligand Cu–N (1.918 Å). The strain of the macrocyclic ligand also imposes two short N–Cu–N angles of 84.85 and 83.95º, with the rest of the N–Cu–N angles ranging 111–128º. Finally, the dangling phenol group is not coordinating the Cu metal center. The metric parameters described here are also in agreement with related Cu(I) complexes that have been previously reported in the literature.[52,250]

Selected bond distances and angles for the first coordination sphere of one of the Cu(I) metal centers of complexes **4**$^{3+}$, **2**$^{2+}$, **5**$^{3+}$, and **6**$^{3+}$ are listed in *Table 4.2.2*.

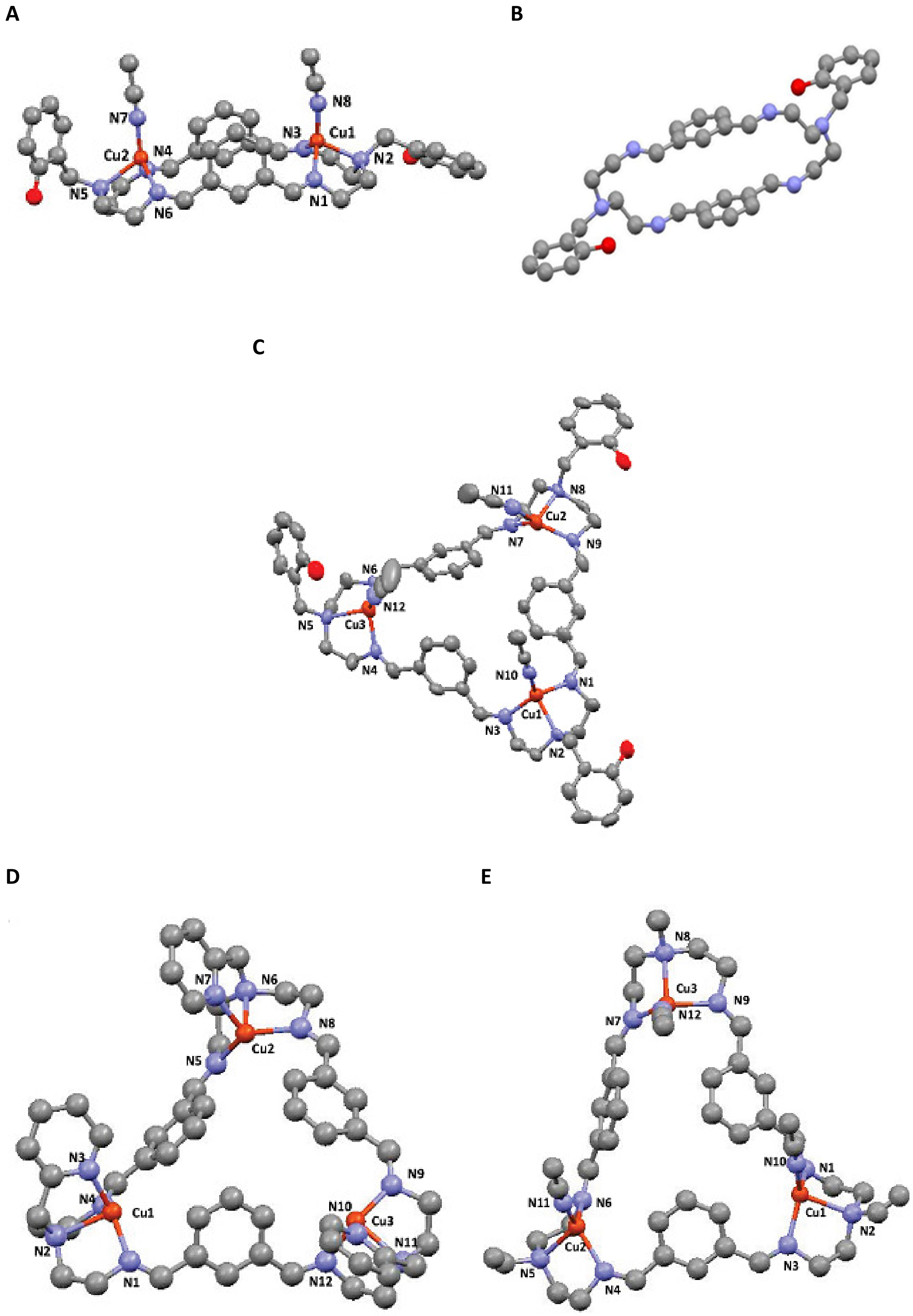
A
N7
N8
N3
Cu1
Cu2
N4
N2
N5
N6
N1
B
C
N11
N8
Cu2
N7
N9
N6
N12
N5
Cu3
N4
N10
N1
Cu1
N3
N2
D
N7
N6
N8
Cu2
N5
N3
N4
Cu1
N2
N1
N9
N10
Cu3
N11
N12
E
N8
Cu3
N9
N7
N12
N10
N1
N11
N6
Cu1
Cu2
N2
N5
N4
N3

Figure 4.2.2. Ball and stick diagrams for the X-ray crystal structure for Cu(I) complexes: (A) $\mathbf{2}^{2+}$; (B) ligand **L74**; (C) $\mathbf{5}^{3+}$; (D) $\mathbf{4}^{3+}$; (E) $\mathbf{6}^{3+}$. Color codes: Cu, orange; N, blue; C, gray; O, red. H atoms are not shown.

Table 4.2.3. Selected bond distances and angles for the first coordination sphere of one of the Cu(I) metal centers of complexes **2**(CF_3SO_3)$_2$, **4**(PF_6)$_3$, **5**(CF_3SO_3)$_3$, and **6**(CF_3SO_3).

2(CF_3SO_3)$_2$		**4**(PF_6)$_3$	
Cu(1)–N$_{\mathrm{MeCN}}$(8)	1.918(2)	Cu(1)–N$_{\mathrm{py}}$(10)	2.043(7)
Cu(1)–N$_{\mathrm{im}}$(3)	2.0223(19)	Cu(1)–N$_{\mathrm{im}}$(1)	1.989(7)
Cu(1)–N$_{\mathrm{im}}$(1)	2.0610(18)	Cu(1)–N$_{\mathrm{im}}$(3)	2.011(7)
Cu(1)–N$_{\mathrm{ter}}$(2)	2.2078(18)	Cu(1)–N$_{\mathrm{ter}}$(2)	2.183(7)
N$_{\mathrm{MeCN}}$(8)–Cu(1)–N$_{\mathrm{im}}$(3)	128.82(8)	N$_{\mathrm{im}}$(3)–Cu(1)–N$_{\mathrm{im}}$(1)	130.9(3)
N$_{\mathrm{MeCN}}$(8)–Cu(1)–N$_{\mathrm{im}}$(1)	116.10(8)	N$_{\mathrm{im}}$(1)–Cu(1)–N$_{\mathrm{py}}$(10)	115.7(3)
N$_{\mathrm{im}}$(3)–Cu(1)–N$_{\mathrm{im}}$(1)	111.32(8)	N$_{\mathrm{im}}$(3)–Cu(1)–N$_{\mathrm{py}}$(10)	110.7(3)
N$_{\mathrm{MeCN}}$(8)–Cu(1)–N$_{\mathrm{ter}}$ (2)	117.68(8)	N$_{\mathrm{im}}$(1)–Cu(1)–N$_{\mathrm{ter}}$ (2)	86.2(3)
N$_{\mathrm{im}}$(3)–Cu(1)–N$_{\mathrm{ter}}$ (2)	83.96(7)	N$_{\mathrm{im}}$(3)–Cu(1)–N$_{\mathrm{ter}}$ (2)	85.1(3)
N$_{\mathrm{im}}$(1)–Cu(1)–N$_{\mathrm{ter}}$(2)	84.85(7)	N$_{\mathrm{py}}$(10)–Cu(1)–N$_{\mathrm{ter}}$(2)	81.8(3)

5(CF_3SO_3)$_3$		**6**(CF_3SO_3)$_3$	
Cu(1)–N$_{\mathrm{MeCN}}$ (10)	1.97(7)	Cu(1)–N$_{\mathrm{MeCN}}$(10)	1.917(10)
Cu(1)–N$_{\mathrm{im}}$(1)	2.04(5)	Cu(1)–N$_{\mathrm{im}}$(1)	2.026(7)
Cu(1)–N$_{\mathrm{im}}$(3)	2.05(5)	Cu(1)–N$_{\mathrm{im}}$(3)	2.036(8)
Cu(1)–N$_{\mathrm{ter}}$(2)	2.19(5)	Cu(1)–N$_{\mathrm{ter}}$(2)	2.209(8)
N$_{\mathrm{MeCN}}$(10)–Cu(1)–N$_{\mathrm{im}}$(3)	122(2)	N$_{\mathrm{MeCN}}$(10)–Cu(1)–N$_{\mathrm{im}}$(1)	113.7(3)
N$_{\mathrm{MeCN}}$(10)–Cu(1)–N$_{\mathrm{im}}$(1)	111(2)	N$_{\mathrm{MeCN}}$(10)–Cu(1)–N$_{\mathrm{im}}$(3)	121.0(3)
N$_{\mathrm{im}}$(3)–Cu(1)–N$_{\mathrm{im}}$(1)	123(2)	N$_{\mathrm{im}}$(1)–Cu(1)–N$_{\mathrm{im}}$(3)	123.7(3)
N$_{\mathrm{MeCN}}$ (10)–Cu(1)–N$_{\mathrm{ter}}$ (2)	120(2)	N$_{\mathrm{MeCN}}$(10)–Cu(1)–N$_{\mathrm{ter}}$ (2)	115.5(3)
N$_{\mathrm{im}}$(3)–Cu(1)–N$_{\mathrm{ter}}$ (2)	85(2)	N$_{\mathrm{im}}$(1)–Cu(1)–N$_{\mathrm{ter}}$ (2)	83.7(3)
N$_{\mathrm{im}}$(1)–Cu(1)–N$_{\mathrm{ter}}$(2)	85(2)	N$_{\mathrm{im}}$(3)–Cu(1)–N$_{\mathrm{ter}}$(2)	84.4(3)

For the trinuclear complexes **5**$^{3+}$ and **6**$^{3+}$, the local Cu(I) coordination is comparable to that of the dinuclear **2**$^{2+}$ complex. In the tricopper complexes, the metal centers are disposed in a triangular arrangement with Cu–Cu distances (ranging from 8.8 to 9.4 Å) that are a bit larger than those for the dinuclear complex. Comparing the **5**$^{3+}$ trinuclear complex and the **2**$^{2+}$ dinuclear complex, the major difference is that the latter has slightly shorter N$_{\mathrm{im}}$–Cu$_{(1)}$–N$_{\mathrm{im}}$ angles, 119–123 vs. 108–111.32, while the Cu bonding distances are practically identical. For the trinuclear complex **4**$^{3+}$, the dangling pyridyl group is coordinating the metal center, replacing the CH_3CN when compared to **5**$^{3+}$. For the trinuclear complexes, it is also interesting to see that the three benzene rings altogether adopt a bowl shape arrangement.

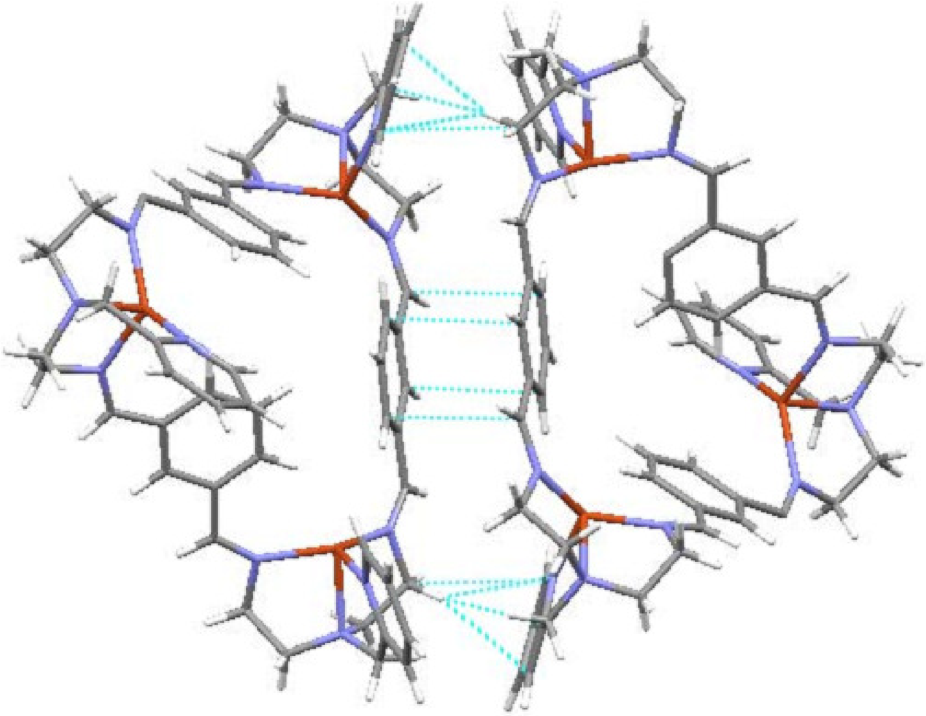

Figure 4.2.3. View of the π–π and CH-π interactions leading to a dimer of trinuclear complexes in the packing structure of **4**(SbF_6)$_3$. The interactions are shown with a dashed blue line.

With regard to the 3D packing of these molecules, it is interesting to realize that those containing the triflate anion have packing that is dominated by H-bonding with triflate oxygen atoms and the macrocycle. A similar situation is found for complex 4^{3+} containing PF_6^- as counteranion that crystallizes with THF, H_2O, and CH_3OH. Here again, packing interactions are dominated by extensive hydrogen bonding between the solvate oxygen atoms and the macrocycle. However, complex **4**$^{3+}$ containing SbF_6^- as counteranion crystallizes with no solvate molecules, and its packing structure is significantly different from the rest. In particular, it is interesting to see the presence of dimers of trinuclear units bonded by π–π and CH–π interactions between macrocyclic ligands, as it is shown in *Figure 4.2.2*.

4.2.5. Stability of the complexes to oxidation.

It must be specified that the Cu(I) complexes described here, in general, when left in contact in an oxygenated atmosphere, react slowly at room temperature (within the time scale of days) with molecular oxygen to the oxidized Cu(II) complexes (as followed by the change of color of the solutions of the complexes left in contact with atmospheric oxygen). Exceptions are the complexes containing the phenolic ligand, **2**$^{2+}$ and **5**$^{3+}$, which are easily oxidized. These low reaction oxidation rates manifest the general capacity of the Schiff base ligand to stabilize the Cu(I) oxidation state in a CH_3CN solution

It must also be noted that, unlike the complex with the analog non substituted ligand **bsM2** $[Cu_2(\mathbf{bsM2})(CH_3CN)_2]^{2+}$,[251] no hydroxylation of the ligand occurs with the complexes described in the present work when the complexes are oxidized under aerobic atmosphere.

4.2.6. Mass Spectroscopy and the [2+2] vs. [3+3] Evolution Process.

Complexes **2^{2+}** and **5^{3+}** were analyzed by ESI-MS, and their spectra are presented in *Figure 4.2.3*. In both cases, their molecular peaks could not be identified, but a series of fragments are found. For complex **2^{2+}**, key monocharged peaks at *m/z* = 615 (**L74** + H, highest intensity), 637 (**L74** + Na), 677 (**L74** + Cu), 739 (**L74** +Cu_2 – 1), and 766 (**L74** + Cu_2Na – 2) could be identified. For complex **5^{3+}**, key peaks are found at *m/z* = 922 (**L77** + H, highest intensity), 984 (**L77** + Cu), and their corresponding doubly charged peaks at *m/z* = 461 and 492, respectively. For both complexes, the relative intensities of their peaks coincide perfectly with the simulated ones.

The reaction of $[Cu^I(CH_3CN)_4]^+$ in CH_3CN with the [2+2] condensation macrocyclic ligand **L74** generates a mixture of the dinuclear and trinuclear complexes as indicated in equation 4 (*Scheme 4.2.3*). Thus, it can be inferred that an equilibrium between the dinuclear and trinuclear complex may exist (equation (6)).

Equation 6

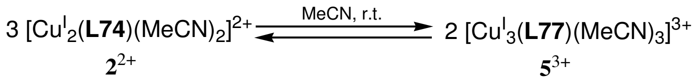

$$\underset{\mathbf{2^{2+}}}{3\,[Cu^I_2(\mathbf{L74})(MeCN)_2]^{2+}} \xrightleftharpoons{\text{MeCN, r.t.}} \underset{\mathbf{5^{3+}}}{2\,[Cu^I_3(\mathbf{L77})(MeCN)_3]^{3+}}$$

This reaction was monitored using MS, following the relative intensities of the peaks at *m/z* = 615 for **2^{2+}** and *m/z* = 922 for **5^{3+}**, at room temperature. The initial concentration of complex **2^{2+}** was 0.026 M, and no **5^{3+}** was observed, as depicted in *Figure 4.2.4*. As time elapsed, the formation of **5^{3+}** was observed. After 1.5 months, the system reaches equilibrium, a steady relation of the intensity of peaks of **5^{3+}** versus **2^{2+}** over time, being the complex **2^{2+}** the main present species despite the formation of **5^{3+}** (see *equation 6*). This indicates that the [2+2] condensation complex **2^{2+}** is more energetically favored than the [3+3] complex **5^{3+}**, probably as a result of entropic factors and also, to a minor extent, of the relative strain of their structures.

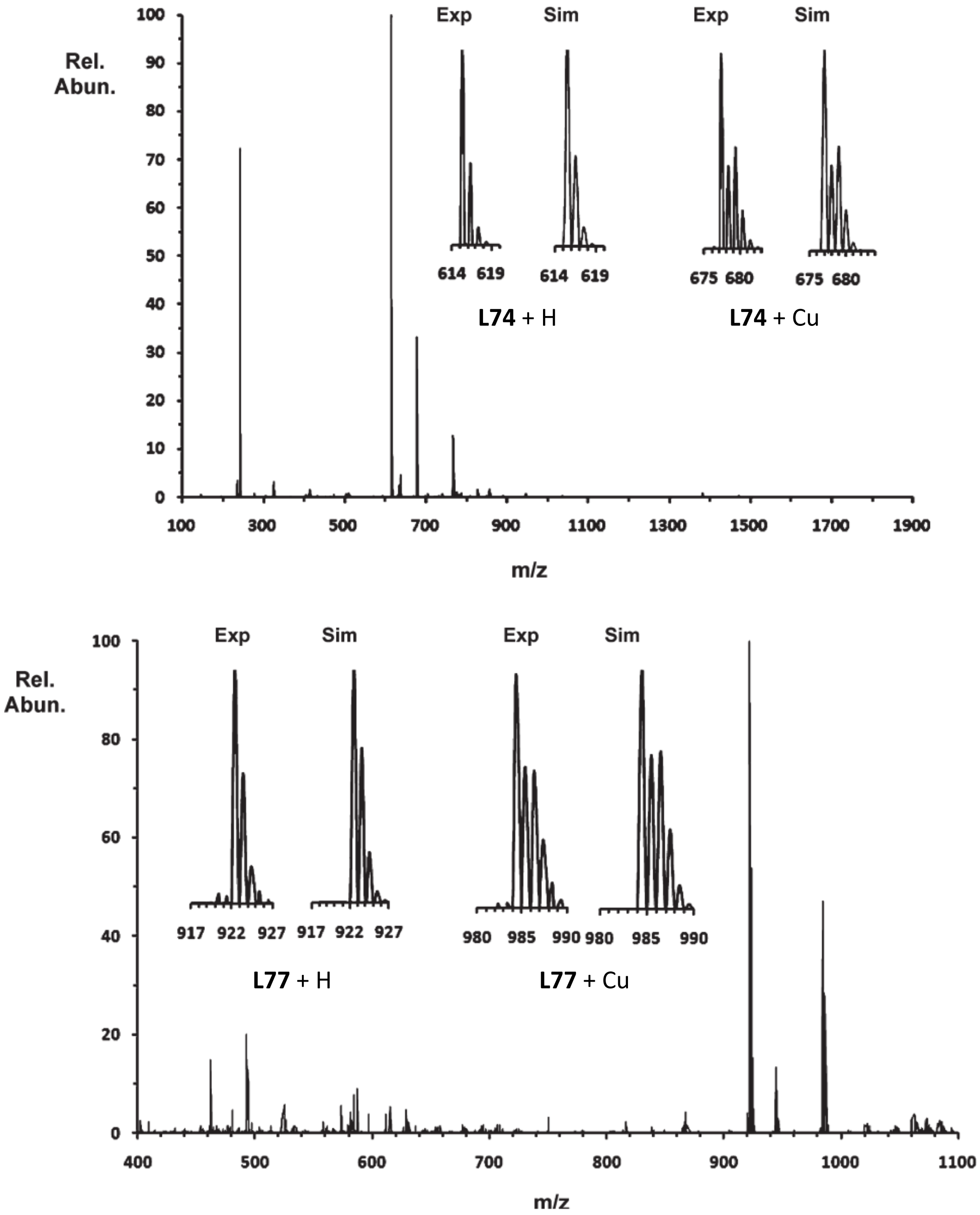

Figure 4.2.4. ESI-MS spectra obtained for **2**$(CF_3SO_3)_2$ (top) and **5**$(CF_3SO_3)_3$ (bottom) in CH_3CN.

It is important to bear in mind that these experiments have been carried out under high dilution conditions so that both complexes are completely soluble. Therefore, these results cannot be extrapolated at a synthetic level with regard to the relative amount of **2**$^{2+}$ and **5**$^{3+}$ because in that case we used a mixture of CH_3CN and ether.

4.2.7. Final remarks

All the results clearly show that, under certain conditions, the studied ligands obtained from the 2+2 reaction of isophthalaldehyde and a substituted triamine with 2 methylenes as spacers may undergo a structural rearrangement, implying an expansion of the macrocyclic ring.

The formation of the trinuclear complex from the dinuclear compound indicates that at least one of the imine C=N of the [2+2] Schiff base ligand has to be broken, and then the fragments have to react again so that the new [3+3] ligand can be formed. This process has not been observed for the free ligand, at least during the time scale of days. Thus, it must be assisted by the Cu(I) dinuclear complex. This is in sharp contrast with the cases of other macrocyclic ligands where this process is known to occur very quickly, as it is the case for the systems derived from pyridine dialdehyde and diamine.[10,249]

Potential condensation products that can be obtained from the reaction of a 1:1 dialdehyde and triamine to illustrate the variety of compounds, including macrocyclic and acyclic compounds are presented in *Scheme 4.2.2*. As mentioned earlier, the **L74** has not shown to undergo any reorganization process by itself, but it does so when complexed to Cu(I) ions. Thus, potential fragments that can lead to the trinuclear complex are as follows:

Equation 7 $$\{Cu^{I}_{2}[2+(o2)]\}^{2+} + \{Cu^{I}[1+2(n2)]\}^{+} \xrightarrow{\text{MeCN, r.t.}} \underset{\mathbf{5}^{3+}}{[Cu^{I}_{3}(\mathbf{L77})(MeCN)_{3}]^{3+}}$$

Equation 8 $$\{Cu^{I}_{2}[2+2(n,o)]\}^{2+} + \{Cu^{I}[1+1(n,o)]\}^{+} \xrightarrow{\text{MeCN, r.t.}} \underset{\mathbf{5}^{3+}}{[Cu^{I}_{3}(\mathbf{L77})(MeCN)_{3}]^{3+}}$$

The ligand nomenclature is described in *Scheme 4.2.2*. For instance, for the case of [2 + 1(o2)], the [2+1] indicates the condensation product of two dialdehydes and one triamine and in the parentheses is indicated the number and nature of unreacted groups, **n** for a primary amine and **o** for aldehyde.

In summary, the ligands described in this section have been synthesised as stable products of a 2+2 condensation of isophthalaldehyde and a functionalised triamine.

Nontheless, when in contact with Cu(I) ions and in acetonitrile solution, they undergo rearrangement reactions in solution, being observed an equilibrium between the [2+2] and [3+3] complexes.

4.3. DNA-Cleavage Induced by New Macrocyclic Schiff base Dinuclear Cu(I)Complexes Containing Pyridyl Pendant Arms

4.3.1. Abstract.

In the past few years, artificial nucleases have been presented as valuable tools in genomic research, as well as promising candidates for application in cancer therapy. Of special interest are multinuclear copper(I) complexes which, in combination with hydrogen peroxide or molecular oxygen can generate reactive species that damage DNA by direct strand scission or base modification.

In this section it is reported the synthesis and characterization of three new dinuclear Cu(I) complexes with hexaazamacrocyclic Schiff base ligand containing pyridyl pendant arms. The nuclease activity of these complexes in presence of hydrogen peroxide towards calf thymus DNA has been investigated by circular dichroism spectroscopy (CD), atomic force microscopy (AFM) and electrophoretic mobility (EM).

All the complexes interact with DNA through a non intercalative way, but each one shows a different degree of nuclease activity in presence of hydrogen peroxide, due to the different electronic factors and complex topology induced by the natures of the different ligands. These results highlight how small modifications introduced in the macrocyclic backbone of the metal complexes lead to dramatic changes in the nuclease activity.

4.3.2. Synthesis, Structure, and Redox Properties of the complexes.

The macrocyclic ligands and their dicopper(I) complexes described in this section (see *Figure 4.3.1*) were prepared analogously to the ligands and complexes in the section 3.2, following the procedure depicted in the *Scheme 4.3.1*.

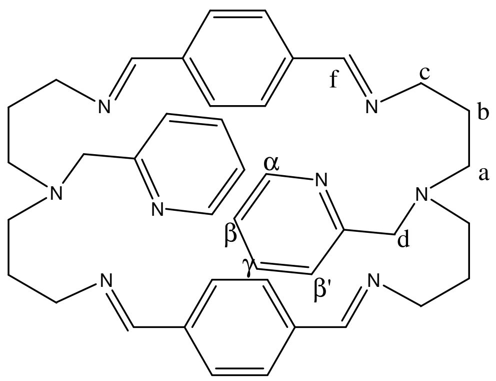

bsp3py - **L79**

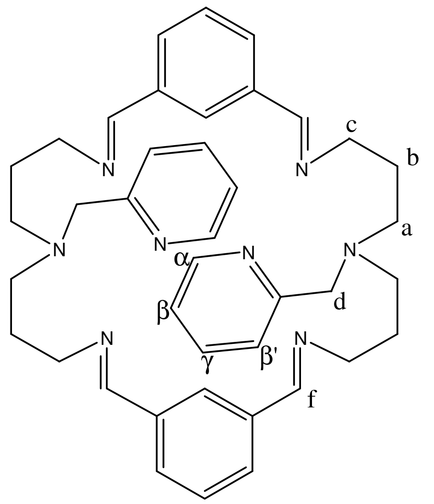

bsm3py - **L80**

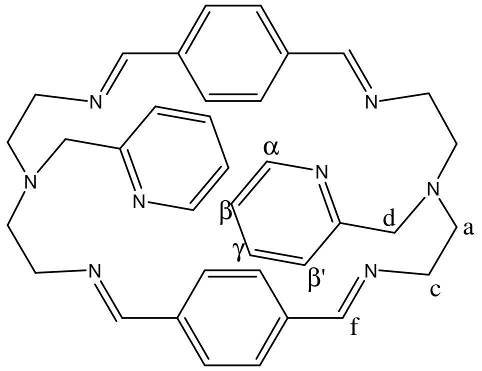

bsp2py - **L81**

Figure 4.3.1. Drawing of the macrocyclic ligands discussed in chapter 4.3 together with the abbreviations and proton labeling.

The macrocyclic ligands were obtained through a 2+2 condensation between the corresponding dialdehydes and the previously prepared diamines affords the desired ligands.

To prepare the functionalized amines, the initial triamines (either diethylenetriamine or *N*-(3-aminopropyl)-1,3-propanediamine) were protected with phthtalic anhydride, followed by functionalization of the central secondary amine and finally deprotecting with hydrazine in ethanol/chloroform at room temperature. Reaction of the triamine either with 2 or 3 methylenes as aliphatic spacers, and the corresponding dialdehyde (either isophthalaldehyde or terephthalaldehyde) in 1:1 ratio afforded the macrocyclic ligands, which differ in the number of the methylenes between the amines and also in the geometry of the aromatic spacer. The dinuclear Cu(I) complexes were easily obtained by direct reaction of the ligands with Cu(I) salts, under anaerobic conditions. No reorganization or expansion of the ring ligands has been observed. A complete structural and spectroscopic characterization is reported in the *Methodology* section.

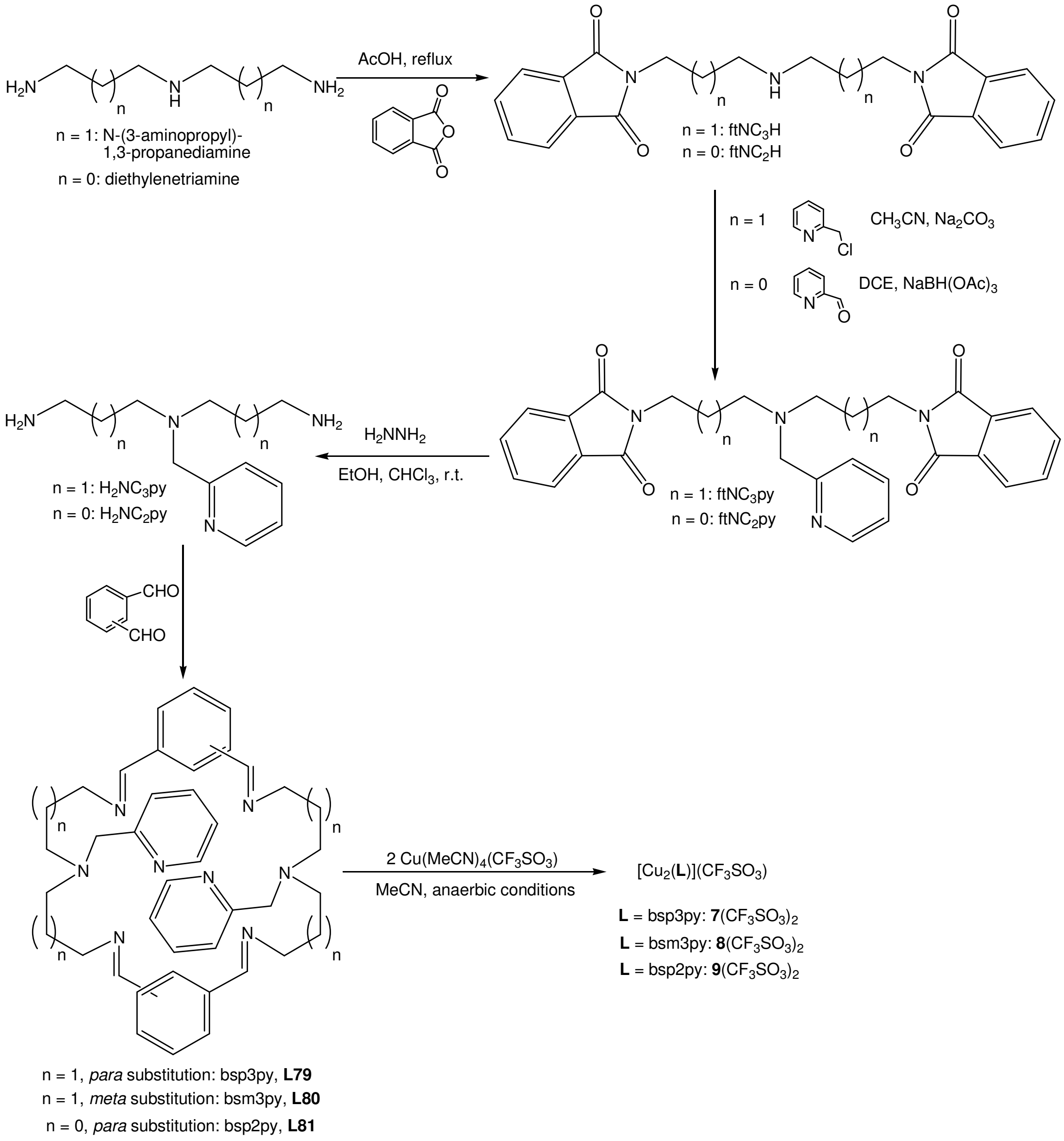
AcOH, reflux
n = 1: N-(3-aminopropyl)-1,3-propanediamine
n = 0: diethylenetriamine
n = 1: ftNC3H
n = 0: ftNC2H
n = 1
CH3CN, Na2CO3
n = 0
DCE, NaBH(OAc)3
H2NNH2
EtOH, CHCl3, r.t.
n = 1: ftNC3py
n = 0: ftNC2py
n = 1: H2NC3py
n = 0: H2NC2py
CHO
CHO
2 Cu(MeCN)4(CF3SO3)
MeCN, anaerbic conditions
[Cu2(L)](CF3SO3)
L = bsp3py: 7(CF3SO3)2
L = bsm3py: 8(CF3SO3)2
L = bsp2py: 9(CF3SO3)2
n = 1, para substitution: bsp3py, L79
n = 1, meta substitution: bsm3py, L80
n = 0, para substitution: bsp2py, L81

Scheme 4.3.1. Synthetic Scheme for Ligands and Complexes discussed in Chapter 4.3.

Complexes **7**(CF_3SO_3)$_2$, **8**(SbF_6)$_2$, and **9**(CF_3SO_3)$_2$ have been characterized by means of X-ray diffraction analysis, their crystallographic data is collected in the *Table 3.1* (see Methodology chapter, page 62), and their ORTEP plots are presented in *Figure 4.3.2*. Bond lengths and angles for the metal coordination environment are listed in *Table 4.3.1*.

The cationic part of the three complexes contains the macrocyclic ligands coordinating two copper atoms. In all three cases each metal center is bonded to four nitrogens of the ligand at each side of the aromatic spacer, showing a distorted tetrahedral coordination. The N_{im}–Cu and N_{py}–Cu distances are very similar ranging from 1.959(4) Å to 2.073(4) Å (see *Table 4.3.1*) whereas the N_{ter}–Cu distance is significantly longer in the range of 2.200(3) Å to 2.221(4) Å which is in agreement with distances previously reported for related complexes.[250,251,253–255] The geometries around the copper centers are relatively similar, although complex **9**$^{2+}$ which forms five member rings is slightly more constrained than **7**$^{2+}$ and **8**$^{2+}$ that form six member rings (see bond angles in *Table 4.3.1*).

Table 4.3.1. Selected Bond Lengths (Å) and Angles (deg) for **7(CF_3SO_3)$_2$**, **8(SbF_6)$_2$**, and **9(CF_3SO_3)$_2$.**

7(CF_3SO_3)$_2$		**8(SbF_6)$_2$**		**9(CF_3SO_3)$_2$**	
Cu(1)—N_{im}(1)	1.959(4)	Cu(1)—N_{im}(1)	1.985(3)	Cu(1)—N_{im}(3)	1.983(3)
Cu(1)—N_{im}(4)	1.993(4)	Cu(1)—N_{im}(3)	1.987(3)	Cu(1)—N_{im}(8)	2.032(3)
Cu(1)—N_{py}(3)	2.073(4)	Cu(1)—N_{py}(7)	2.031(3)	Cu(1)—N_{py}(1)	2.004(3)
Cu(1)—N_{ter}(2)	2.205(4)	Cu(1)—N_{ter}(2)	2.206(3)	Cu(1)—N_{ter}(2)	2.207(3)
Cu(2)—N_{im}(8)	2.002(4)	Cu(2)—N_{im}(6)	1.982(3)	Cu(2)—N_{im}(7)	1.985(3)
Cu(2)—N_{im}(5)	2.002(4)	Cu(2)—N_{im}(4)	2.005(3)	Cu(2)—N_{im}(4)	2.018(3)
Cu(2)—N_{py}(7)	2.031(4)	Cu(2)—N_{py}(8)	2.019(3)	Cu(2)—N_{py}(6)	2.038(3)
Cu(2)—N_{ter}(6)	2.221(4)	Cu(2)—N_{ter}(5)	2.203(3)	Cu(2)—N_{ter}(5)	2.200(3)
Cu(1)—Cu(2)	7.364	Cu(1)—Cu(2)	4.517	Cu(1)—Cu(2)	6.956
N_{im}(1)—Cu(1)—N_{im}(4)	131.71(15)	N_{im}(1)—Cu(1)—N_{im}(3)	121.37(14)	N_{im}(3)—Cu(1)—N_{im}(8)	116.30(12)
N_{im}(1)—Cu(1)—N_{py}(3)	125.60(16)	N_{im}(1)—Cu(1)—N_{py}(7)	123.62(13)	N_{im}(3)—Cu(1)—N_{py}(1)	129.81(12)
N_{im}(4)—Cu(1)—N_{py}(3)	100.33(15)	N_{im}(3)—Cu(1)—N_{py}(7)	114.87(13)	N_{im}(8)—Cu(1)—N_{py}(1)	110.72(11)
N_{im}(1)—Cu(1)—N_{ter}(2)	99.70(16)	N_{im}(1)—Cu(1)—N_{ter}(2)	95.51(13)	N_{im}(3)—Cu(1)—N_{ter}(2)	85.90(11)
N_{im}(4)—Cu(1)—N_{ter}(2)	102.32(15)	N_{im}(3)—Cu(1)—N_{ter}(2)	97.05(13)	N_{im}(8)—Cu(1)—N_{ter}(2)	85.25(11)
N_{py}(3)—Cu(1)—N_{ter}(2)	80.12(15)	N_{py}(7)—Cu(1)—N_{ter}(2)	81.02(12)	N_{py}(1)—Cu(1)—N_{ter}(2)	81.32(11)
N_{im}(8)—Cu(2)—N_{im}(5)	113.13(17)	N_{im}(6)—Cu(2)—N_{im}(4)	119.84(13)	N_{im}(7)—Cu(2)—N_{im}(4)	125.76(12)
N_{im}(8)—Cu(2)—N_{py}(7)	119.68(16)	N_{im}(6)—Cu(2)—N_{py}(8)	122.54(13)	N_{im}(7)—Cu(2)—N_{py}(6)	120.05(12)
N_{im}(5)—Cu(2)—N_{py}(7)	126.64(16)	N_{im}(4)—Cu(2)—N_{py}(8)	117.60(13)	N_{im}(4)—Cu(2)—N_{py}(6)	111.21(12)
N_{im}(8)—Cu(2)—N_{ter}(6)	98.11(15)	N_{im}(6)—Cu(2)—N_{ter}(5)	95.29(13)	N_{im}(7)—Cu(2)—N_{ter}(5)	85.46(11)
N_{im}(5)—Cu(2)—N_{ter}(6)	97.97(15)	N_{im}(4)—Cu(2)—N_{ter}(5)	94.89(13)	N_{im}(4)—Cu(2)—N_{ter}(5)	85.41(11)
N_{py}(7)—Cu(2)—N_{ter}(6)	82.21(17)	N_{py}(8)—Cu(2)—N_{ter}(5)	81.14(13)	N_{py}(6)—Cu(2)—N_{ter}(5)	81.70(12)

It is interesting to mention here that the distances between metal centers are basically controlled by the *meta* or *para* substitution in the phenylic spacer, rather than being affected by the number of methylenic units between amine moieties (around 7 Å for *para* substituted and 4.5 Å for *meta* substituted) even though in solution there will be a certain flexibility, and also influences the 3D topography of the molecule. Thus the *meta* molecule has a spherical shape whereas the *para* substituted resemble a rectangular cuboid.

In addition to the geometry of the aromatic spacer, the methylenic spacers between the amine nitrogen atoms have also a strong influence on the relative disposition of the metal centers, as has been previously shown by related macrocyclic complexes[255]. This is neatly reflected by the angles between the pyridylic rings ($\theta_{py–py}$ = 50.88º for **7**, 80.36º for **8**, and 79.61º for **9**) and also to the angle between the phenylic rings ($\theta_{ph\text{-}ph}$ = 17.14º for **7**, 52.85º for **8**, and 85.51º for **9**) due to their relative rotational capacity.

The redox properties of the complexes **7–9** were investigated by CV and SQWV, and the voltammograms are shown in *Figure 4.3.3.*

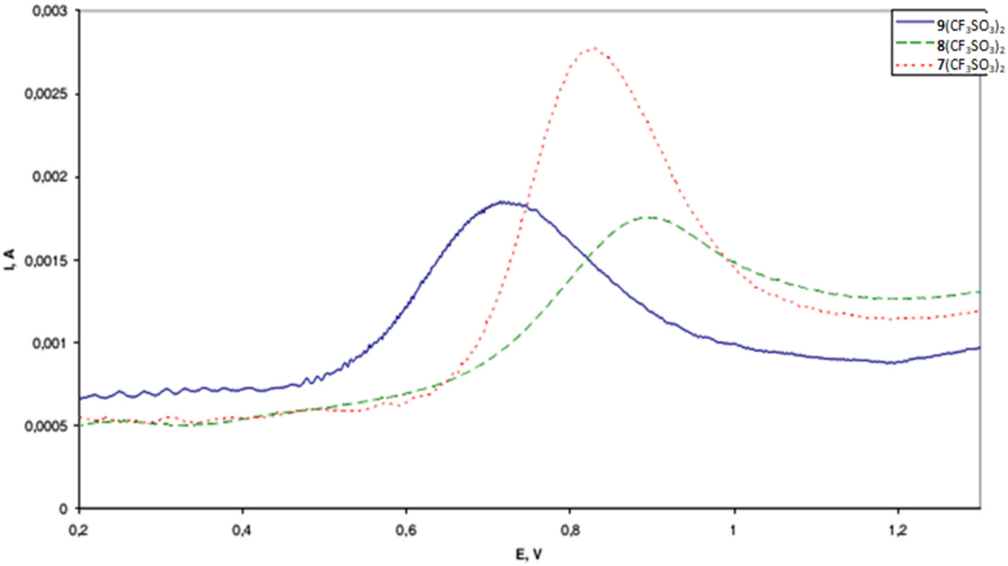

Figure 4.3.2. Square Wave Voltammetrys of complexes **7**($CF_3SO_3)_2$, **8**($CF_3SO_3)_2$ and **9**($CF_3SO_3)_2$.

The CV of complexes **7–9** show chemically irreversible waves in the anodic region indicating the irreversibility of the Cu(II)/ Cu(I) redox couple which is not unusual for this type of compound given the different coordination preferences of these two oxidation states of Cu. On the other hand SQWV experiments with a pulse frequency of 10 Hz allows the formal redox potentials of the Cu(II)/Cu(I) couple to be calculated, and they are 0.82, 0.89, and 0.71 V for **7**, **8**, and **9** respectively. These redox potentials are a consequence of the number of methylenic units bonding the amines and the effective overlap involved in the Cu–N bonding that is influenced by the ligand geometry.

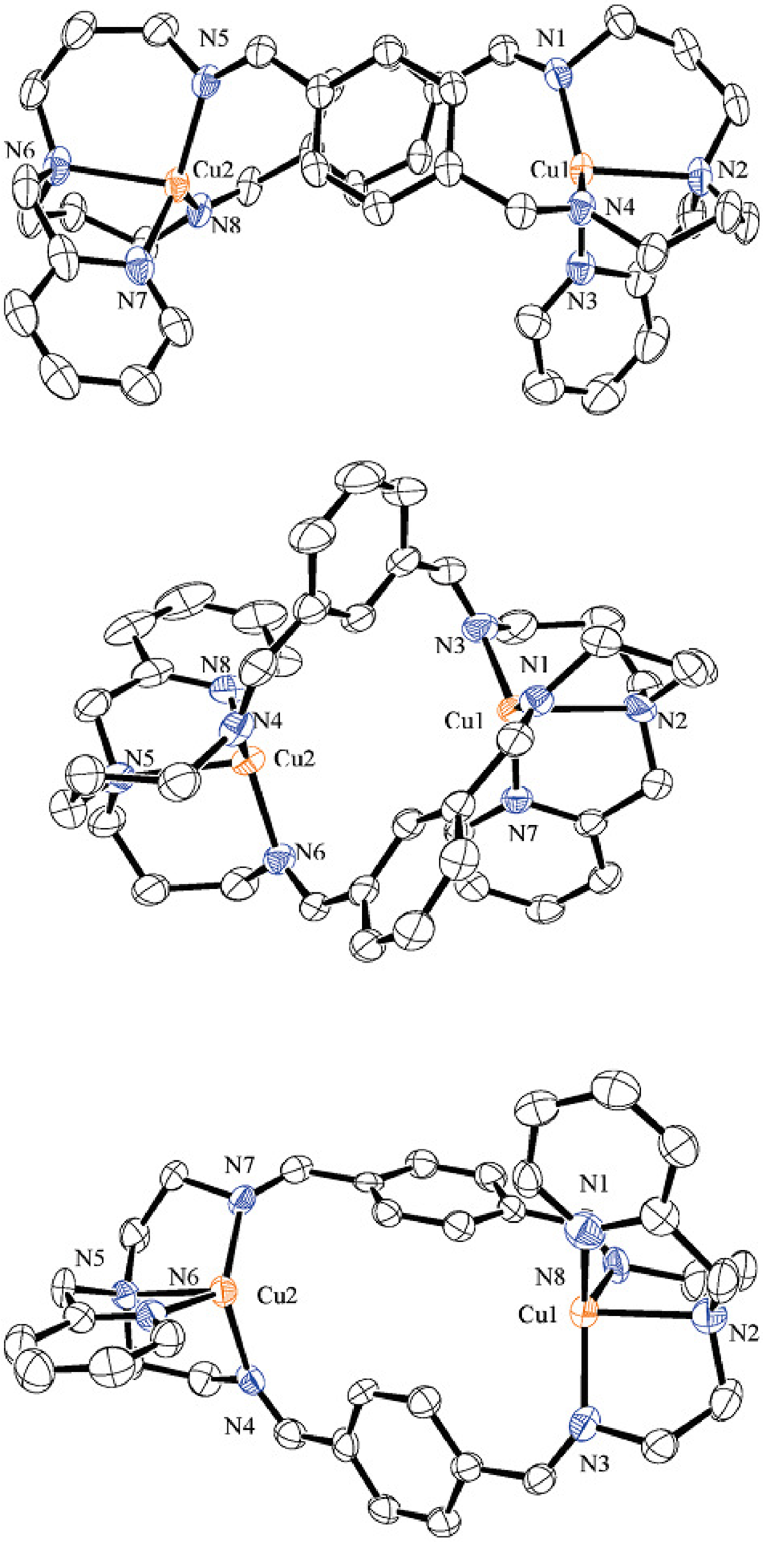
N5
N1
N6
Cu2
Cu1
N2
N8
N4
N7
N3
N3
N8
N1
N4
Cu1
N2
Cu2
N5
N7
N6
N7
N1
N5
N6
N8
Cu2
Cu1
N2
N4
N3

Figure 4.3.3. ORTEP plots (80% probability) for the cationic structures of the Cu(I) complexes: **7**$^{2+}$ (top), **8**$^{2+}$, (middle) and **9**$^{2+}$ (bottom).

These results are in accordance with the IR spectra of the dissolved CO complexes. The band corresponding to the C-O bond of the copper coordinated carbon monoxide is equivalent for complexes **7** and **8**, being displaced to slightly higher frequencies for complex **9**.

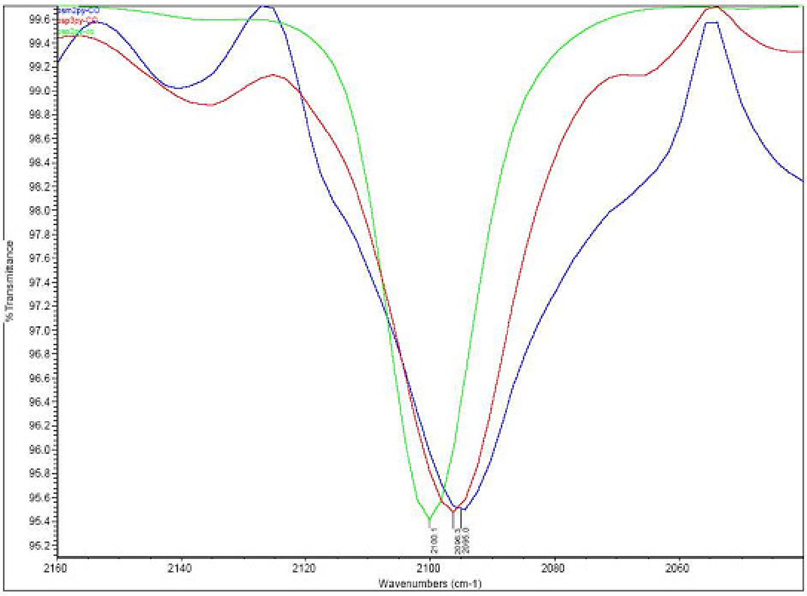

Figure 4.3.4. FT-IR spectroscopy of the CO adducts measured in a CH_2Cl_2 solution of each BARF-complex after bubbling with CO for a couple of minutes. ν(CO) of 2096 cm^{-1} for **7**(BArF)$_2$ (red line), 2095 for **7**(BArF)$_2$ (blue line) and 2101 cm^{-1} for **9**(BArF)$_2$ (light green line).

4.3.3. DNA–Copper Complex Interaction Studies.

The mode and propensity of binding of the Cu(I) complexes to DNA were studied by CD spectroscopy to observe changes in the DNA secondary structure, EM in agarose gel to appreciate changes in the DNA tertiary structure, and AFM to visualize changes in the DNA topography and morphology.

4.3.3.1. CD Spectroscopy.

CD spectroscopy is a powerful technique to provide useful information on changes in DNA morphology and secondary structure as a consequence of complex–DNA interactions.[256]

The CD spectra of Calf Thymus DNA incubated 24 h at 37ºC with the corresponding copper complexes at several ratios (r_i = 0.1, 0.3, 0.5) were recorded and they are shown in *Figure 4.3.5*. The DMSO used for the sample preparation presents some overlapping bands near the minima of ellipticity but does not interfere at the corresponding maxima.[257,258]

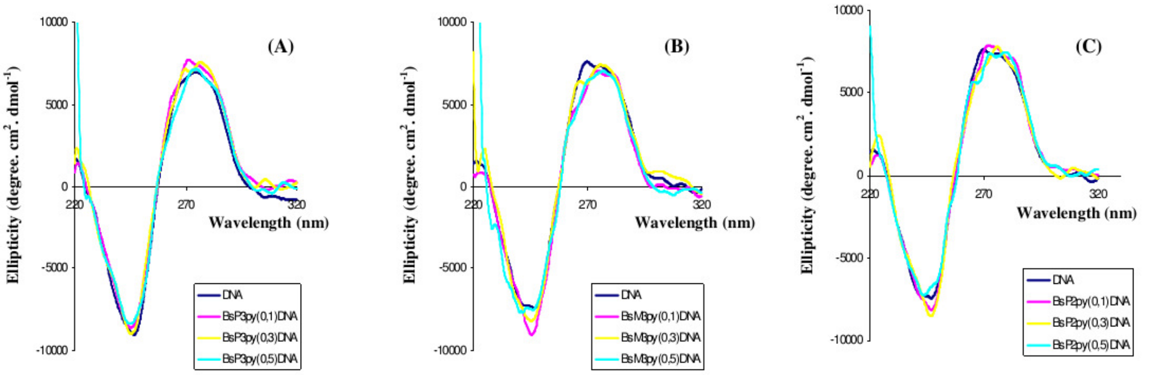

Figure 4.3.5. CD Spectra of Calf Thymus DNA incubated with Cu(I) Complexes: **7**($CF_3SO_3)_2$ (A), **8**($CF_3SO_3)_2$ (B), **9**($CF_3SO_3)_2$ (C) at different r_i(input molar ratio of the complex to nucleotide) values. Ellipticity θ(degree·cm^2·dmol^{-1}). Wavelength, λ(nm). (DNA concentration 20 μg/mL, molar ratios r_i = 0.10, 0.30, 0.50).

For complexes **7–9** no large perturbations in ellipticity and wavelength of the two bands on the CD spectra of CT–DNA were observed, although some slight differences can be appreciated. This indicates that the stacking mode and the orientation of base pairs in DNA is slightly disturbed, and thus the B-form character of CT DNA is still maintained. Therefore, the nature of the interaction of the Cu(I) complexes with DNA is mainly of a non–intercalative type.[259–261] This can also be supported by the crystal structures of the different Cu(I) complexes described in this work, since their geometrical nature does not produce a good fit for DNA with this type of interaction. These conclusions are in agreement with previously reported examples in the literature that have shown that the right-handed B form of free CT DNA shows a typical CD spectrum with a positive band (maximum about 268–272 nm) due to base stacking and a negative band (maximum about 245–243 nm) due to right-handed helicity[262,263] and that the intercalation of small molecules to DNA would cause a characteristic decrease in both positive and negative bands.[259]

On the other hand simple groove binding and electrostatic interaction of small molecules with DNA shows little or no perturbations on the two bands[262,264] as observed in our case.

4.3.3.2. EM in Agarose Gel.

The influence of complexes **7**–**9** on the tertiary structure of DNA was determined by its ability to modify the EM (electrophoretic mobility through the agarose gel) of the pBR322 plasmid DNA, which presents a circular shape with two main forms: a relaxed open circular form (OC) and a supercoiled covalently closed form (CCC) that is much more compacted than the former one.

OC form is presented naturally, as a relaxed form of the CCC, but can also be obtained if the complex performs a single strand scission to CCC DNA form.

A linear form can be obtained through a metal mediated double strand scission of the CCC form of DNA, or from a second scission of the OC form.

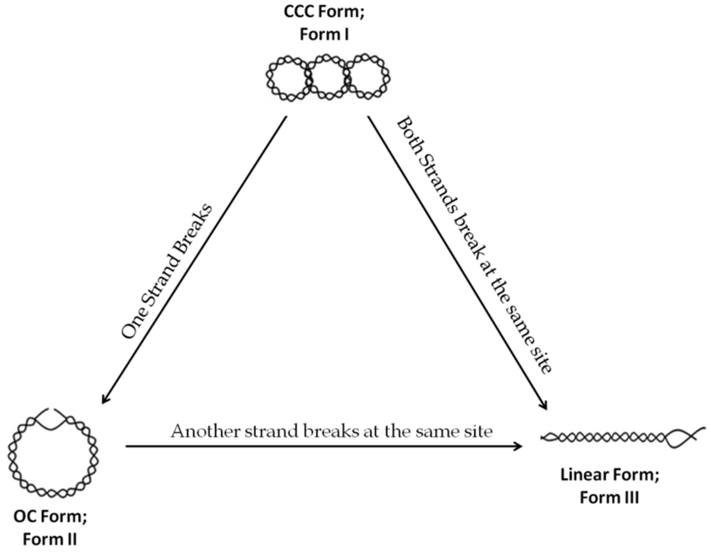
CCC Form;
Form I
One Strand Breaks
Both Strands break at the same site
Another strand breaks at the same site
OC Form;
Form II
Linear Form;
Form III

Figure 4.3.6. Forms adopted by circular plasmid depending on the nicking degree.

Plasmid conformations of equivalent molecular weight have dramatically different mobilities when electrophoresed through an agarose gel. Relatively fast migration will be observed for the uncleaved supercoiled form (CCC form, Form I). If scission occurs on one strand (nicking), the supercoil will relax to generate a slower moving open circular form (OC form, Form II). If both strands are cleaved, a linear form (form III) that migrates between CCC form and form OC will be generated.

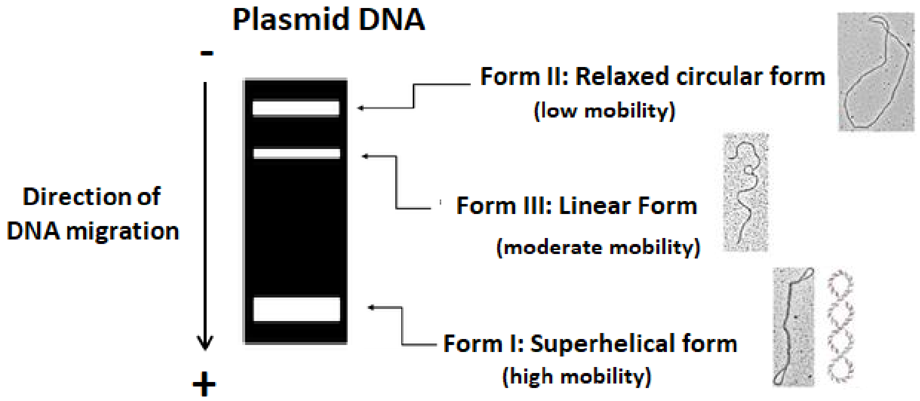
Plasmid DNA
-
+
Direction of DNA migration
Form II: Relaxed circular form
(low mobility)
Form III: Linear Form
(moderate mobility)
Form I: Superhelical form
(high mobility)

Figure 4.3.7. Summary of the Electrophoretic Mobility of each form of the circular plasmid.

In *Figure 4.3.8*, it is presented the EM of complexes **7**–**9** (r_i = 6.9) in the absence and presence of H_2O_2, showing their capacity to promote important changes in the EM of the pBR322 plasmid DNA under aerobic and physiological conditions (pH = 7.0, 37ºC).

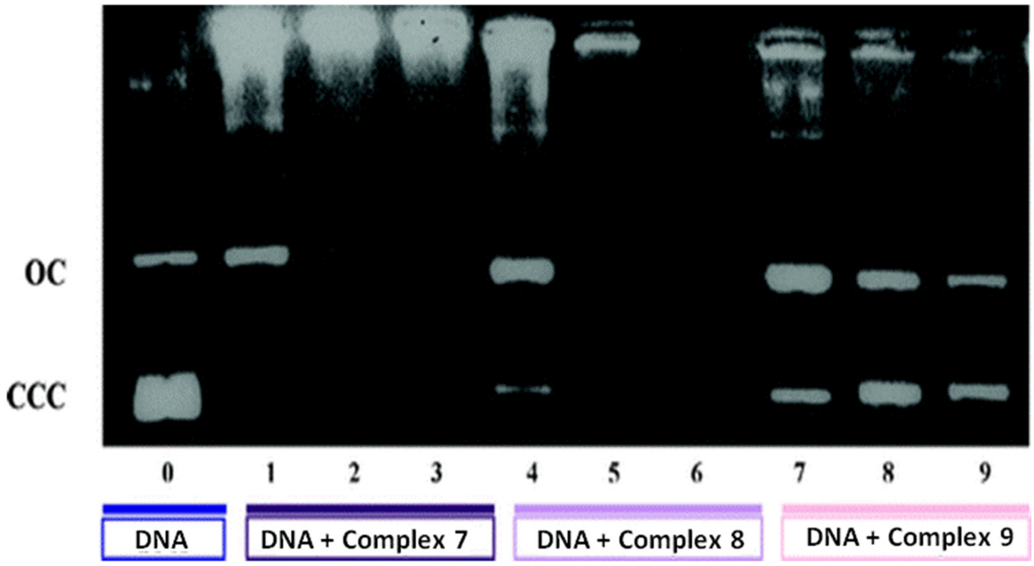
OC
CCC
0
1
2
3
4
5
6
7
8
9
DNA
DNA + Complex 7
DNA + Complex 8
DNA + Complex 9

Figure 4.3.8. Agarose gel EM of pBR322 plasmid DNA treated with Cu(I) compounds (DNA concentration 0.017 µg/µL, 6 × 10^{-3} µM, molar ratio r_i = 6.9; r_i: input molar ratio of the complex to nucleotide). Incubation time 2 h (37 °C). Lane 0, pBR322 plasmid DNA; Lane 1, DNA + Complex **7**; Lane 2, DNA + complex **7** treated with 1 µL H_2O_2 (33% w/v) for *t* = 3 min, after incubation; Lane 3, DNA + complex **7** treated with 1 µL H_2O_2 (33% w/v) for *t* = 30 min, after incubation; Lane 4, DNA + complex **8**; Lane 5, DNA + complex **8** treated with 1 µL H_2O_2 (33% w/v) for *t* = 3 min, after incubation; Lane 6, DNA + complex **8** treated with 1 µL H_2O_2 (33% w/v) for *t* = 30 min, after incubation; Lane 7, DNA + complex **9**; Lane 8, DNA + complex **9** treated with 1 µL H_2O_2 (33% w/v) for *t* = 3 min, after incubation; Lane 9, DNA + complex **9** treated with 1 µL H_2O_2 (33% w/v) for *t* = 30 min, after incubation. (OC, open circular form; CCC, covalently closed circular form).

Time course experiments reveal that, without H_2O_2, all complexes are capable of inducing conversion of supercoiled plasmid DNA form(CCC) into relaxed circular form (OC) (lanes 1, 4, and 7 for complexes **7**, **8**, and **9** respectively) and other slower moving forms of DNA (bands migrating higher than OC) (lanes 1 and 4 for complexes 1 and 2, respectively). The degree of induction under these conditions is **7** > **8** >> **9**, as is evident from the relative decrease in the intensity of the supercoiled bands.

The addition of H_2O_2, with different exposition times, produces much stronger damage to the DNA than the Cu(I) alone for cases **7** and **8** (see lanes, 2–3 for complex **7** and 5–6 for **8**) but now the relative reactivity is reversed; that is, **8** is more active than **7**. In sharp contrast the addition of H_2O_2 to complex **9** (lanes 8–9) basically does not modify its activity as compared to its performance without H_2O_2. Under similar conditions no cleavage of pBR322 DNA occurred for free H_2O_2 (see **Figure A3.16**, Supporting Information). Electrophoresis of complexes **7**–**9** ($r_i = 6.9$), under anaerobic conditions, in the absence of H_2O_2, has also been performed (**Figure A3.18**, Supporting Information).

The results show that all complexes can effectively promote similar changes in the EM of the pBR322 plasmid DNA to those obtained under aerobic conditions suggesting that atmospheric oxygen is not involved in the cleavage process. The results obtained are consistent with the fact that copper(I) complexes examined here are capable of promoting important interactions with DNA, producing a sequential decrease of the CCC form folding, but do not cleave pBR322 plasmid DNA in the absence of hydrogen peroxide. That these interactions may lead to relaxed open conformation (bands OC) and other aggregation of DNA molecules originated by cross-links between the complexes and more or less relaxed different molecules of plasmid DNA (bands migrating higher than OC) in agreement with the results observed in EF (*Figure 4.3.8*). The nuclease activity of these Cu(I) complexes take place by direct strand scission when H_2O_2 is present.

The DNA degraded completely into small pieces, and it could not induce the linear form in the tested experiment.

4.3.3.4. AFM. Atomic Force Microscopy.

Direct visualization of three conformers of plasmid DNA can be achieved using tapping mode atomic force microscopy (TMAFM) and thus allows graphically evaluating plasmid DNA cleavage by metallonucleases.[163,265,266]

AFM images of free pBR322 plasmid DNA and pBR322 incubated with complexes **7**–**9** ($r_i = 6.9$) with and without H_2O_2 under the same conditions as in the EM experiments are presented in *Figures 4.3.9* and *Figure 4.3.10*.

Image b in *Figure 4.3.9* shows the plasmid DNA modifications produced by **7**, where the largest part of DNA has started to relax in the OC form of DNA, although it is possible to observe some molecules with an intermediate degree of folding and some others containing several crossing points. *Image c*, taken 30 min after the addition of 1 µL of H_2O_2, shows that most of the DNA has been completely destroyed as a result of the cleavage activity of the complex. *Image d* in *Figure 4.3.9* shows the effect produced by **8** where CCC and OC DNA forms can be observed. The addition of H_2O_2 is shown in *image e* where, after 3 min, complex **8** exhibits clear evidence of DNA-strand scission to give short fragments.

Finally, *Figure 4.3.10.* shows the reaction of **9** with the plasmid DNA where CCC and OC forms can be observed. *Image b* shows the effect of adding H_2O_2 together with complex **9**, showing that it is able to cause a small amount of double strand scission of pBR322 but not able to fully convert the CCC form into the OC form. This behavior is in agreement with the results observed in the EM pattern.

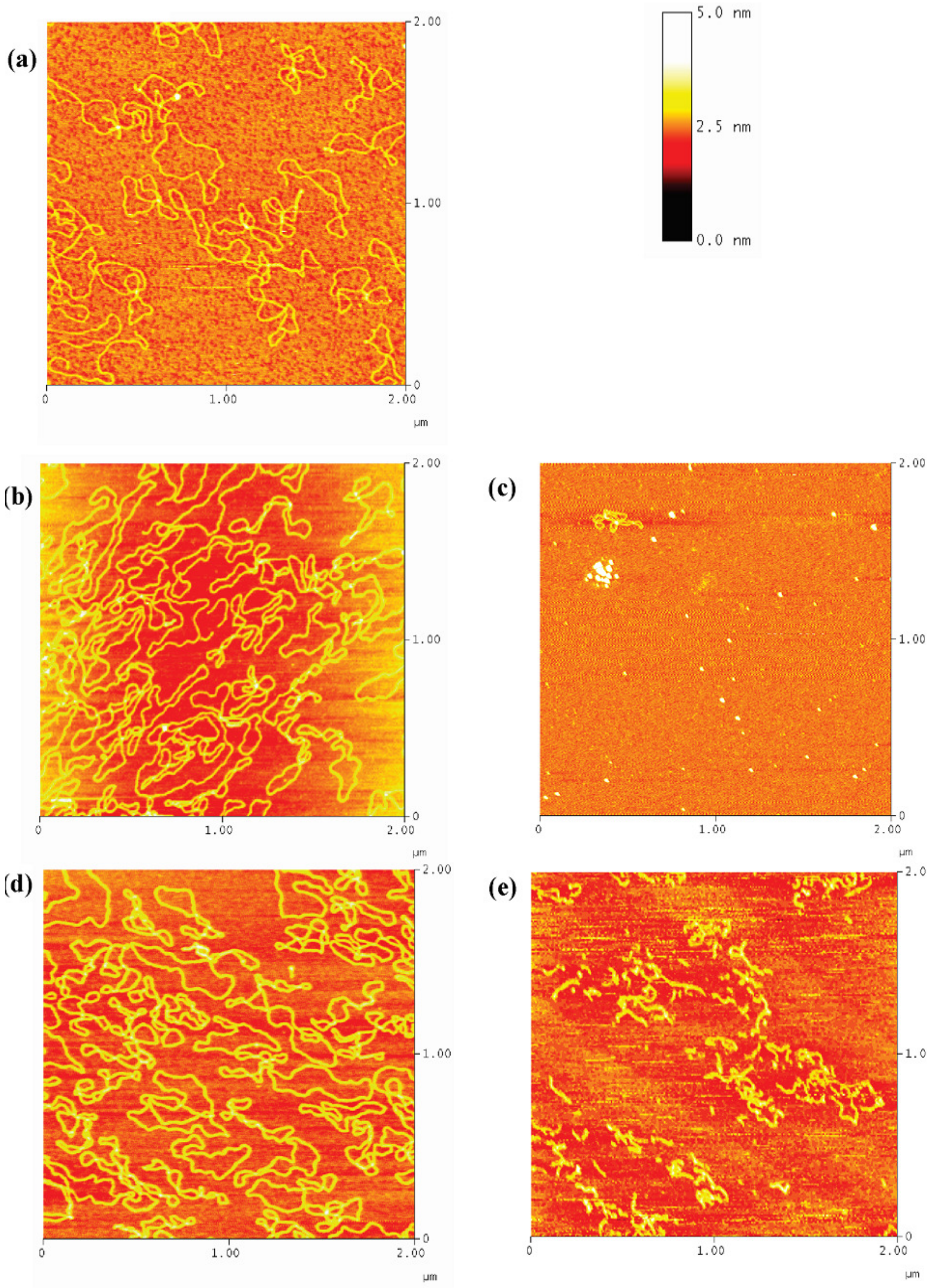

Figure 4.3.9. TMAFM images of pBR322 plasmid DNA treated with Cu(I) compounds (DNA concentration 0.0043 µg/µL, 1.510^{-3} µM, molar ratio r_i=6.9; r_i: input molar ratio of the complex to nucleotide) (a) free pBR322 DNA; (b) pBR322 DNA incubated with **7**, 2 h (37ºC); (c) pBR322 DNA incubated with **7**, 2 h (37ºC), sample treated with 1µL H_2O_2 (33%w/v) for t= 30 min, after incubation; (d) pBR322 DNA incubated with **8**, 2 h (37ºC); (e) pBR322 DNA incubated with **8**, 2 h (37ºC), sample treated with 1 µL H_2O_2 (33% w/v) for t = 2 min, after incubation.

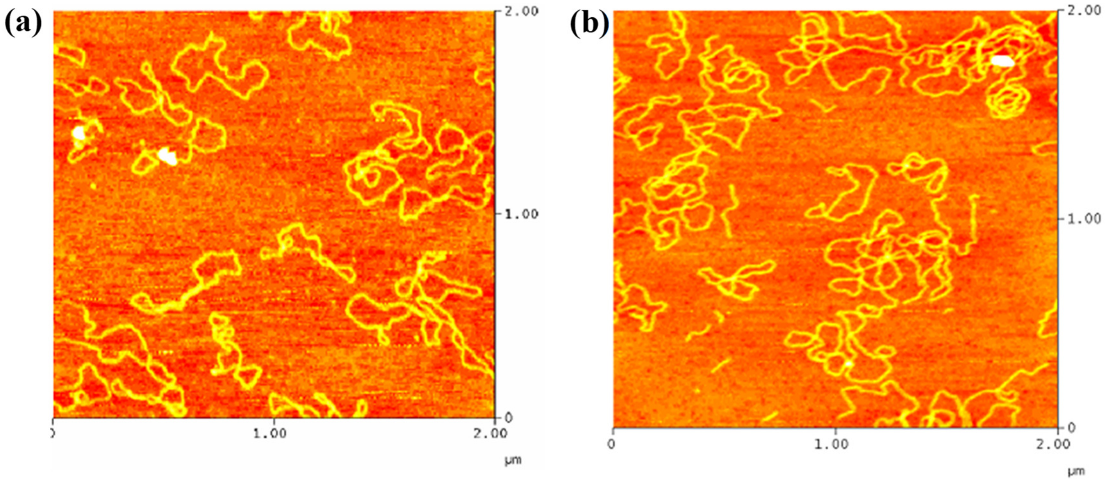

Figure 4.3.10. TMAFM images of pBR322 plasmid DNA treated with Cu(I) complex **9** (DNA concentration 0.0043 µg/µL, 1.510^{-3} µM, molar ratio r_i=6.9; r_i: input molar ratio of the complex to nucleotide) (a) pBR322 DNA incubated with **9**, 2h (37ºC); (b) pBR322 DNA incubated with **9**, 2h (37ºC), sample treated with 1µl H_2O_2 (33% w/v) for t = 50 min, after incubation.

4.3.4. Final remarks

In overall, complexes **7**–**9** belong to a family of dinuclear Cu(I) complexes containing octaaza dinucleating macrocyclic ligands that can be envisaged as formed by a phenylic spacer linked to two different coordination sites (see *Figure 4.3.1*). The properties of these ligands are finely modulated by changing the number of methylenic spacers between the aminic N atoms and by the *meta* or *para* substitution at the aromatic spacer. These small variations in the ligands produce a significantly different 3D topography for the three Cu(I) complexes **7**–**9**, as revealed by their crystal structures (see *Figure 4.3.2*) described above. On the other hand the redox properties of the metal centers change depending on the macrocyclic ligand used, as indicated previously.

CD spectroscopy indicates that the interaction of complexes **7**–**9** with DNA is weak, not of an intercalative nature. Under EM conditions with no peroxide, the supramolecular complex generated is then responsible for the transformation of the CCC form of the DNA into the OC. The different reactivities of the complexes **7**–**9** are thus associated with the two differentiated properties of the complexes: the redox potential and the shape of the molecule. With regard to the latter it is interesting to bear in mind the work of Rodger et al. and others[156,267] for dinuclear Fe(II) complexes where relative orientation of the aromatic rings play a key role in the non-intercalating interaction with DNA. In our particular case it is important to realize that for the *para*-substituted cases **7** and **9**, the relative orientation of their pyridylic rings will dictate the degree of interaction with DNA. Thus a quasi-orthogonal disposition of this type of nonintercalative supramolecular interaction will generate a very weak interaction (which is the case for complex **9**) whereas a 50.88º angle will produce a chelate sort of interaction with the two pyridylic rings properly oriented and thus be able to produce a much stronger interaction (which is the case of complex **7**).[267]

For the *meta* case, complex **8**, its spherical shape also seems to have a good contact with DNA as evidenced by having a relative similar interaction as with **7** under similar redox potentials conditions. We have recently shown that the reaction of related Cu(I) complexes, containing similar macrocyclic ligands with no pyridylic pendant arms, with oxygen generates Cu_2O_2–peroxo type of intermediates.[255,268] In the case of the complexes where the macrocyclic ligand has a *para* substitution, a trans-μ-1,2-peroxo is likely to be formed due to the large distance between the Cu centers imposed by spacer. However, in the case of the *meta* the distance is highly reduced and a μ-η_2:η_2–peroxo is more probably formed. The different nature of the peroxo complex formed could explain the reversal of reactivity observed for the Cu(I) complexes in the presence of H_2O_2. On the other hand the much lesser activity of complex **9** is hampered by the weak supramolecular interaction of the plain Cu(I) complex that seems to be a requirement for the reaction with DNA to proceed.

Finally the relatively similar reactivity observed for complex **9** in the presence and absence of hydrogen peroxide and the different reactivity of **7** and **8** with H_2O_2 rule out the formation of free hydroxyl radical species and point out that the main chemistry produced in our case may be the nucleophilic addition of peroxide to the Cu(I) complex, in a similar manner as had been found in previous reports with related complexes.[269,270]

In overall, this section shows another example of how small variations in the ligand backbone can cause significant differences in the complex structure and performance, specifically in their respective Cu(I) complexes that in turn are responsible for radically differentiated biological reactivity.

5. Conclusions

This work shows the behavior of macrocyclic ligands and complexes under three points of view, emphasizing how small differences in the backbone of the macrocyclic ligand produce changes in their chemistry.

- It has been studied the interaction of the macrocyclic ligand **L9** with the aromatic dicarboxylic acids phthalic acid (*ph*), isophthalic acid (*is*) and terephthalic acid (*te*) through potentiometric titrations, NMR studies and theoretical calculations.
- Each diacid interacts with the receptor with different strength, depending on the geometry of the diacid, following the order *is* > *ph* > *te*. Moreover, the receptor **L9** shows a high selectivity for the *is* diacid, especially over *te* diacid, with which presents a higher complexation constant over all pH range.
- The **L9** receptor interacts with the three diacids through coulombic interaction and H bonding, but not π-stacking.
- When comparing the interaction of the three diacids with the two receptors **L9** and **L12**, it is clear that the two methylenic groups in **L12** central amines induce a notable decrease in the selectivity of the receptor towards the diacid substrates, resulting in a higher difference in the affinity of the **L9** ligand for each diacid.

- It has been synthesized a new family of imine macrocyclic ligands with pyridil pendant arms, through a 2+2 condensation of an aromatic dialdehyde and a pendant arm triamine. The ligands of the family differ in the geometry of the aromatic spacer (*ortho* or *para*), as well as in the length of the aliphatic spacers (two or three methylenes).
- The macrocyclic ligand with *meta* geometry and spacer of 2 methylenic units bearing a pyridyl (**bsm2py**) undergoes a ring expansion when complexed with Cu(I) in acetonitrile solution, obtaining the trinuclear complex of the 3+3 ligand, in contrast with the other three pendant arm imine macrocyclic ligands of the family (***bsp3py***, ***bsm3py*** and ***bsp2py***), which do not perform any ligand expansion in presence of Cu(I).
- In order to study the ring expansion of the **bsm2py**, it have also been synthesized two analog ligands to **bsm2py**, but bearing different pendant arms: one with a phenol group (**bsm2phOH**) and another with an ethyl group (**bsm2Et**) as pendant arms. All of them undergo ring expansion when complexed with Cu(I) in acetonitrile.
- The ligand rearrangement of these ligands with pendant arms (**bsm2py**, **bsm2phOH** and **bsm2Et**) is in sharp contrast with the analog imine macrocyclic ligand without pendant

arms ***bsM2*** described in the literature, which does not undergo any ligand rearrangement when complexed with Cu(I).

- The dinuclear Cu(I) complexes with the ligands ***bsp3py***, ***bsm3py*** and ***bsp2py*** have been synthesized and fully characterized, and their nuclease activity towards plasmid DNA pBR322 has been studied by means of Electrophoresis Mobility in Agarose Gel, Circular Dichroism spectroscopy and Atomic Force Microscopy.
- All complexes interact with DNA and produce nicking in presence of H_2O_2, clearly being the complex with the ligand ***bsp2py*** the one with less activity.
- The interaction mode of the complexes with DNA is non intercalative in all three cases as evidenced by CD spectroscopy.
- In absence of H_2O_2 the order of the complexes interaction with DNA is $\mathbf{7}^{2+}$ > $\mathbf{8}^{2+}$ >$\mathbf{9}^{2+}$., whereas with H_2O_2, the nuclease activity of the complexes follows the order $\mathbf{8}^{2+}$ > $\mathbf{7}^{2+}$ >$\mathbf{9}^{2+}$.
- The difference in reactivity among the complexes can be associated with the properties of the products, both electronic and geometric.

6. References

(1) Casas, J.S.; Moreno, V.; Sánchez, A.; Sánchez, J.L.; Sordo, J. *Química Bioinorgánica*; Editorial Síntesis, 2002.

(2) Vallet, M.; Faus, J.; García-España, E.; Moratal, J. *Introducción a La Química Bioinorgánica.*; Editorial Síntesis, 2003.

(3) Ochiai., E.-I. *Química Bioinorgánica. Una Introducción.*; Ed. Reverté, 1985.

(4) Lippard, S.J., Berg, J. M. *Principles of Bioinorganic Chemistry*; University Science Books, 1994.

(5) Johnstone, T. C.; Suntharalingam, K.; Lippard, S. J. *Chem. Rev.* **2016**, *116* (5), 3436–3486. https://doi.org/10.1021/acs.chemrev.5b00597.

(6) Kaim, W.; Schwederski, B. *Bioinorganic Chemistry: Inorganic Elements in the Chemistry of Life.*; Ed. Wiley, 1994.

(7) Holm, Richard H.; Solomon, E. I. *Chem. Rev.* **2004**, *104* (2), 347–348.

(8) Mateus, P.; Bernier, N.; Delgado, R. *Coord. Chem. Rev.* **2010**, *254* (15–16), 1726–1747. https://doi.org/10.1016/j.ccr.2009.11.005.

(9) Bazzicalupi, C.; Bencini, A.; Bianchi, A.; Danesi, A.; Faggi, E.; Giorgi, C.; Santarelli, S.; Valtancoli, B. *Coord. Chem. Rev.* **2008**, *252* (10–11), 1052–1068. https://doi.org/10.1016/j.ccr.2007.07.024.

(10) Vigato, P. A.; Tamburini, S. *Coord. Chem. Rev.* **2004**, *248*, 1717–2128. https://doi.org/10.1016/j.cct.2003.09.003.

(11) Vigato, P. A.; Tamburini, S.; Bertolo, L. *Coord. Chem. Rev.* **2007**, *251*, 1311–1492. https://doi.org/10.1016/j.ccr.2006.11.016.

(12) Vigato, P. A.; Peruzzo, V.; Tamburini, S. *Coord. Chem. Rev.* **2012**, *256* (11–12), 953–1114. https://doi.org/10.1016/j.ccr.2012.01.009.

(13) Korybut-Daszkiewicz, B.; Bilewicz, R.; Woźniak, K. *Coord. Chem. Rev.* **2010**, *254* (15–16), 1637–1660. https://doi.org/10.1016/j.ccr.2009.12.004.

(14) Rezaeivala, M.; Keypour, H. *Coord. Chem. Rev.* **2014**, *280*, 203–253. https://doi.org/10.1016/j.ccr.2014.06.007.

(15) Gavey, E. L.; Pilkington, M. *Coord. Chem. Rev.* **2015**, *296*, 125–152. https://doi.org/10.1016/j.ccr.2015.03.017.

(16) Alexander, V. *Chem. Rev.* **1995**, *95* (2), 273–342. https://doi.org/10.1021/cr00034a002.

(17) McKee, V.; Nelson, J.; Town, R. M. *Chem. Soc. Rev.* **2003**, *32* (5), 309–325. https://doi.org/10.1039/b200672n.

(18) Lehn, J.-M. *Supramolecular Chemistry: Concepts and Perspectives.*; VCH: Weinheim, 1995.

(19) Bianchi, A.; García-España, E. *Inorganica Chim. Acta* **2014**, *417*, 1–2. https://doi.org/10.1016/j.ica.2014.01.021.

(20) Brooker, S. *Coord. Chem. Rev.* **2001**, *222*, 33–56. https://doi.org/10.1016/S0010-

8545(01)00300-9.

(21) Bligh, S. W. A.; Choi, N.; Geraldes, C. F. G. C.; Knoke, S.; Mcpartlin, M.; Sanganee, M. J.; Woodroffe, T. M. *J. Chem. Soc., Dalt. Trans.* **1997**, 4119–4125.

(22) Cabbiness, D. K.; Margerum, D. W. *J. Am. Chem. Soc.* **1969**, *91* (23), 6540–6541. https://doi.org/10.1021/ja01051a091.

(23) Weller, M.; Overton, T.; Rourke, Jonathan; Armstrong, F. *Inorganic Chemistry*; Oxford University Press, 2014.

(24) Melson, G. A. *Coordination Chemistry of Macrocyclic Compounds.*, Melson, G.; New York: Plenum Press, 1979.

(25) Zhong, D. C.; Lu, T. B. *Chem. Commun.* **2016**, *52* (68), 10322–10337. https://doi.org/10.1039/c6cc03660k.

(26) Lindoy, L. F.; Park, K. M.; Lee, S. S. *Chem. Soc. Rev.* **2013**, *42* (4), 1713–1727. https://doi.org/10.1039/c2cs35218d.

(27) Nelson, S. M. *Pure Appl. Chem.* **1980**, *52* (11), 2461–2476. https://doi.org/10.1351/pac198052112461.

(28) Salvadeo, E.; Dubois, L.; Latour, J. M. *Coord. Chem. Rev.* **2018**, *374*, 345–375. https://doi.org/10.1016/j.ccr.2018.07.005.

(29) McKee, V. *Adv. Inorg. Chem.* **1993**, *40*, 323–410.

(30) Brooker, S. *Eur. J. Inorg. Chem.* **2002**, 2535–2547.

(31) Zanello, P.; Tamburini, S.; Vigato, P. A.; Mazzocchin, G. A. *Coord. Chem. Rev.* **1987**, *77*, 165–273. https://doi.org/10.1016/0010-8545(87)85034-8.

(32) Vigato, P. A.; Tamburini, S.; Fenton, D. E. *Coord. Chem. Rev.* **1990**, *106*, 25–170. https://doi.org/10.1016/0010-8545(60)80002-1.

(33) Guerriero, P.; Tarnburini, S.; Vigato, P. A. *Coord. Chem. Rev.* **1995**, *139*, 17–243. https://doi.org/10.1016/0010-8545(93)01105-7.

(34) Jastrzab, R.; Kaczmarek, M. T.; Nowak, M.; Trojanowska, A.; Zabiszak, M. *Coord. Chem. Rev.* **2017**, *351*, 32–44. https://doi.org/10.1016/j.ccr.2017.05.001.

(35) Clares, M. P.; Acosta-Rueda, L.; Castillo, C. E.; Blasco, S.; Jiménez, H. R.; García-España, E.; Basallote, M. G. *Inorg. Chem.* **2017**, *56* (8), 4400–4412. https://doi.org/10.1021/acs.inorgchem.6b03070.

(36) Caneschi, A.; Sorace, L.; Casellato, U.; Tomasin, P.; Vigato, P. A. *Eur. J. Inorg. Chem.* **2004**, No. 19, 3887–3900. https://doi.org/10.1002/ejic.200400135.

(37) Di Bernardo, P.; Zanonato, P. L.; Tamburini, S.; Tomasin, P.; Vigato, P. a. *Dalton Trans.* **2006**, No. 39, 4711–4721. https://doi.org/10.1039/b604211b.

(38) Weitzer, M.; Brooker, S. *Dalt. Trans.* **2005**, 2448–2454.

(39) Sessler, J. L.; Callaway, W.; Dudek, S. P.; Date, R. W.; Bruce, D. W. *Chem. Commun.* **2003**, 2422–2423.

(40) Gerasimchuk, N. N.; Gerges, A.; Clifford, T.; Danby, A.; Bowman-james, K.; March, R. V. *Inorg. Chem.* **1999**, No. 38, 5633–5636.

(41) Brooker, S.; Kelly, P. R. J.; Moubaraki, B.; Murray, K. S. *Chem. Commun.* **1996**, *2*, 2579–2580.

(42) Brandt, C. D.; Plieger, P. G.; Kelly, R. J.; Geest, D. J. De; Kennepohl, D. K.; Iremonger, S. S.; Brooker, S. *Inorganica Chim. Acta* **2004**, *357*, 4265–4272. https://doi.org/10.1016/j.ica.2004.06.013.

(43) Gao, J.; Reibenspies, J. H.; Martell, A. E. *Angew. Chem. Int. Ed.* **2003**, *42*, 6008–6012. https://doi.org/10.1002/anie.200351978.

(44) Gao, J.; Reibenspies, J. H.; Zingaro, R. A.; Woolley, F. R.; Martell, A. E.; Clearfield, A. *Inorg. Chem.* **2005**, *44* (2), 232–241.

(45) Ito, T.; Matsumoto, T.; Wakizaka, M.; Chang, H. C. *Eur. J. Inorg. Chem.* **2017**, 3498–3507. https://doi.org/10.1002/ejic.201700433.

(46) Nakamura, T.; Tsukuda, S.; Nabeshima, T. *J. Am. Chem. Soc.* **2019**, *141* (16), 6462–6467. https://doi.org/10.1021/jacs.9b00171.

(47) Chang, F. F.; Zhang, L.; Zhao, P. C.; Huang, W. *Inorg. Chem.* **2018**, *57* (3), 1438–1448. https://doi.org/10.1021/acs.inorgchem.7b02835.

(48) Sessler, J. L.; Callaway, W. B.; Dudek, S. P.; Date, R. W.; Bruce, D. W.; Uni, V.; Road, S.; Ex, E. *Inorg. Chem.* **2004**, *43* (21), 6650–6653.

(49) Givaja, G.; Blake, A. J.; Wilson, C.; Schro, M.; Love, J. B. *Chem. Commun.* **2005**, *9380* (2), 4423–4425. https://doi.org/10.1039/b507729j.

(50) Givaja, G.; Blake, A. J.; Wilson, C.; Der, M. S.; Love, J. B. *Chem. Commun.* **2003**, 2508–2509.

(51) Arnold, P. L.; Blake, A. J.; Wilson, C.; Love, J. B.; Uni, V.; Park, U. V; Ng, N. *Inorg. Chem.* **2004**, *43* (26), 8206–8208.

(52) Veauthier, J. M.; Tomat, E.; Lynch, V. M.; Sessler, J. L.; Mirsaidov, U.; Markert, J. T.; Uni, V.; Station, C.; Uni, T. *Inorg. Chem.* **2005**, *44* (19), 6736–6743.

(53) Veauthier, J. M.; Cho, W.; Lynch, V. M.; Sessler, J. L. *Inorg. Chem.* **2004**, *43* (4), 1220–1228.

(54) Sessler, J. L.; Tomat, E.; Mody, T. D.; Lynch, V. M.; Veauthier, J. M.; Mirsaidov, U.; Markert, J. T.; Uni, V.; Station, C. *Inorg. Chem.* **2005**, *44* (7), 2125–2127.

(55) L, P. M.; Brooker, S.; Hay, S. J.; Plieger, P. G. *Angew. Chem. Int. Ed.* **2000**, No. 11, 1995–1997.

(56) Brooker, S.; Kelly, R. J. *J. Chem. Soc. Dalt. Trans.* **1996**, 2117–2122.

(57) Christensen, A.; Mayer, C.; Jensen, F.; Bond, A. D.; Mckenzie, C. J. *Dalt. Trans.* **2006**, 108–120. https://doi.org/10.1039/b512068c.

(58) Kuhnert, N.; Rossignolo, G. M.; Lopez-periago, A. *Org. Biomol. Chem.* **2003**, *1*, 1157–1170.

(59) Korupoju, S. R.; Mangayarkarasi, N.; Ameerunisha, S.; Valente, E. J.; Zacharias, P. S. *J. Chem. Soc., Dalt. Trans.* **2000**, 2845–2852. https://doi.org/10.1039/b002700f.

(60) Lu, Q.; Motekaitis, R. J.; Reibenspies, J. J.; Martell, A. E. *Inorg. Chem.* **1995**, *34* (20), 4958–4964. https://doi.org/10.1021/ic00124a008.

(61) Evans, N. H.; Beer, P. D. *Angew. Chem. Int. Ed.* **2014**, *53*, 11716–11754. https://doi.org/10.1002/anie.201309937.

(62) Langton, M. J.; Serpell, C. J.; Beer, P. D. *Angew. Chem. Int. Ed.* **2016**, *55* (6), 1974–1987. https://doi.org/10.1002/anie.201506589.

(63) Ulatowski, F.; Dabrowa, K.; Jurczak, J. *Tetrahedron Lett.* **2016**, *57*, 1820–1824. https://doi.org/10.1016/j.tetlet.2016.03.043.

(64) Katayev, E. A.; Pantos, G. D.; Reshetova, M. D.; Khrustalev, V. N.; Lynch, V. M.; Ustynyuk, Y. A.; Sessler, J. L. *Angew. Chem. Int. Ed.* **2005**, *44*, 7386–7390. https://doi.org/10.1002/anie.200502393.

(65) Katayev, E. A.; Sessler, J. L.; Khrustalev, V. N.; Ustynyuk, Y. A. *J. Org. Chem.* **2007**, *72* (19), 7244–7252.

(66) Lehn, J. *Angew. Chemie Int. Ed. English* **1988**, *27* (1), 89–112. https://doi.org/10.1002/anie.198800891.

(67) Lehn, J.-M. *Science (80-.).* **1985**, *227* (4689), 849–856. https://doi.org/10.1126/science.227.4689.849.

(68) Lehn, J. M. *Pure Appl. Chem.* **1978**, *50* (9–10), 871–892. https://doi.org/10.1351/pac197850090871.

(69) Bianchi, A.; Bowman-james, K.; Garcia-España, E. *Supramolecular Chemistry of Anions*; Wiley-VCH: New York, 1997.

(70) Morita, T.; Westh, P.; Nishikawa, K.; Koga, Y. *J. Phys. Chem. B* **2014**, *29* (118), 8744–8749.

(71) García-España, E.; Díaz, P.; Llinares, J. M.; Bianchi, A. *Coord. Chem. Rev.* **2006**, *250* (23–24), 2952–2986. https://doi.org/10.1016/j.ccr.2006.05.018.

(72) Kimura, E.; Sakonaka, A.; Yatsunami, T.; Kodama, M. *J. Am. Chem. Soc.* **1981**, *103* (11), 3041–3045.

(73) Cavallero, A.; Marte, A.; Fedele, E. *J. Neurochem.* **2009**, *110* (3), 924–934. https://doi.org/10.1111/j.1471-4159.2009.06187.x.

(74) Mycielska, M. E.; Patel, A.; Rizaner, N.; Mazurek, M. P.; Keun, H.; Patel, A.; Ganapathy, V.; Djamgoz, M. B. A. *BioEssays* **2009**, *31* (1), 10–20. https://doi.org/10.1002/bies.080137.

(75) Nelson, D. I.; Lehninger, A. L.; Cox, M. M. *Principles of Biochemistry*; W. H. Freeman: New York, 2008.

(76) Curiel, D.; Más-Montoya, M.; Sánchez, G. *Coord. Chem. Rev.* **2015**, *284*, 19–66. https://doi.org/10.1016/j.ccr.2014.09.010.

(77) Zeikus, J. G.; Jain, M. K.; Elankovan, P. *Appl. Microbiol. Biotechnol.* **1999**, *51* (5), 545–552. https://doi.org/10.1007/s002530051431.

(78) Khose, V. N.; John, M. E.; Pandey, A. D.; Borovkov, V.; Karnik, A. V. *Symmetry (Basel).* **2018**, *10* (2), 34. https://doi.org/10.3390/sym10020034.

(79) Chakraborty, S.; Saha, S.; Lima, L. M. P.; Warzok, U.; Sarkar, S.; Akhuli, B.; Nandi, M.; Bej, S.; Adarsh, N. N.; Schalley, C. A.; et al. *J. Org. Chem.* **2017**, *82* (19), 10007–10014. https://doi.org/10.1021/acs.joc.7b01431.

(80) Saha, I.; Wang, E. B.; Parish, C. A.; Ghosh, K. *ChemistrySelect* **2017**, *2* (17), 4794–4799. https://doi.org/10.1002/slct.201700756.

(81) Mateus, P.; Lima, L. M. P.; Delgado, R. *Polyhedron* **2013**, *52*, 25–42. https://doi.org/10.1016/j.poly.2012.07.073.

(82) Mateus, P.; Delgado, R.; Brando, P.; Følix, V. *Chem. - a Eur. J.* **2011**, No. 17, 7020–7031. https://doi.org/10.1002/chem.201100428.

(83) Fitzmaurice, R. J.; Kyne, G. M.; Douheret, D.; Kilburn, J. D. *J. Chem. Soc. Perkin Trans. 1* **2002**, No. 7, 841–864. https://doi.org/10.1039/b009041g.

(84) Yang, Y. D.; Sessler, J. L.; Gong, H. Y. *Chem. Commun.* **2017**, *53* (70), 9684–9696. https://doi.org/10.1039/c7cc04661h.

(85) Rhaman, M. M.; Hasan, M. H.; Alamgir, A.; Xu, L.; Powell, D. R.; Wong, B. M.; Tandon, R.; Hossain, M. A. *Sci. Rep.* **2018**, *8* (Article Number 286), 1–11. https://doi.org/10.1038/s41598-017-18322-w.

(86) Dietrich, B.; Hosseini, M. W.; Lehn, J. M.; Sessions, R. B. *J. Am. Chem. Soc.* **1981**, *103*, 1282–1283.

(87) Kimura, E.; Kodama, M.; Yatsunami, T. *J. amer* **1982**, *103* (11), 3182–3187.

(88) Anda, C.; Llobet, A.; Martell, A. E.; Reibenspies, J.; Berni, E.; Solans, X. *Inorg. Chem.* **2004**, *43* (9), 2793–2802. https://doi.org/10.1021/ic035121p.

(89) Carvalho, S.; Delgado, R.; Fonseca, N.; Félix, V. *New J. Chem.* **2006**, *30*, 247–257. https://doi.org/10.1039/b512661d.

(90) Miranda, C.; Escartí, F.; Lamarque, L.; Yunta, M. J. R.; Navarro, P.; García-España, E.; Jimeno, M. L. *J. Am. Chem. Soc.* **2004**, *126* (3), 823–833. https://doi.org/10.1021/ja035671m.

(91) Bazzicalupi, C.; Bencini, A.; Bianchi, A.; Borri, C.; Danesi, A.; Garcia-España, E.; Giorgi, C.; Valtancoli, B. *J. Org. Chem.* **2008**, *73* (21), 8286–8295. https://doi.org/10.1021/jo801366w.

(92) Kondo, S. I.; Sato, K.; Matsuta, Y.; Osawa, K. *Bull. Chem. Soc. Jpn.* **2018**, *91* (6), 875–881. https://doi.org/10.1246/bcsj.20180028.

(93) Sokolov, J.; Šindelář, V. *Chem. - A Eur. J.* **2018**, *24* (58), 15482–15485. https://doi.org/10.1002/chem.201802748.

(94) González-Álvarez, A.; Alfonso, I.; Díaz, P.; García-España, E.; Gotor, V. *Chem. Commun.* **2006**, No. 11, 1227–1229. https://doi.org/10.1039/b517729d.

(95) Gonza, A.; Alfonso, I.; Dı, P.; Garcı, E. *J. Org. Chem.* **2008**, *73*, 374–382.

(96) Bencini, A.; Bianchi, A.; Burguete, M. I.; Garcia-España, E.; Luis, S. V; Ramirez, J. A. *J. Am. Chem. Soc.* **1992**, *114* (5), 1919–1920.

(97) Bencini, A.; Bianchi, A.; Burguete, M. I.; Dapporto, P.; Domenech, A.; Garcia-Espafia, E.; Luis, S. V; Paoli, P.; Ramirez, J. A. *J. Chem. Soc. Perkin Trans. 2* **1994**, 569–577.

(98) Bazzicalupi, C.; Bencini, A.; Bianchi, A.; Borsari, L.; Giorgi, C.; Valtancoli, B.; Anda, C.; Llobet, A. *J. Org. Chem.* **2005**, *70* (11), 4257–4266. https://doi.org/10.1021/jo048142p.

(99) Nelson, J.; Nieuwenhuyzen, M.; Pál, I.; Town, R. M. *Dalton Trans.* **2004**, No. 2, 229–235. https://doi.org/10.1039/b311379e.

(100) Nelson, J.; Nieuwenhuyzen, M.; Pál, I.; Town, R. M. *Chem. Commun. (Camb).* **2002**, 2266–2267. https://doi.org/10.1039/b207964j.

(101) Mateus, P.; Delgado, R.; Brandão, P.; Félix, V. *J. Org. Chem.* **2012**, *77* (10), 4611–4621. https://doi.org/10.1021/jo300320w.

(102) Arranz-Mascarós, P.; Bazzicalupi, C.; Bianchi, A.; Giorgi, C.; Godino-Salido, M. L.; Gutiérrez-Valero, M. D.; Lopez-Garzón, R.; Valtancoli, B. *New J. Chem.* **2011**, *35* (9), 1883–1891. https://doi.org/10.1039/c1nj20393b.

(103) Andrea Bencini, D.; Biagini, S.; Giorgi, C.; Handell, H.; Michel Le Baccon, L.; Mariani, P.; Paoletti, P.; Paoli, P.; Rossi, P.; Tripier, R.; et al. *European J. Org. Chem.* **2009**, No. 32, 5610–5621. https://doi.org/10.1002/ejoc.200900770.

(104) Boyer, P. D. *Biochemistry* **1987**, *26* (26), 8503–8507. https://doi.org/10.1021/bi00400a001.

(105) Anda, C.; Llobet, A.; Martell, A. E.; Donnadieu, B.; Parella, T. *Inorg. Chem.* **2003**, *42* (25), 8545–8550. https://doi.org/10.1021/ic034205v.

(106) Develay, S.; Tripier, R.; Le Baccon, M.; Patinec, V.; Serratrice, G.; Handel, H. *Dalton Trans.* **2006**, 3418–3426. https://doi.org/10.1039/b517695f.

(107) Develay, S.; Tripier, R.; Le Baccon, M.; Patinec, V.; Serratrice, G.; Handel, H. *Dalton Trans.* **2005**, 3016–3024. https://doi.org/10.1039/b507819a.

(108) Bazzicalupi, C.; Bencini, A.; Bianchi, A.; Cecchi, M.; Escuder, B.; Fusi, V.; Garcia-España, E.; Giorgi, C.; Luis, S. V.; Maccagni, G.; et al. *J. Am. Chem. Soc.* **1999**, *121* (29), 6807–6815. https://doi.org/10.1021/ja983947y.

(109) Anda, C.; Bazzicalupi, C.; Bencini, A.; Berni, E.; Bianchi, A.; Fornasari, P.; Llobet, A.; Giorgi, C.; Paoletti, P.; Valtancoli, B. *Inorganica Chim. Acta* **2003**, *356*, 167–178. https://doi.org/10.1016/S0020-1693(03)00405-5.

(110) Anda, C.; Llobet, A.; Salvado, V.; Reibenspies, J.; Motekaitis, R. J.; Martell, A. E. *Inorg. Chem.* **2000**, *39* (14), 2986–2999. https://doi.org/10.1021/ic990818p.

(111) Anda, C.; Llobet, A.; Salvado, V.; Martell, A. E.; Motekaitis, R. J. *Inorg. Chem.* **2000**, *39* (14), 3000–3008. https://doi.org/10.1021/ic9908468.

(112) Burguete, M. I.; García-España, E.; López-Diago, L.; Luis, S. V; Miravet, J.; Sroczynski, D. *Org. Biomol. Chem.* **2007**, *5*, 1935–1944. https://doi.org/10.1039/b704305h.

(113) Bazzicalupi, C.; Bencini, A.; Bianchi, A.; Faggi, E.; Giorgi, C.; Santarelli, S.; Valtancoli, B. *J. Am. Chem. Soc.* **2008**, *130* (8), 2440–2441. https://doi.org/10.1021/ja7106977.

(114) Miravet, J. F.; Ramireza, J. A.; Sorianob, C. *J. Chem. Soc. Chem. Commun.* **1995**, 2237–2239.

(115) Aguilar, J. a.; García-España, E.; Guerrero, J.; Luis, S. V.; Llinares, J.; Ramírez, J.; Soriano, C. *Inorganica Chim. Acta* **1996**, *246*, 287–294. https://doi.org/10.1016/0020-1693(96)05075-X.

(116) Aguilar, J. a.; Celda, B.; Fusi, V.; García-España, E.; Luis, S. V.; Martínez, M. C.; Ramírez, J. a.; Soriano, C.; Tejero, R. *J. Chem. Soc. Perkin Trans. 2* **2000**, 1323–1328. https://doi.org/10.1039/b000118j.

(117) Delépine, A.-S.; Tripier, R.; Handel, H. *Org. Biomol. Chem.* **2008**, *6*, 1743–1750. https://doi.org/10.1039/b719514a.

(118) Delépine, A. S.; Tripier, R.; Le Bris, N.; Bernard, H.; Honraedt, A.; Handel, H. *Inorganica Chim. Acta* **2009**, *362* (10), 3829–3834. https://doi.org/10.1016/j.ica.2009.05.003.

(119) Bazzicalupi, C.; Bencini, A.; Bianchi, A.; Danesi, A.; Faggi, E.; Giorgi, C.; Lodeiro, C.; Oliveira, E.; Pina, F.; Valtancoli, B. *Inorganica Chim. Acta* **2008**, *361* (12–13), 3410–3419. https://doi.org/10.1016/j.ica.2008.02.056.

(120) Arturoni, E.; Bazzicalupi, C.; Bencini, A.; Caltagirone, C.; Danesi, A.; Garau, A.; Giorgi, C.; Lippolis, V.; Valtancoli, B. *Inorg. Chem.* **2008**, *47* (14), 6551–6563. https://doi.org/10.1021/ic800549e.

(121) Inclán, M.; Albelda, M. T.; Carbonell, E.; Blasco, S.; Bauzá, A.; Frontera, A.; García-España, E. *Chem. - A Eur. J.* **2014**, *20* (13), 3730–3741. https://doi.org/10.1002/chem.201303861.

(122) González, J.; Llinares, J. M.; Belda, R.; Pitarch, J.; Soriano, C.; Tejero, R.; Verdejo, B.; García-España, E. *Org. Biomol. Chem.* **2010**, *8* (10), 2367–2376. https://doi.org/10.1039/b927418a.

(123) González-García, J.; Tomić, S.; Lopera, A.; Guijarro, L.; Piantanida, I.; García-España, E. *Org. Biomol. Chem.* **2015**, *13* (6), 1732–1740. https://doi.org/10.1039/C4OB02084G.

(124) Kuchelmeister, H. Y.; Schmuck, C. *Chem. - A Eur. J.* **2011**, *17* (19), 5311–5318. https://doi.org/10.1002/chem.201003393.

(125) Bazzicalupi, C.; Bencini, A.; Bianchi, A.; Fusi, V.; Giorgi, C.; Granchi, A.; Paoletti, P.; Valtancoli, B. *J. Chem. Soc. Perkin Trans. 2* **1997**, No. 4, 775–781.

(126) *Comprehensive Inorganic Chemistry II. 2nd Edition. From Elements to Applications*; Reedijk, J., Poeppelmeier, K. R., Eds.; Elsevier, 2013.

(127) Crichton, R. R. *Biological Inorganic Chemistry. An Introduction.*; Elsevier, 2008.

(128) Mjos, K. D.; Orvig, C. *Chem. Rev.* **2014**, *114* (8), 4540–4563. https://doi.org/10.1021/cr400460s.

(129) Wende, C.; Lüdtke, C.; Kulak, N. *Eur. J. Inorg. Chem.* **2014**, *2014* (16), 2597–2612. https://doi.org/10.1002/ejic.201400032.

(130) Zaki, M.; Arjmand, F.; Tabassum, S. *Inorganica Chim. Acta* **2016**, *444*, 1–22. https://doi.org/10.1016/j.ica.2016.01.006.

(131) Timmons, J. C.; Hubin, T. J. *Coord. Chem. Rev.* **2010**, *254* (15–16), 1661–1685. https://doi.org/10.1016/j.ccr.2009.09.018.

(132) Santini, C.; Pellei, M.; Gandin, V.; Porchia, M.; Tisato, F.; Marzano, C. *Am. Chem. Soc.* **2014**, *114*, 815–862. https://doi.org/10.1021/cr400135x.

(133) Nishino, T.; Morikawa, K. *Oncogene* **2002**, *21* (8), 9022–9032. https://doi.org/10.1038/sj.onc.1206135.

(134) Li, F. Z.; Feng, F. M.; Yu, L.; Xie, J. Q. *Prog. React. Kinet. Mech.* **2014**, *39* (3), 209–232. https://doi.org/10.3184/146867814X14043731662981.

(135) Steinreiber, J.; Ward, T. R. *Coord. Chem. Rev.* **2008**, *252* (5–7), 751–766. https://doi.org/10.1016/j.ccr.2007.09.016.

(136) Silva, F.; Fernandes, C.; Campello, M. P. C.; Paulo, A. *Polyhedron* **2017**, *125*, 186–205. https://doi.org/10.1016/j.poly.2016.11.040.

(137) Aiba, Y.; Sumaoka, J.; Komiyama, M. *Chem. Soc. Rev.* **2011**, *40* (12), 5657–5668. https://doi.org/10.1039/c1cs15153c.

(138) Silavi, R.; Divsalar, A.; Saboury, A. A. *J. Biomol. Struct. Dyn.* **2012**, *30* (6), 752–772. https://doi.org/10.1080/07391102.2012.689704.

(139) Agbale, C. M.; Cardoso, M. H.; Galyuon, I. K.; Franco, O. L. *Metallomics* **2016**, *8* (11), 1159–1169. https://doi.org/10.1039/c6mt00133e.

(140) Amatori, S.; Ambrosi, G.; Errico Provenzano, A.; Fanelli, M.; Formica, M.; Fusi, V.; Giorgi, L.; Macedi, E.; Micheloni, M.; Paoli, P.; et al. *J. Inorg. Biochem.* **2016**, *162*, 154–161. https://doi.org/10.1016/j.jinorgbio.2016.06.027.

(141) Kuah, E.; Toh, S.; Yee, J.; Ma, Q.; Gao, Z. *Chem. - A Eur. J.* **2016**, *22* (25), 8404–8430. https://doi.org/10.1002/chem.201504394.

(142) Guo, Z.; Sadler, P. J. *Angew. Chemie Int. Ed.* **1999**, *38* (11), 1512–1531. https://doi.org/10.1002/(SICI)1521-3773(19990601)38:11<1512::AID-ANIE1512>3.0.CO;2-Y.

(143) Hambley, T. W. *Science (80-.).* **2007**, *318* (5855), 1392–1393. https://doi.org/10.1126/science.1150504.

(144) Marzano, C.; Pellei, M.; Tisato, F.; Santini, C. *Anticancer. Agents Med. Chem.* **2009**, *9* (2), 185–211. https://doi.org/10.2174/187152009787313837.

(145) Barton, J. K. In *Bioinorganic Chemistry*; University Press, 1994.

(146) Pages, B. J.; Ang, D. L.; Wright, E. P.; Aldrich-Wright, J. R. *Dalt. Trans.* **2015**, *44* (8), 3505–3526. https://doi.org/10.1039/c4dt02700k.

(147) Jany, T.; Moreth, A.; Gruschka, C.; Sischka, A.; Spiering, A.; Dieding, M.; Wang, Y.; Samo, S. H.; Stammler, A.; Bögge, H.; et al. *Inorg. Chem.* **2015**, *54* (6), 2679–2690. https://doi.org/10.1021/ic5028465.

(148) Erxleben, A. *Coord. Chem. Rev.* **2018**, *360*, 92–121. https://doi.org/10.1016/j.ccr.2018.01.008.

(149) Rosenberg, B.; Van Camp, L.; Krigas, T. *Nature* **1965**, *205* (4972), 698–699. https://doi.org/10.1038/205698a0.

(150) Rosenberg, B.; Van Camp, L.; Trosko, J. E.; Mansour, V. H. *Nature* **1969**, *222* (5191), 385–386. https://doi.org/10.1038/222385a0.

(151) Oun, R.; Moussa, Y. E.; Wheate, N. J. *Dalt. Trans.* **2018**, *47* (19), 6645–6653. https://doi.org/10.1039/c8dt00838h.

(152) Deo, K. M.; Pages, B. J.; Ang, D. L.; Gordon, C. P.; Aldrich-Wright, J. R. *Int. J. Mol. Sci.* **2016**, *17* (11), 1818. https://doi.org/10.3390/ijms17111818.

(153) Todd, R. C.; Lippard, S. J. *Metallomics* **2009**, *1* (4), 280–291. https://doi.org/10.1039/b907567d.

(154) Chikira, M.; Ng, C. H.; Palaniandavar, M. *Int. J. Mol. Sci.* **2015**, *16* (9), 22754–22780. https://doi.org/10.3390/ijms160922754.

(155) Mewis, R. E.; Archibald, S. J. *Coord. Chem. Rev.* **2010**, *254* (15–16), 1686–1712. https://doi.org/10.1016/j.ccr.2010.02.025.

(156) Boer, D. R.; Canals, A.; Coll, M. *Dalt. Trans.* **2009**, No. 3, 399–414. https://doi.org/10.1039/b809873p.

(157) McGivern, T. J. P.; Afsharpour, S.; Marmion, C. J. *Inorganica Chim. Acta* **2018**, *472*, 12–39. https://doi.org/10.1016/j.ica.2017.08.043.

(158) Barone, G.; Terenzi, A.; Lauria, A.; Almerico, A. M.; Leal, J. M.; Busto, N.; García, B. *Coord. Chem. Rev.* **2013**, *257* (19–20), 2848–2862. https://doi.org/10.1016/j.ccr.2013.02.023.

(159) Joyner, J. C.; Reichfield, J.; Cowan, J. a. *J. Am. Chem. Soc.* **2011**, *199* (39), 15613–15626. https://doi.org/10.1021/ja2052599.

(160) Chakraborty, A.; Kumar, P.; Ghosh, K.; Roy, P. *Eur. J. Pharmacol.* **2010**, *647* (1–3), 1–12. https://doi.org/10.1016/j.ejphar.2010.08.003.

(161) Dhar, S.; Senapati, D.; Das, P. K.; Nethaji, M.; Chakravarty, A. R. *J. Am. Chem. Soc.* **2003**, *125* (9), 12118–12124. https://doi.org/10.1021/ja036681q.

(162) Desbouis, D.; Troitsky, I. P.; Belousoff, M. J.; Spiccia, L.; Graham, B. *Coord. Chem. Rev.* **2012**, *256* (11–12), 897–937. https://doi.org/10.1016/j.ccr.2011.12.005.

(163) Jiang, Q.; Xiao, N.; Shi, P.; Zhu, Y.; Guo, Z. *Coord. Chem. Rev.* **2007**, *251* (15–16), 1951–1972. https://doi.org/10.1016/j.ccr.2007.02.013.

(164) Yu, L.; Li, F. Z.; Wu, J. Y.; Xie, J. Q.; Li, S. *J. Inorg. Biochem.* **2016**, *154*, 89–102. https://doi.org/10.1016/j.jinorgbio.2015.09.011.

(165) Boerner, L. J. K.; Zaleski, J. M. *Curr. Opin. Chem. Biol.* **2005**, *9* (2), 135–144. https://doi.org/10.1016/j.cbpa.2005.02.010.

(166) Dumont, E.; Monari, A. *Front. Chem.* **2015**, *3*, Article 43.

https://doi.org/10.3389/fchem.2015.00043.

(167) Mancin, F.; Scrimin, P.; Tecilla, P.; Tonellato, U. *Chem. Commun.* **2005**, No. 20, 2540–2548. https://doi.org/10.1039/b418164f.

(168) Liu, C.; Wang, L. *Dalt. Trans.* **2009**, No. 2, 227–239. https://doi.org/10.1039/b811616d.

(169) Neelakantan, M. A.; Balakrishnan, C.; Balamurugan, K.; Mariappan, S. S. *Appl. Organomet. Chem.* **2018**, *32*, e4400. https://doi.org/10.1002/aoc.4400.

(170) Yu, Z.; Cowan, J. A. *Curr. Opin. Chem. Biol.* **2018**, *43*, 37–42. https://doi.org/10.1016/j.cbpa.2017.10.029.

(171) Amendola, V.; Bergamaschi, G. *Photochemistry* **2018**, *45*, 101–132. https://doi.org/10.1039/9781788010696-00101.

(172) Maldotti, A. *Photochemistry* **2011**, *39*, 88–111.

(173) Pradeep Kumar, M.; Vamsikrishna, N.; Ramesh, G.; Subhashini, N. J. P.; Nanubolu, J. B.; Shivaraj. *J. Coord. Chem.* **2017**, *70* (8), 1368–1388. https://doi.org/10.1080/00958972.2017.1292503.

(174) Lin, C. J.; Hsu, C. S.; Wang, P. Y.; Lin, Y. L.; Lo, Y. S.; Wu, C. H. *Inorg. Chem.* **2014**, *53* (10), 4934–4943. https://doi.org/10.1021/ic4031238.

(175) Zhang, Y.; Zhou, Q.; Zheng, Y.; Li, K.; Jiang, G.; Hou, Y.; Zhang, B.; Wang, X. *Inorg. Chem.* **2016**, *55* (9), 4296–4300. https://doi.org/10.1021/acs.inorgchem.6b00028.

(176) Vinay Kumar, B.; Bhojya Naik, H. S.; Girija, D.; Sharath, N.; Pradeepa, S. M.; Joy Hoskeri, H.; Prabhakara, M. C. *Spectrochim. Acta - Part A Mol. Biomol. Spectrosc.* **2012**, *94*, 192–199. https://doi.org/10.1016/j.saa.2012.03.071.

(177) Ramakrishnan, S.; Rajendiran, V.; Palaniandavar, M.; Periasamy, V. S.; Srinag, B. S.; Krishnamurthy, H.; Akbarsha, M. A. *Inorg. Chem.* **2009**, *48* (4), 1309–1322. https://doi.org/10.1021/ic801144x.

(178) Ros, T. Da; Spalluto, G.; Boutorine, A. S.; Bensasson, R. V; Prato, M. *Curr. Pharm. Des.* **2001**, *7* (17), 1781–1821.

(179) Lin, R. K.; Chiu, C. I.; Hsu, C. H.; Lai, Y. J.; Venkatesan, P.; Huang, P. H.; Lai, P. S.; Lin, C. C. *Chem. - A Eur. J.* **2018**, *24* (16), 4111–4120. https://doi.org/10.1002/chem.201705640.

(180) Chitrapriya, N.; Wang, W.; Jang, Y. J.; Kim, S. K.; Kim, J. H. *J. Inorg. Biochem.* **2014**, *140*, 153–159. https://doi.org/10.1016/j.jinorgbio.2014.06.017.

(181) Anbu, S.; Killivalavan, A.; Alegria, E. C. B. A.; Mathan, G.; Kandaswamy, M. *J. Coord. Chem.* **2013**, *66* (22), 3989–4003. https://doi.org/10.1080/00958972.2013.858136.

(182) Shiva Shankar, D.; Rambabu, A.; Vamsikrishna, N.; Ganji, N.; Daravath, S.; Shivaraj. *Inorg. Chem. Commun.* **2018**, *98*, 48–57. https://doi.org/10.1016/j.inoche.2018.09.033.

(183) Marnett, L. J.; Riggins, J. N.; West, J. D. *J. Clin. Invest.* **2003**, *111* (5), 583–593. https://doi.org/10.1172/JCI200318022.

(184) Heinrich, J.; König, N. F.; Sobottka, S.; Sarkar, B.; Kulak, N. *J. Inorg. Biochem.* **2019**, *194* (August 2018), 223–232. https://doi.org/10.1016/j.jinorgbio.2019.01.016.

(185) Detmer, C. A.; Pamatong, F. V.; Bocarsly, J. R. *Inorg. Chem.* **1996**, *35* (21), 6292–6298.

(186) Elwell, C. E.; Gagnon, N. L.; Neisen, B. D.; Dhar, D.; Spaeth, A. D.; Yee, G. M.; Tolman, W. B. *Chem. Rev.* **2017**, *117* (3), 2059–2107. https://doi.org/10.1021/acs.chemrev.6b00636.

(187) Nunes, C. J.; Borges, B. E.; Nakao, L. S.; Peyroux, E.; Hardré, R.; Faure, B.; Réglier, M.; Giorgi, M.; Prieto, M. B.; Oliveira, C. C.; et al. *J. Inorg. Biochem.* **2015**, *149*, 49–58. https://doi.org/10.1016/j.jinorgbio.2015.05.007.

(188) Pogozelski, W. K.; Tullius, T. D. *Chem. Rev.* **1998**, *98* (3), 1089–1108. https://doi.org/10.1021/cr960437i.

(189) Trawick, B. N.; Daniher, A. T.; Bashkin, J. K. *Chem. Rev.* **1998**, *98* (3), 939–960. https://doi.org/10.1021/cr960422k.

(190) Mirica, L. M.; Ottenwaelder, X.; Stack, T. D. P. *Chem. Rev.* **2004**, *104*, 1013–1045.

(191) Inclán, M.; Guijarro, L.; Pont, I.; Frías, J. C.; Rotger, C.; Orvay, F.; Costa, A.; García-España, E.; Albelda, M. T. *Chem. - A Eur. J.* **2017**, *23* (63), 15966–15973. https://doi.org/10.1002/chem.201702934.

(192) Hormann, J.; Van Der Meer, M.; Sarkar, B.; Kulak, N. *Eur. J. Inorg. Chem.* **2015**, *2015* (28), 4722–4730. https://doi.org/10.1002/ejic.201500596.

(193) Sundaravadivel, E.; Kandaswamy, M.; Varghese, B. *Polyhedron* **2013**, *61*, 33–44. https://doi.org/10.1016/j.poly.2013.04.057.

(194) Fang, M.; Wei, L.; Lin, Z.; Lu, G. Y. *Chinese J. Chem.* **2014**, *32* (2), 142–150. https://doi.org/10.1002/cjoc.201300699.

(195) Massoud, S. S.; Perkins, R. S.; Knierim, K. D.; Comiskey, S. P.; Otero, K. H.; Michel, C. L.; Juneau, W. M.; Albering, J. H.; Mautner, F. A.; Xu, W. *Inorganica Chim. Acta* **2013**, *399*, 177–184. https://doi.org/10.1016/j.ica.2013.01.020.

(196) Liu, C.; Zhu, Y.; Tang, M. *J. Mol. Graph. Model.* **2016**, *64*, 11–29. https://doi.org/10.1016/j.jmgm.2015.12.003.

(197) Li, J. L.; Jiang, L.; Wang, B. W.; Tian, J. L.; Gu, W.; Liu, X.; Yan, S. P. *New J. Chem.* **2015**, *39* (1), 529–538. https://doi.org/10.1039/c4nj00876f.

(198) Zhao, Y.; Gong, T.; Yu, Z.; Zhu, S.; He, W.; Ni, T.; Guo, Z. *Inorganica Chim. Acta* **2013**, *399*, 112–118. https://doi.org/10.1016/j.ica.2013.01.008.

(199) Zhou, W.; Wang, X.; Hu, M.; Guo, Z. *J. Inorg. Biochem.* **2013**, *121* (3), 114–120. https://doi.org/10.1016/j.jinorgbio.2012.12.018.

(200) Hernández-Gil, J.; Ferrer, S.; Castiñeiras, A.; Lloret, F. *Inorg. Chem.* **2012**, *51* (18), 9809–9819. https://doi.org/10.1021/ic301168k.

(201) Chetana, P. R.; Srinatha, B. S.; Somashekar, M. N.; Policegoudra, R. S. *J. Mol. Struct.* **2016**, *1106*, 352–365. https://doi.org/10.1016/j.molstruc.2015.10.010.

(202) Mames, I.; Rodger, A.; Kowalski, J. *Eur. J. Inorg. Chem.* **2015**, *2015* (4), 630–639. https://doi.org/10.1002/ejic.201403042.

(203) Zuin Fantoni, N.; Molphy, Z.; Slator, C.; Menounou, G.; Toniolo, G.; Mitrikas, G.; McKee, V.; Chatgilialoglu, C.; Kellett, A. *Chem. - A Eur. J.* **2019**, *25* (1), 221–237. https://doi.org/10.1002/chem.201804084.

(204) Serre, D.; Erbek, S.; Berthet, N.; Ronot, X.; Martel-Frachet, V.; Thomas, F. *J. Inorg. Biochem.* **2018**, *179*, 121–134. https://doi.org/10.1016/j.jinorgbio.2017.11.006.

(205) Cao, S.; Cheng, R.; Wang, D.; Zhao, Y.; Tang, R.; Yang, X.; Chen, J. *J. Inorg. Biochem.* **2019**, *192*, 126–139. https://doi.org/10.1016/j.jinorgbio.2018.12.014.

(206) Mistry, C. H. E.; Sigman, D. S.; Graham, D. R.; Aurora, V. D.; Stern, A. M.; Aurora, D. *J. Biol. Chem.* **1979**, *254* (24), 12269–12272.

(207) Stockert, J. C. *J. Theor. Biol.* **1989**, *137* (1), 107–111. https://doi.org/10.1016/S0022-5193(89)80152-3.

(208) Nakahata, D. H.; de Paiva, R. E. F.; Lustri, W. R.; Ribeiro, C. M.; Pavan, F. R.; da Silva, G. G.; Ruiz, A. L. T. G.; de Carvalho, J. E.; Corbi, P. P. *J. Inorg. Biochem.* **2018**, *187*, 85–96. https://doi.org/10.1016/j.jinorgbio.2018.07.011.

(209) İnci, D.; Aydın, R.; Vatan, Ö.; Zorlu, Y.; Çinkılıç, N. *J. Biomol. Struct. Dyn.* **2018**, *36* (15), 3878–3901. https://doi.org/10.1080/07391102.2017.1404936.

(210) Prisecaru, A.; McKee, V.; Howe, O.; Rochford, G.; McCann, M.; Colleran, J.; Pour, M.; Barron, N.; Gathergood, N.; Kellett, A. *J. Med. Chem.* **2013**, *565*, 8599–8615.

(211) Wang, Q.; Mao, H.; Wang, W.; Zhu, H.; Dai, L.; Chen, Y.; Tang, X. *BioMetals* **2017**, *30* (4), 575–587. https://doi.org/10.1007/s10534-017-0028-8.

(212) Thederahn, T. B.; Kuwabara, M. D.; Larsen, T. A.; Sigman, D. S. *J. Am. Chem. Soc.* **1989**, *111* (13), 4941–4946. https://doi.org/10.1021/ja00195a057.

(213) Hormann, J.; Perera, C.; Deibel, N.; Lentz, D.; Sarkar, B.; Kulak, N. *Dalt. Trans.* **2013**, *42* (13), 4357–4360. https://doi.org/10.1039/c3dt32857k.

(214) Pradhan, A.; Haldar, S.; Mallik, K. B.; Ghosh, M.; Bera, M.; Sepay, N.; Schollmeyer, D.; Ghatak, S. K.; Roy, S.; Saha, S. *Inorganica Chim. Acta* **2019**, *484* (August 2018), 197–205. https://doi.org/10.1016/j.ica.2018.09.026.

(215) Zhao, Z.; Zhang, J.; Zhi, S.; Song, W.; Zhao, J. *J. Inorg. Biochem.* **2019**, *197*, 110696. https://doi.org/10.1016/j.jinorgbio.2019.110696.

(216) Barrera-Guzmán, V. A.; Rodríguez-Hernández, E. O.; Ortíz-Pastrana, N.; Domínguez-González, R.; Caballero, A. B.; Gamez, P.; Barba-Behrens, N. *J. Biol. Inorg. Chem.* **2018**, *23* (7), 1165–1183. https://doi.org/10.1007/s00775-018-1598-9.

(217) Brissos, R. F.; Caubet, A.; Gamez, P. *Eur. J. Inorg. Chem.* **2015**, *2015* (16), 2633–2645. https://doi.org/10.1002/ejic.201500175.

(218) Molphy, Z.; Montagner, D.; Bhat, S. S.; Slator, C.; Long, C.; Erxleben, A.; Kellett, A. *Nucleic Acids Res.* **2018**, *46* (19), 9918–9931. https://doi.org/10.1093/nar/gky806.

(219) Zhao, Y.; Zhu, J.; He, W.; Yang, Z.; Zhu, Y.; Li, Y.; Zhang, J.; Guo, Z. *Chem. - A Eur. J.* **2006**, *12* (25), 6621–6629. https://doi.org/10.1002/chem.200600044.

(220) Radecka-Paryzek, W.; Patroniak, V.; Lisowski, J. *Coord. Chem. Rev.* **2005**, *249* (21–22),

2156–2175. https://doi.org/10.1016/j.ccr.2005.02.021.

(221) Anbu, S.; Kandaswamy, M.; Suthakaran, P.; Murugan, V.; Varghese, B. *J. Inorg. Biochem.* **2009**, *103* (3), 401–410. https://doi.org/10.1016/j.jinorgbio.2008.12.013.

(222) Khoramdareh, Z. K.; Hosseini-Yazdi, S. A.; Spingler, B.; Khandar, A. A. *J. Incl. Phenom. Macrocycl. Chem.* **2014**, *80* (3–4), 391–399. https://doi.org/10.1007/s10847-014-0425-3.

(223) Khoramdareh, Z. K.; Hosseini-Yazdi, S. A.; Spingler, B.; Khandar, A. A. *Inorganica Chim. Acta* **2014**, *415*, 7–13. https://doi.org/10.1016/j.ica.2014.02.022.

(224) Karthick, C.; Karthikeyan, K.; Korrapati, P. S.; Rahiman, A. K. *Appl. Organomet. Chem.* **2017**, *31* (8), 1–15. https://doi.org/10.1002/aoc.3669.

(225) Arthi, P.; Haleel, A.; Srinivasan, P.; Prabhu, D.; Arulvasu, C.; Kalilur Rahiman, A. *Spectrochim. Acta - Part A Mol. Biomol. Spectrosc.* **2014**, *129*, 400–414. https://doi.org/10.1016/j.saa.2014.03.058.

(226) Qian, J.; Gu, W.; Liu, H.; Gao, F.; Feng, L.; Yan, S.; Liao, D.; Cheng, P. *Dalt. Trans.* **2007**, *2* (10), 1060–1066. https://doi.org/10.1039/b615148e.

(227) Cheng, Q. R.; Zhang, F. Q.; Zhou, H.; Pan, Z. Q.; Liao, G. Y. *J. Coord. Chem.* **2015**, *68* (11), 1997–2005. https://doi.org/10.1080/00958972.2015.1032272.

(228) Arthi, P.; Shobana, S.; Srinivasan, P.; Mitu, L.; Kalilur Rahiman, A. *Spectrochim. Acta - Part A Mol. Biomol. Spectrosc.* **2015**, *143*, 49–58. https://doi.org/10.1016/j.saa.2015.01.122.

(229) Liu, J.; Lu, T. B.; Li, H.; Zhang, Q. L.; Ji, L. N.; Zhang, T. X.; Qu, L. H.; Zhou, H. *Transit. Met. Chem.* **2002**, *27* (6), 686–690. https://doi.org/10.1023/A:1019888918621.

(230) Chen, Y.; Song, H.; Mao, J.; Liu, M.; Ding, C.; Pan, Z. *Inorg. Chem. Commun.* **2013**, *27*, 131–137. https://doi.org/10.1016/j.inoche.2012.10.037.

(231) Chang, C. A.; Wu, T. T.; Lee, H. Y. *J. Coord. Chem.* **2016**, *69* (8), 1388–1405. https://doi.org/10.1080/00958972.2016.1157177.

(232) Gran, G. *Analyst* **1952**, *77*, 661–663.

(233) Rossotti, F. J. C.; Rossotti, H. *J. Chem. Educ.* **1965**, *42* (7), 375. https://doi.org/10.1021/ed042p375.

(234) Pettit, L. D. .; Powell, K. J. Academic Software: Sourby Old Farm: Timble, Otley, Yorks, U.K. 2004.

(235) Smith, R. M. .; Martell, A. E. National Institute of Standards and Technology: Gaithersburg 1995.

(236) Gans, P.; Sabatini, A.; Vacca, A. *Talanta* **1996**, *43* (10), 1739–1753. https://doi.org/10.1016/0039-9140(96)01958-3.

(237) Schro ¨dinger, LLC: New York 2005.

(238) Weiner, S. J.; Kollman, P. A.; Nguyen, D. T.; Case, D. A. *J. Comput. Chem.* **1986**, *7* (2), 230–252. https://doi.org/10.1002/jcc.540070216.

(239) Weiner, S. J.; Kollman, P. A.; Case, D. A.; Singh, U. C.; Ghio, C.; Alagona, G.; Profeta, S.; Weinerl, P. *J. Am. Chem. Soc.* **1984**, *106* (17), 765–784. https://doi.org/10.1021/ja00315a051.

(240) Frisch, M. J.; Trucks, G. W.; Schlegel, H. B.; Scuseria, G. E.; A., R. M.; Cheeseman, J. R. Zakrzewski, V. G. Montgomery, J. A., J.; Stratmann, R. E.; Burant, J. C.; Dapprich, S.; Millam, J. M.; et al. Gaussian, Inc.: Pittsburgh 2001.

(241) Case, D. A. .; Pearlman, D. A. .; Caldwell, J. W. .; Cheatham, T. E., I.; Wang, J. .; Ross, W. S. .; Simmerling, C. .; Darden, T. .; Merz, K. M. .; Stanton, R. V. .; et al. University of California 2002.

(242) Wang, J. M.; Wolf, R. M.; Caldwell, J. W.; Kollman, P. a; Case, D. a. *J. Comput. Chem.* **2004**, *25* (9), 1157–1174. https://doi.org/10.1002/jcc.20035.

(243) Spek, A. L. Utrecht University: Utrecht, The Netherlands p 2005.

(244) Mier-Vinué, J. de; Lorenzo, J.; Montaña, Á. M.; Moreno, V.; Avilés, F. X. *J. Inorg. Biochem.* **2008**, *102* (4), 973–987. https://doi.org/10.1016/j.jinorgbio.2007.12.026.

(245) Ng, C. Y.; Motekaitis, R. J.; Martell, A. E. *Inorg. Chem.* **1979**, *18* (11), 2982–2986.

(246) Fielding, L. *Tetrahedron* **2000**, *56* (34), 6151–6170.

(247) Anda, C.; Martínez, M. A.; Llobet, A. *Supramol. Chem.* **2005**, *17* (3), 257–266. https://doi.org/10.1080/10610270412331337330.

(248) Menif, R.; Martell, A. E.; Squattrito, P. J.; Clearfield, A. *Inorg. Chem.* **1990**, *29* (23), 4723–4729. https://doi.org/10.1021/ic00348a028.

(249) Hutin, M.; Bernardinelli, G.; Nitschke, J. R. *Proc. Natl. Acad. Sci.* **2006**, *103*, 17655–17660.

(250) Robles, J.; Solà, M.; Costas, M.; Xifra, R.; Parella, T.; Stoeckli-Evans, H.; Llobet, A.; Neuburger, M. *Inorg. Chem.* **2003**, *42* (14), 4456–4468. https://doi.org/10.1021/ic0261833.

(251) Ma, H.; Allmendinger, M.; Thewalt, U.; Lentz, A.; Klinga, M.; Rieger, B. *Eur. J. Inorg. Chem.* **2002**, No. 11, 2857–2867. https://doi.org/10.1002/1099-0682(200211)2002:11<2857::AID-EJIC2857>3.0.CO;2-#.

(252) Burrows, C. J.; Muller, J. G. *Chem. Rev.* **1998**, *98* (3), 1109–1152. https://doi.org/10.1021/cr960421s.

(253) Koval, I. A.; Belle, C.; Selmeczi, K.; Philouze, C.; Saint-Aman, E.; Schuitema, A. M.; Gamez, P.; Pierre, J. L.; Reedijk, J. *J. Biol. Inorg. Chem.* **2005**, *10* (7), 739–750. https://doi.org/10.1007/s00775-005-0016-2.

(254) Mizuno, M.; Hayashi, H.; Fujinami, S.; Furutachi, H.; Nagatomo, S.; Otake, S.; Uozumi, K.; Suzuki, M.; Kitagawa, T. *Inorg. Chem.* **2003**, *42* (25), 8534–8544. https://doi.org/10.1021/ic0345166.

(255) Costas, M.; Ribas, X.; Poater, A.; López Valbuena, J. M.; Xifra, R.; Company, A.; Duran, M.; Solà, M.; Llobet, A.; Corbella, M.; et al. *Inorg. Chem.* **2006**, *45* (9), 3569–3581. https://doi.org/10.1021/ic051800j.

(256) Kypr, J.; Kejnovská, I.; Renčiuk, D.; Vorlíčková, M. *Nucleic Acids Res.* **2009**, *37* (6), 1713–1725. https://doi.org/10.1093/nar/gkp026.

(257) Moradell, S.; Lorenzo, J.; Rovira, A.; Robillard, M. S.; Avilés, F. X.; Moreno, V.; De Llorens, R.; Martinez, M. A.; Reedijk, J.; Llobet, A. *J. Inorg. Biochem.* **2003**, *96* (4), 493–502. https://doi.org/10.1016/S0162-0134(03)00252-6.

(258) Moradell, S.; Lorenzo, J.; Rovira, A.; Van Zutphen, S.; Avilés, F. X.; Moreno, V.; De Llorens, R.; Martinez, M. A.; Reedijk, J.; Llobet, A. *J. Inorg. Biochem.* **2004**, *98* (11), 1933–1946. https://doi.org/10.1016/j.jinorgbio.2004.08.011.

(259) Wang, X.; Shao, Y.; Xu, Q.; Li, Y.; Zhu, Y.; Zhu, J.; Guo, Z.; Chen, J. *Inorg. Chem.* **2007**, *46* (8), 3306–3312. https://doi.org/10.1021/ic0614162.

(260) McMillin, D. R.; McNett, K. M. *Chem. Rev.* **2002**, *98* (3), 1201–1220. https://doi.org/10.1021/cr9601167.

(261) Mounir, M.; Lorenzo, J.; Ferrer, M.; Prieto, M. J.; Rossell, O.; Avilès, F. X.; Moreno, V. *J. Inorg. Biochem.* **2007**, *101* (4), 660–666. https://doi.org/10.1016/j.jinorgbio.2006.12.009.

(262) Kong, D. M.; Wang, J.; Zhu, L. N.; Jin, Y. W.; Li, X. Z.; Shen, H. X.; Mi, H. F. *J. Inorg. Biochem.* **2008**, *102* (4), 824–832. https://doi.org/10.1016/j.jinorgbio.2007.12.002.

(263) Lincoln, P.; Tuite, E.; Nordén, B. *J. Am. Chem. Soc.* **1997**, *119* (6), 1454–1455. https://doi.org/10.1021/ja9631965.

(264) Li, J. H.; Wang, J. T.; Hu, P.; Zhang, L. Y.; Chen, Z. N.; Mao, Z. W.; Ji, L. N. *Polyhedron* **2008**, *27* (7), 1898–1904. https://doi.org/10.1016/j.poly.2008.02.032.

(265) Coury, J. E.; Anderson, J. R.; McFail-Isom, L.; Williams, L. D.; Bottomley, L. A. *J. Am. Chem. Soc.* **1997**, *119* (16), 3792–3796. https://doi.org/10.1021/ja9623774.

(266) Coury, J. E.; McFail-Isom, L.; Williams, L. D.; Bottomley, L. A. *Proc. Natl. Acad. Sci.* **1996**, *93* (22), 12283–12286. https://doi.org/10.1073/pnas.93.22.12283.

(267) Khalid, S.; Hannon, M. J.; Rodger, A.; Mark Rodger, P. *Chem. - A Eur. J.* **2006**, *12* (13), 3493–3506. https://doi.org/10.1002/chem.200501168.

(268) Llobet, A.; Solà, M.; Cavallo, L.; Ribas, X.; Poater, A. *J. Am. Chem. Soc.* **2008**, *130* (52), 17710–17717. https://doi.org/10.1021/ja801913b.

(269) Sawyer, D. T.; Kang, C.; Llobet, A.; Redman, C. *J. Am. Chem. Soc.* **1993**, *115* (13), 5817–5818. https://doi.org/10.1021/ja00066a057.

(270) Qui, A.; Liu, X.; Sawyer, D. T.; Sobkowiak, A.; Llobet, A. *J. Am. Chem. Soc.* **1993**, *115* (2), 609–614. https://doi.org/10.1021/ja00055a033.

Annex. Supporting Information.

Supporting information for Chapter 4.1.

Figure A1.1. ^{1}H-NMR (500 MHz) spectra in D_2O at pD = 5.84 and T = 298 K (A) free **L9** (2 mM); (B) free *is* (2 mM) and (C) **L9**-*is* system (2 mM, 1:1).

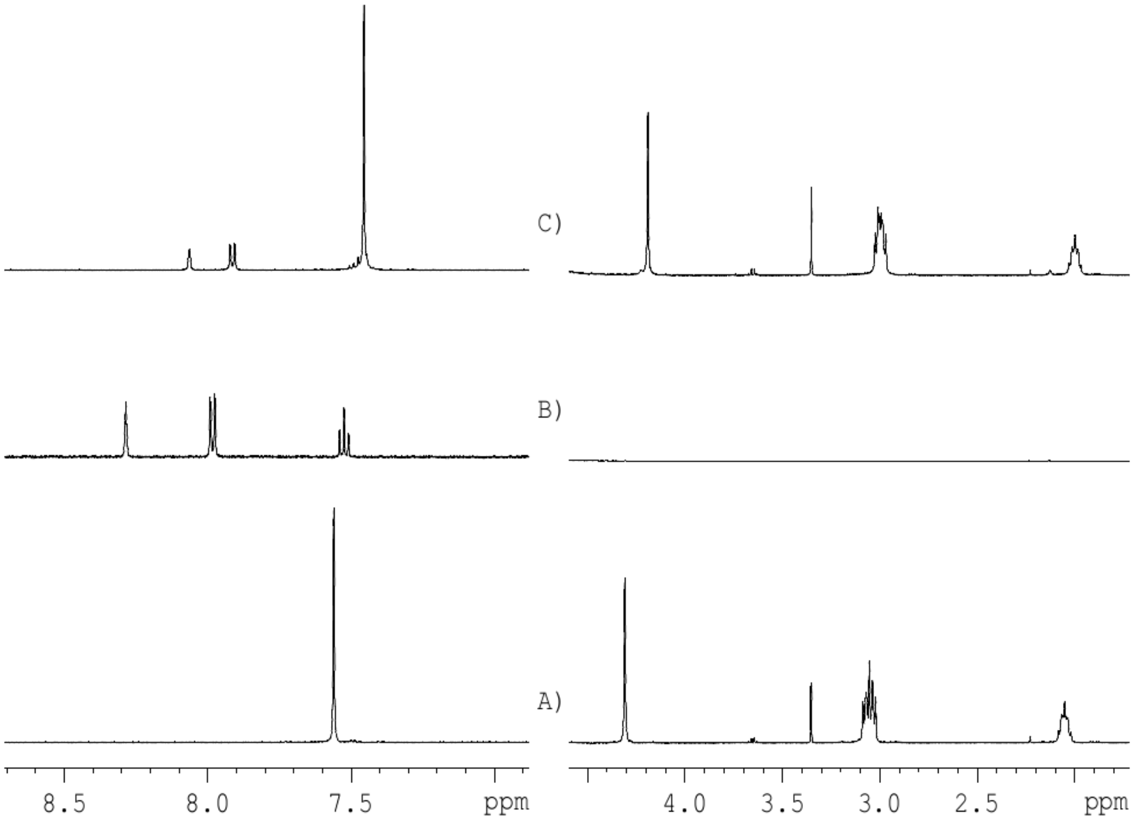

Figure A1.2. 2D ^{1}H-^{1}H NOESY (500 MHz) spectra of **L9**-*is* system (2 mM, 1:1) in D_2O at pD = 5.84, T = 298 K.

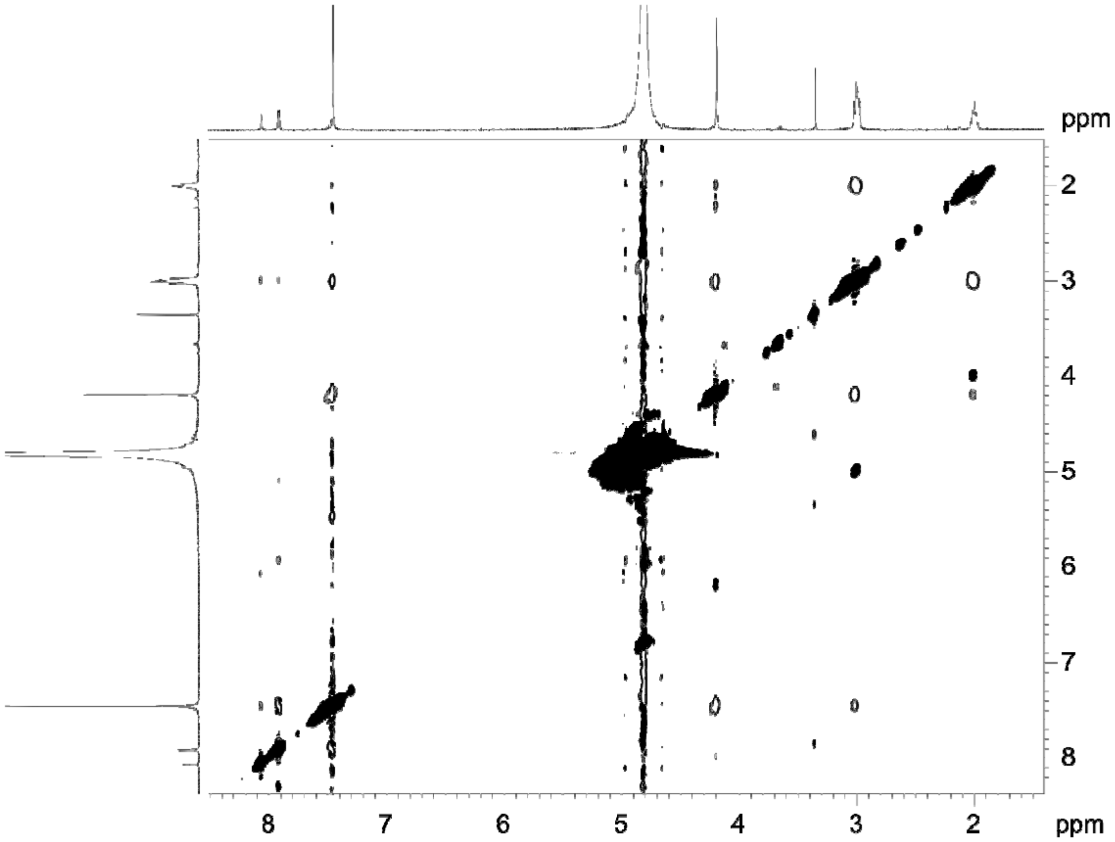

Figure A1.3. Expansions of the 2D ^{1}H-^{1}H NOESY (500 MHz) spectra of the **L9**-*is* system (2 mM, 1:1) in D_2O at pD = 5.84, T = 298 K.

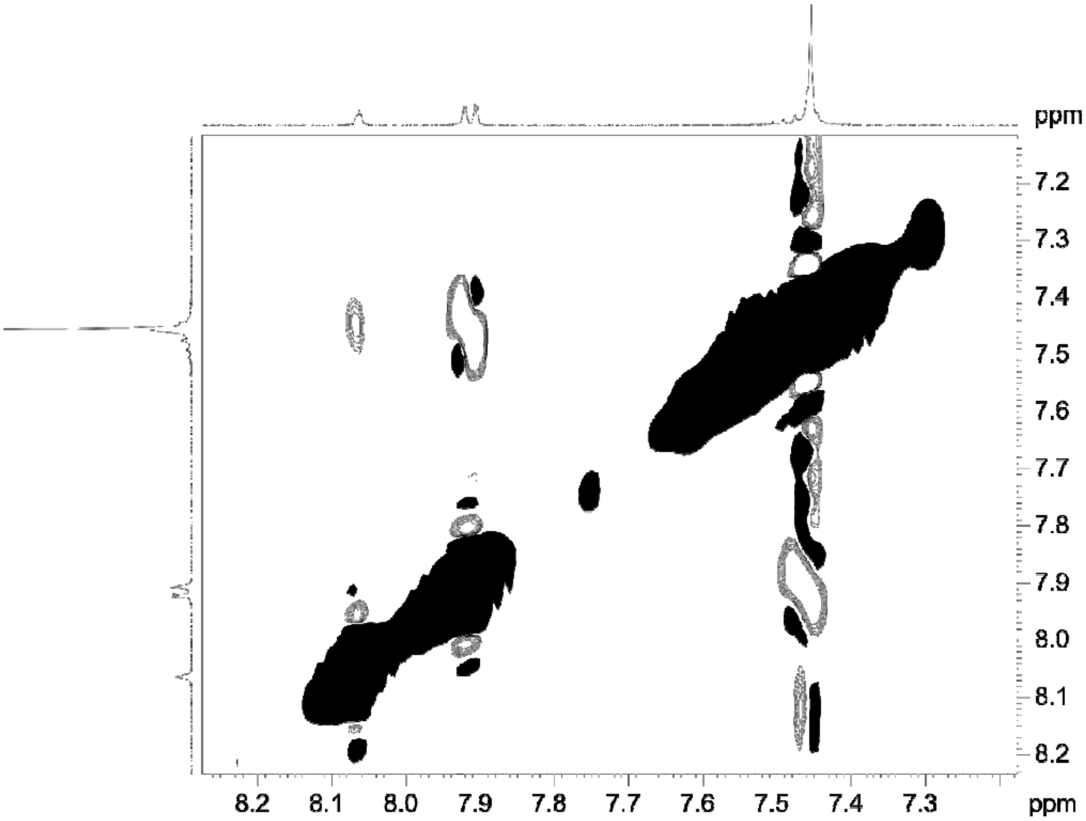

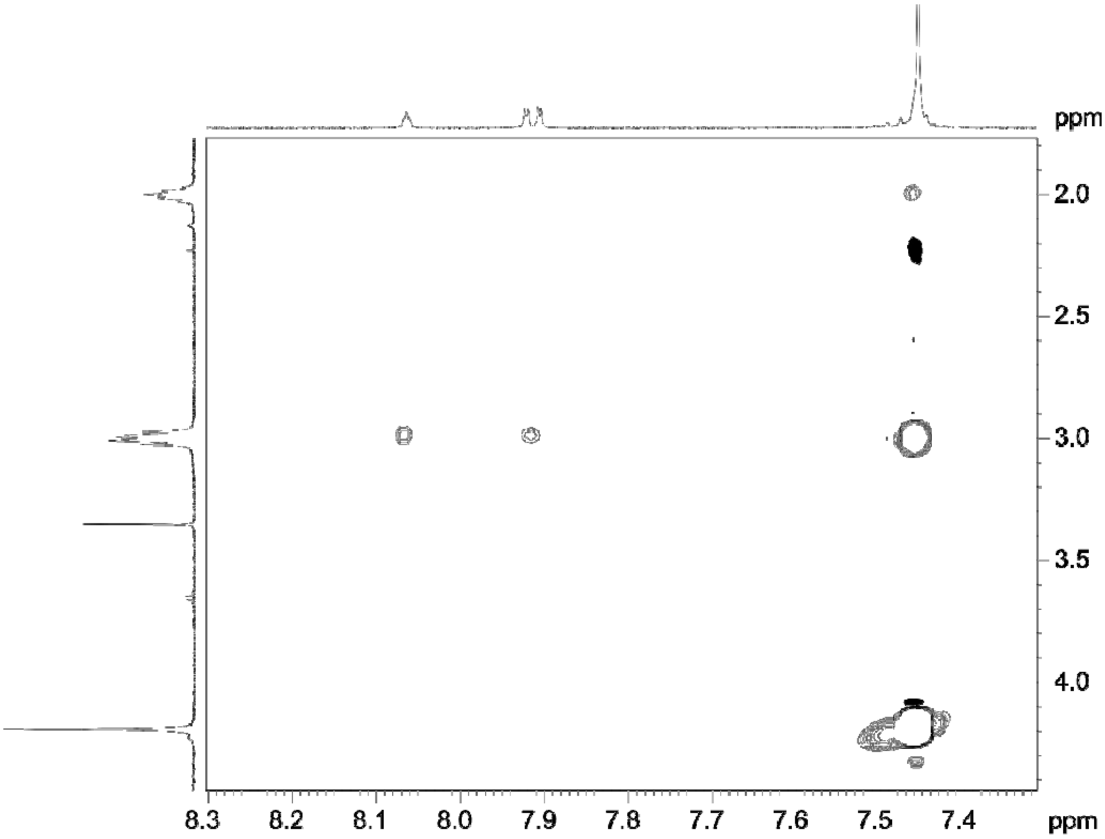

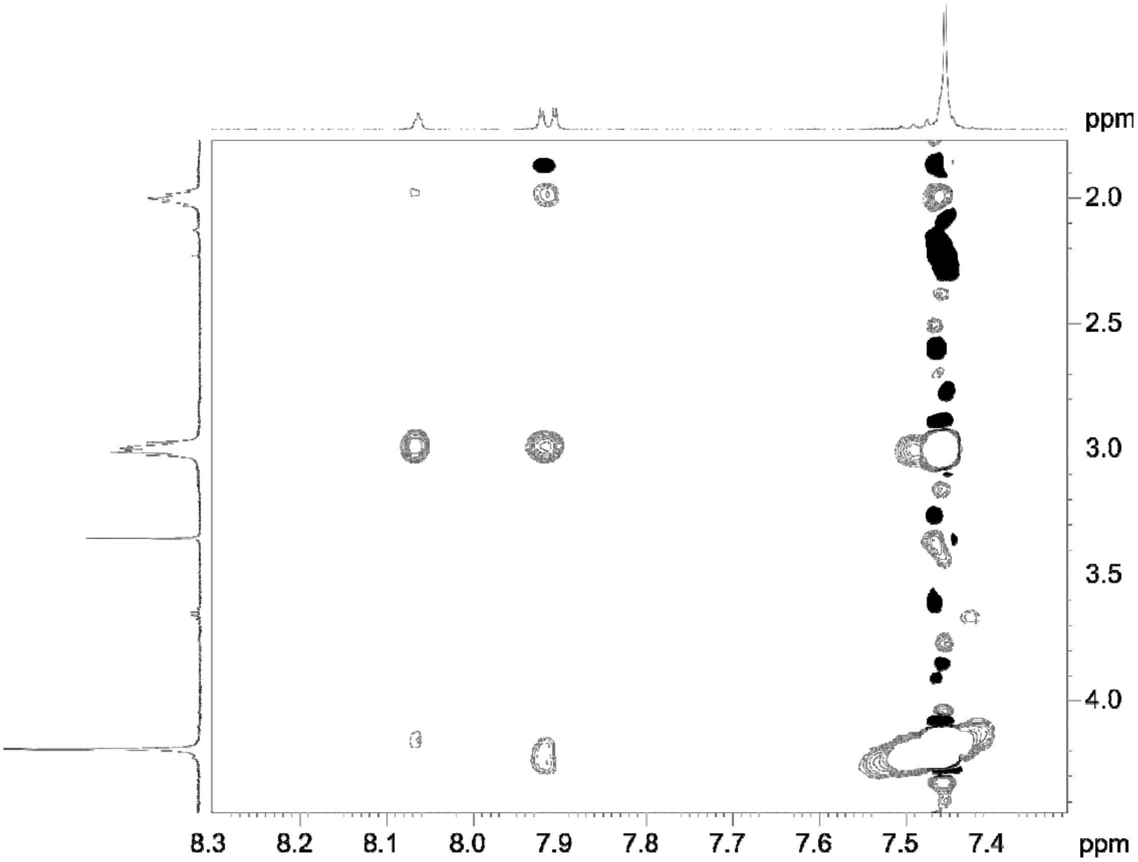
ppm
2.0
2.5
3.0
3.5
4.0
8.3
8.2
8.1
8.0
7.9
7.8
7.7
7.6
7.5
7.4
ppm

Figure A1.4. Diffusion experiments in D_2O at pD = 5.84 and T = 298 K (A) free **L9** (B) free *is* (C) ternary **L9**-*is* system (2 mM, 1:1).

Figure A1.4. (A)

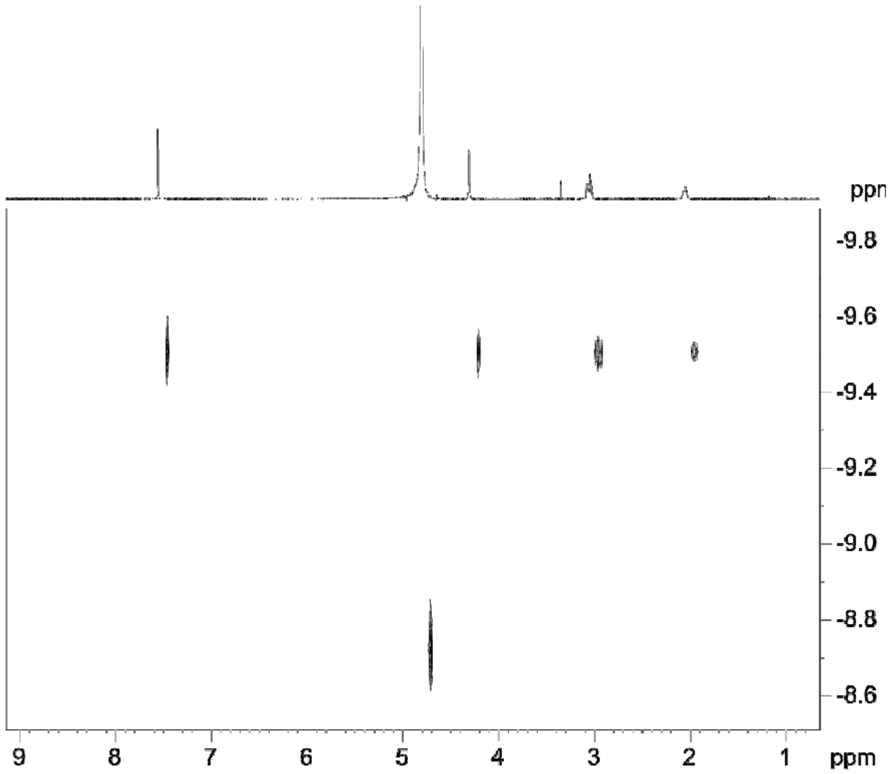

Figure A1.4. (B)

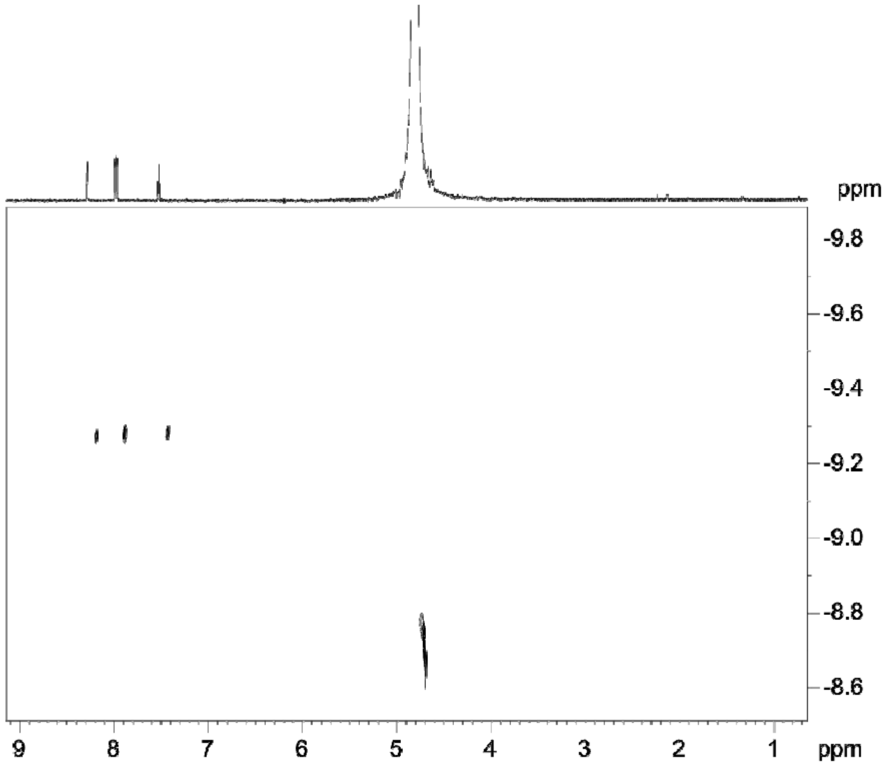

Figure A1.4. (C)

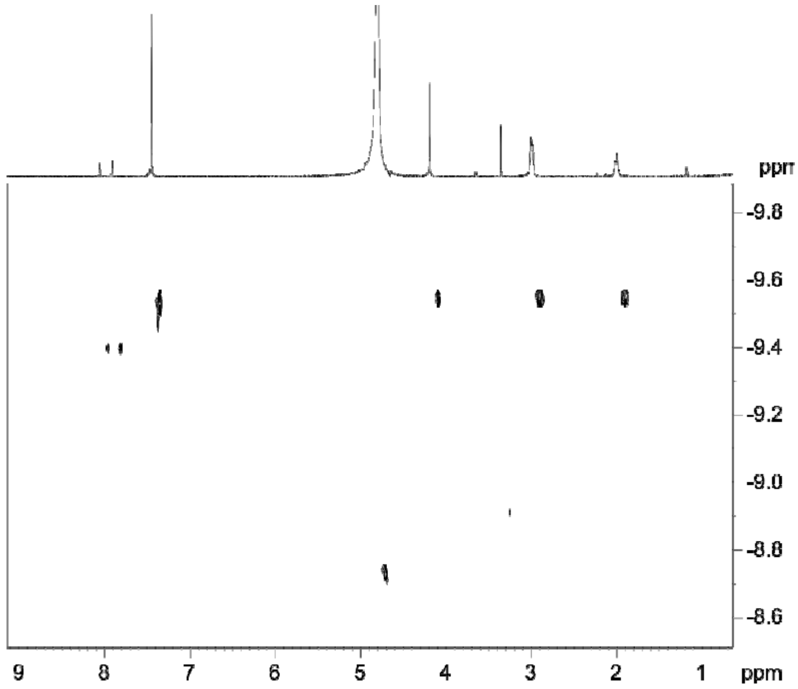

Figure A1.5.Spectra of **L9**-*is* systems in D_2O, pD = 5.84, T = 298 K, [**L9**] = 2mM in different **L9**:*is* ratio (A) 1:0.1 ([*is*]=0.2mM) (B) 1:0.5 ([*is*]=1mM), (C) 1:1 ([*is*]=2mM), (D) 1:1.5 ([*is*]=3mM) and (E) 1:2 ([*is*]=4mM).

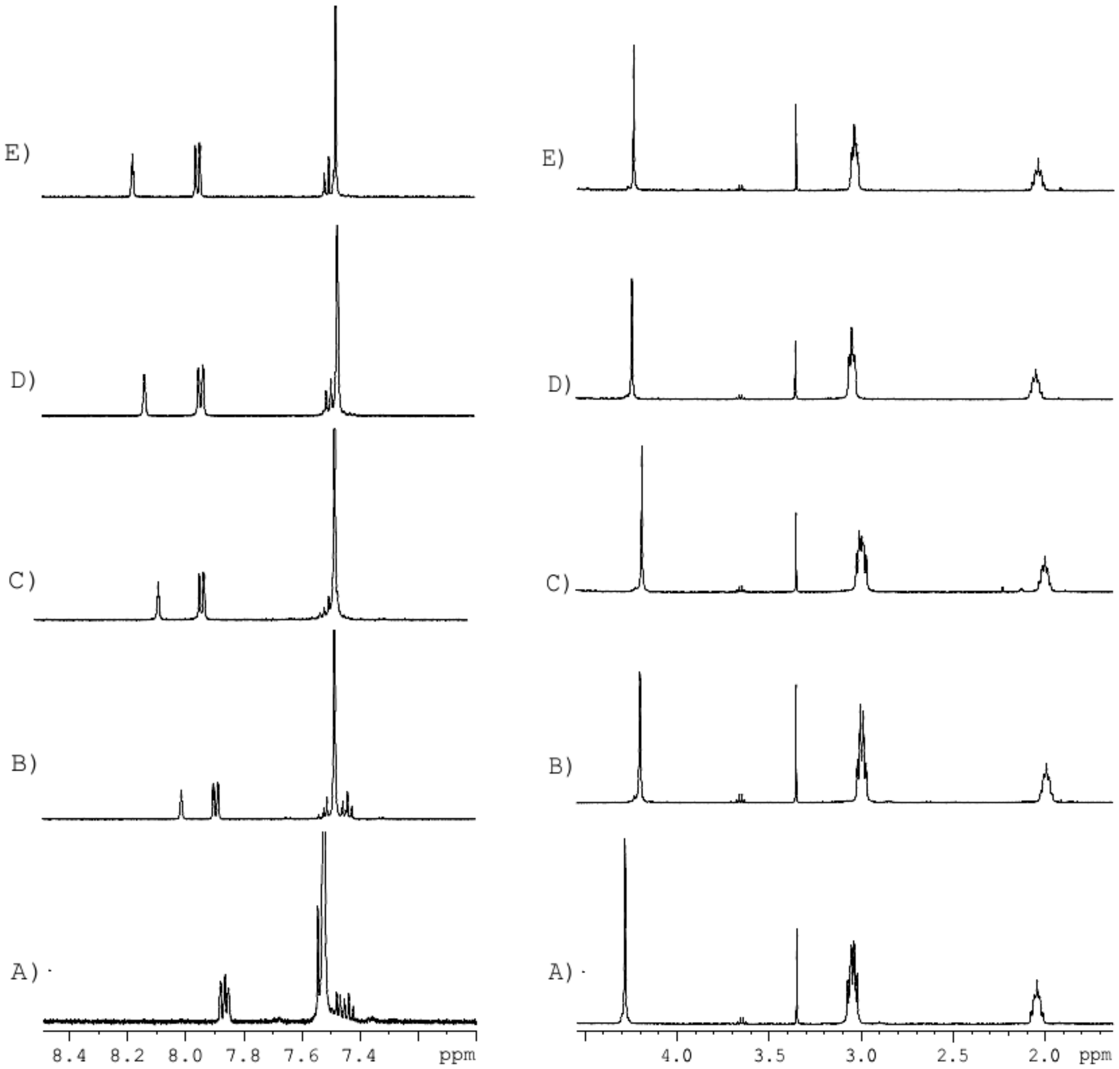

Figure A1.6. 2D ^{1}H-^{1}H NOESY (500 MHz) spectra of **L9**-*ph* system (2 mM, 1:1) in D_2O at pD = 5.84, T = 298 K.

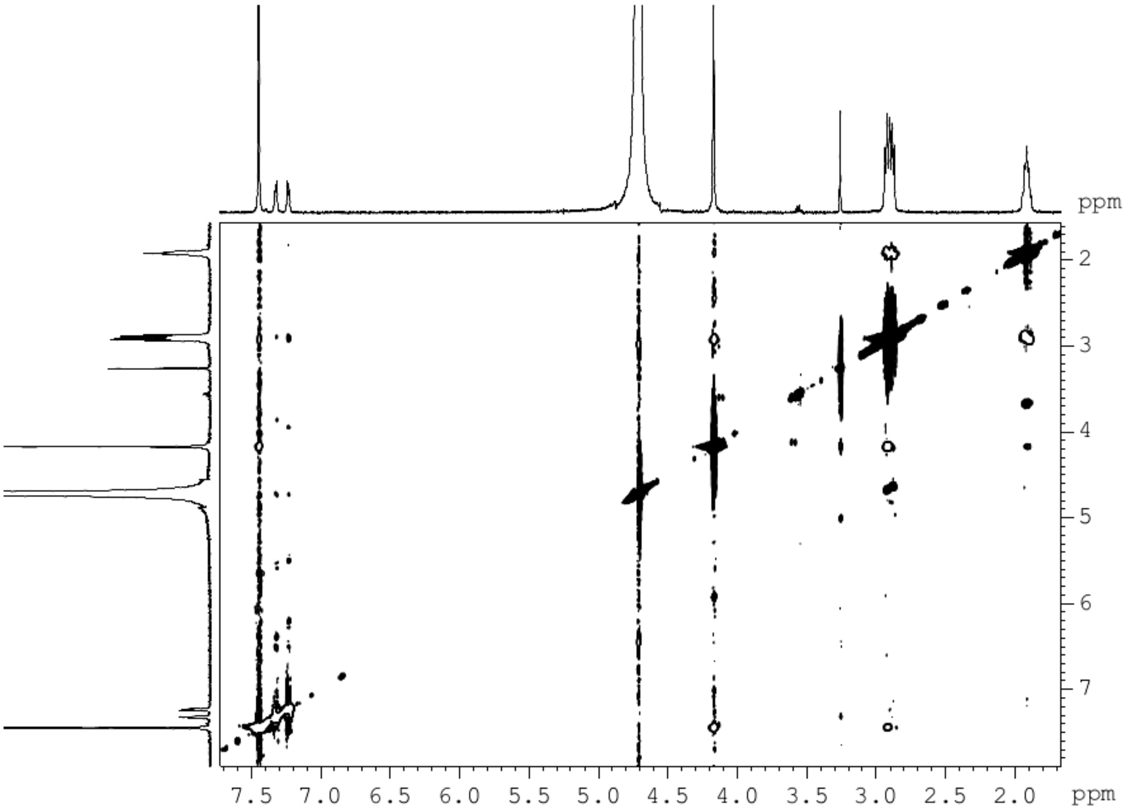

Figure A1.7. Expansions of the 2D ^1H-^1H NOESY (500 MHz) spectra of **L9**-*ph* system (2 mM, 1:1) in D_2O at pD = 5.84, T = 298 K.

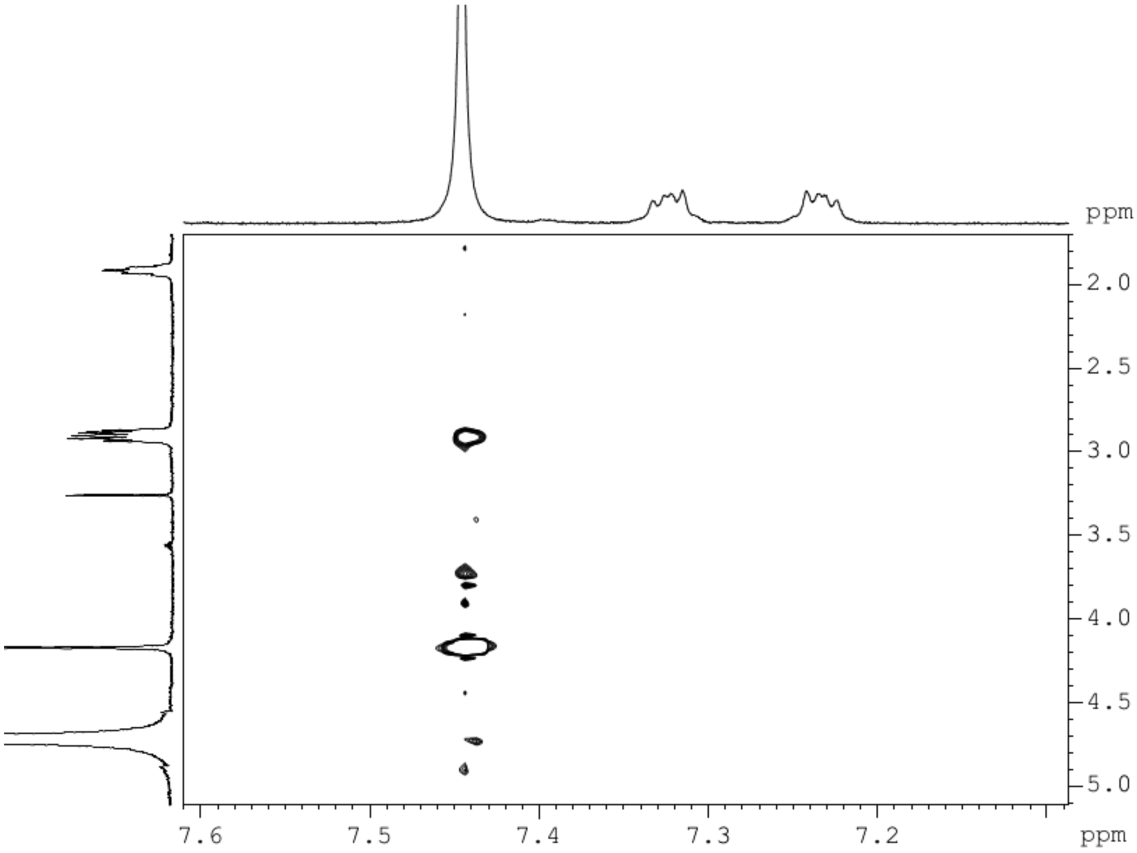

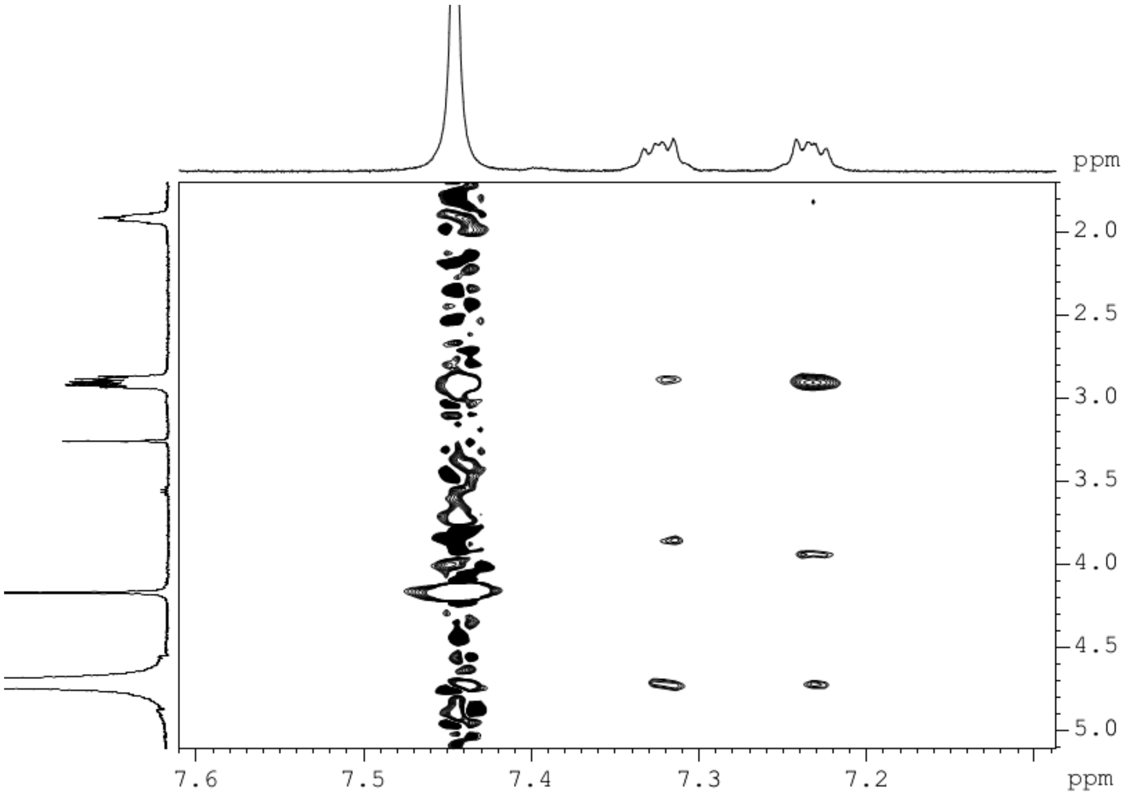

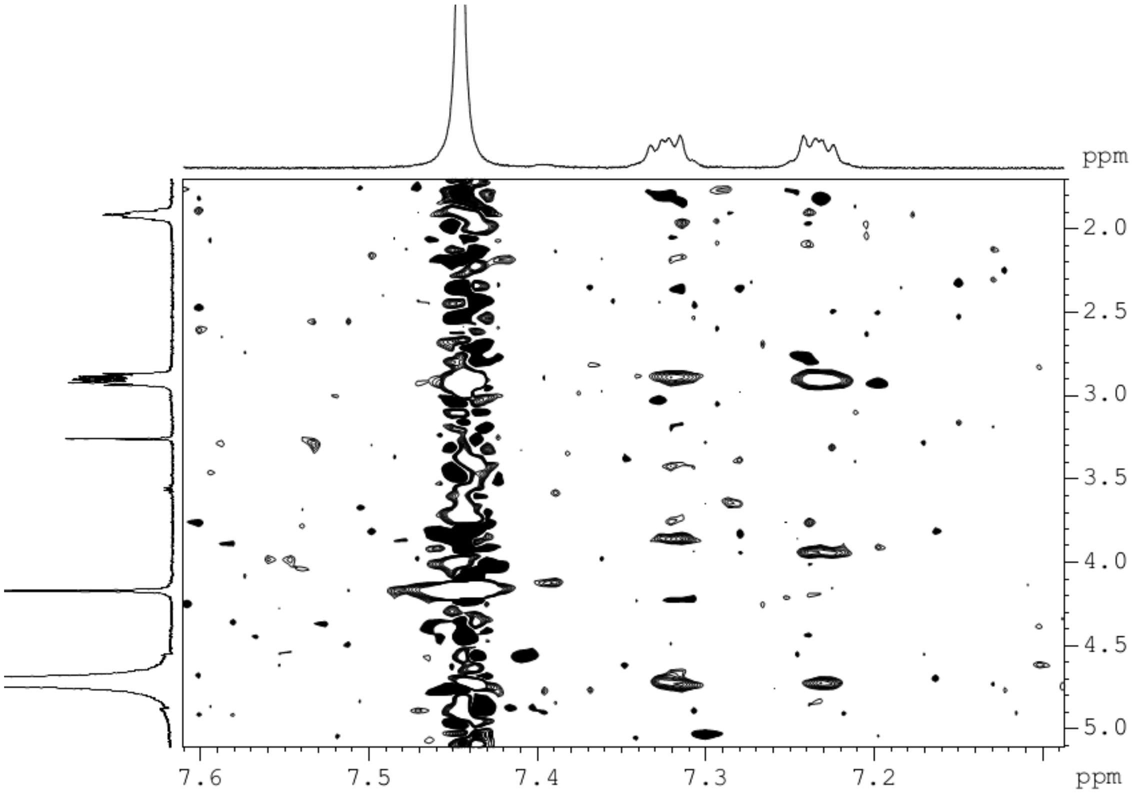
ppm
2.0
2.5
3.0
3.5
4.0
4.5
5.0
7.6
7.5
7.4
7.3
7.2
ppm

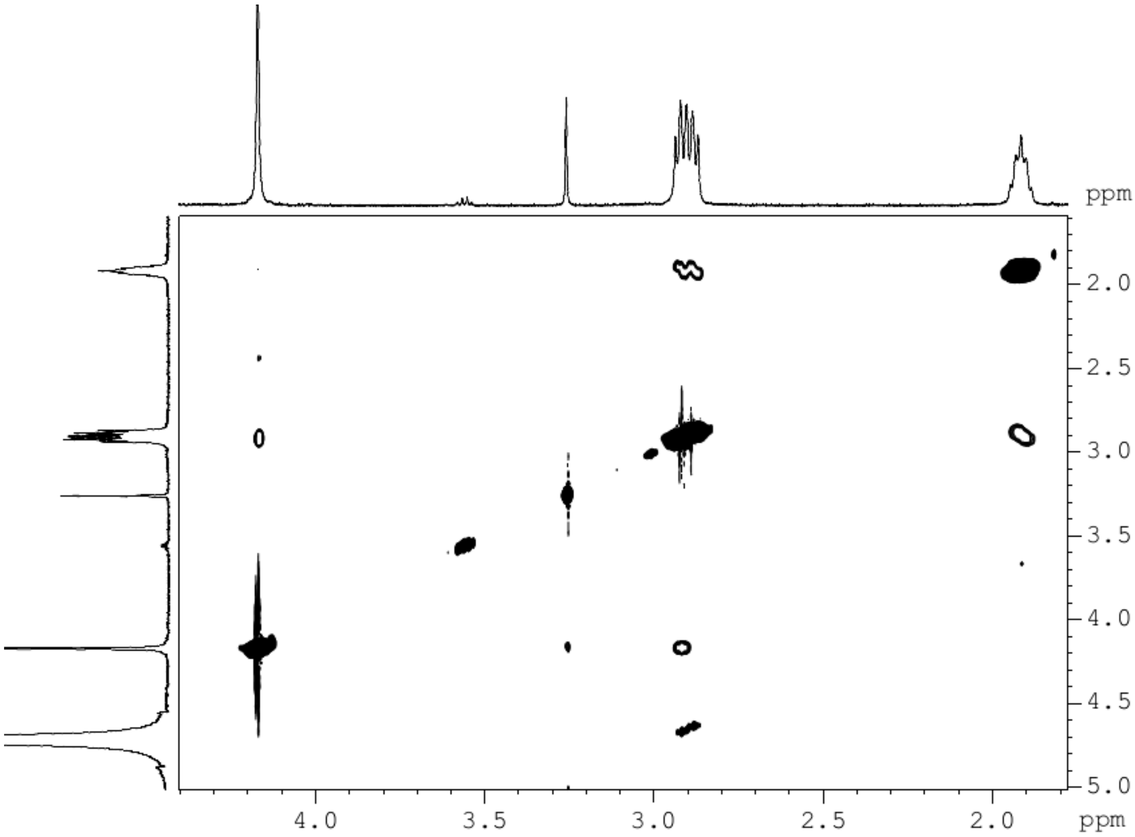
ppm
2.0
2.5
3.0
3.5
4.0
4.5
5.0
4.0
3.5
3.0
2.5
2.0
ppm

Figure A1.8. 2D ^{1}H-^{1}H NOESY (500 MHz) spectra of **L9**-*te* system (2 mM, 1:1) in D_2O at pD = 5.84, T = 298 K.

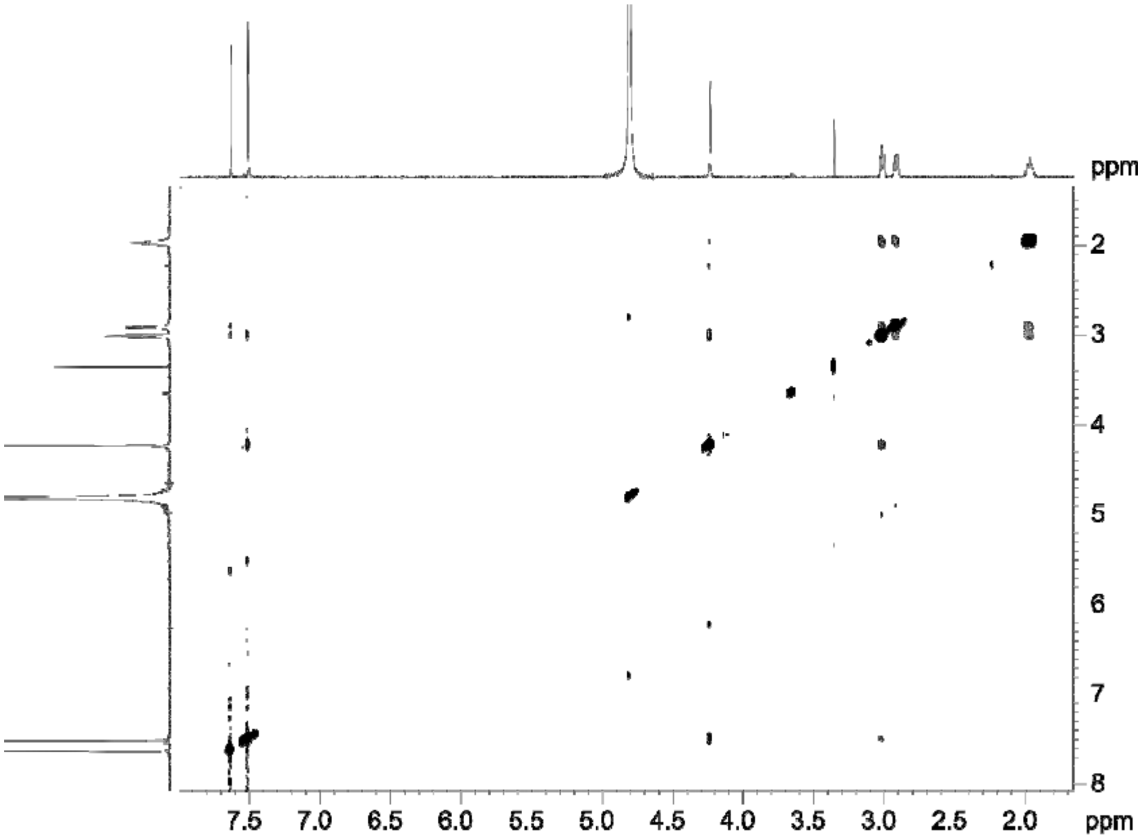

Figure A1.9. Expansions of the 2D ^{1}H-^{1}H NOESY (500 MHz) spectra of **L9**-*te* system (2 mM, 1:1) in D_2O at pD = 5.84, T = 298 K.

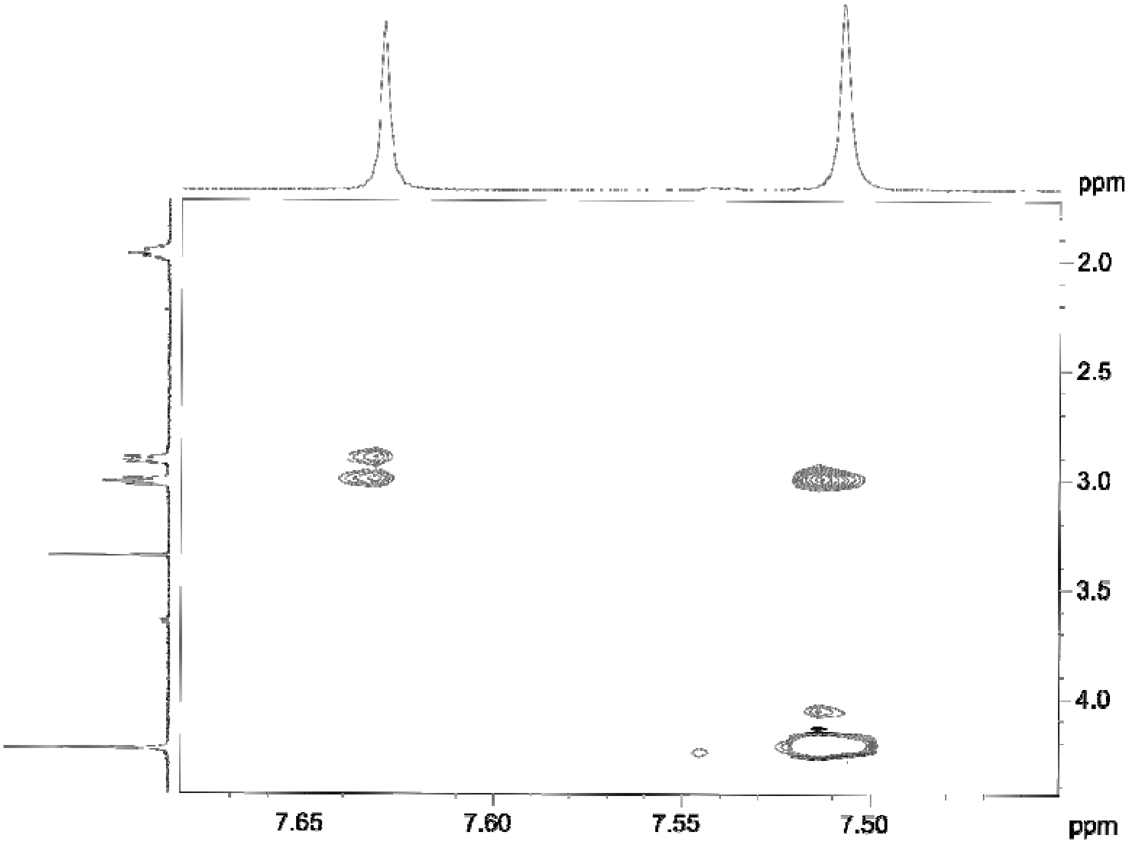

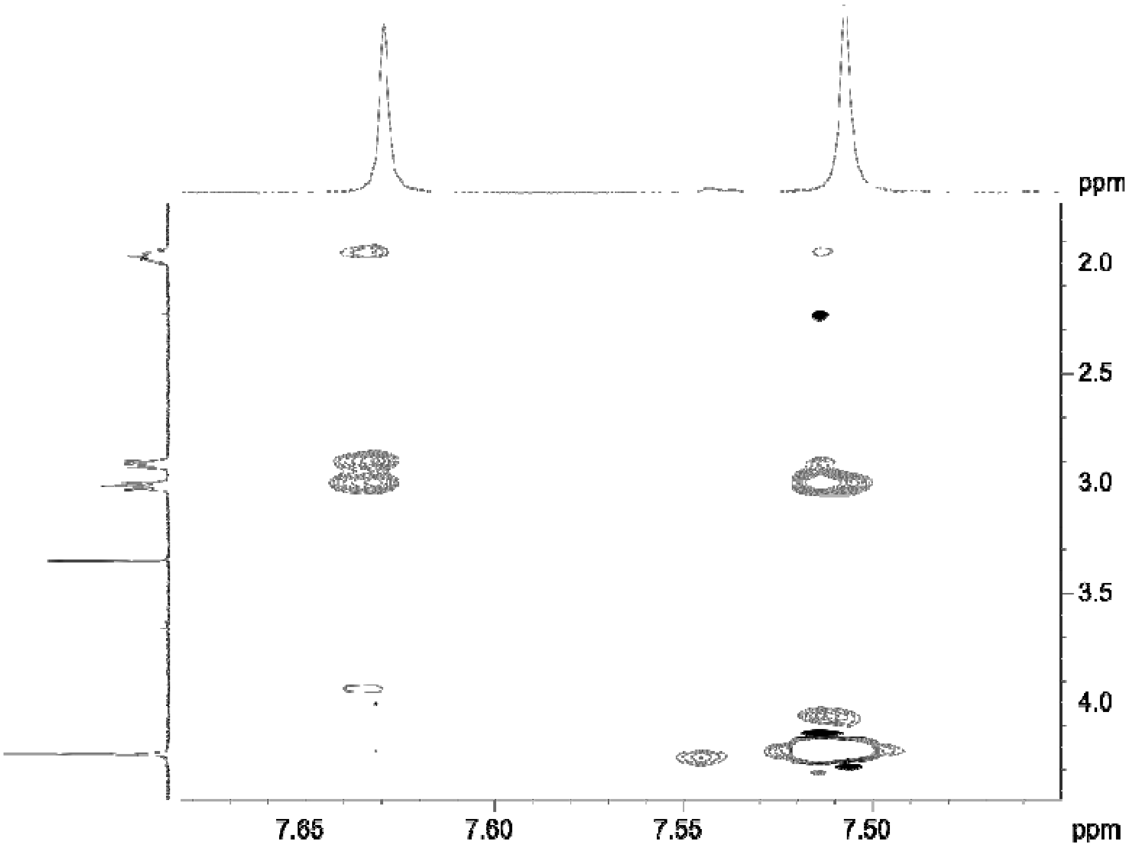

Figure A1.10. Two stick views of 25 overlayed lower energy structures (out of a total of 100) taken from 1 fs dynamic simulation. (A) **L9**-*is*, (B) **L9**-*ph*, and (C) **L9**-*te* systems.

Figure A1.10. (A)

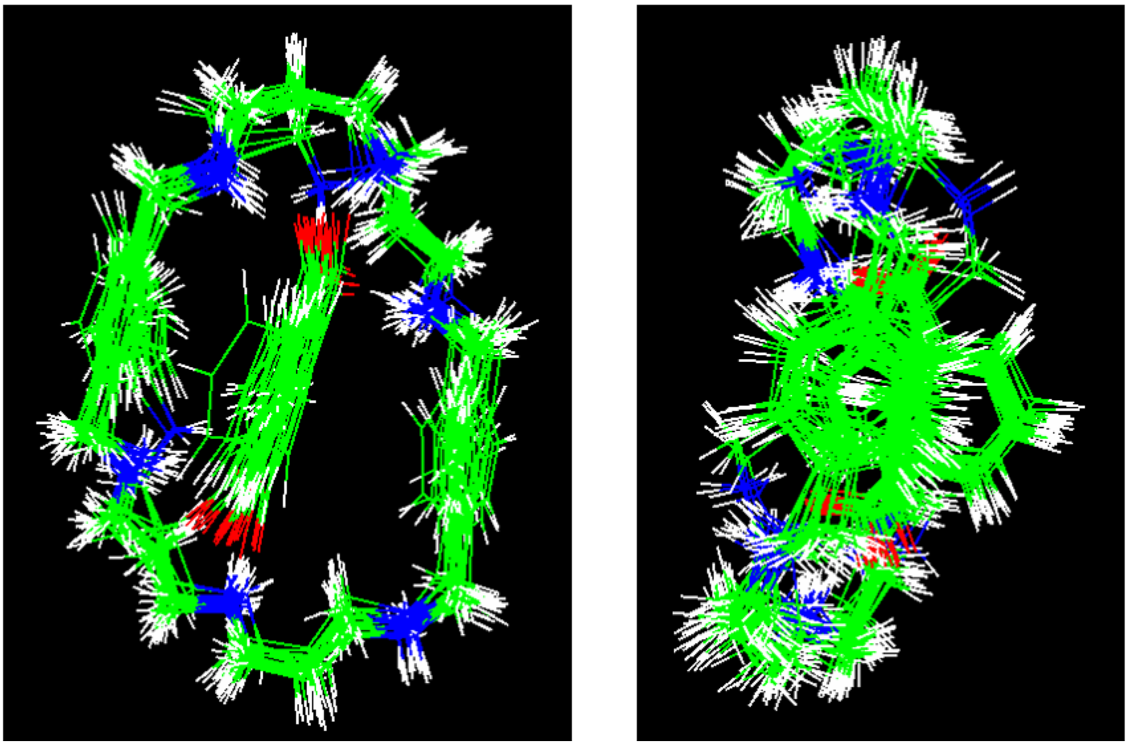

Figure A1.10. (B)

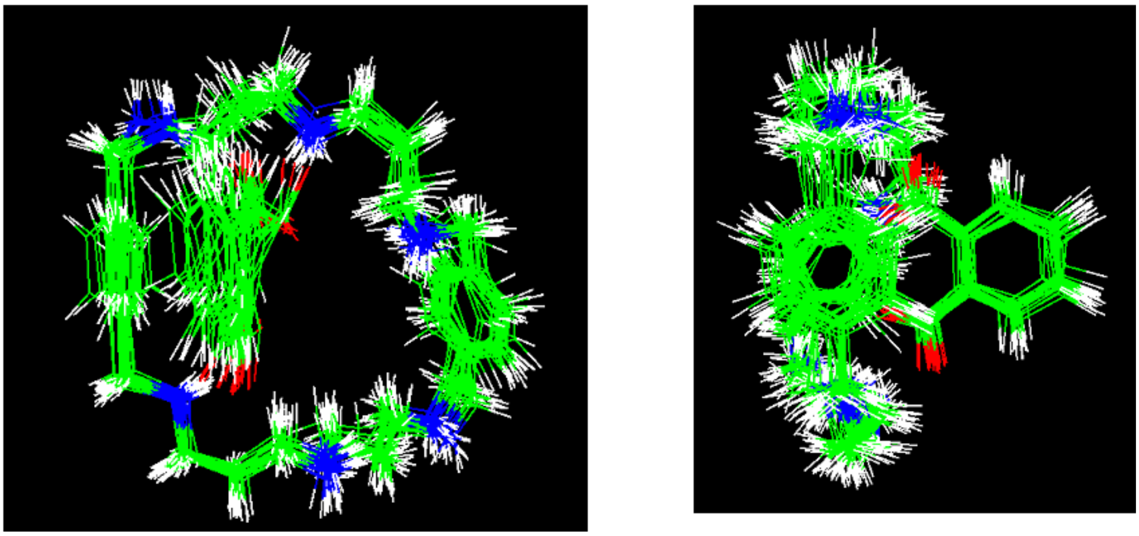

Figure A1.10. (C)

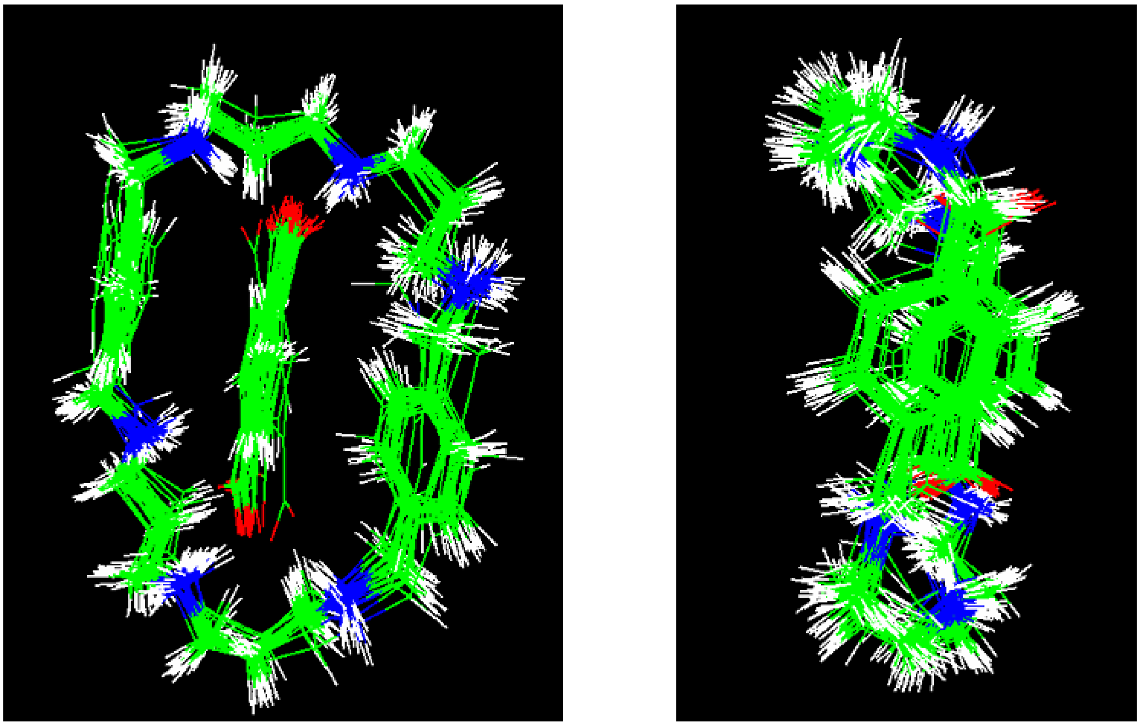

Supporting information for Chapter 4.2.

Figure A2.1. ^{1}H-NMR (400 MHz) spectra (A) and the ^{13}C-NMR (400 MHz) (B) of the compound ftNC$_2$PhOH in CDCl$_3$.

Figure A2.1. (A)

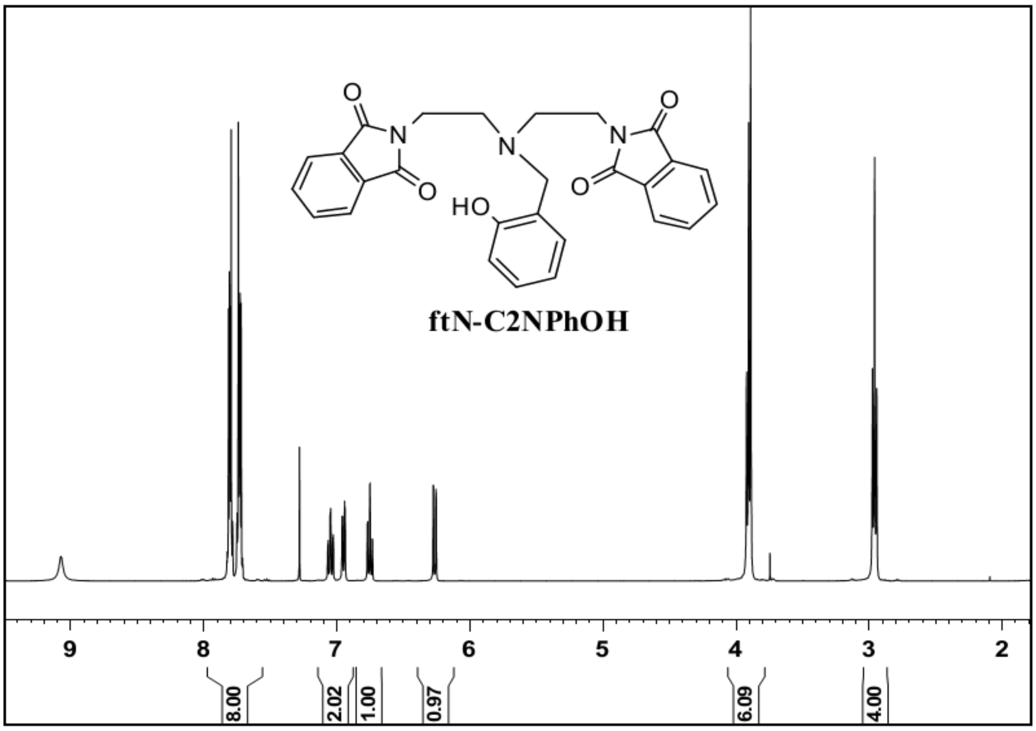

Figure A2.1. (B)

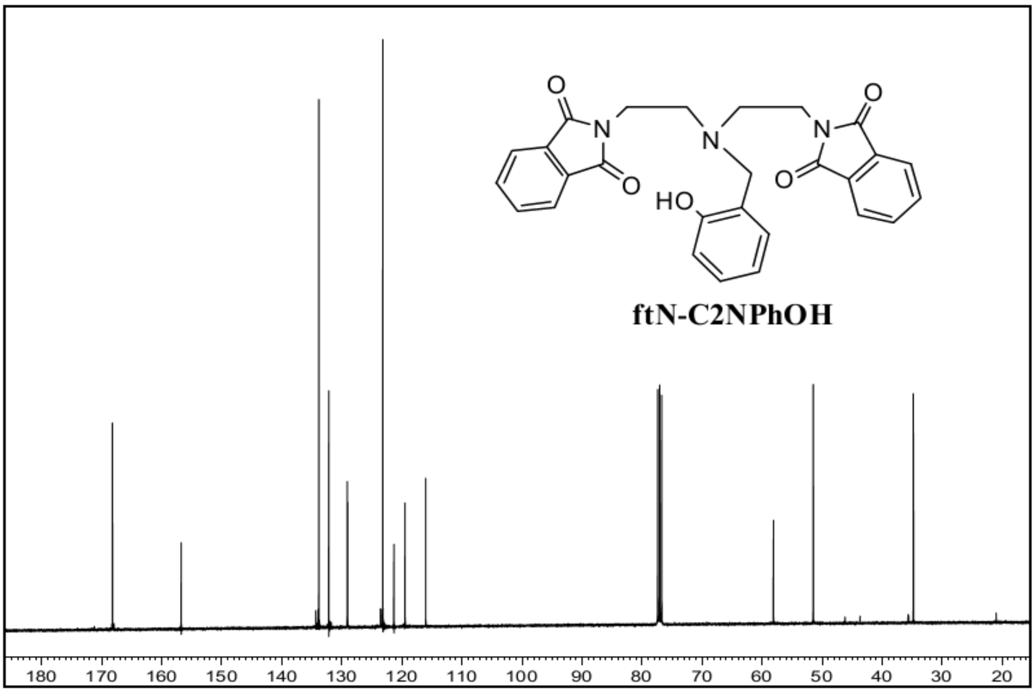

Figure A2.2. ^{1}H-NMR (400 MHz) spectra (A) and the ^{13}C-NMR (400 MHz) (B) of the compound H_2NC_2PhOH spectra in $CDCl_3$.

Figure A2.2. (A)

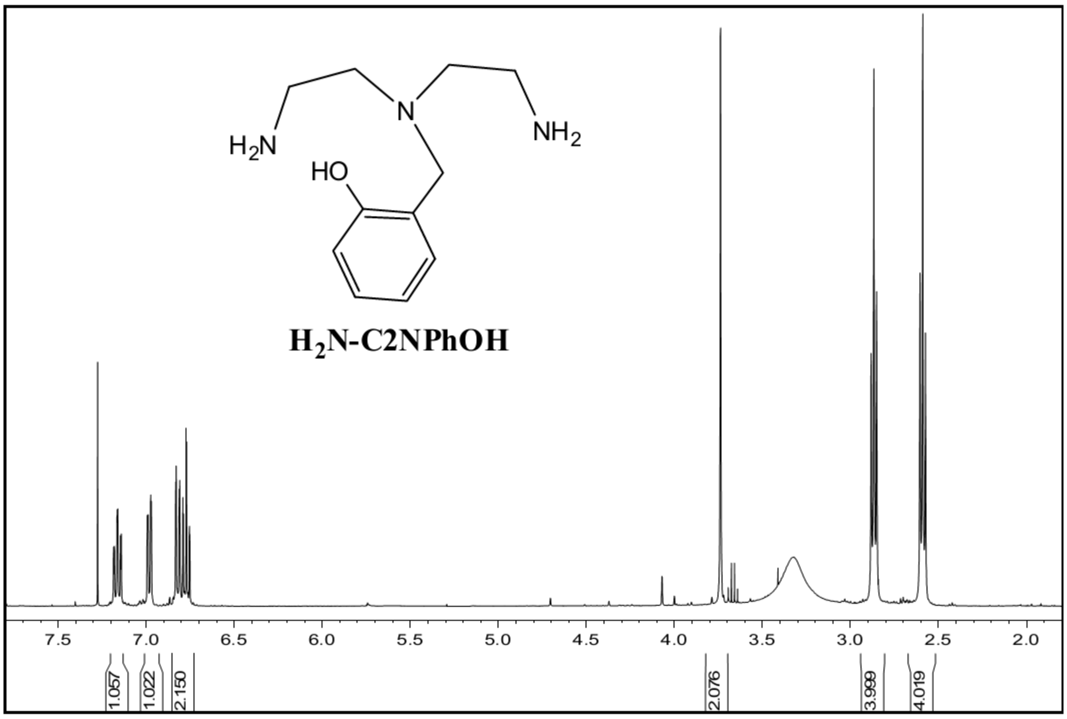

Figure A2.2. (B)

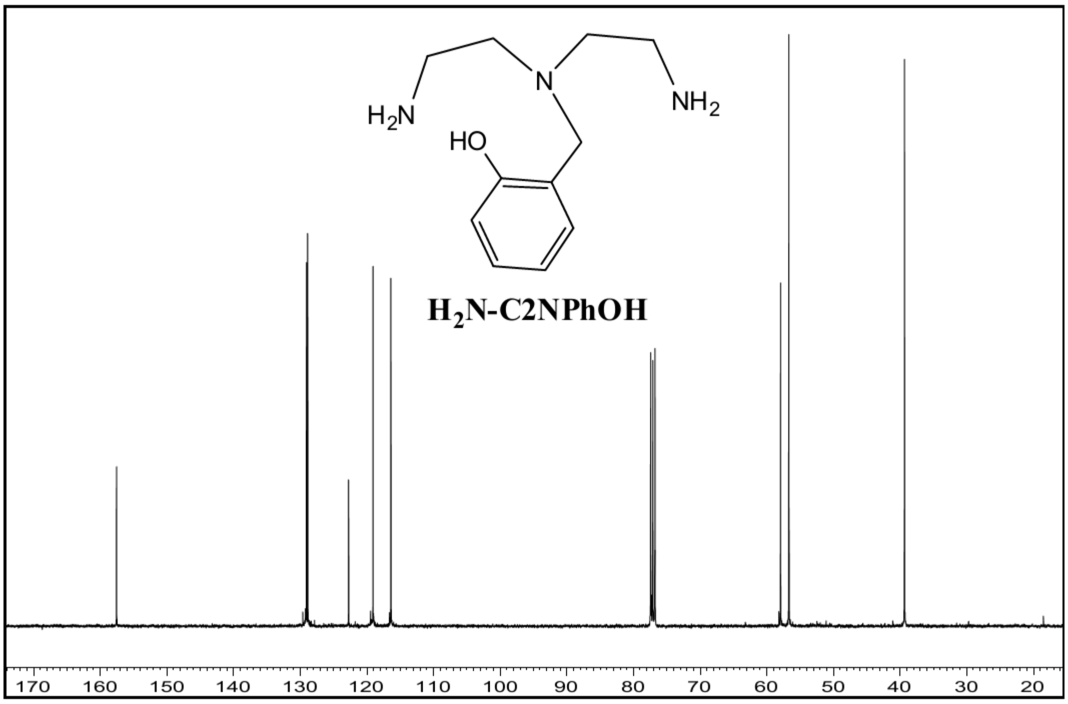

Figure A2.3. ^{1}H-NMR (400 MHz) spectra (A) and the ^{13}C-NMR (400 MHz) (B) of the compound $EtN(CH_2CN)_2$ in $CDCl_3$.

Figure A2.3. (A)

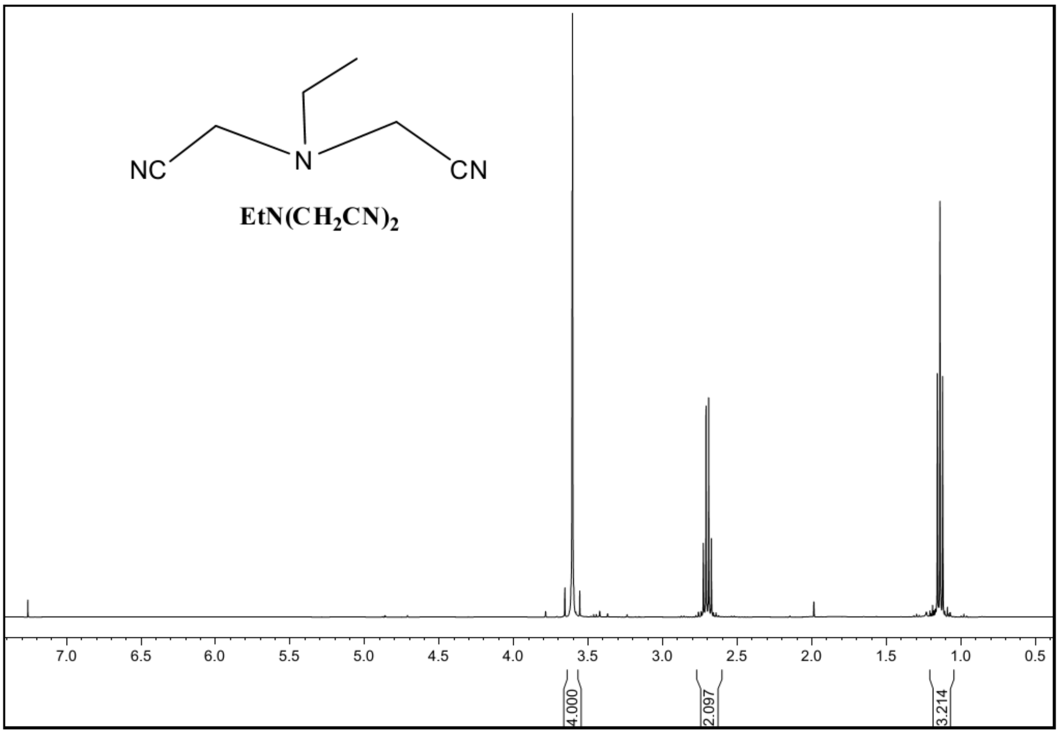

Figure A2.3. (B)

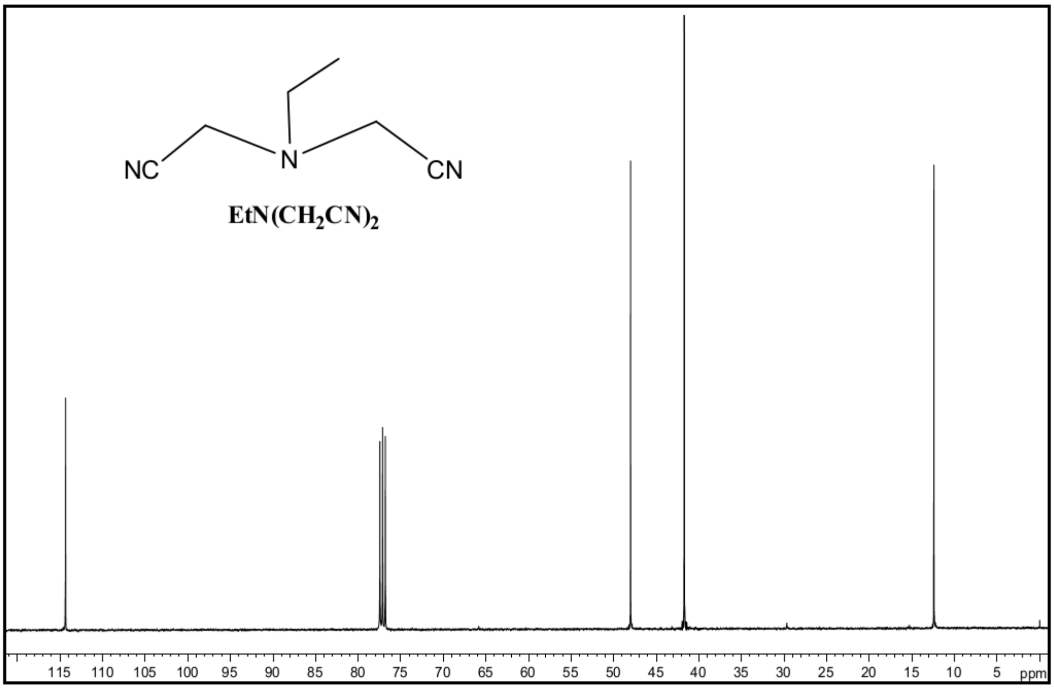

Figure A2.4. ^{1}H-NMR (400 MHz) spectra (A) and the ^{13}C-NMR (400 MHz) (B) of the compound ftNC$_2$Et in CDCl$_3$.

Figure A2.4. (A)

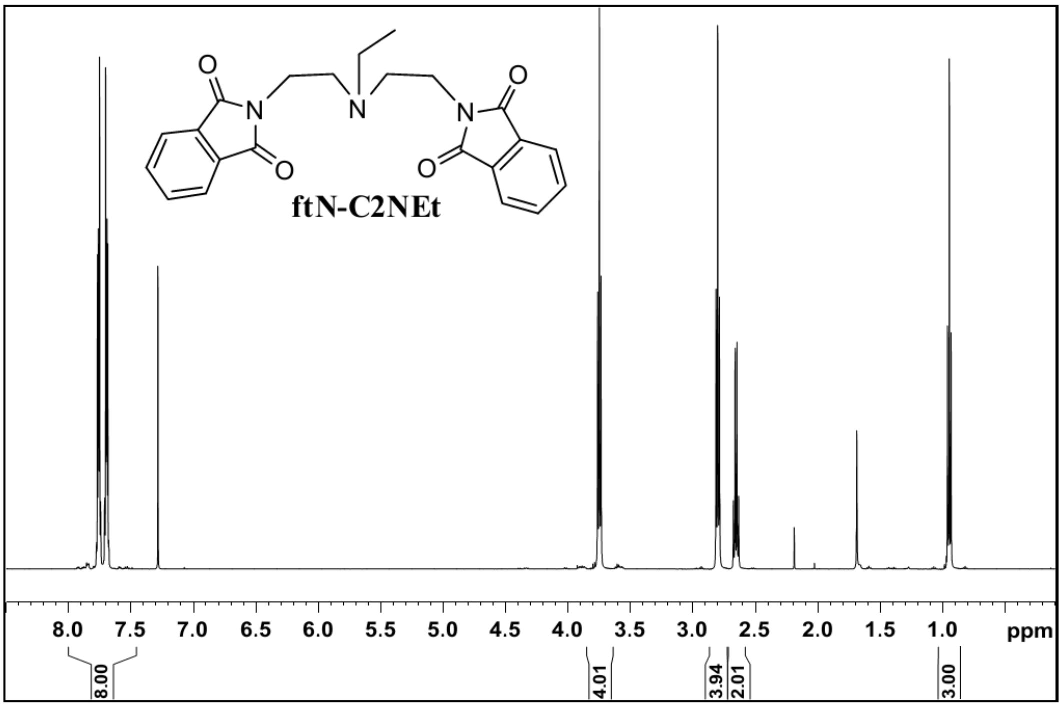

Figure A2.4. (B)

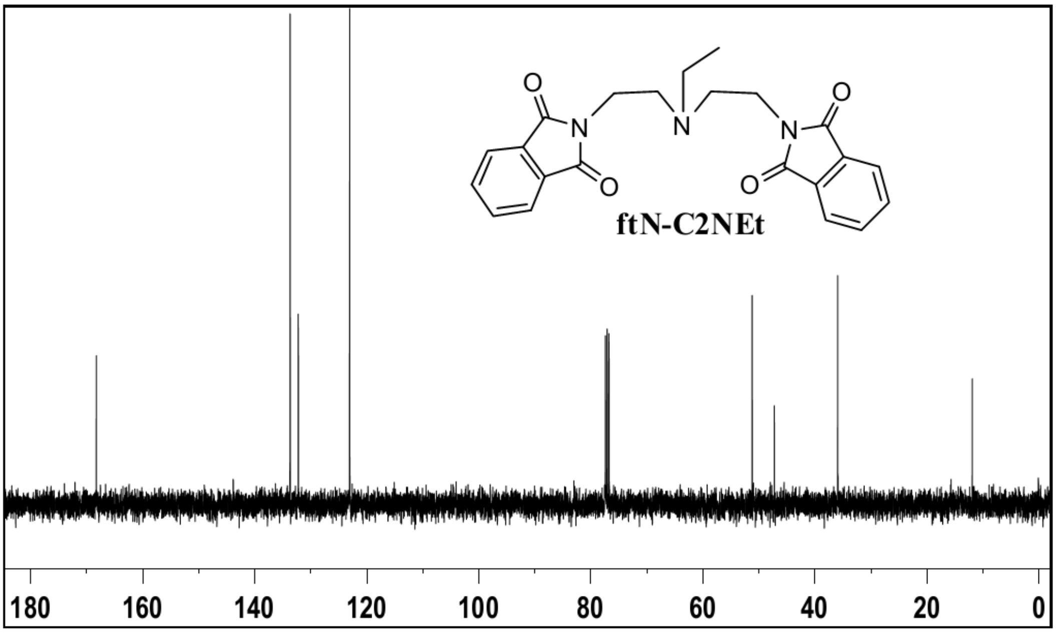

Figure A2.5. ^{1}H-NMR (400 MHz) spectra (A) and the ^{13}C-NMR (400 MHz) (B) of the compound H_2NC_2Et in $CDCl_3$.

Figure A2.5. (A)

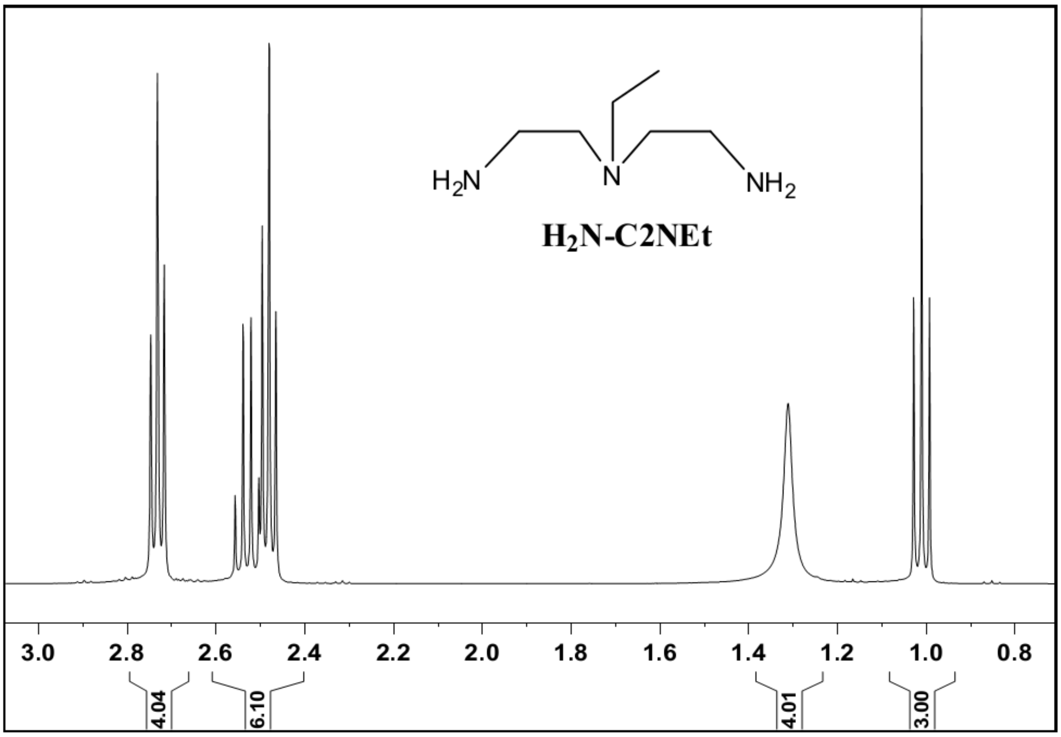

Figure A2.5. (B)

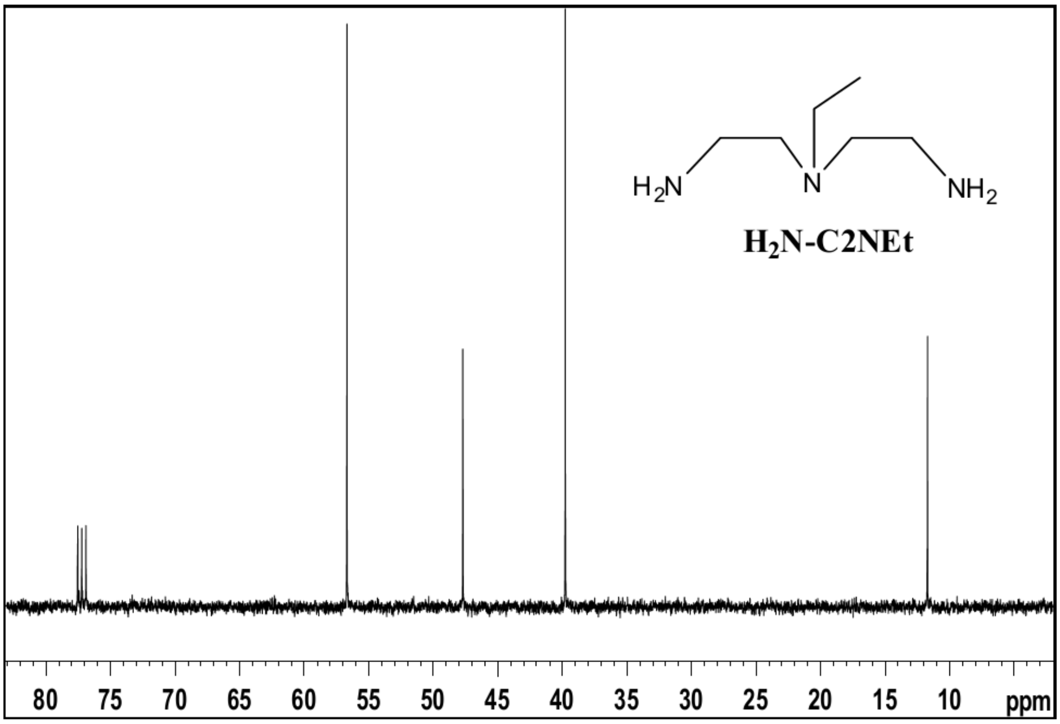

Figure A2.6. ^{1}H-NMR (400 MHz) spectra (A) and the ^{13}C-NMR (400 MHz) (B) of the compound **bsm2py** (**L73**) in $CDCl_3$.

Figure A2.6. (A)

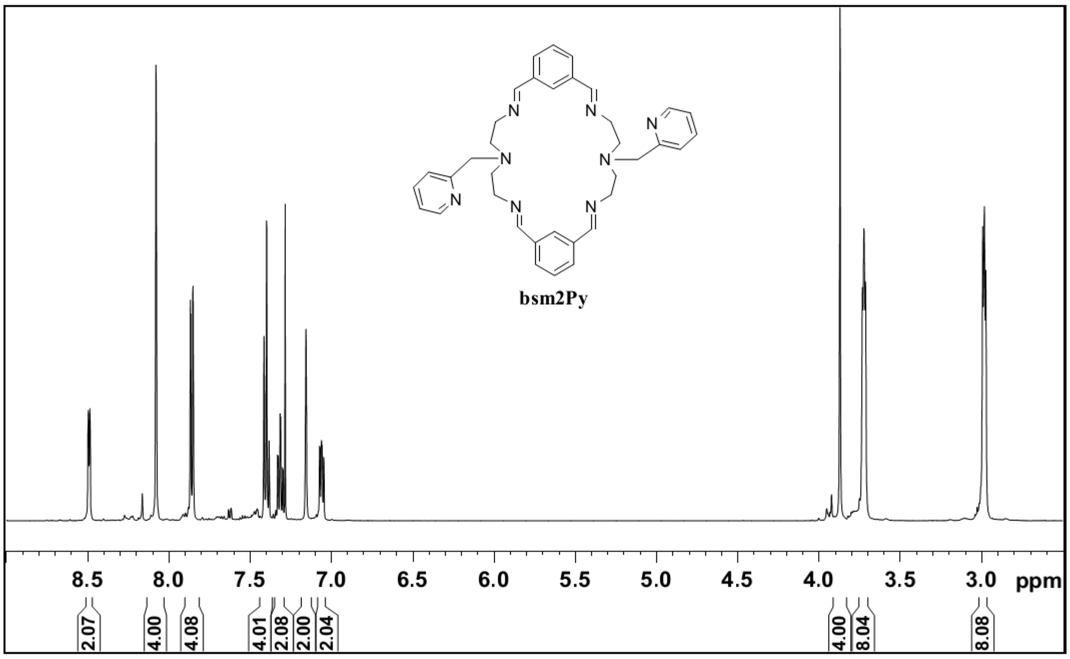

Figure A2.6. (B)

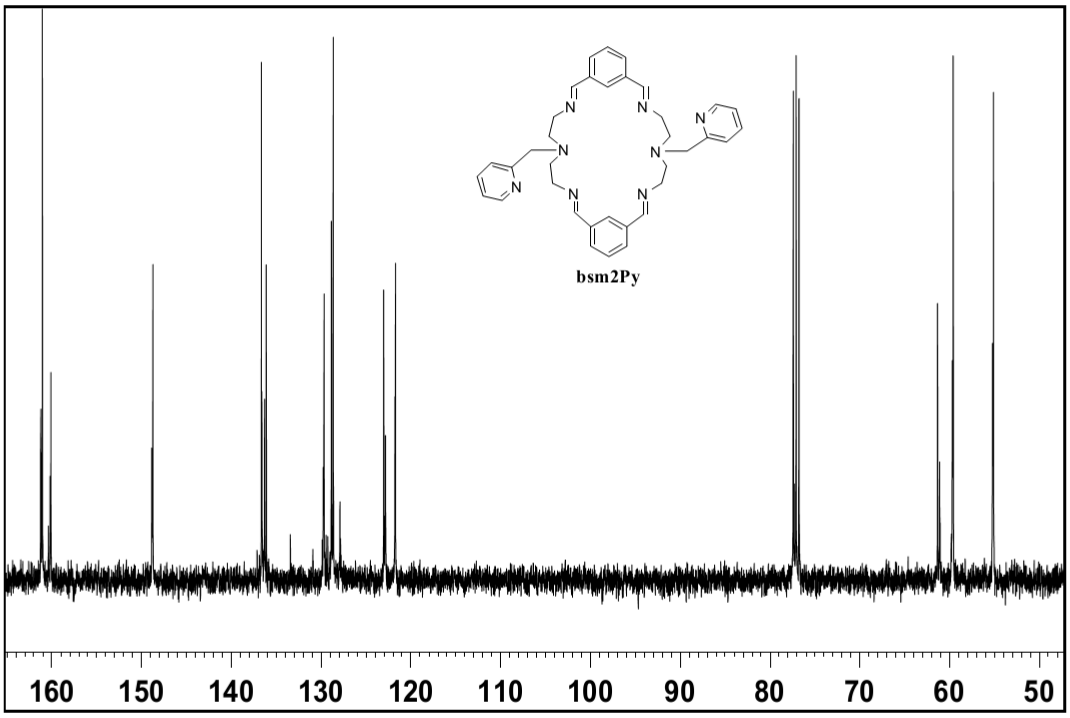

Figure A2.7. ^{1}H-NMR (400 MHz) spectra (A) and the ^{13}C-NMR (400 MHz) (B) of the compound **bsm2PhOH** (**L74**) in $CDCl_3$.

Figure A2.7. (A)

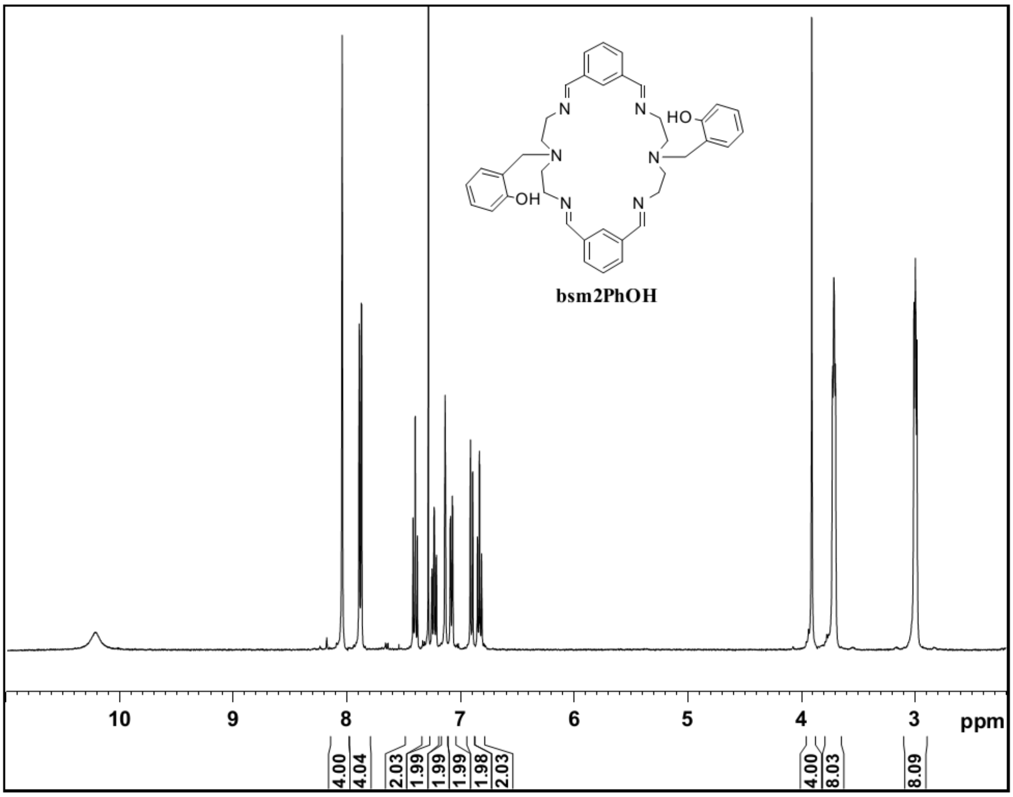

Figure A2.7. (B)

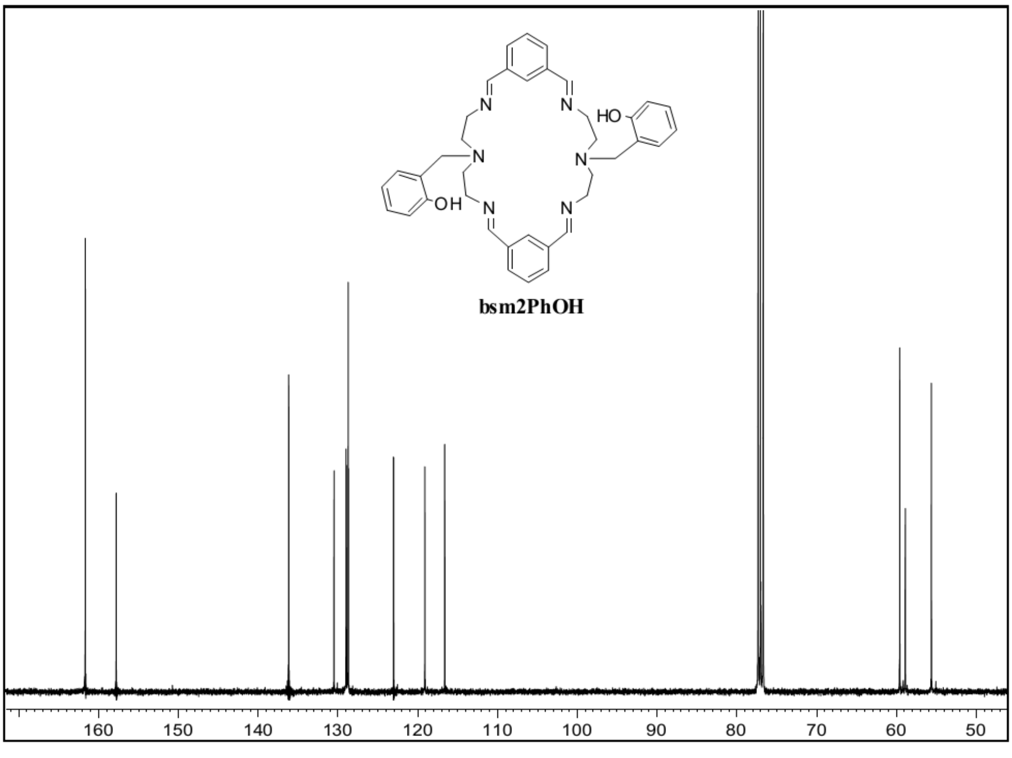

Figure A2.8. ^{1}H-NMR (400 MHz) spectra (A) and the ^{13}C-NMR (400 MHz) (B) of the compound **bsm2Et** (**L75**) in CDCl$_3$.

Figure A2.8. (A)

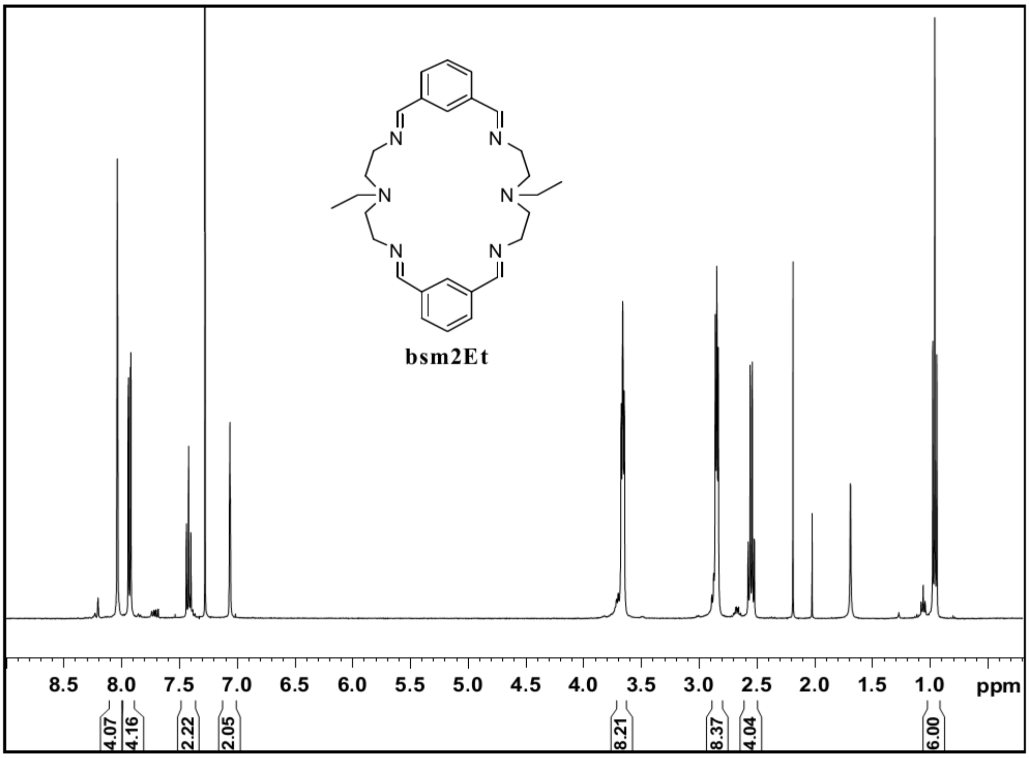

Figure A2.8. (B)

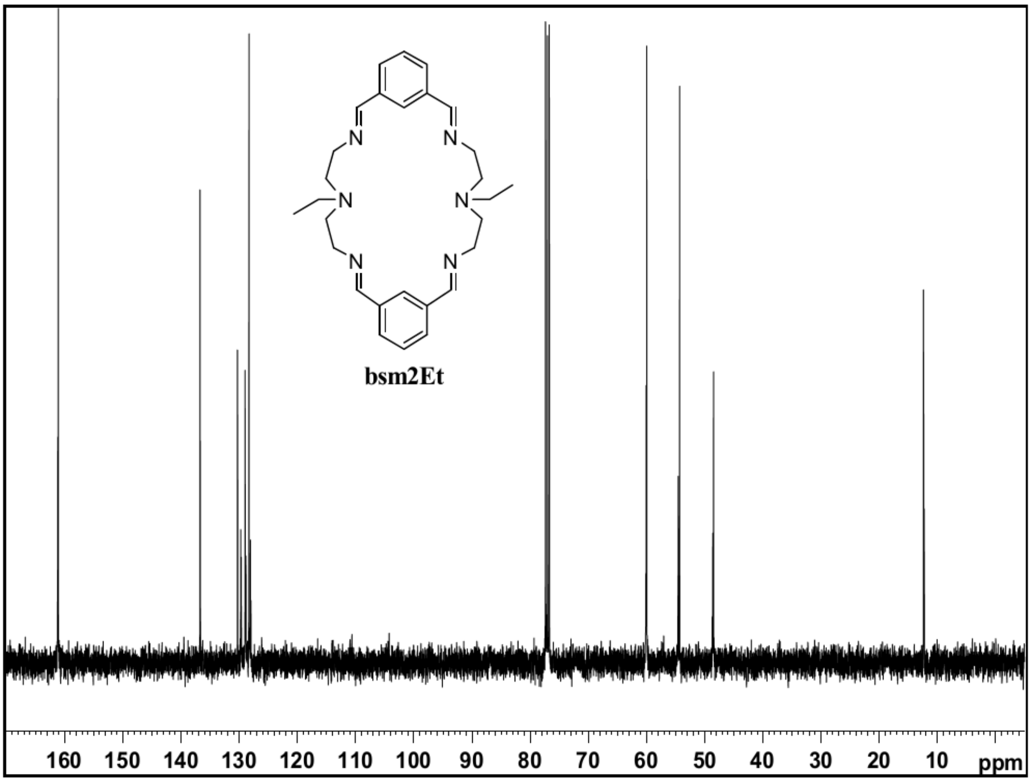

Figure A2.9. HRMS of the compound **bsm2py** (**L73**).

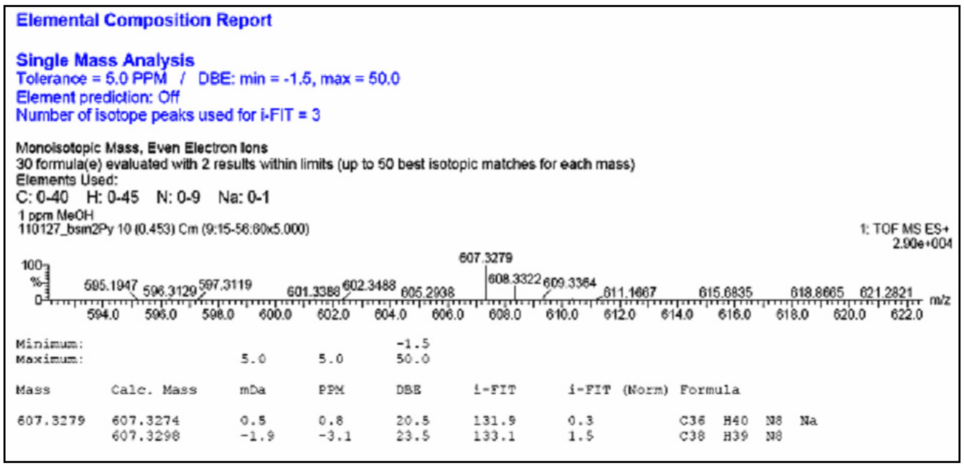

Elemental Composition Report

Single Mass Analysis
Tolerance = 5.0 PPM / DBE: min = -1.5, max = 50.0
Element prediction: Off
Number of isotope peaks used for i-FIT = 3

Monoisotopic Mass, Even Electron Ions
30 formula(e) evaluated with 2 results within limits (up to 50 best isotopic matches for each mass)
Elements Used:
C: 0-40 H: 0-45 N: 0-9 Na: 0-1
1 ppm MeOH
110127_bsm2Py 10 (0.453) Cm (9:15-56:60x5.000)
1: TOF MS ES+
2.90e+004

100
%
0
607.3279
595.1947
596.3129
597.3119
601.3388
602.3488
605.2938
608.3322
609.3364
611.1667
615.6835
618.8665
621.2821
m/z
594.0
596.0
598.0
600.0
602.0
604.0
606.0
608.0
610.0
612.0
614.0
616.0
618.0
620.0
622.0

```
Minimum:                                   -1.5
Maximum:                  5.0       5.0    50.0

Mass       Calc. Mass     mDa       PPM    DBE       i-FIT      i-FIT (Norm) Formula

607.3279   607.3274       0.5       0.8    20.5      131.9      0.3          C36  H40  N8  Na
           607.3298       -1.9      -3.1   23.5      133.1      1.5          C38  H39  N8
```

Figure A2.10. HRMS of the compound **bsm2PhOH** (**L74**).

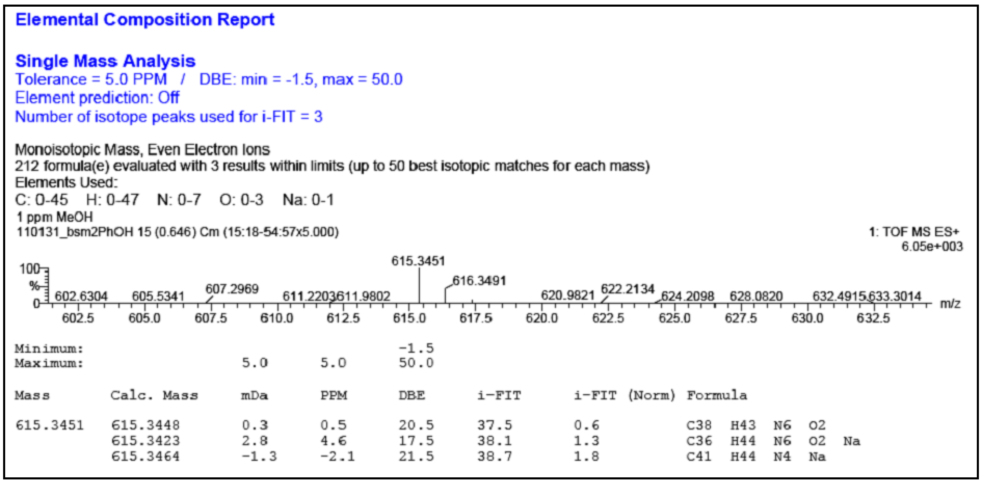

Elemental Composition Report

Single Mass Analysis
Tolerance = 5.0 PPM / DBE: min = -1.5, max = 50.0
Element prediction: Off
Number of isotope peaks used for i-FIT = 3

Monoisotopic Mass, Even Electron Ions
212 formula(e) evaluated with 3 results within limits (up to 50 best isotopic matches for each mass)
Elements Used:
C: 0-45 H: 0-47 N: 0-7 O: 0-3 Na: 0-1
1 ppm MeOH
110131_bsm2PhOH 15 (0.646) Cm (15:18-54:57x5.000)
1: TOF MS ES+
6.05e+003

100
%
0
615.3451
602.6304
605.5341
607.2969
611.2203
611.9802
616.3491
620.9821
622.2134
624.2098
628.0820
632.4915
633.3014
m/z
602.5
605.0
607.5
610.0
612.5
615.0
617.5
620.0
622.5
625.0
627.5
630.0
632.5

```
Minimum:                                   -1.5
Maximum:                  5.0       5.0    50.0

Mass       Calc. Mass     mDa       PPM    DBE       i-FIT      i-FIT (Norm) Formula

615.3451   615.3448       0.3       0.5    20.5      37.5       0.6          C38  H43  N6  O2
           615.3423       2.8       4.6    17.5      38.1       1.3          C36  H44  N6  O2  Na
           615.3464       -1.3      -2.1   21.5      38.7       1.8          C41  H44  N4  Na
```

Figure A2.11. HRMS of the compound **bsm2Et** (**L75**).

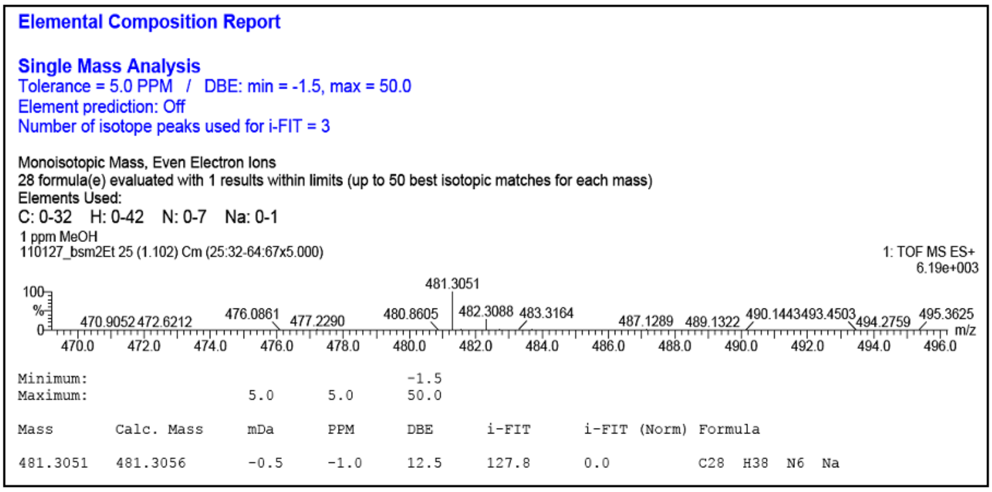

Elemental Composition Report

Single Mass Analysis
Tolerance = 5.0 PPM / DBE: min = -1.5, max = 50.0
Element prediction: Off
Number of isotope peaks used for i-FIT = 3

Monoisotopic Mass, Even Electron Ions
28 formula(e) evaluated with 1 results within limits (up to 50 best isotopic matches for each mass)
Elements Used:
C: 0-32 H: 0-42 N: 0-7 Na: 0-1
1 ppm MeOH
110127_bsm2Et 25 (1.102) Cm (25:32-64:67x5.000)
1: TOF MS ES+
6.19e+003

100
%
0
481.3051
470.9052
472.6212
476.0861
477.2290
480.8605
482.3088
483.3164
487.1289
489.1322
490.1443
493.4503
494.2759
495.3625
m/z
470.0
472.0
474.0
476.0
478.0
480.0
482.0
484.0
486.0
488.0
490.0
492.0
494.0
496.0

```
Minimum:                                   -1.5
Maximum:                  5.0       5.0    50.0

Mass       Calc. Mass     mDa       PPM    DBE       i-FIT      i-FIT (Norm) Formula

481.3051   481.3056       -0.5      -1.0   12.5      127.8      0.0          C28  H38  N6  Na
```

Figure A2.12. ^{1}H-NMR (400 MHz) spectra in CD_3COCD_3 of the complex [Cu_2(**L73**)]$(SbF_6)_2$, **1**$(SbF_6)_2$ and [Cu_3(**L76**)]$(SbF_6)_3$, **4**(SbF6)$_3$.

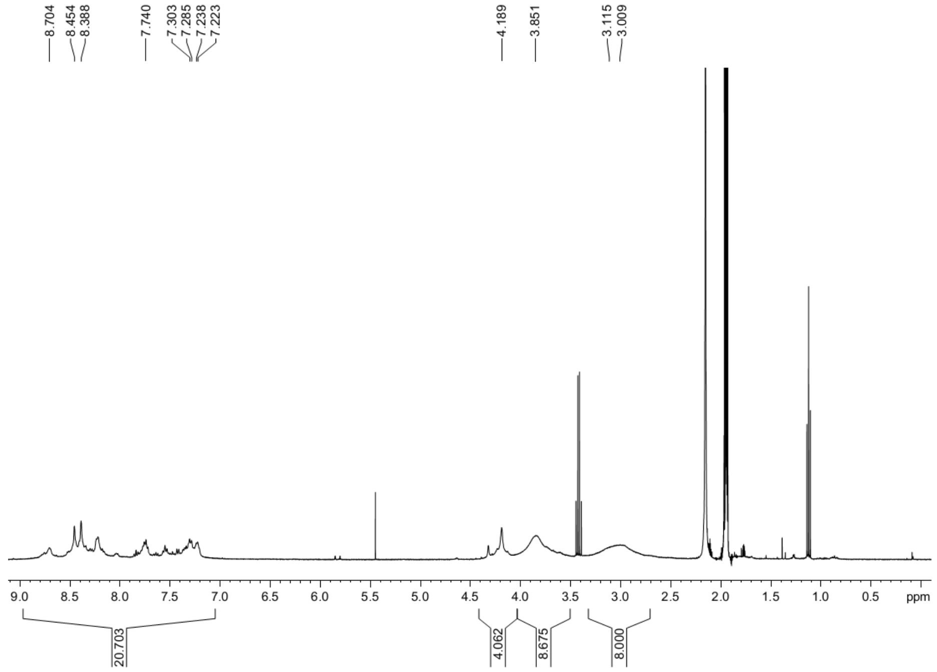

Figure A2.13. ^{1}H-NMR (400 MHz) spectra in CD_3COCD_3 of the complex [Cu_2(**L74**)]$(OTf)_2$, **2**$(OTf)_2$ and [Cu_3(**L77**)]$(OTf)_3$, **5**$(OTf)_3$.

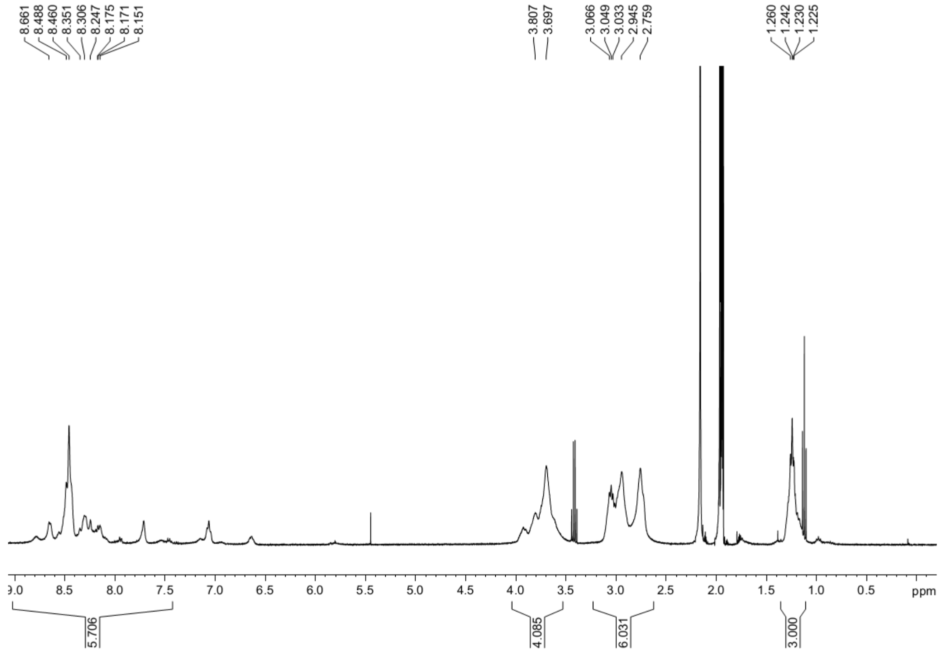

Figure A2.14. ^{1}H-NMR (400 MHz) spectra in CD_3COCD_3 of the complex [Cu$_3$(**L78**)](OTf)$_3$, **6**(OTf)$_3$.

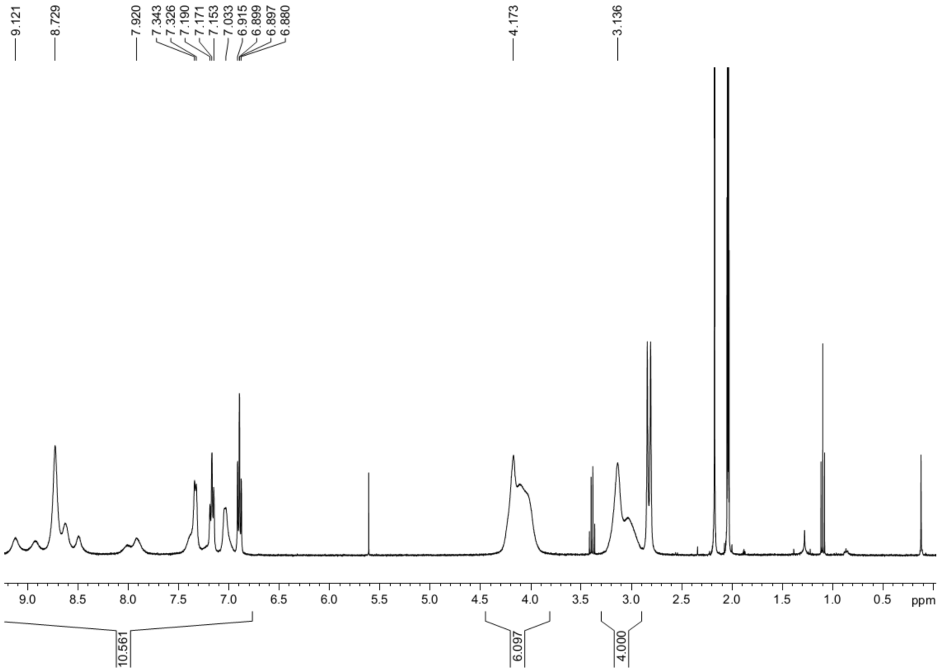

Supporting information for Chapter 4.3.

Figure A3.1. ^{1}H-NMR (200 MHz) spectra in $CDCl_3$ (A) and FT-IR spectra (B) of the compound $ftNC_3H$.

Figure A3.1. (A)

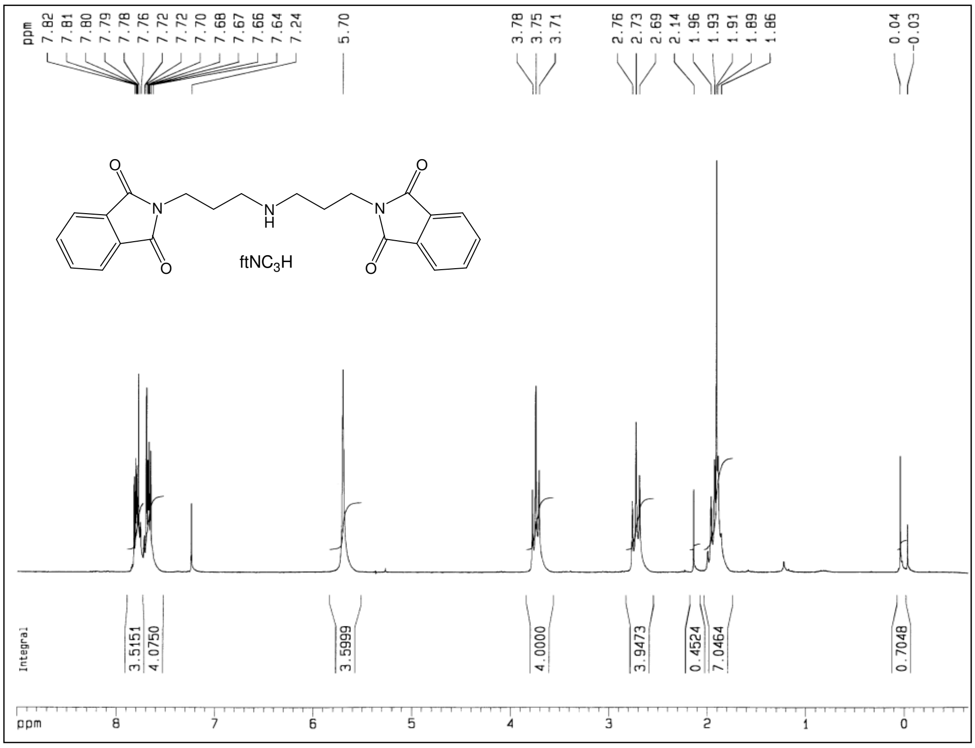

Figure A3.1. (B)

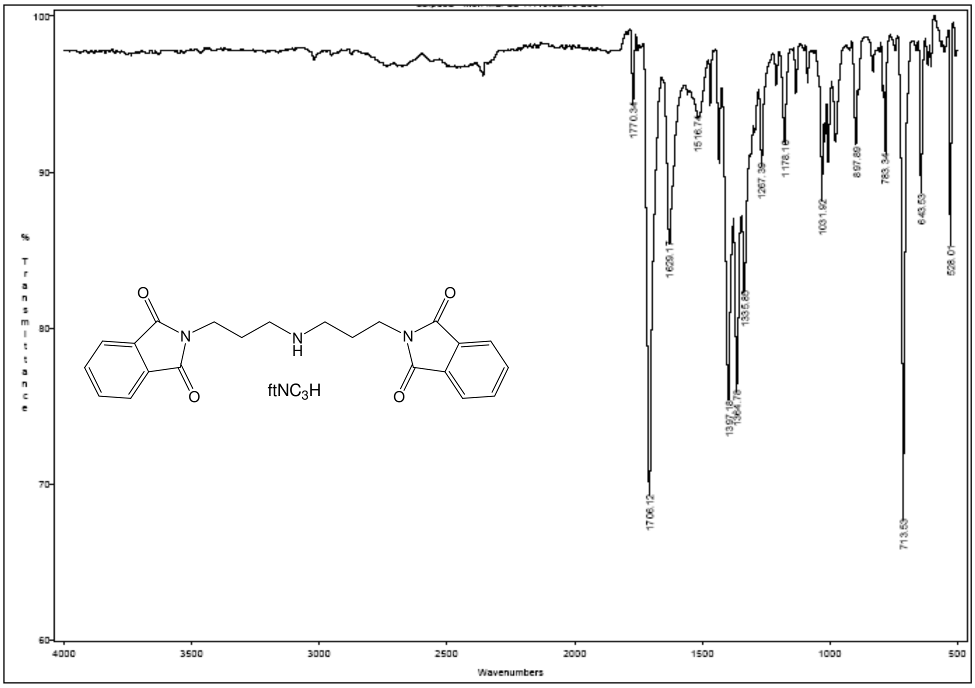

Figure A3.2. ^{1}H-NMR (200 MHz) spectra in $CDCl_3$ (A) and FT-IR spectra (B) of the compound ftNC$_3$py.

Figure A3.2. (A)

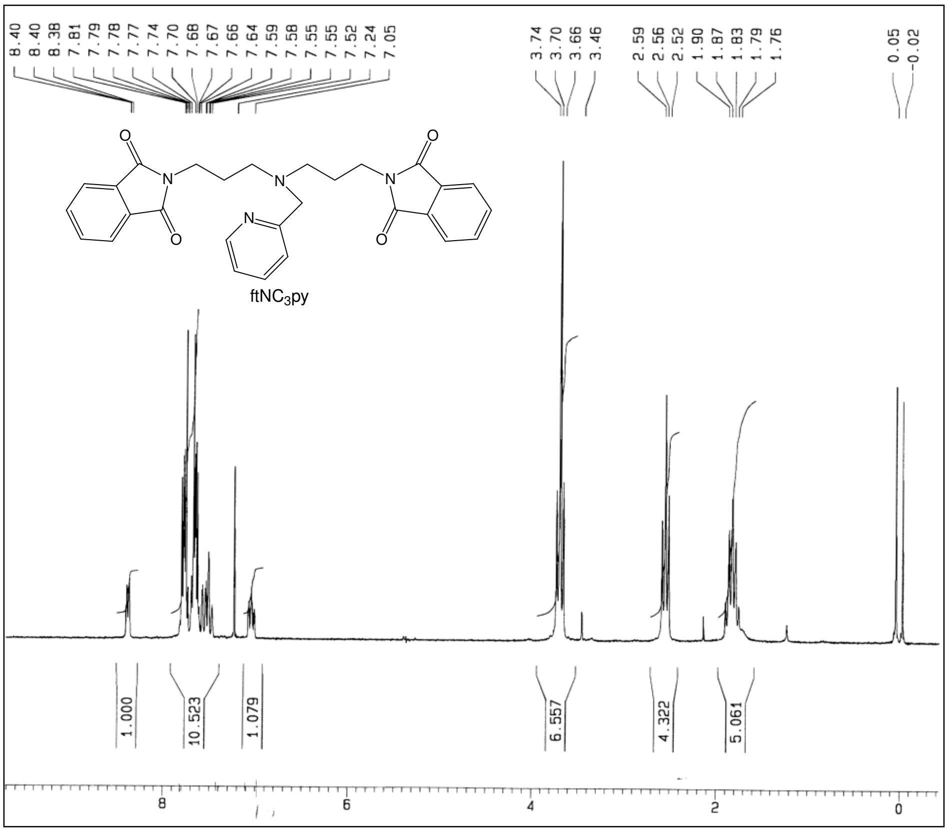

Figure A3.2. (B)

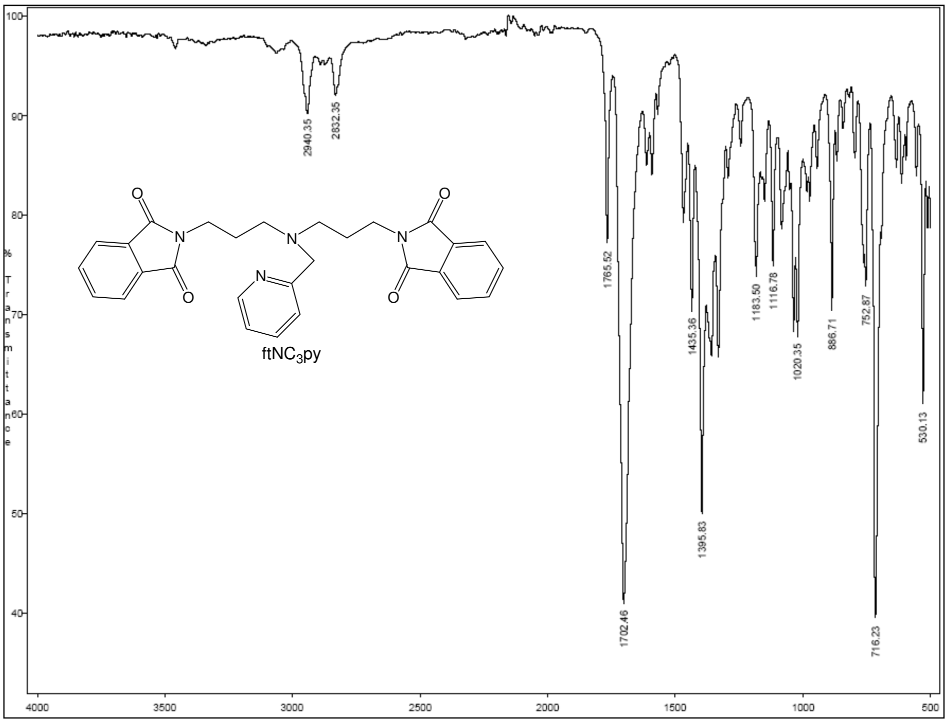

Figure A3.3. ^{1}H-NMR (200 MHz) spectra in $CDCl_3$ (A) and FT-IR spectra (B) of the compound H_2NC_3py.

Figure A3.3. (A)

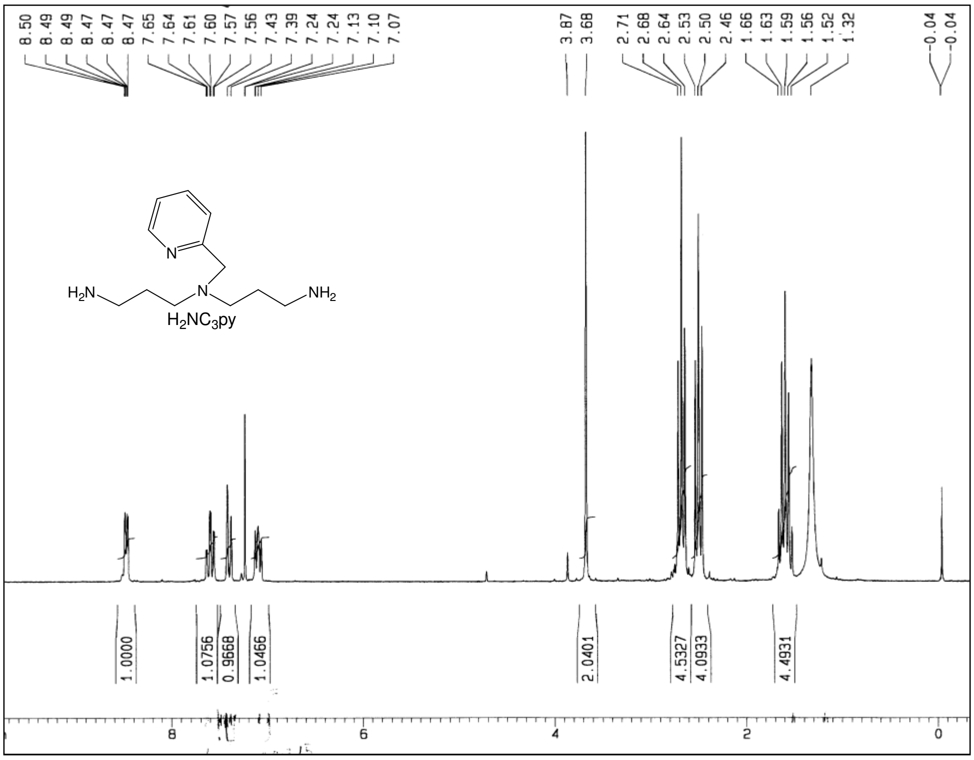

Figure A3.3. (B)

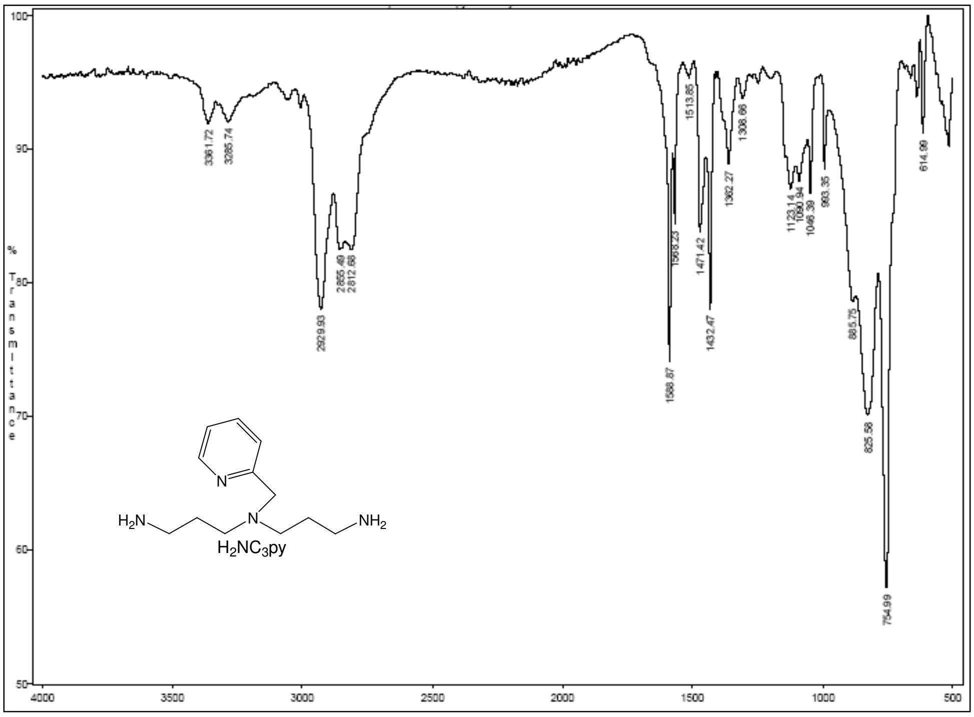

Figure A3.4. ^{1}H-NMR (200 MHz) spectra in $CDCl_3$ (A) and FT-IR spectra (B) of the compound ftNC$_2$H.

Figure A3.4. (A)

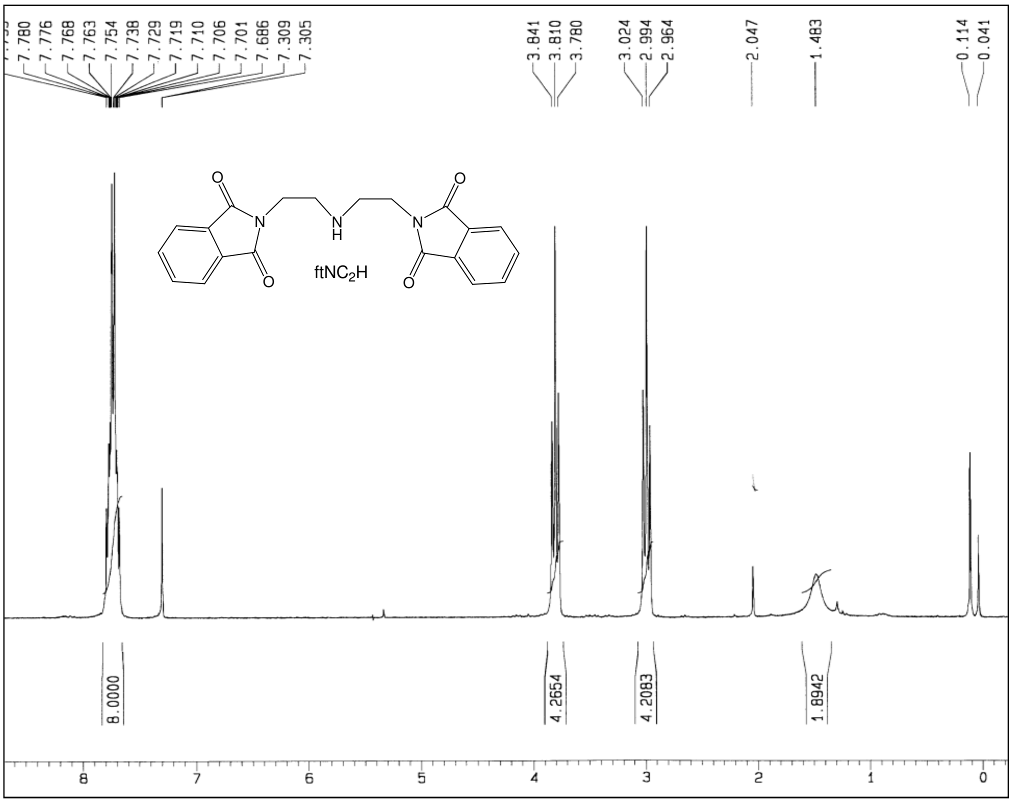

Figure A3.4. (B)

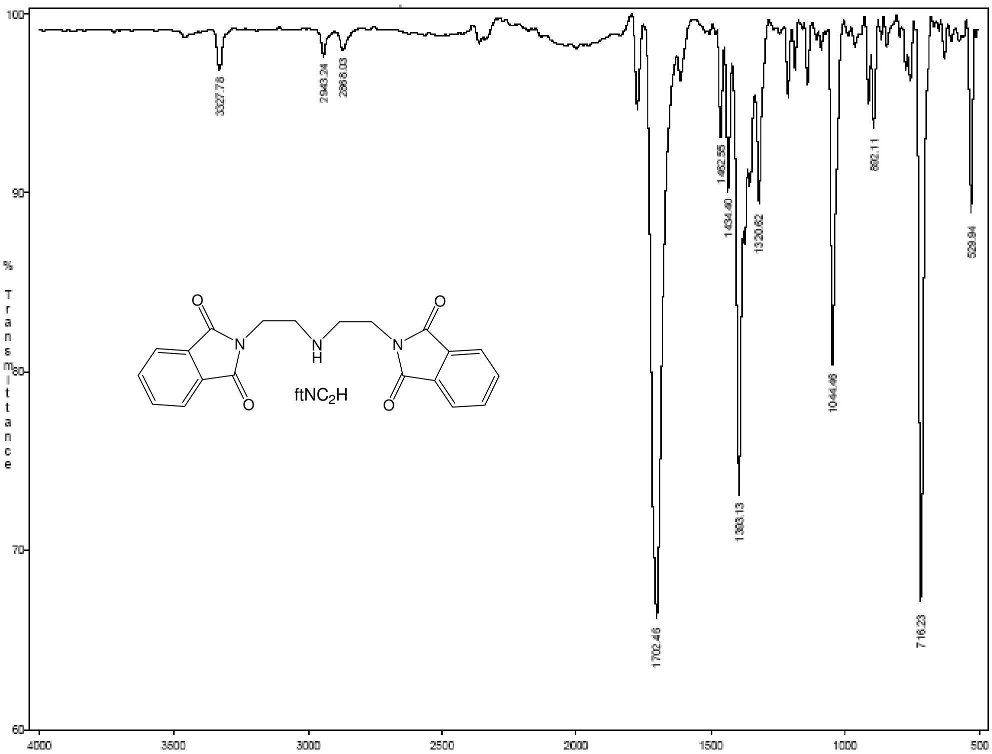

Figure A3.5. ^{1}H-NMR (200 MHz) spectra in $CDCl_3$ (A) and FT-IR spectra (B) of the compound ftNC$_2$py.

Figure A3.5. (A)

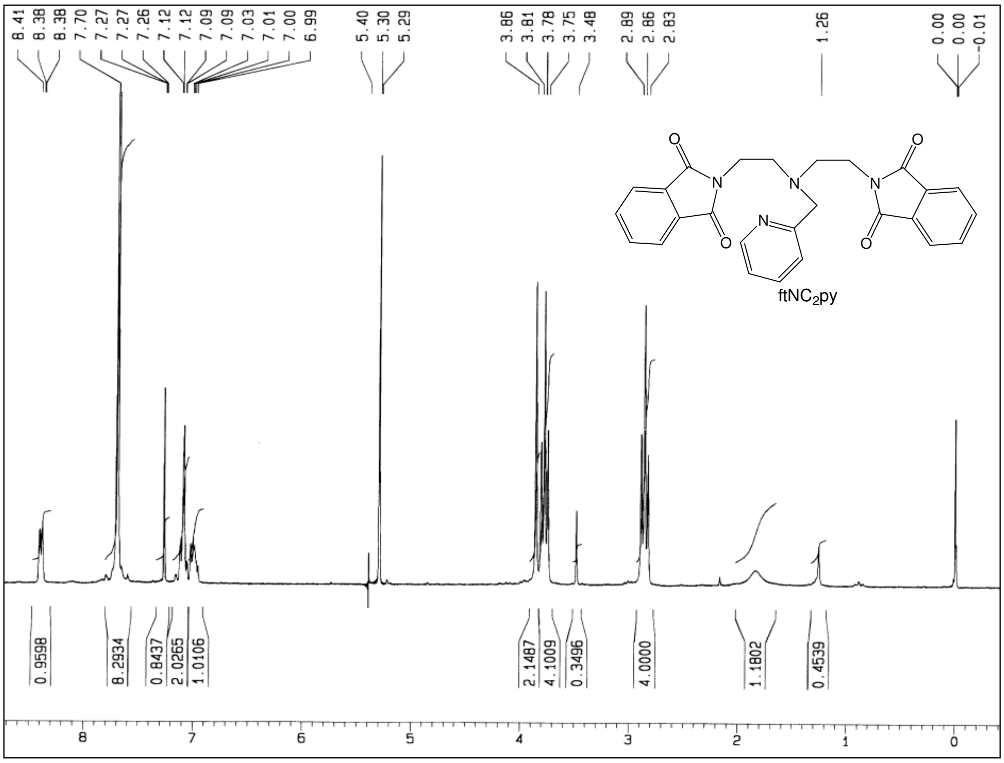

Figure A3.5. (B)

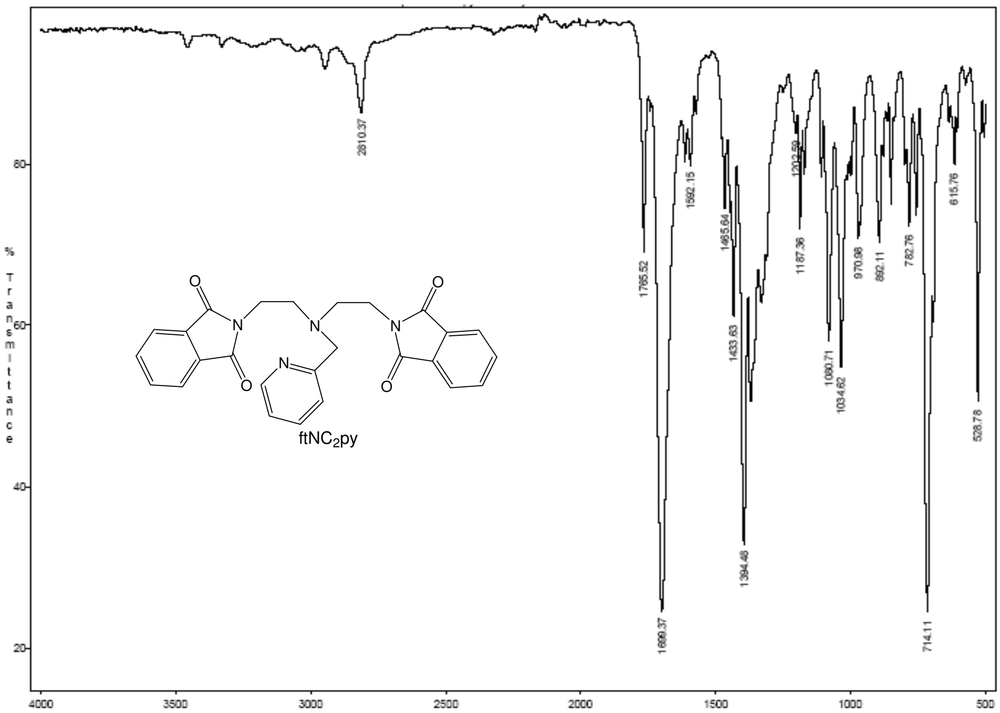

Figure A3.6. ^{1}H-NMR (200 MHz) spectra in $CDCl_3$ (A) and FT-IR spectra (B) of the compound H_2NC_2py.

Figure A3.6. (A)

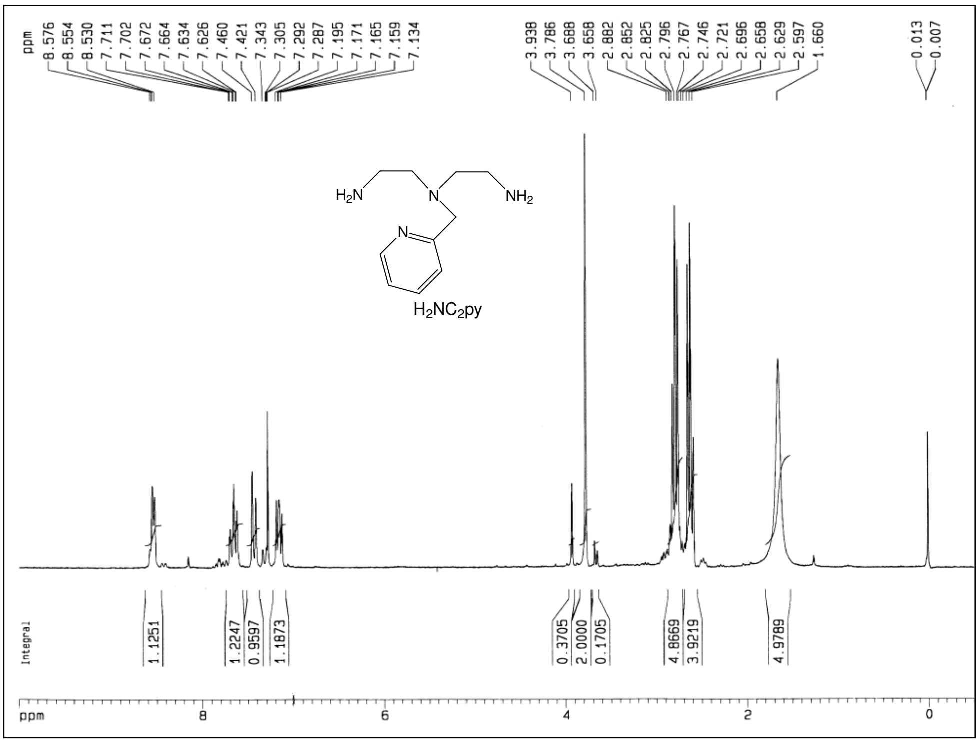

Figure A3.6. (B)

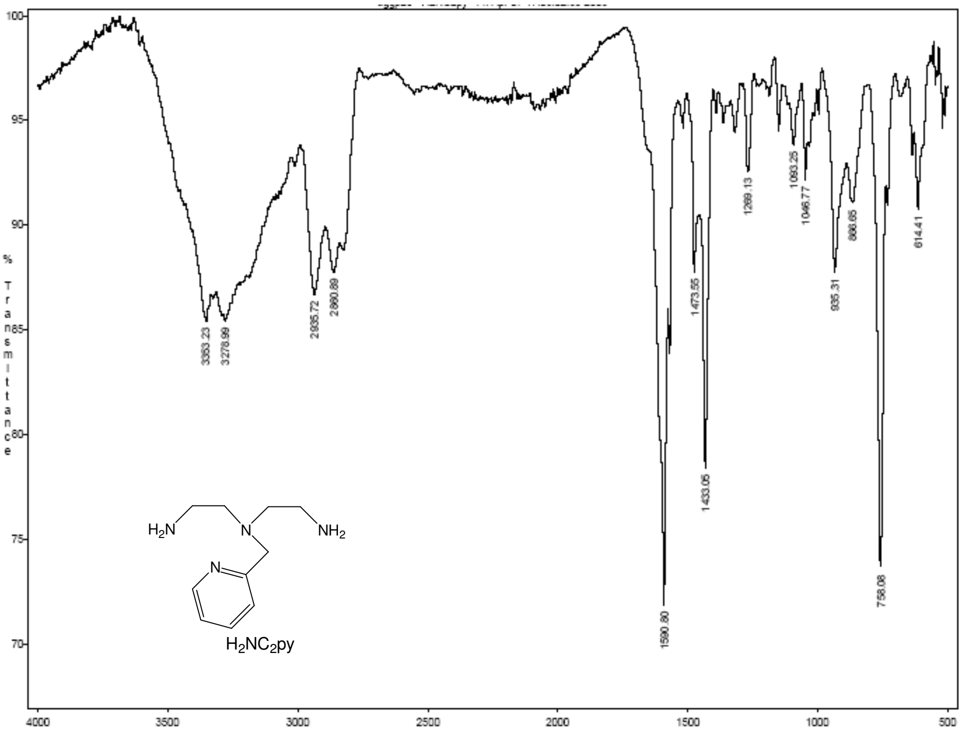

Figure A3.7. ^{1}H-NMR (200 MHz) spectra in $CDCl_3$ FT-IR spectra (B) and ESI-MS spectra (C) of the compound **bsp3py** (**L79**).

Figure A3.7. (A)

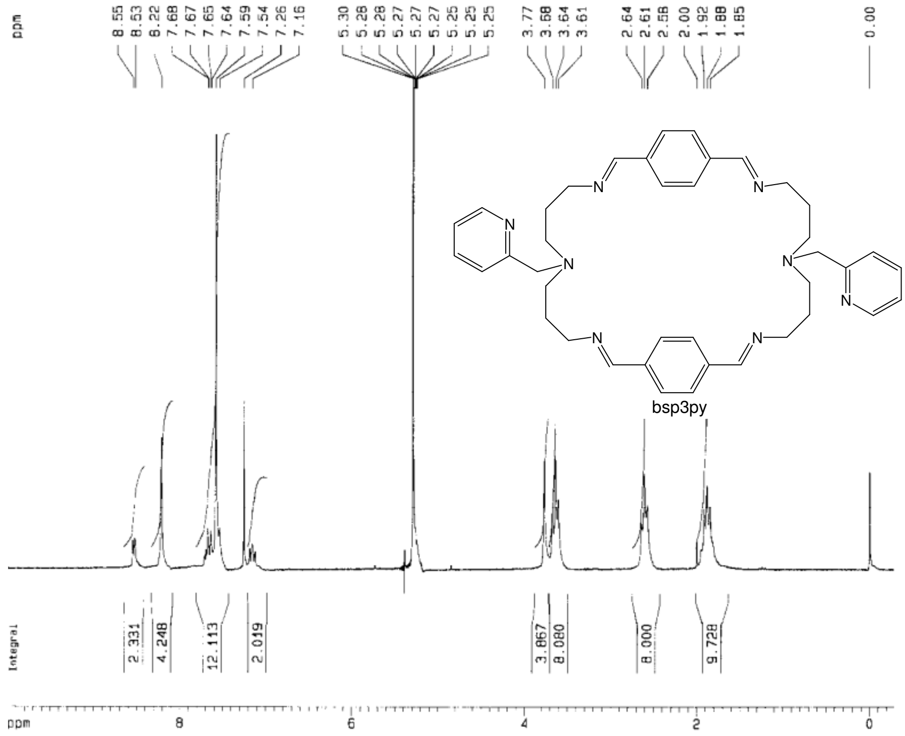

Figure A3.7. (B)

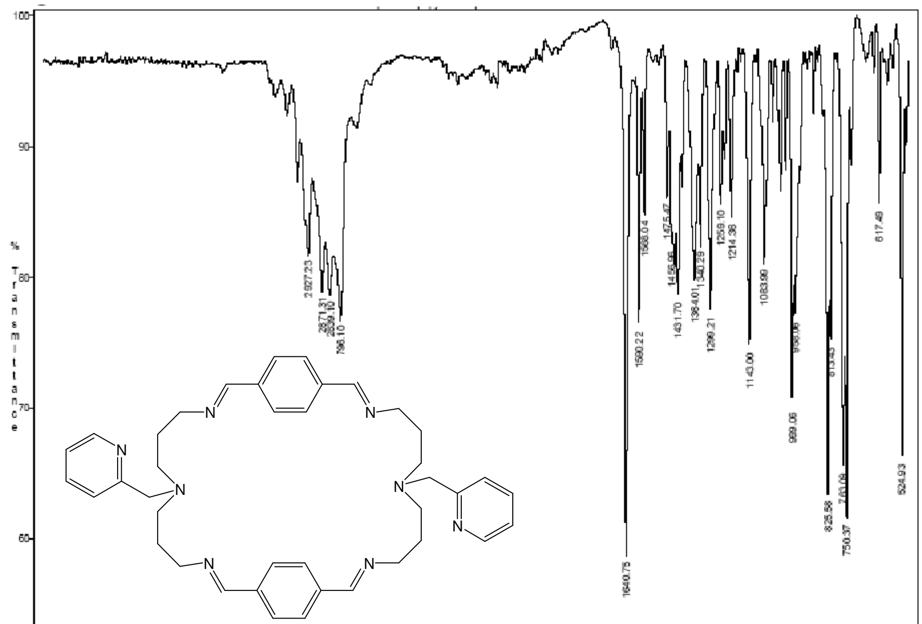

Figure A3.7. (C)

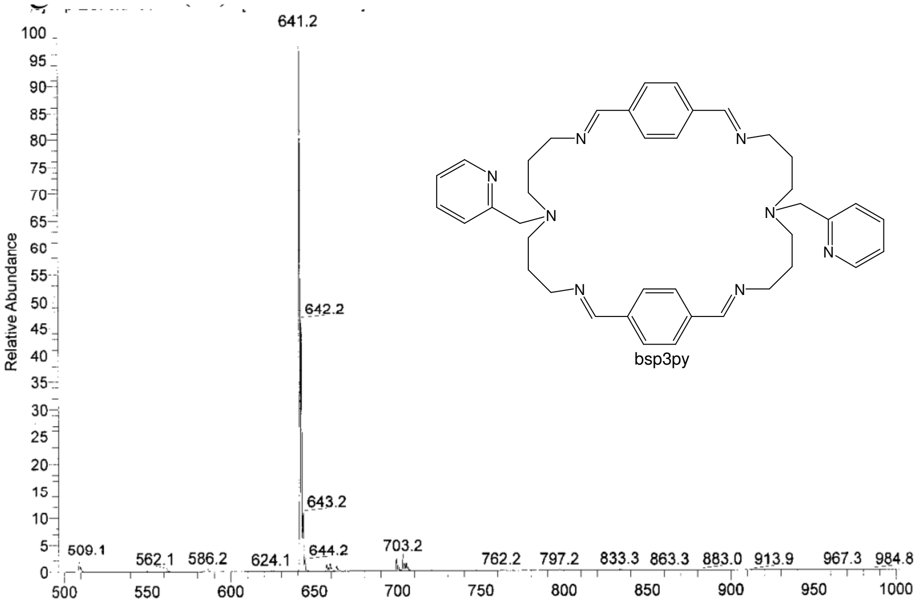
641.2
642.2
643.2
509.1
562.1
586.2
624.1
644.2
703.2
762.2
797.2
833.3
863.3
883.0
913.9
967.3
984.8
Relative Abundance
0
5
10
15
20
25
30
35
40
45
50
55
60
65
70
75
80
85
90
95
100
500
550
600
650
700
750
800
850
900
950
1000
N
bsp3py

Figure A3.8. ^{1}H-NMR (200 MHz) spectra in $CDCl_3$ FT-IR spectra (B) and ESI-MS spectra (C) of the compound **bsm3py** (**L80**).

Figure A3.8. (A)

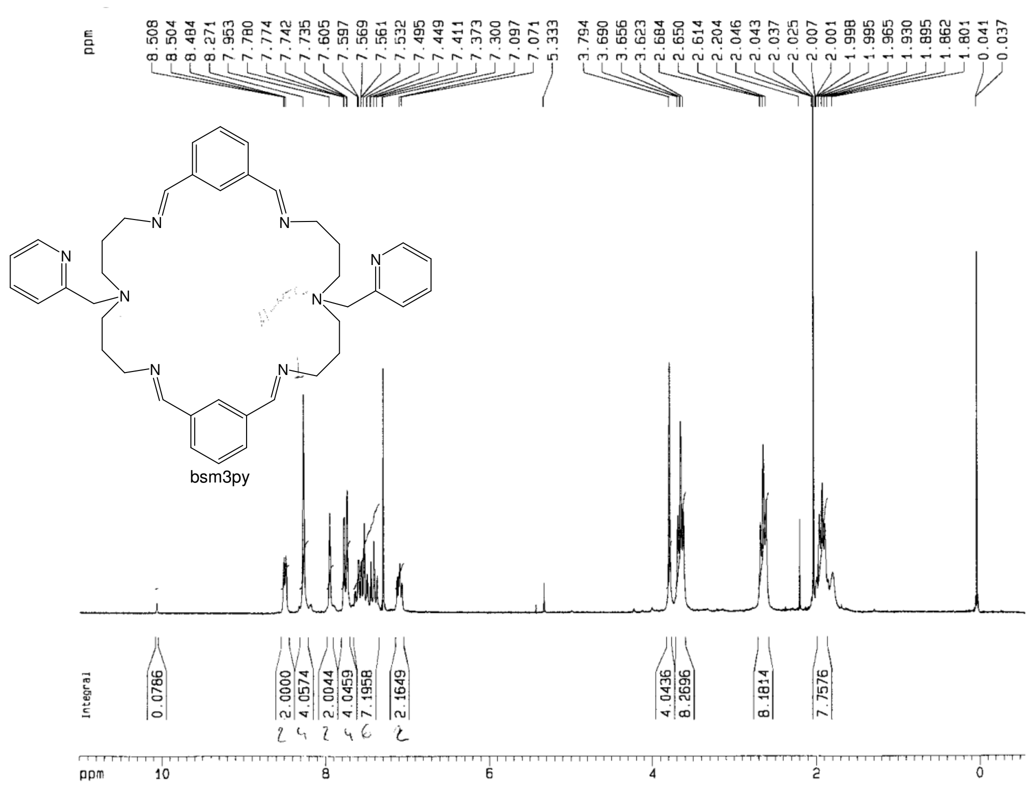

Figure A3.8. (B)

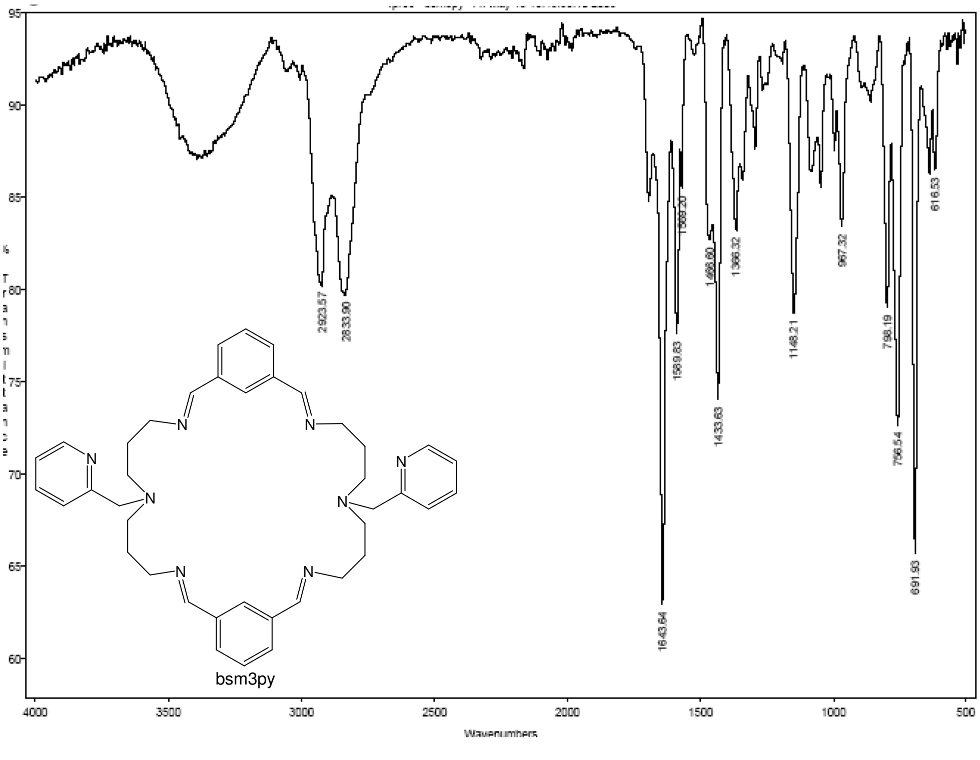

Figure A3.8. (C)

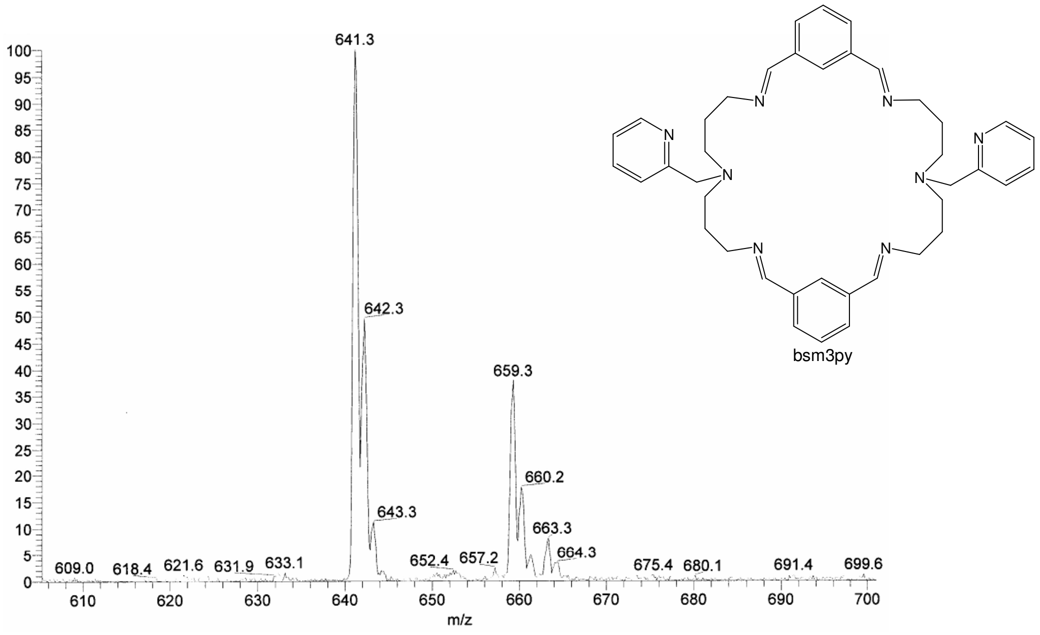
641.3
642.3
643.3
659.3
660.2
663.3
664.3
609.0
618.4
621.6
631.9
633.1
652.4
657.2
675.4
680.1
691.4
699.6
0
5
10
15
20
25
30
35
40
45
50
55
60
65
70
75
80
85
90
95
100
610
620
630
640
650
660
670
680
690
700
m/z
N
bsm3py

Figure A3.9. ^{1}H-NMR (200 MHz) spectra in $CDCl_3$ (A), FT-IR spectra (B) and ESI-MS spectra (C) of the compound **bsp2py** (**L81**).

Figure A3.9. (A)

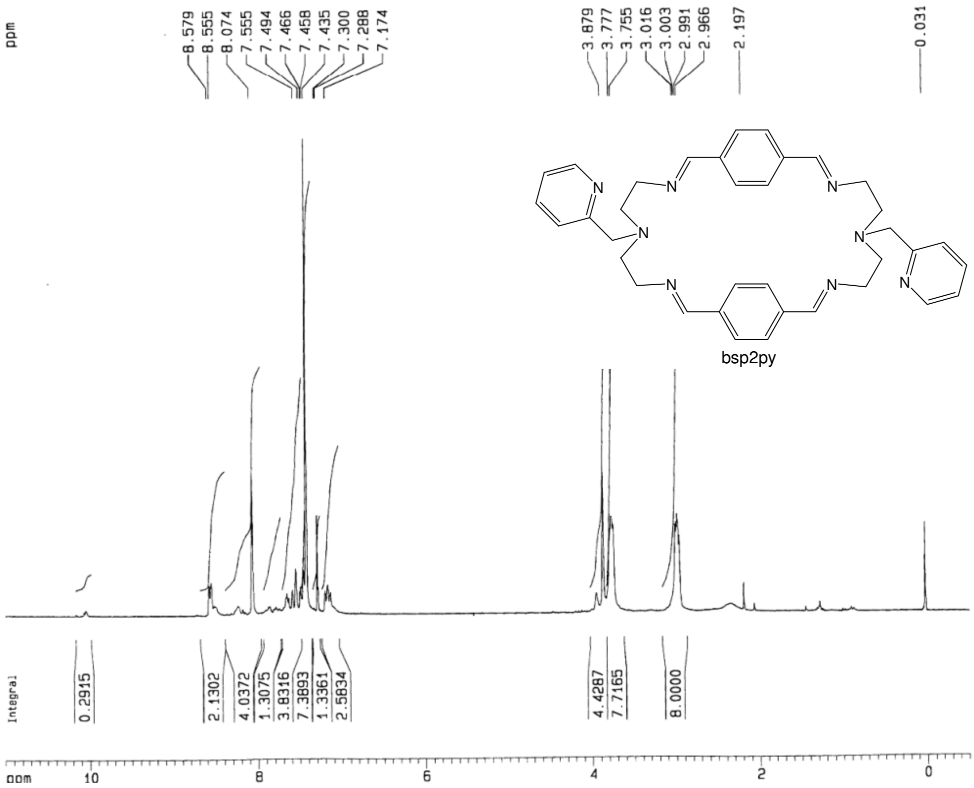

Figure A3.9. (B)

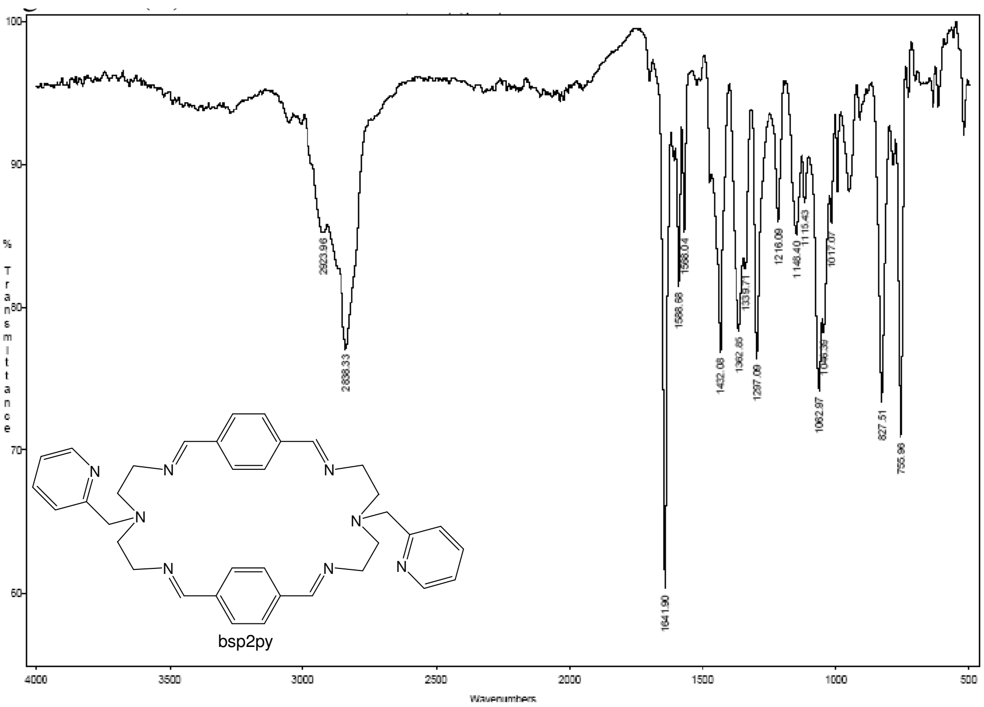

Figure A3.9. (C)

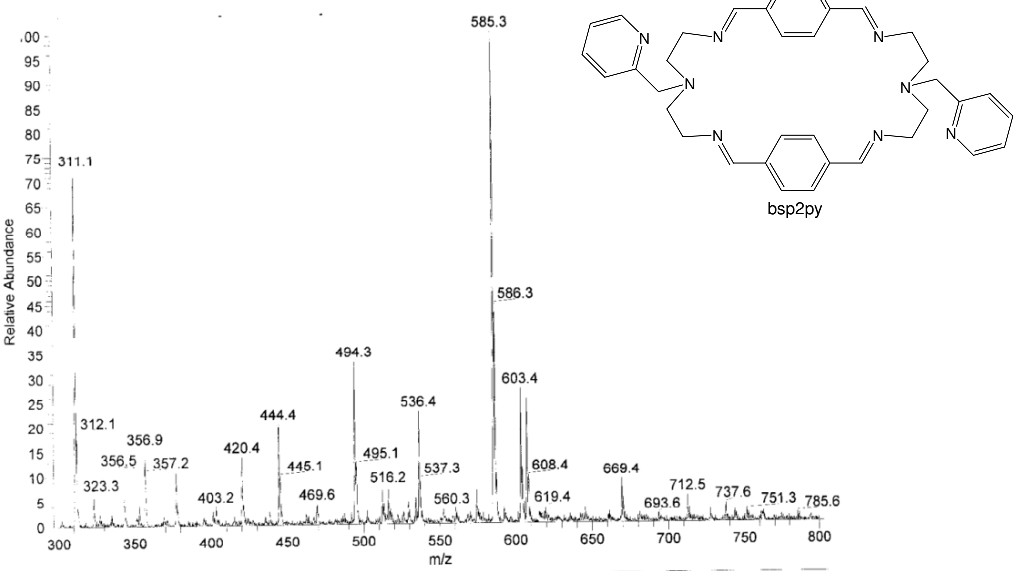
Relative Abundance
100
95
90
85
80
75
70
65
60
55
50
45
40
35
30
25
20
15
10
5
0
585.3
311.1
586.3
494.3
603.4
536.4
444.4
312.1
356.9
420.4
495.1
356.5
357.2
445.1
537.3
608.4
669.4
516.2
323.3
712.5
737.6
403.2
469.6
560.3
619.4
751.3
785.6
693.6
300
350
400
450
500
550
600
650
700
750
800
m/z
N
N
N
N
N
N
N
N
bsp2py

Figure A3.10. ^{1}H-NMR (400 MHz) spectra in D_2O:d_6-DMSO (4:1) (A), ^{13}C-NMR (100 MHz) spectra in d_6-DMSO (B) and ESI-MS spectra (C) of the compound **7**$(CF_3SO_3)_2$.

Figure A3.10. (A)

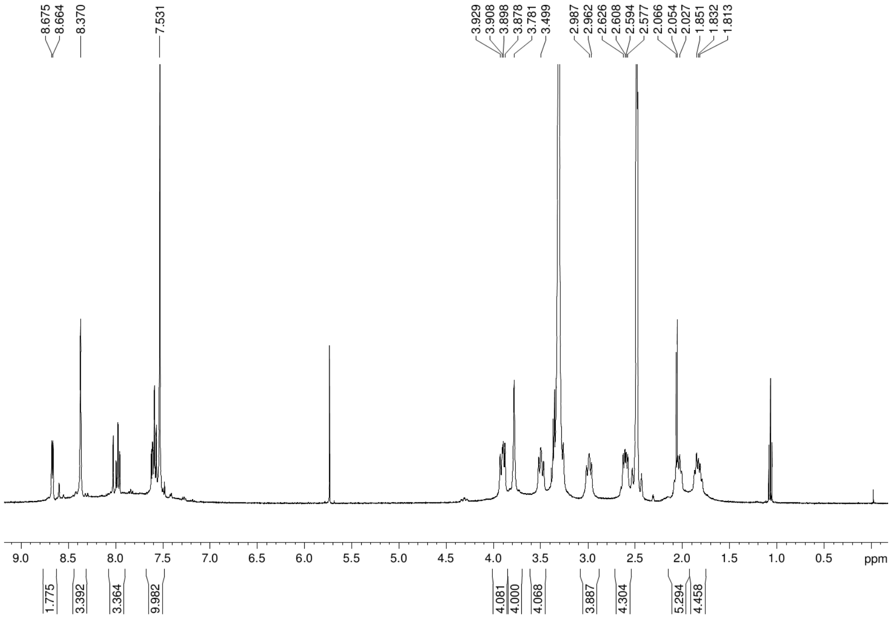

Figure A3.10. (B)

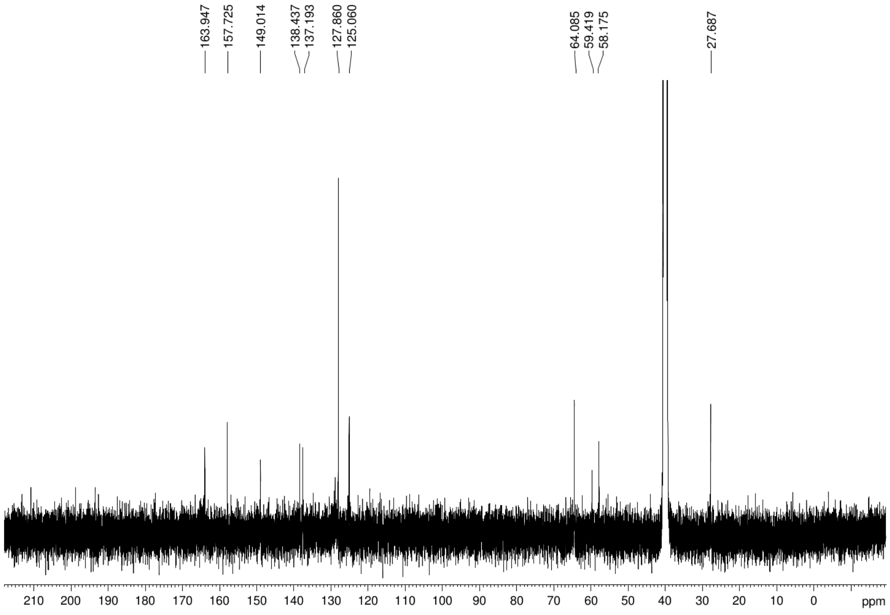

Figure A3.10. (C)

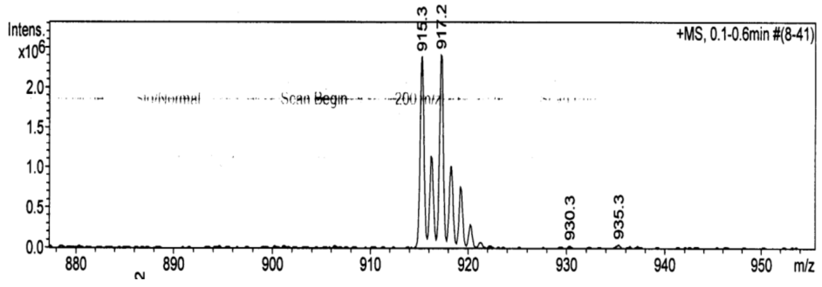

Figure A3.11. ^{1}H-NMR (400 MHz) spectra in d$_6$-DMSO (A), ^{1}H-NMR (400 MHz) spectra in D$_2$O:d$_6$-DMSO (4:1) (B), ^{13}C-NMR (100 MHz) spectra in d$_6$-DMSO (C) of the compound **8**(CF$_3$SO$_3$)$_2$.

Figure A3.11. (A)

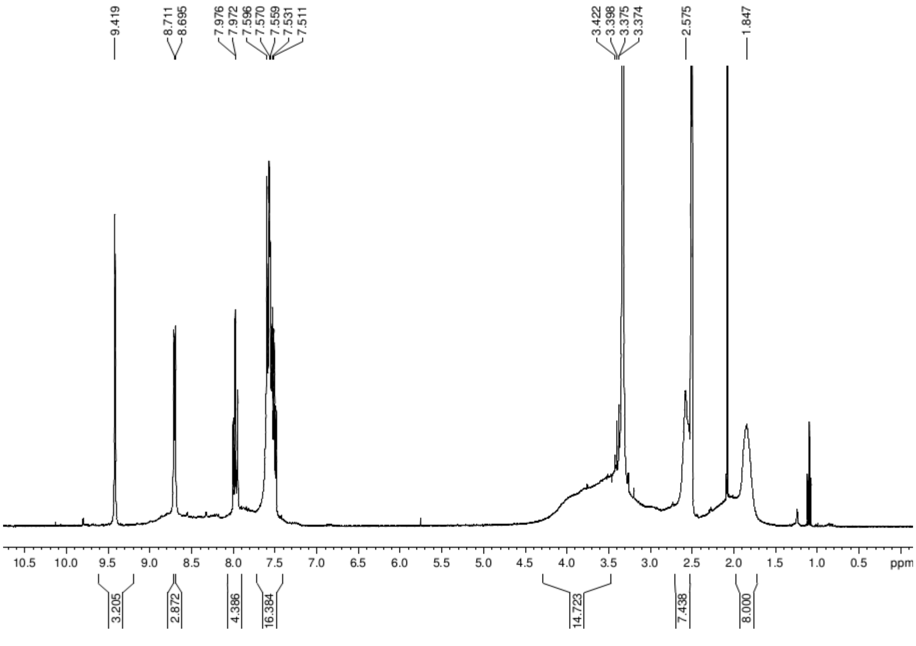

Figure A3.11. (B)

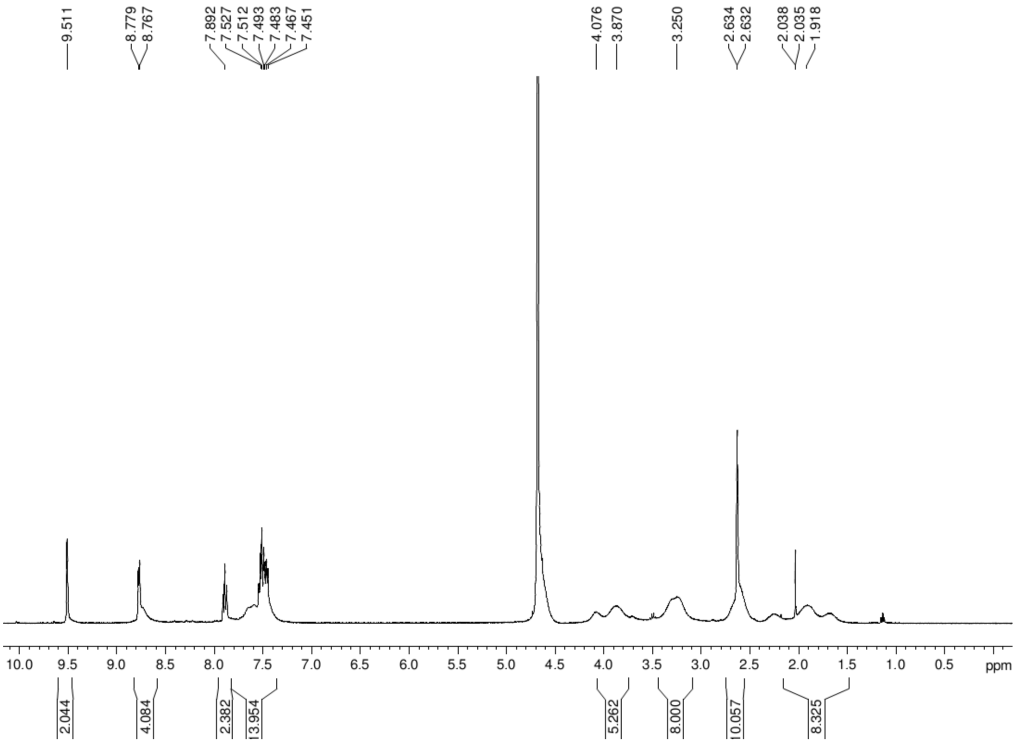

Figure A3.11. (C)

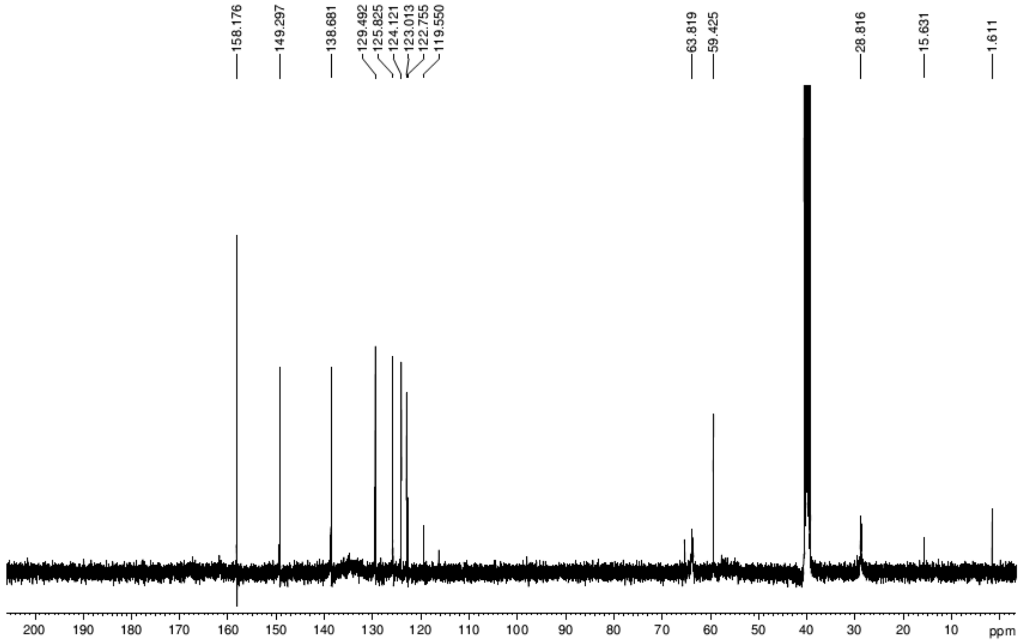

Figure A3.12. ^{1}H-NMR (400 MHz) spectra in D_2O:d_6-DMSO (4:1) (A), ^{13}C-NMR (100 MHz) spectra in d_6-DMSO (B) and ESI-MS spectra (C) of the compound **9**(CF_3SO_3)$_2$.

Figure A3.12. (A)

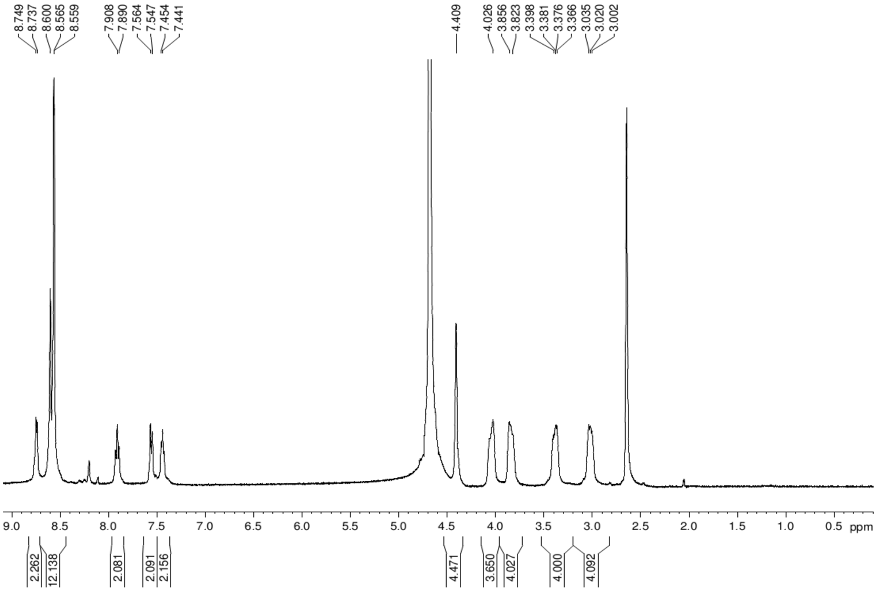

Figure A3.12. (B)

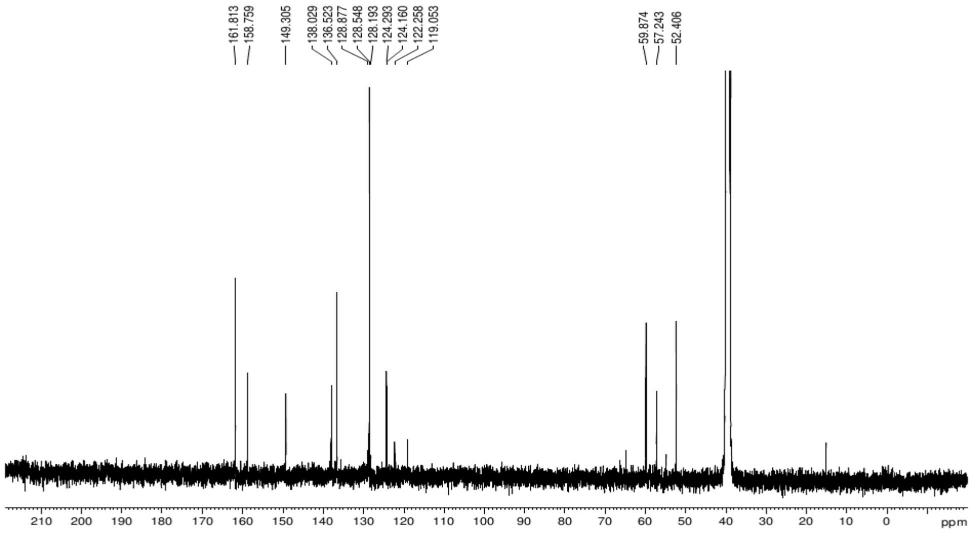

Figure A3.12. (C)

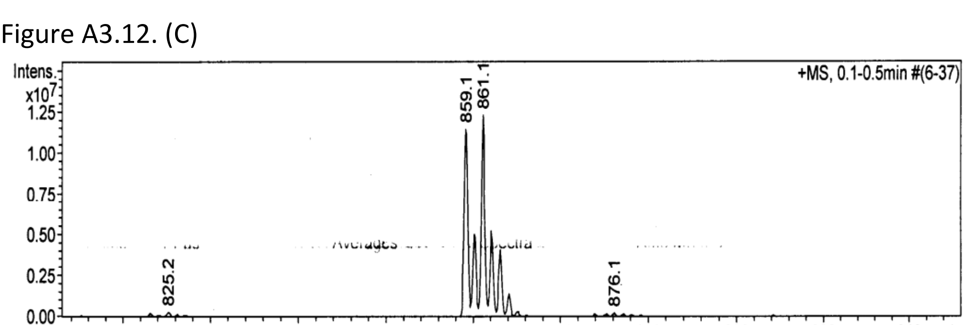

Figure A3.13. ^{1}H-NMR (200 MHz) spectra in CD_3CN of the compound **7**(BArF)$_2$.

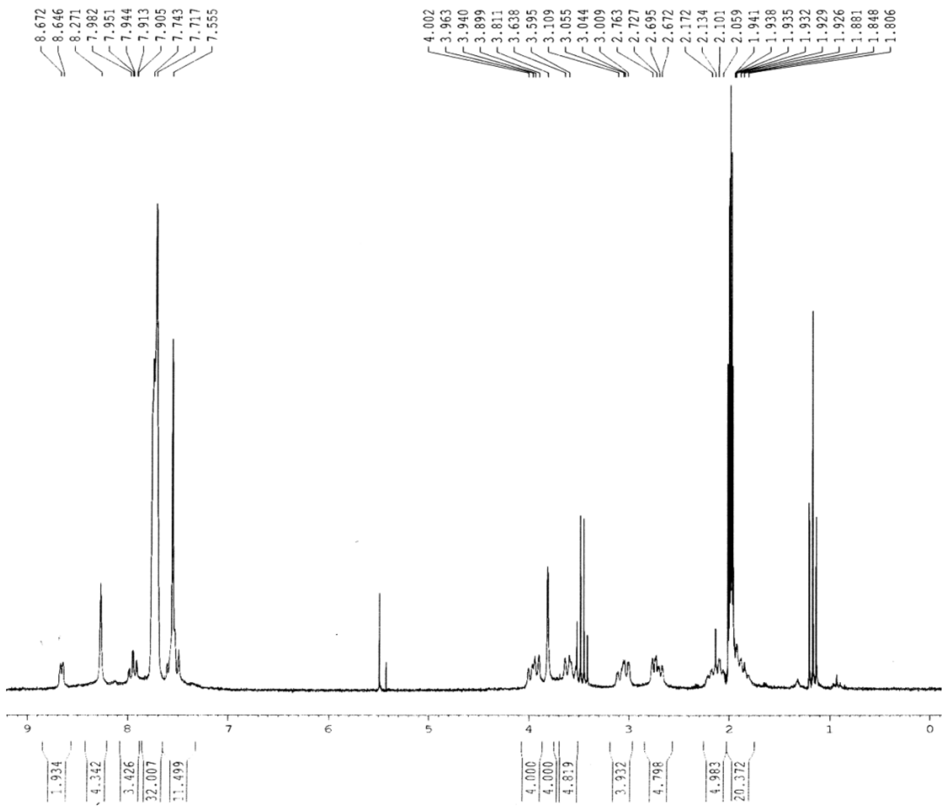

Figure A3.14. ^{1}H-NMR (200 MHz) spectra in CD_2Cl_2 (A) and ESI-MS spectra (B) of the compound **8**$(BArF)_2$.

Figure A3.14. (A)

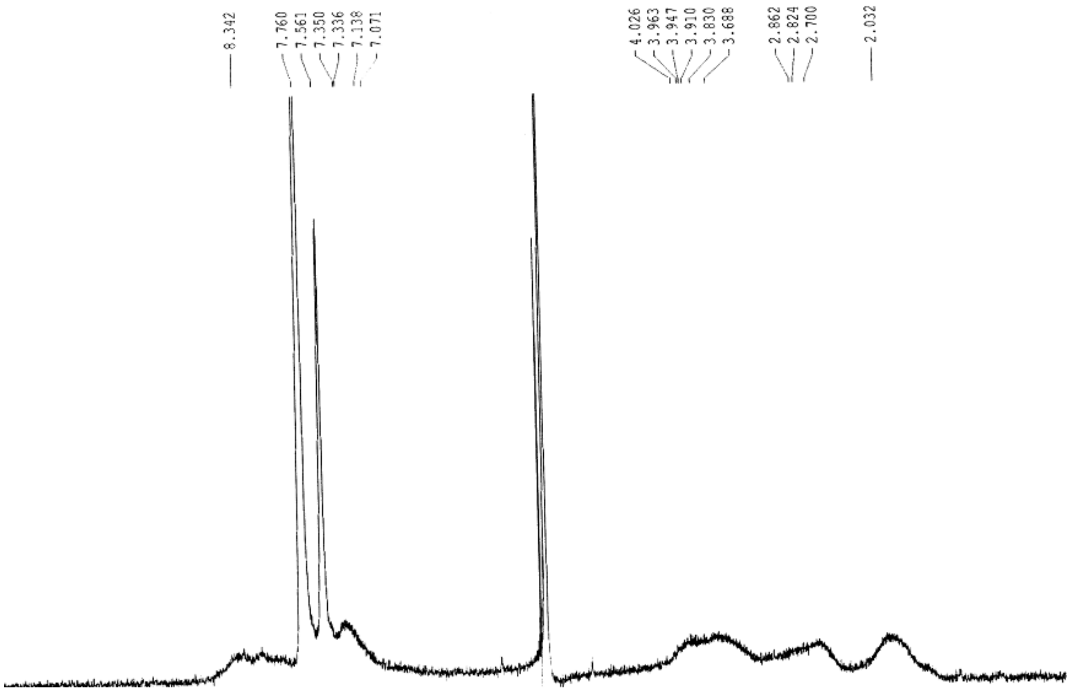

Figure A3.14. (B)

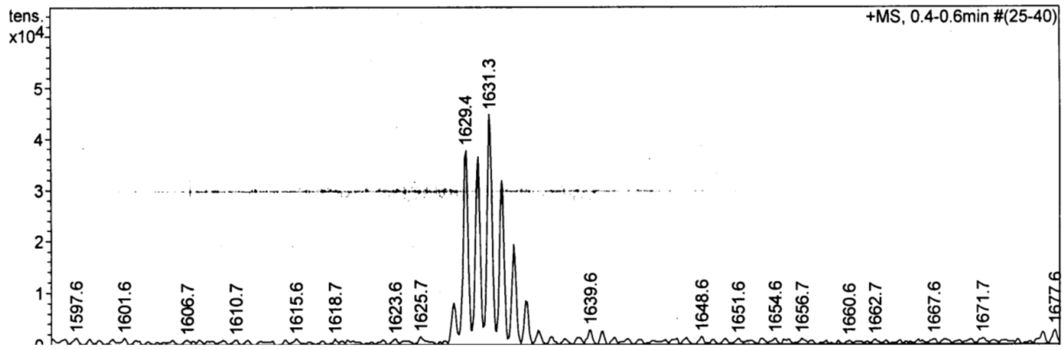

Figure A3.15. ^{1}H-NMR (200 MHz) spectra in CD_2Cl_2 (A), ^{1}H-NMR (200 MHz) spectra in CD_3CN (B) of the compound **9**(BArF)$_2$.

Figure A3.15. (A)

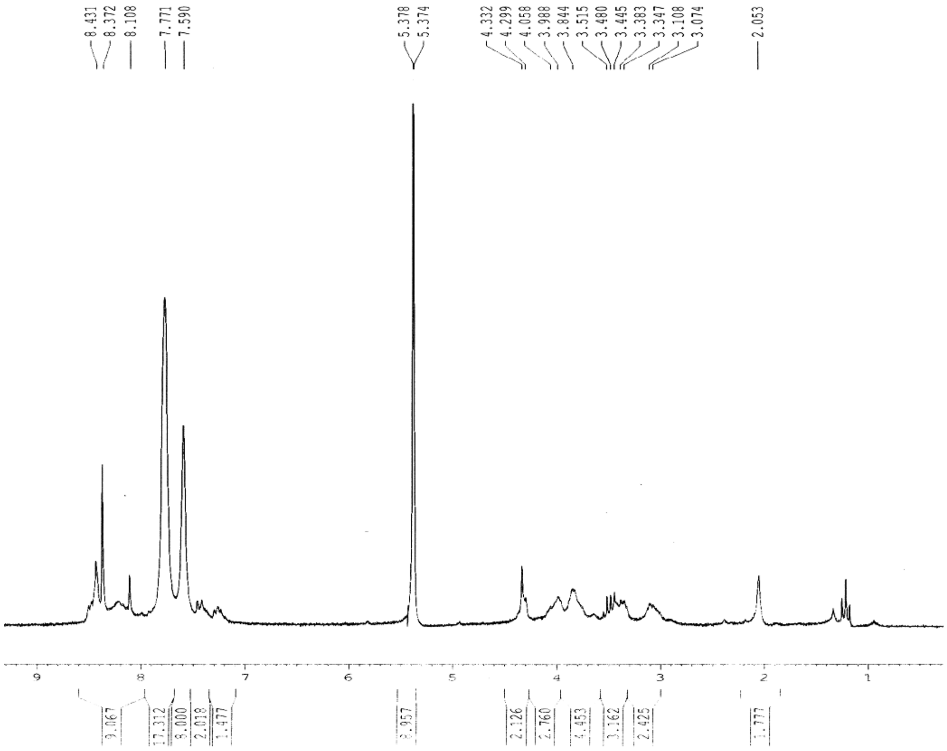

Figure A3.15. (B)

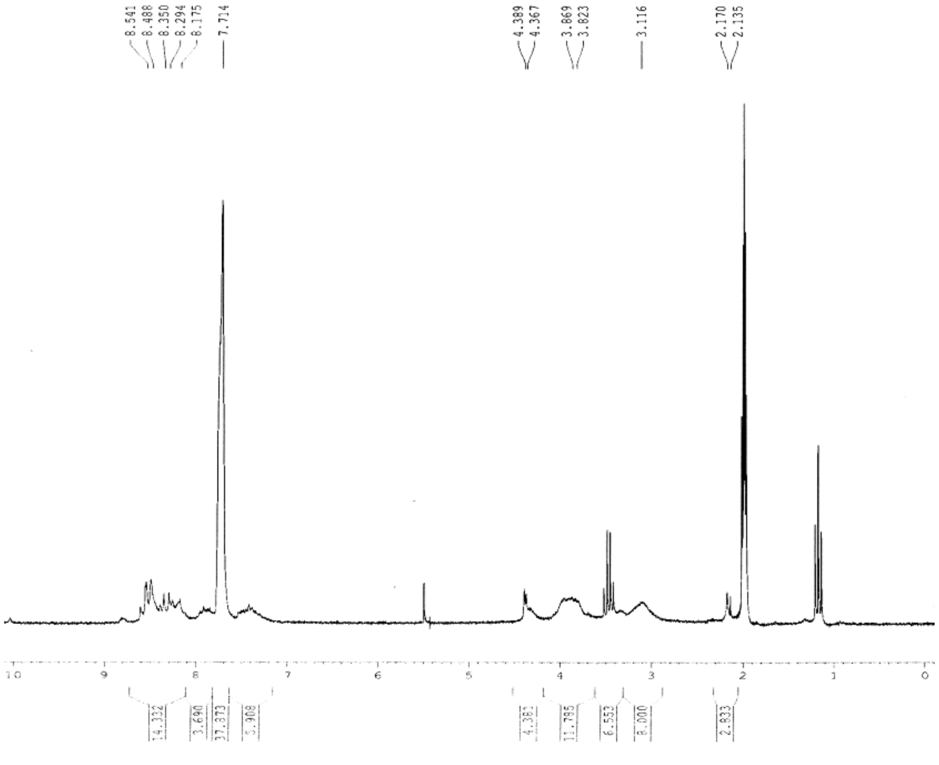

Figure A3.16. Agarose Gel Electrophoretic Mobility of pBR322 plasmid DNA (DNA concentration 0.017 µg/µL, 6 x 10^{-3} µM). Incubation time 2h (37ºC). Lane 1, pBR322 plasmid DNA in TE (3µL of the pBR322 DNA (0.25 µg/µL) in 41 µL of a TE buffer solution); Lane 2, control experiment with DNA in TE treated with milli-Q water with 20% DMSO solution (3µL of the pBR322 DNA (0.25 µg/µL) in 20 µL of a TE buffer solution + 21 µL of milli-Q water with 20% DMSO solution); Lane 3, control experiment with DNA in TE treated with milli-Q water with 20% DMSO solution + 1µl H_2O_2 (33% w/v) for t = 3 min, after incubation (3µL of the pBR322 DNA (0.25 µg/µL) in 20 µL of a TE buffer solution + 21 µL of milli-Q water with 20% DMSO solution + 1µl H_2O_2 (33% w/v)); Lane 4, control experiment with DNA in TE treated with milli-Q water with 20% DMSO solution + 1µl H_2O_2 (33% w/v) for t = 30 min, after incubation (3µL of the pBR322 DNA (0.25 µg/µL) in 20 µL of a TE buffer solution + 21 µL of milli-Q water with 20% DMSO solution + 1µl H_2O_2 (33% w/v)). (OC, open circular form; CCC, covalently closed circular form).

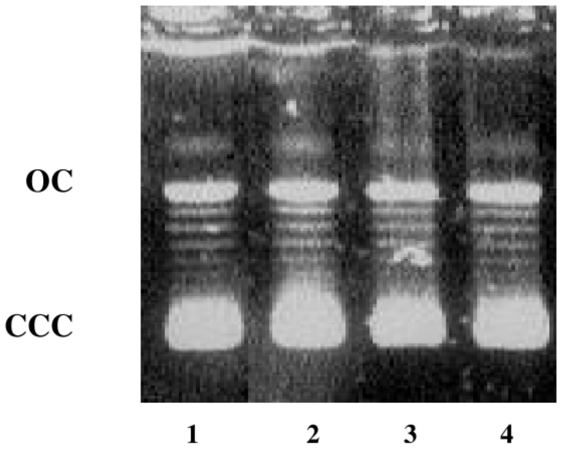

Figure A3.17. Agarose Gel Electrophoretic Mobility of pBR322 plasmid DNA treated with Cu(I) Compounds under nitrogen atmosphere (lane 1, 3 and 5 for complexes **7**, **8** and **9** respectively) and under aerobic conditions (lane 2, 4 and 6 for complexes **7**, **8** and **9** respectively). Lane 0, pBR322 plasmid DNA (control). Incubation time 2h (37ºC). (DNA concentration 0.017 µg/µL, 6 x 10^{-3} µM, molar ratio $r_i = 6.9$; r_i: input molar ratio of the complex to nucleotide) (OC, open circular form; CCC, covalently closed circular form).